THE UNIVERSITY OF HULL

Steel slag leachates: environmental risks and metal recovery opportunities

Being a Thesis submitted for the Degree of Doctor of Philosophy

In the University of Hull

By

Uchenna Victor Oty (M.Sc, PGDip)

Department of Chemistry, Faculty of Science and Engineering,

University of Hull, United Kingdom.

December 2015

Contents

Chapter 3. Methodology 38

List of Figures

List of Tables

List of Abbreviations

BET – Brunauer Emmett Teller (BET)

BF – Blast Furnace

BJH – Barrett Joyner Halenda

BOF – Basic Oxygen Furnace

COD – Chemical Oxygen Demand

CRM – Certified Reference Material

DI – Deionised

DOC – Dissolved Organic Carbon

DOM – Dissolved Organic Matter

EAF – Electric Arc Furnace

EDX – Energy Dispersive X-ray

EQS – Environmental Quality Standards

EU –European Union

FAAS – Flame Atomic Absorption Spectroscopy

GFAAS – Graphite Furnace Atomic Absorption Spectroscopy

IC – Ion Chromatography

ICP/OES – Inductively Coupled Plasma / Optical Emission Spectroscopy

ICP/MS – Inductively Coupled Plasma / Mass Spectroscopy

LLNL – Lawrence Livermore National Laboratory

LOD – Limit of Detection

RSD – Relative Standard Deviation

RF – Radiofrequency

SEM – Scanning Electron Microscopy

SI – Saturation Index

TGA – Thermogravimetric Analysis

UHQ – Ultra High Quality

XRD – X-ray Diffraction

WFD – Water Framework Directive

List of Photographic plates

Declaration

This thesis is the result of the independent investigation of the author, unless otherwise stated. Other sources of material relating to this work have been duly acknowledged. This work has not been previously submitted to any other higher educational institution for the purpose of gaining a higher degree.

Uchenna Victor Oty

Acknowledgements

I would like to give special thanks to my principal supervisor, Dr. Will Mayes, for the invaluable support and encouragement provided throughout this challenging PhD process, and also for his extensive academic advice and assistance during field visits. I am extremely grateful to my Co-supervisors, Dr. Mike Rogerson, for sharing some of his amazing ideas on experimental design on leaching experiments, solid phase characterisation, as well as for his extensive academic advice, Prof. Gillian Greenway, for providing guidance and advice on the analytical methods used in this research.

I sincerely appreciate all the administrative and technical staffs that have contributed towards the success of this work. Bob Knight, for providing me with a workspace, and also training on the use and troubleshooting of ICP (MS/OES). Nigel Parkin, for assistance with fabricating the columns for the leaching experiments. Dean Moore, for providing specialist training on the use of various chromatography and spectroscopy instruments. I would like to thank Tony Sinclair for SEM analyses, and Ian Dobson for TGA analyses. I appreciate the efforts of Kim Rosewell and Mark Anderson, for providing assistance with the establishment of my column experiments and microscopy analyses. Thanks to Mr Harri Wyn-williams (Leeds) for providing assistance with thin section preparation.

I am grateful to the University of Hull UK for providing funding for this PhD, as well as Tata Steel Scunthorpe, for granting site access. I would like to thank Mike Horne, Richard Coe, the Analytical chemistry group, all my friends in the UK and worldwide, for their amazing moral support and encouragement throughout this process.

Finally, I am highly indebted to my family, without their help, words of encouragement, prayers and support, this thesis would have been a lot more challenging. I love you all. Thank you for believing in me and I hope I made you all proud.

Abstract

Steel slag wastes are large volume residues generated in increasing quantities globally during steel production. While there are many afteruses for slag, roughly a quarter produced globally is stockpiled or landfilled where it may pose environmental risks. Furthermore as resource pressures increase there is a growing interest in recovering valuable metals from industrial by-products. Given the uncertainties in environmental risks and opportunities for further valorisation of wastes, an improved understanding of leaching processes from steel slag would help inform long term management of these industrial by-products.

This thesis aims to investigate a series of alkaline disposal sites (both steel slag and limespoil) to improve our understanding of the geochemical nature and fate of notable contaminants, as well as valuable metals of interest, in highly alkaline settings. The results of the field investigations show that leachates are characterised by high pH (> 11) and negative redox potential, excess deposition of secondary precipitates, and increased mobility of lithium (>800 ppb), strontium (>2500 ppb) and vanadium (>50 ppb), present in concentrations greater than those typically encountered in natural surface waters. Furthermore, these slag deposits were enriched with less mobile elements such as molybdenum (60 ppb) and nickel (61 ppb) with associated low environmental concern, but high resource value.

Laboratory batch tests showed that acid leaching promotes the leaching of the elements of interest particularly vanadium. However, such approach may not be viable at legacy sites due to cost. On the other hand, compost amendment of slag enhanced the leaching of molybdenum and vanadium by a factor of 3.6 and 2.5 respectively above water leaching alone. Column experiments reinforced these patterns in showing enhanced leaching of vanadium, molybdenum, and lithium when organic amendment is in contact with hyperalkaline leachate under aerobic conditions. This is most likely due to alkaline hydrolysis of organics within the system and subsequent metal complexation.

Analysis of secondary precipitates (notably calcium and magnesium carbonates) forming around the slag suggest these are key in controlling solubility of contaminants and metals of potential resource value (e.g. Ni).

1

Introduction

1.1 Context of the research

The research presented herein was conducted between 2012 and 2015 at a time of rising interest in the need for alternative sources of valuable metals especially from waste. Around 2000 Mt of caustic (i.e alkaline) waste are generated globally each year by major industries (Gomes *et al.*, 2015). These include industries involved with steelmaking (about 170 – 250 Mt/yr; Hendrick, 2015), coal-fired power generation (415 Mt/yr; Heidrich *et al.*, 2013) and alumina refining (> 70 Mt/yr; Sutar *et al.*, 2014). Some proportion of these waste are recycled and have after-uses. For example, 53 % of fly ash is recycled predominantly in cement (Heidrich *et al.*, 2013), while steel slag are used as aggregrates in construction, remediation of acid mine drainage and soil amendments (Charles and Nemmer, 2006; Geiseler, 1996; Mack and Gutta, 2009). Bauxite processing residue (red mud) from alumina refining also have afteruses such as adsorbents for heavy metal removal and also in the preparation of catalysts (Kumar *et al.*, 2006; Pradhan *et al.*, 1999). However despite these extensive afteruses, a significant proportion of these by-products are stockpiled or disposed in landfills since the recycling option is not widespread enough for efficient management of the residues. Traditionally, landfilling is a common option for the disposal of these residues however landfilling of alkaline waste can pose significant environmental risks primarily due to its inherent high alkalinity and toxic trace metal content (Environment Agency, 2010).

In addition, these residues are rich in elements, termed E-tech metals in a recent mineral security strategy review, which are crucial to development of green technologies (La, Li, Co, V, Te, Ga, Se; Naden, 2013). For example, the use of vanadium in high grade steel manufacture, rare earth metals essential for development of next-generation solar power systems and the use of lithium and cobalt for vehicle fuel cells. Consequently, the potential of highly alkaline waste for metal recovery is enormous because not only is waste produced in large amounts daily, but also due to the abundance of over a century-old "legacy" stockpiles in some areas (Milodowski *et al*., 2013).

Many of these elements of interest are also highly soluble at high pH (Mayes et al., 2011 a, 2011 b), and so potentially recoverable from leachates. Recovery of these resources would be a major step in addressing some of the key mineral security challenges highlighted in recent strategic reviews (Naden, 2013) whilst decreasing the environmental impact associated with the disposal of these residues in landfills. However, some challenges are associated with the recovery of metals from leachates at landfill sites. The concentration of metals within the leachate is low thus making the recovery process uneconomical in its own right. Also, there is also the issue of high energy requirements related to digging up legacy sites and associated environmental disturbance (Johnston *et al*., 2008).

1.2 Aim and objectives

The core aim of this project was to investigate the environmental risks and metal recovery opportunities associated with steel slag deposits and trial novel approaches towards *in-situ* metal recovery. To achieve this aim, a number of specific objectives were identified and are expanded below.

They include:

1. An outline of key literature;
    - Highlighting current sources, chemistry and management options for alkaline waste, as well as identifying the need for novel management strategies.
    - Exploring the underlying principles governing the leaching of trace metals from steel slag and alkaline waste in general.
    - Critically assessing gaps in understanding that currently prevent widespread resource recovery from steel slag.
2. Characterise alkaline waste (steel slag and lime spoil) disposal sites in the field to help improve the understanding of pollutant presence, transport and pathways in hyperalkaline systems.
3. Investigate the leaching behaviour of vanadium, molybdenum, nickel and lithium in novel multi-scale laboratory experiments with acid additions and organic amendments to assess the potential scope for metal recovery.
4. Determine and optimize the biogeochemical controls on the leaching rates of e-tech metals from steel slag under varying conditions using batch and column trials.

1.3 Thesis outline

This thesis has 8 chapters. Chapter 2 is a review of literature that provides context to the new data presented in Chapters 4, 5, 6 and 7. Chapter 2 introduces the reader to the concept of high pH systems, highlighting both natural and anthropogenic sources (primarily steel slag and lime spoil). The synergies between these waste types in terms of composition, leaching processes and management are highlighted. The concept of accelerated weathering of steel slag and the incorporation of trace elements into calcite as a means of controlling trace metal mobility is also introduced in this chapter.

Chapter 3 presents the generic analytical methods used for measurement and characterisation of samples throughout subsequent chapters. This chapter also provides the reader with details regarding field sample collection and Quality Assurance / Quality Control procedures related to this work.

To gain a better understanding of the geochemistry of alkaline waste systems, a number of steel slag disposal sites and lime spoil affected systems were studied, with results presented in Chapter 4. By doing this, the Chapter aims to identify the metals of interest (either in terms of environmental risk or recovery value) and their partitioning between the solid and aqueous phases within alkaline waste systems. By studying leaching products under ambient environmental weathering conditions, some of the key management challenges and future opportunities can be better understood.

Chapter 5 assesses the relative effectiveness on different approaches to leaching metals from steel slag in laboratory conditions. A comparison of acid leaching alongside organic amendments and control treatments is presented. Batch experiments were conducted under controlled conditions to explore the influence of these differing leaching approaches on the behaviour of vanadium, lithium, molybdenum and nickel from steel slag.

In Chapter 6, the effect of aerobic and anaerobic leaching of compost amended steel slag on metal release in solution is investigated using batch tests. Furthermore, column trials were used to investigate the effect of the physical structural arrangement between the compost and steel slag on the leaching of selected elements (V, Li, Mo, Ni). Chapter 7 covers the solid phase analyses of steel slag obtained from the column experiments in Chapter 6. By combining aqueous analyses of leaching products with solid phase assessment of source material and secondary mineral precipitates, Chapter 6 and 7 aim to provide a model for understanding the sources and fate of elements of interest in steel slag deposits.

Chapter 8 is a conclusion of the thesis and integrates the key findings throughout the thesis. An evaluation of future management opportunities for steel slags are considered which could minimise their environmental risks and maximise potential resource value is provided. Key lines of future research enquiry are also considered.

The outcomes of this research have already been disseminated to scientists (Hull *et al.*, 2014), local and international scientific community

(Environmental Mineralogy Research meeting, 2013; Goldschmidt 2014; International Mineralogical Association conference, 2014). These are presented in Appendix A1.

2

Literature review

Hyperalkaline wastes, unlike acidic waste, are a class of waste stream that are understudied. Hence, limited knowledge exists on its chemistry and particularly in the aspect of metal recovery. As a result, this chapter aims to introduce the various sources of high pH (pH > 9) waste, their adverse effects on humans and the environment and the existing management options for these residues. Furthermore, more emphasis was placed on steel slag and lime spoil mainly due to large volumes of production of these residues and the availability of study sites for these residues. Finally, a review of the mechanisms of leaching of trace metals from hyperalkaline solid residues, concept of accelerated weathering of steel slag and the possibility of the use of calcite as sink for trace metals is presented.

2.1 Natural and Industrial hyperalkaline systems

Hyper alkaline systems (pH 9 - 14) rarely occur in natural settings although there are a few exceptions in some areas of the world relating to local geological conditions. These include soda lakes and some ultramafic rocks rich in silicate and hydroxide phases. Soda lakes are strongly alkaline and distributed around the world. Some examples include Lonar lake (India; pH > 10.5), Lake Magadi (Kenya; pH 10.5), Mono Lake (United States; 9.8), Lake Chitu (Ethiopia; pH 10.3), Lake

Manyara (Tanzania; pH > 9.5), Lake Van (Turkey; pH 9.7), Goodenough lake (Canada; pH 10.2) and Kelemen-Szek (Hungary; pH 9.7) (Carini and Joye, 2008; Czop *et al*., 2011; Felfoldi *et al*., 2009; Hsieh *et al*., 2011; Lanzen *et al*., 2013; Nandy and Deod, 1961; Siddiqi, 2008). Most of these lakes are enriched with sodium, potassium, dissolved salts, sulphate and carbonate ions. Ultramafic rocks such as forsterite (Mg_2SiO_4) and enstatite ($MgSiO_3$) also give rise to high pH (pH 12) waters upon interacting with Mg–HCO_3 type solutions (Barnes *et al*., 1978).

While an increasing number of natural hyperalkaline sites have been reported and described, these are a small minority compared to those created from anthropogenic activity, which mostly involves the combustion of carbonate rich material to form oxides of Ca, Mg and other minerals. Examples of industrial waste with high native pH and elevated trace metal content include steel slag, lime spoil, red mud, fly ash, chromite ore processing residues, construction and demolition waste (concrete), paper and pulp waste (Adriano *et al*., 1980; Asokan *et al*., 2005; Burke *et al*., 2012b; Geelhoed *et al*., 2002; Mayes *et al*., 2011a, b; Pokhrel and Viraraghavan, 2004; USEPA, 1995; Whitthleston *et al*., 2011; see Table 2.1), comprising approximately 2 billion tonnes globally each year (Gomes *et al*., 2015).

Table 2.1: Current global production volumes for industrial alkaline residues

Residues	Production volume (million tonnes/yr)	Reference
Steel slag	170 – 250	Hendrick , 2015
Bauxite processing residues (red mud)	70 – 120	Power *et al*., 2009
Fly ash	415	Dwivedi and Jain, 2014; Heidrich *et al*., 2013
Construction and demolition wastes	44.8 (UK alone)	DEFRA, 2015

However, for the purpose of this research, emphasis has been placed primarily on steel slag and to a lesser extent, lime spoil. This is partly due to their increasing volume of production and landfilling in places such as Europe (see Figure 2.1), the abundance of these wastes especially at legacy disposal sites and also the availability of potential study sites during the period in which this research was conducted.

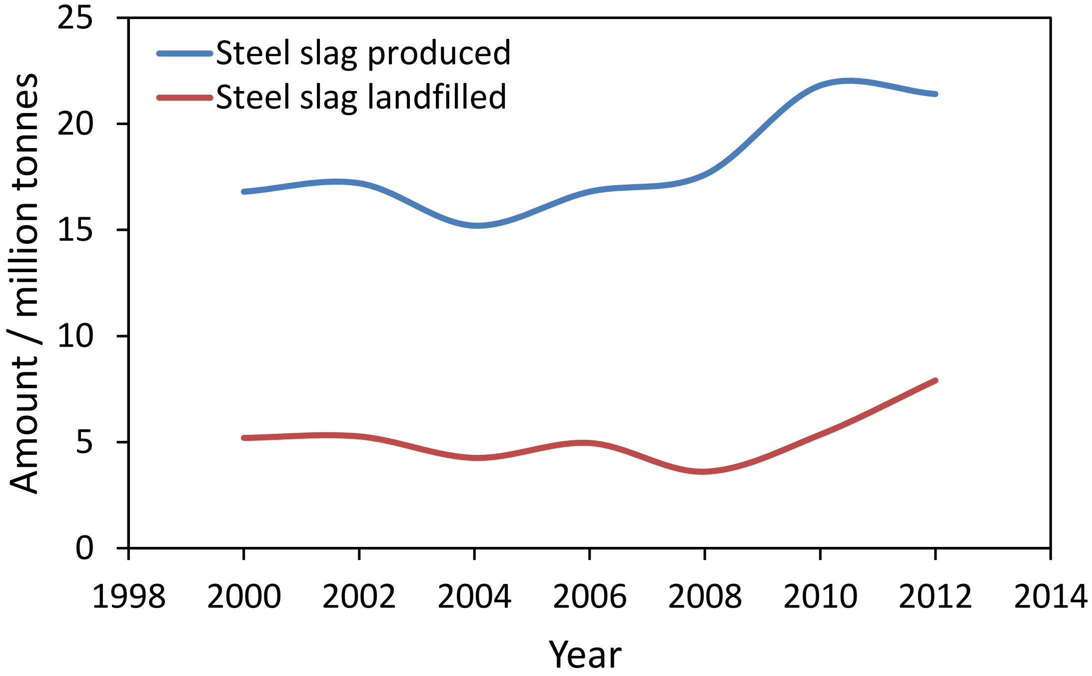

Figure 2.1: Trend showing statistics of production and landfilling of steel slag in Europe. Blue line – amount of slag produced. Red line – amount of slag landfilled. (Source: Euroslag, 2013. http://www.euroslag.com/products/statistics/2012/).

2.2 Steel slag and lime spoil: production and chemistry

2.2.1 Steel slag

Slag is a general term used to refer to all non-metallic co-products generated during the separation of a metal from its ore. The morphology and chemistry of slag is dependent on the cooling process applied, ore composition and the metallurgical process used for producing the material (Proctor *et al.*, 2000; Yildirim and Prezzi, 2015). Slag can be broadly classified as ferrous (iron / steel) and non-ferrous (copper, lead, zinc) depending on the industry of origin. The majority of slag types fall under the ferrous category while non-ferrous slag account for about 12 % of total annual production (National Slag Association, 2013; Proctor *et al.*, 2000).

2.2.1.1 Ferrous slag

Iron and steel slag is a non-metallic co-product generated during the production of iron and steel (Hendrick, 2015; Proctor *et al.*, 2000). Blast furnaces are used for production of iron while basic oxygen furnaces and electric arc furnaces are used for manufacture of steel (Proctor *et al.*, 2000; Yildirim and Prezzi, 2015). Steel slag is a by-product of the steelmaking process. It is formed during the separation of molten steel from impurities in steel-making furnaces. Molten steel slag is a complex mixture of oxides and silicates, and this crystallises into solids with the same bulk composition when cooled (Proctor *et al.*, 2000). Currently, in the UK, almost all steel plants have replaced the open hearth furnace system for steel-making with either the basic oxygen process (BOF) or the electric arc furnace (EAF) process (Steelconstruction.info).

2.2.1.1.1 Blast furnace slag (BF)

The production of iron takes place in a blast furnace (Figure 2.2; Proctor *et al.*, 2000). During this process, iron ore is mixed with coke and heated to form an iron-rich clinker called ‘sinter’. Limestone is fed into the top of the blast furnace containing the sinter. A hot air blast, from which the furnace gets its name, is injected through nozzles, called ‘tuyeres’, in the base of the furnace. The blast air may be oxygen-enriched and coal or oil is sometimes also injected to provide additional heat and reduce coke requirements. The heat generated in the furnace (reaching 1000 °C) allows the iron in the ore and sinter to melt out and settle at the bottom of the furnace. The limestone combines with impurities and molten rock from the iron ore and sinter, forming molten slag which, being lighter than the metal, floats on top of it (FHWA, 2012; Juckes, 2011).

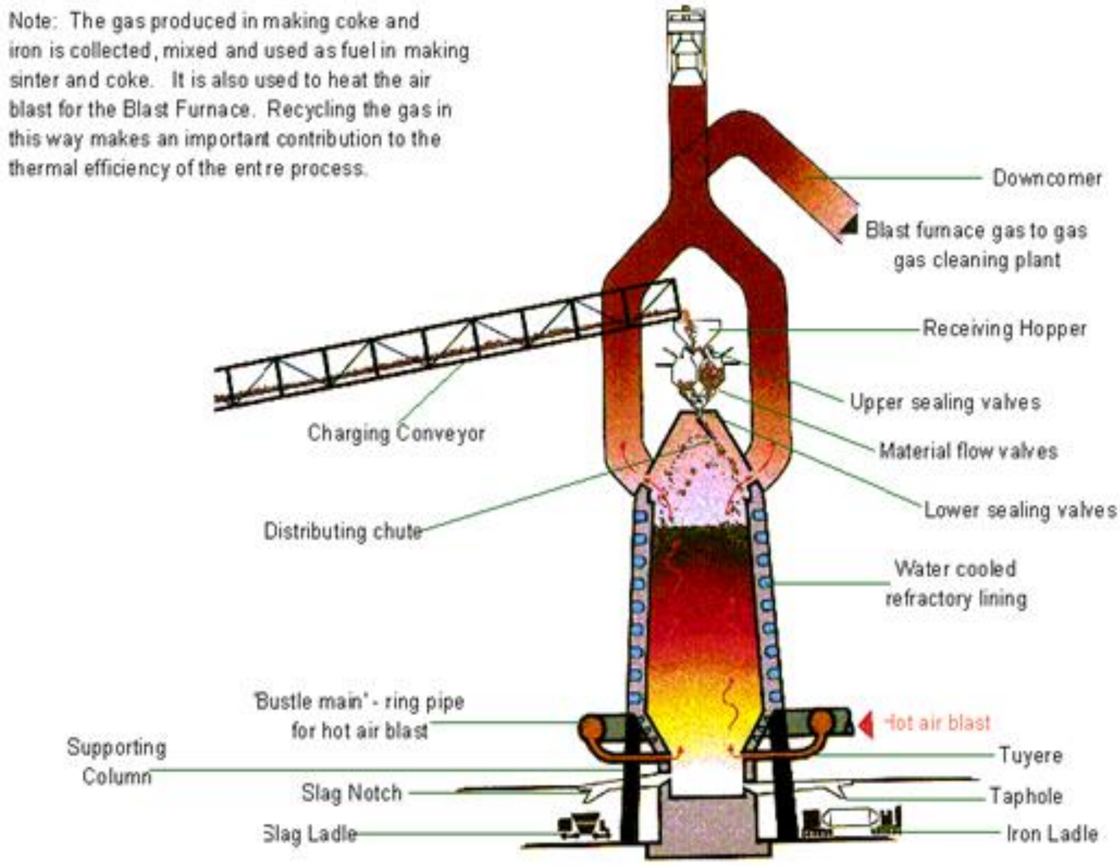

Figure 2.2: A typical blast furnace used in the iron-making process (Source: Steelconstruction.info, http://www.steelconstruction.info/Steel_manufacture)

2.2.1.1.2 Basic oxygen furnace slag (BOF)

In the basic oxygen process, molten pig iron from the blast furnace is first pre-treated externally to lower the silicon, sulphur and phosphorus content (Steelconstruction.info; Stubbles, 2015). This step is however optional depending on the quality of the hot metal and the required final quality of the steel. A typical basic oxygen steelmaking process has been presented in Figure 2.3.

The hot metal, scrap and fluxes (lime, dolomite) are charged to a furnace and high purity oxygen is injected at a pressure of 100 - 150 psi at supersonic speed through a water-cooled lance, which is suspended in the vessel. The oxygen ignites the carbon dissolved in the steel, to form carbon monoxide and carbon dioxide, and causing the temperature in the furnace to rise to about 1700 °C. It also combines and removes the impurities in the charged furnace consisting mainly of oxides of carbon, silicon, manganese, phosphorus and iron. These impurities combine with the fluxes to create the **steel slag**. At the end of the refining operation, the liquid steel is tapped (poured) into a ladle while the steel slag is retained in the vessel and subsequently tapped into a separate slag pot (Juckes, 2011; Stubbles, 2015).

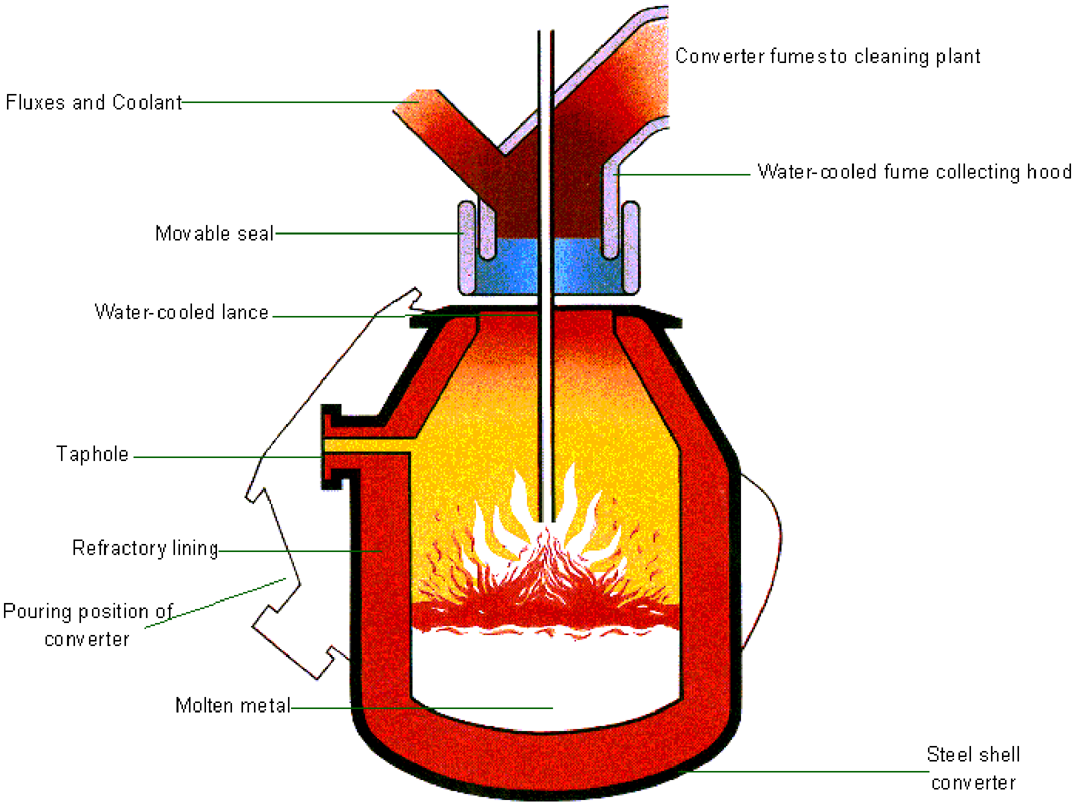

Figure 2.3: The Basic oxygen steelmaking furnace (image adapted from Steelconstruction.info: http://www.steelconstruction.info/Steel_manufacture)

After being tapped from the furnace, the molten steel is transferred in a ladle for further refining to remove additional impurities still contained within the steel. This operation is called ladle refining because it is completed within the transfer ladle. During ladle refining, additional steel slag is generated by again adding fluxes to the ladle to melt. These slag are combined with any carryover of furnace slag and assist in absorbing deoxidation products (inclusions), heat insulation, and protection of ladle refractories. The steel slag produced at this stage of steel making is generally referred to as **raker and ladle slag** (National Slag Association, 2007; Steelconstruction.info). In some BOF steelmaking plants where low sulphur steel grades are required, the co-injection of lime and magnesium into the hot metal is carried out in order to accomplish this aim. The post desulphurisation slag is comprised of blast furnace slag carryover, the residual from previous heat(s) in the hot metal ladle and the reaction products of the injected CaO and Mg, and is termed **desulphurised skimmed slag** (Li *et al.*, 2012).

2.2.1.1.3 Chemistry of blast furnace and basic oxygen slag

The chemical composition of most steel slag vary depending on the method of steel production applied and the characteristics of raw materials used while its physical properties is controlled mainly by the choice of cooling techniques used (Costa, 2009). For example, BOF slag have more iron and manganese compared to BF slag. On the other hand, BF slag are richer in aluminium, silicon and sulphur compared to BOF slag. Table 2.2 and 2.3 presents the typical composition of blast furnace and basic oxygen furnace slag.

Table 2.2: Typical physical parameters and major ion composition of blast furnace, basic oxygen furnace and desulphurised slag (All values are reported in %).

Reference	Slag type	Ca	Si	**Al**	**Mg**	**Fe**	S	**Mn**	P
Proctor *et al.*,2000 [a]	BF	27.4	17.0	4.1	7.0	1.7	1.0	0.6	0.02
Euroslag, 2010	BF	35.0 – 42.0	33.0 – 42.0	10.0 – 15.0	7.0 – 12.0	≤ 1.0	1.0 – 1.5	≤ 1.0	-
Proctor *et al.,*2000 [a]	BOF	28.0	6.0	2.4	5.5	18.4	0.1	3.3	0.3
Juckes, 2003 [b]	BOF	36.4 – 45.8	10.7 – 15.2	1.0 - 3.4	4.1 – 7.8	19.0 – 24.0	0.1 – 0.2	2.7 – 4.3	1.0 – 1.5
Emery, 1982	BOF	40.0 – 52.0	10.0 – 19.0	1.0 – 3.0	5.0 – 10.0	10.0 – 40.0	< 1.0	5.0 – 8.0	0.5 – 1.0
Yildirim and Prezzi, 2011	BOF	39.4	12.0	2.2	9.7	30.2	0.1	2.7	1.0
Chang *et al.*, 2011a, b	Desulphurised slag[c]	43 – 49	16 -19	2 – 4	1 – 5	10 -20	-	-	-

[a] The values are compiled based on mean chemical composition data from 73 slag samples collected from 58 different steel mills in the United States and Canada. [b] The range of values are compiled based on chemical composition data from 4 different sources in Great Britain. [c] expressed as % metal oxides

Table 2.3: Typical minor elements composition of blast furnace BF and basic oxygen furnace BOF slag (All values are reported in mg/kg).

Reference	Material/Slag type	Sb	As	Ba	**Cr** (total)	**Co**	Cu	Pb	**Mo**	**Ni**	Se	**V**	**Zn**
Proctor *et al.*,2000 [a]	BF	N.D	1.3	273.0	132.0	3.0	5.3	3.6	0.8	1.4	3.9	54.0	20.0
Proctor *et al.*,2000 [a]	BOF	3.3	N.D	75.0	1271.0	3.8	30.0	50.0	11.0	4.9	15.0	992.0	46.0
Background levels	Soil	0.5[c], 0.7[d]	5.2[c], 7.2[d]	440.0[c], 588.0[d]	37.0[c], 54.0[d]	6.7[c], 9.1[d]	17.0[c], 25.0[d]	16.0[c], 19.0[d]	0.6[c], 1.0[d]	13.0[c], 19.0[d]	0.3[c], 555.0[d]	58.0[c], 81.0[d]	48.0[c], 60.0[d]

[a] The values are compiled based on mean chemical composition data from 73 slag samples collected from 58 different steel mills in the United states and Canada.

[c] Mean background concentrations for metals in soil from Shacklette and Boerngen, 1984.

[d] Background concentrations from Dragun and Chiasson, 1991. Elements highlighted in bold are typical E-tech elements.

2.2.2 Lime waste spoil

Limestone is a naturally occurring sedimentary rock rich in minerals such as calcite, magnesite and dolomite. It is used as a precursor in the production of lime via burning and mostly obtained from quarries and mines. Lime products have various applications in the construction, metallurgical, chemical and environmental industries (Singleton Birch, 2015). In construction, lime is added to asphalt to reduce stripping, decelerate the ageing process and improve its cohesion. It is also used to stabilise low quality soils for road construction and also as an ingredient in plaster and mortar production (British Lime Association, 2015). Environmental applications of lime include the use for drinking water purification, contaminated land and wastewater treatment (British Lime Association, 2015). In metallurgy, lime is used to remove impurities during steel production (British Lime Association, 2015). In the chemical industry, lime is used as an additive in the manufacture of glass, paper, sugar and pharmaceuticals (British Lime Association, 2015).

To produce lime, limestone is heated in a rotary kiln using traditional fuel (coal) which generates sufficient heat to convert the limestone to quicklime and carbondioxide (Watkinson and Brimacombe, 1982).

$$CaCO_{3(s)} \rightarrow CaO_{(s)} + CO_{2(g)} \qquad (2.1)$$

Limestone is fed into the upper end of the kiln, while fuel and combustion air are fired into the lower end of the kiln. The limestone is heated as it moves down the kiln toward the lower end. As the preheated limestone moves through the kiln, it is “calcined” into lime (Watkinson and Brimacombe, 1982). The lime is discharged from the kiln into a cooler where it is used to preheat the combustion air. Lime can either be sold as is or crushed to make hydrated lime.

At most lime legacy sites such as that investigated in this research (Harpur Hill; see Chapter 4 for site description), the lime production process was inefficient and led to the generation of large volumes of waste in the form of partially and over - calcined limestone, coal ash, fused glassy lime clinker, coal clinker and lime fines which make up the lime spoil. Subsequently, these lime spoil becomes a source of hyperalkaline leachates. The presence of quicklime (CaO) in the spoil greatly increase the pH, [Ca^{2+}], alkalinity and carbonate ion concentration of waters via the hydration of slaked lime $Ca(OH)_2$ which dissociates to liberate hydroxide (Andrews *et al* 1997).

$$CaO + H_2O \rightarrow Ca(OH)_2 \qquad (2.2)$$

Upon hydration, calcium hydroxide dissociates to give the hydroxide ion responsible for the high alkalinity of the lime spoil associated waters (pH > 12; Burke *et al*., 2012a; Mayes *et al*., 2005).

$$Ca(OH)_2 \rightarrow Ca^{2+} + 2OH^- \qquad (2.3)$$

The process of calcite precipitation is a common feature of both lime and steel disposal sites. High pH leachates, upon interaction with atmospheric carbondioxide, leads to the formation of carbonate tufas (Anon, 2008; Burke *et al*., 2012a). The mechanism for this process is described by eqns. 2.4 – 2.7 (Clark *et al*, 1992).

$$CO_{2(g)} \rightarrow CO_{2(aq)} \qquad (2.4)$$

$$CO_{2(aq)} + OH^{-} \rightarrow HCO^{-}_{3(aq)} \quad (2.5)$$

$$HCO^{-}_{3(aq)} \rightarrow CO^{2-}_{3\,(aq)} + H^{+} \quad (2.6)$$

$$Ca^{2+}_{(aq)} + CO^{2-}_{3\,(aq)} \rightarrow CaCO_{3(s)} \quad (2.7)$$

2.3 Environmental effects of hyperalkaline systems

There are relatively few studies on the environmental and health effects of highly alkaline systems (Dethlefsen and Rosenthal, 1973; Koryak *et al.*, 2002; Mayes *et al.*, 2009). This is partly due to the fact that hyperalkaline residues and associated waters sites are less common compared to the acidic counterpart. Consequently, the actual adverse effects are less certain – for example, laboratory toxicity tests rarely go the extreme alkaline end of the pH range. Therefore there are a whole range of uncertainties surrounding risk assessment for these sites. Alkaline waste residues and wastewaters have adverse effects on human, invertebrates, ecology, aquatic life and the environment.

(a) Impact of pH and dissolved oxygen

Leachates emanating from fly ash waste are detrimental to benthic fauna and fish populations particularly salmonids due to the high pH exhibited by these waters (Cairns *et al.*, 1972; Haslam, 1990). The pH of alkaline leachates is also responsible for DNA damage in plant tissues and earthworms, point mutations in the bacteria *Salmonella typhimurium* strains TA97 and TA102 and can have genotoxic effects on invertebrates (Manerikar *et al.*, 2008; Mukherjee and Chakraborty, 2009). The high alkalinity also contaminates surface water and renders it unfit for purpose.

Hyperalkaline leachates when in contact with surface waters, leads to an increase in the chemical oxygen demand (COD) and a decrease in amount of dissolved oxygen which is vital to the survival of most aquatic organisms (Dethlefsen and Rosenthal, 1973). High pH waters reduce microbial activities because hyperalkaline conditions are not favourable for most bacteria e.g. sulfate reducing bacteria (Czop *et al.,* 2011). Red mud (bauxite residue) adversely affect the exchange of oxygen between the eggs of marine invertebrates and their surrounding environment, thus decreasing their chance of survival (Dethlefsen and Rosenthal, 1973). They also cause problems in the development and reproduction of Mediterranean Sea urchin *Paracentrotus lividus,* the extent of toxicity however depends on composition of the bauxite ore and the manufacturing process (Pagano *et al*., 2002; Trieff *et al.,* 1995).

(b) Impact of precipitates smothering

Leachates from alkaline wastes e.g. steel slag, adversely affect the ecology of surface waters due to the excess rate of calcite precipitation on these waters (Mayes *et al*., 2009). Calcite precipitation in these waters (as calcareous crystalline crust) hinder light from penetrating into the water to the primary producers which is usually found at the littoral and deep zones of the habitat (Koryak *et al*., 2002). Calcite smothering in high pH affected waters is also detrimental to fish, macrophyte, zooplankton and benthos populations (Auer *et al*., 1996; Effler 1987; Effler *et al*., 2001). The precipitation of calcite on the surface of these waters reduces the amount of nutrient available to these organisms because the nutrients especially phosphorus tend to coprecipitate with the calcite, thus adversely affecting their survival (Patrick and Khalid, 1974). Calcite smothering also affects vegetation by destroying plant tissue and hindering photosynthesis (Madsen *et al.*, 1996).

(c) Impact of fugitive dust

Fugitive dust is the particulate matter released into the atmosphere from outdoor processes or operations and controlled by forces of the wind (MDEQ, 2014). Typical activities include those occurring at steel slag, red mud, coal ash disposal sites etc (Dellantonio *et al.*, 2010; Posfai *et al.*, 2011; Ruhl *et al.*, 2009). Fugitive dust originating from high pH waste poses significant environmental concern. For example, red mud consists of very fine grained particles with average particle size of 2 – 100 μm and prone to resuspension into the atmosphere especially under dry conditions (Klauber *et al.*, 2009). Given the relatively long residence time of these particles, they may remain resuspended in the air long enough to cause severe respiratory problems in human by affecting the bronchus and lungs (Dellantonio *et al.*, 2010).

(d) Impact of toxic trace elements

Some trace metals present in alkaline waste have adverse ecological and health effects. For example, the presence of mercury in alkaline waste like coal ash can have adverse ecological effects depending on the chemical lability of mercury in the solids and the tendency for mercury methylation to occur in the area of impact (Mukherjee and Zevenhoven, 2006). Also, the accumulation of fly ash with high arsenic content in the deep zone of an aquatic system could lead to fish poisoning through food chains and reduction of benthic fauna, an important source of food (Ruhl *et al.*, 2009). Furthermore, toxic trace elements such as chromium in the hexavalent state Cr^{VI} is carcinogenic to the lungs either through oral or dermal exposure; due to its high solubility it tends to be mobile within the terrestrial environment (Geelhoed *et al.,* 2002). In some cases, the toxic trace metals especially B, Mo, As, Se are accumulated within plant tissues via uptake mechanisms. This accumulation has subsequent effects on animals causing diseases like Mo- induced hypocuprosis when such plants are consumed (Mukherjee and Zevenhoven, 2006).

2.4 Management options for steel slag

2.4.1 Landfilling

Conventionally, landfilling is the most common option for management of alkaline waste. However, this option occupies land that would otherwise be useful for other purposes and is also expensive particularly in form of landfill costs (HM Revenue & Customs, 2015). For example, as of April 2015, landfill tax in the UK had risen to £82.60 standard rate and £2.60 lower rate per tonne of waste landfilled thus making this option unattractive to waste producers (HM Revenue & Customs, 2015). There is also the issue of non-regulated landfill disposal particularly at legacy disposal sites. Many of these sites were not subject to such stringent requirements and remain enduring sources of hyperalkaline drainage because legislations such as the Council Directive 1999/31/EC on landfilling of waste and Council Decision 2003/33/EC for landfilling of hazardous and non-hazardous waste targeted at ensuring that waste are in compliance with limit values before disposal in landfills were not in place at the time (Mayes *et al.*, 2008). Landfilling also has associated environmental and ecological effects (see section 2.3). Hence, globally there is a growing awareness that landfilling should be applied as a temporary measure or a last resort, and that a more resource efficient alkaline waste management system is required.

2.4.2 Recycling

In as much as the majority of steel slag end up in landfill, some proportion are recycled and find uses in aspects of construction, agriculture and metal recovery.

2.4.2.1 Reuse as secondary source for metals recovery

In recent times, the rising demand for metals in the world has led to series of intensive research for alternative sources of metals, with more focus on the extraction of metals from low-grade ores and/or secondary resources (Anjum *et al.*, 2012). The high rate of population growth coupled with natural resource consumption and the need for the development of more environmental friendly approaches for metal extraction and processing are key reasons for the high demand on available global metal supplies (Naden, 2013).

Recently, the need for the global security of supply of certain e-tech elements and ways for ensuring their continuity have been highlighted in various strategic reviews at both national and EU level (Naden, 2013). These elements are classified as being of importance or significant to environmental technologies and / or science opportunities (Li, V, Co, Te, Ga, Se, La; Figure 2.4).

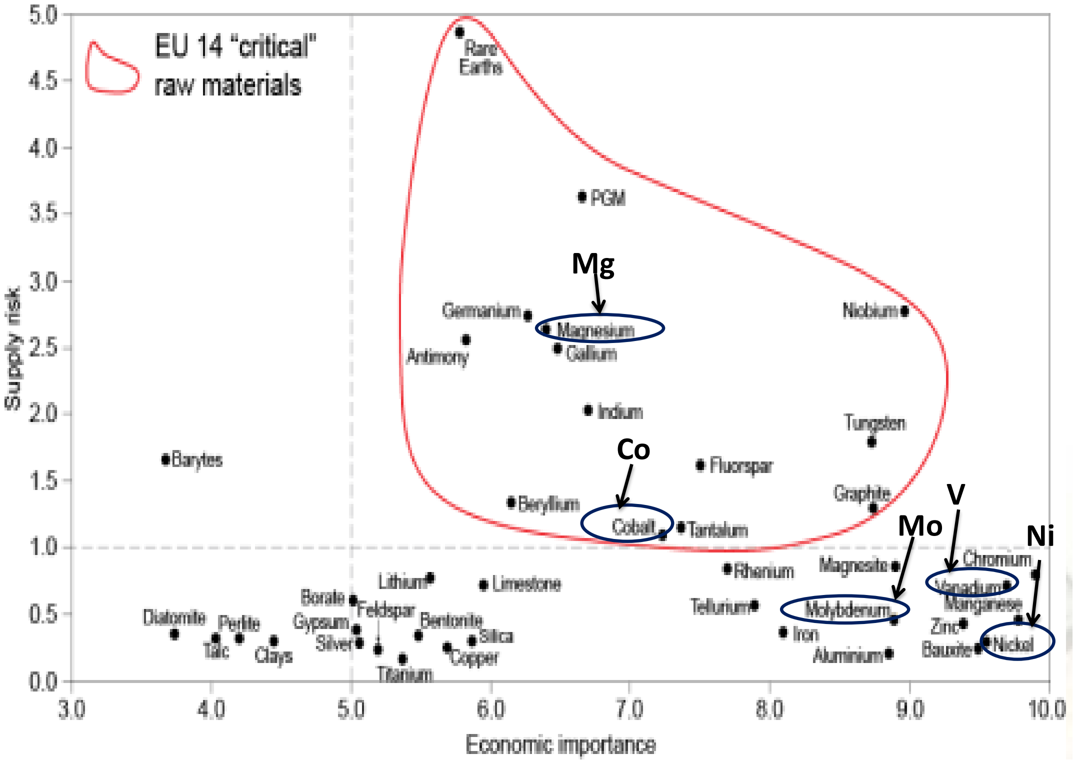

Figure 2.4: . Diagram illustrating the 14 “critical” raw materials identified by the European Union (image obtained from Naden, 2013).

Some of these elements (highlighted in blue circles; Figure 2.4) are highly soluble at high pH (Mayes *et al*., 2011a, b), and so are potentially recoverable from steel slag leachates. As a result, steel slag leachates and high pH leachates in general have attracted considerable attention as secondary sources of e-tech elements with potentially globally significant reserves (Table 2.4). Recovery of metals from steel slag would therefore be a major step in tackling the current EU mineral security challenge and reduce the amount of residues that end up in landfills.

Table 2.4: Typical E-tech element composition (mg/kg: values in parenthesis give the % of global annual production in respective residue assuming a 5 % metal recovery rate)

Residue	Cobalt	Gallium	Lanthanum	Lithium	Selenium	Vanadium
Steel slag[1]	40-700 *(0.3-5.7%)*	30-60 *(99-198%*	60-75 *(4.3-5.4%)*	1-140 *(0.02-3.4%)*	<1 (-)	100-1500 *(1.4-21.4%)*
Red mud[2]	90-110 *(0.5-0.6%)*	70-80 *(154-176%)*	141-282 *(6.7-13.5%)*	50-60 *(0.8-1.0%)*	<1 (-)	860-1100 *(8.2-10.5%)*
Fly ash[3]	3-10 *(0.1-0.2%)*	40-60 *(304-456%)*	80-100 *(13.3-16.6%)*	300-400 *(16.8-22.4%)*	2-5 *(2.1-5.2%)*	50-100 *(1.6-3.3%)*
2012 production(t/yr)[4]	110000	273	12500	37000	2000	63000

[1] Dyson, 2013; [2]Mayes *et al.* (2011a; b); [3]Dai *et al.* (2011); [4]USGS (2013)

2.4.2.1.1 Methods of metal recovery from high pH waste

The extraction and recovery of metals from alkaline industrial waste can be achieved through either hydrometallurgical or bioleaching methods. The conventional hydrometallurgical approach is capital intensive and has associated pollution risks (Mishra *et al*., 2004; Pradhan *et al*., 2006). On the other hand, the latter method is gaining popularity, since it is more environmentally - friendly and requires less energy (Akcil, 2004; Brierley, 2010).

(a) Hydrometallurgical approach

Several workers have investigated the hydrometallurgical method of metal recovery from high pH residues. Hydrometallurgical method of extraction of metals from the feedstock, in this case, steel slag can be achieved either via acid leaching or alkaline leaching, or a combination of both. The use of acids (nitric, sulphuric, acetic acid) for extraction of metals from steel slag has been investigated by various workers (Doucet, 2010; Eloneva *et al*., 2008a, 2008b). This approach is appealing, simply because it generates high extraction efficiency, sometimes up to 80 % (Shafyei *et al*., 2006). Alkaline leaching of steel slag using NaOH is less efficient but allows for selective leaching of elements such as vanadium and molybdenum (Vahidi *et al*., 2012). These approaches are however capital intensive, energy intensive and are not environmentally friendly. Also, several studies have also been carried out on the use of ammonium salts for leaching of metals from waste residues. This process is economical due to simultaneous solvent regeneration associated with it, but less efficient compared to acid extraction (Teir, 2015).

(b) Bioleaching method

Bioleaching is a process which involves the transformation of insoluble solid compounds into soluble and extractable elements which can be recovered through the action of micro-organisms e.g. fungi and bacteria (Akcil and Deveci, 2010). Bioleaching helps to overcome the problem encountered during processing of ore deposits by conventional means (Brierley, 2010) and also reduces cost of production of metals (Akcil *et al*., 2013). Bioleaching process occurs via a route similar to natural biochemical cycles. Bioleaching of metals from industrial waste helps reduce the amount of waste that ends up in landfill (Akcil *et al*., 2013).

Heterotrophic microbes are able to solubilise metals from waste through the use of organic and inorganic acids released as a product of metabolism of fungi and bacteria (Burgstaller, 1993). Heterotrophs require organic carbon sources for leaching to occur. Metal dissolution of minerals by organic acids is achieved through the protonation and subsequent chelation of the mineral / waste into soluble organometallic complexes (Burgstaller, 1993). Some of the ligands produced have the ability to dissolve oxides and silicates from the mineral matrix e.g. humic acid, citric acid and gluconic acid (Duff *et al.*, 1963). Heterotrophic bioleaching can either occur in a single or two – step process (Mishra and Rhee, 2010). In a one – step process, the microbe producing the leaching agent is incubated with the waste at the beginning of the bioleaching process while in a two – step process, the microorganism is first pre-cultured for a few days to obtain the leaching agent and then brought in contact with the waste or mineral in a separate stage (Mishra and Rhee, 2010). Two – stage bioleaching leads to improved metal recovery. The use of heterotrophic microbes for leaching is useful for minerals or waste that are low in sulphur and sulphides and unable to sustain autotrophic acidophiles.

2.4.2.2 Utilization in the agriculture and construction sectors

Steel slag is utilized in the agriculture sector as soil conditioners and fertilizers to amend soil properties. Addition of steel slag to soils increases the soil pH and improves the exchange complex within the soil thereby improving soil productivity (Maslehuddin *et al.*, 2003). Steel slag rich in lime and phosphorus are also used as substitutes in the manufacture of fertilizers (Lopez Gomez *et al.*, 1999). Steel slag particularly those with low free lime content are useful for construction purposes. Due to the mineralogy and physical properties of steel slag, they serve as concrete aggregates for road and harbour construction, road stone and ballast for railways for railway tracks (Ozeki, 1997).

2.4.2.2.1 Accelerated weathering of steel slag

Prior to the use of alkaline residues (steel slag) for the various applications, they have to be weathered so as to ensure stabilisation of the waste. Naturally, this weathering process occurs on relatively slow timescales hence the concept of accelerated weathering is introduced below because it is paramount in the context of metal recovery.

Accelerated weathering is the process of reacting alkaline materials with high purity CO_2 in the presence of moisture in order to achieve carbonation within minutes or hours, unlike natural weathering which occurs at a slow rate due to the relatively low atmospheric CO_2 concentration, about 0.03 – 0.06 % (Costa *et al.*, 2007; Lackner, 2002; Lim *et al.*, 2010). The iron and steel industry is responsible for about 6 – 7 % of global CO_2 emissions (Doucet, 2010). The industry is therefore continually working towards developing environmentally sustainable technologies for managing CO_2 emissions and waste residues generated from the steel plants. Steel slag is an ideal feedstock for accelerated carbonation because it is highly abundant in metal oxides including calcium, magnesium, aluminium, iron and manganese oxides (Pan *et al.*, 2012). In addition, carbonation can also be made to occur in-situ at disposal sites e.g. steelworks, therefore overcoming the problem of fugitive dust encountered during transport.

Accelerated weathering of generated steel slag has therefore gained plenty of interest in recent years as a viable option for offsetting some of the emissions associated with carbon-intensive industries (e.g. Huijgen *et al.*, 2005; Bonenfant *et* *al*., 2008; Teir, 2008; Eloneva *et al*., 2008a; Kodama *et al*., 2008; Costa, 2009; Wang and Yan, 2010; Chang *et al*., 2011a, b; De Windt *et al*., 2011). Carbonation of steel slag is estimated to reduce global CO_2 emissions from steel plants by about 170 Mt/year (Eloneva *et al*., 2009). Weathering can lead to a decrease in solution pH thereby affecting the solubility and leaching of metals that are mobile at high pH and fixed at lower pH (Costa et al., 2007). It leads to waste stabilization and also decreases the porosity of solid waste since the pore space is usually filled with calcite after carbonation, thus giving the material a finer structure (Fernández - Bertos *et al*., 2004; Ishida and Maekawa, 2000).

Generally, several mechanisms have been listed for the process of accelerated carbonation of alkaline solid waste. Pan e*t al*, 2012 concluded that aqueous carbonation of steelmaking slag occurred in three stages including;

a) the dissolution of CO_2-reactive species (e.g. portlandite, calcium silicate hydrates (CSH), larnite) from a solid matrix to yield calcium ions. Smaller particle size, lower pH, increasing temperature , high pressure and increased surface area are some of the factors that encourages calcium leaching from steel slag (Iizuka *et al*., 2004; Tai *et al*., 2006; Costa *et al.,* 2007; Gerdemann *et al.*, 2007; Lekakh *et al*., 2008; Teir, 2008; De Windt *et al*., 2011).

b) the contemporary dissolution of CO_2 into a liquid phase and conversion of carbonic acid to carbonate/bicarbonate ions depending on pH (see equations 2.3 – 2.5). pH determines the ions produced during the dissociation of carbonic acid. At a low pH (~4), the production of H_2CO_3 dominates, at a mid pH (~8) HCO_3^-dominates, and at a high pH (~12) CO_3^{2-}dominates (Morel and Hering, 1993). Therefore, accelerated carbonation is favoured at an alkaline pH due to the availability of carbonate ions (Pan *et al*., 2012).

c) the consequent nucleation and precipitation of carbonates (equation 2.6). The balance between dissolution and precipitation is dependent on the kinetics and solubility of the present feedstock and possible products, where carbonates are probably the most important products.

Some of the factors that can affect the rate and extent of the carbonation process include (a) transportation-controlled mechanisms such as CO_2 and Ca^{2+}-ions diffusion to/from reaction sites; (b) boundary layer effects (diffusion across precipitate coatings on particles); (c) dissolution of $Ca(OH)_2$ at the particle surface; (d) pore blockage; and (e) precipitate coating (Huijgen *et al*., 2005).

2.5 Mechanisms of trace element mobility in soils and waste systems

The mobility of trace elements in high pH waste is controlled largely by physico-chemical processes and to a limited extent by biological processes depending on the toxicity of the metal of interest (Carrillo-González *et al*., 2006; Kotuby-Amacher and Gambrell, 1988). Physico-chemical processes such as adsorption, mineral solubility and precipitation, and complexation promote and regulate the mobility of trace elements in waste materials whereas the sorption process sequesters trace element mobility and greatly controls the partitioning of the trace elements between the solid and solution phase (Carrillo-González et al., 2006; Kotuby-Amacher and Gambrell, 1988).

2.5.1 Physico-chemical processes

Most trace elements in soils and waste usually occur in association with the solid phase, only a small portion of trace elements occur within the solution phase (Carrillo-González et al., 2006; Yang *et al*., 2012). In the solid phase, trace elements are bound via surface adsorption, mineral precipitation or coprecipitation within various forms whereas in solution, they exists in form of free ions or bound to organic acids (Carrillo-González et al., 2006).

2.5.1.1 Mineral solubility and precipitation

The mobility of trace elements in waste is governed by the solubility of the mineral phase associated with the trace element and this in turn is controlled by the pH of the waste environment. In the case of alkaline leachates, the native pH is usually controlled by the dissolution of various Ca-bearing minerals such as calcite ($CaCO_3$), portlandite ($Ca(OH)_2$), ettringite ($Ca_6[Al(OH)_6]_{2}$-$(SO_4)_3 \ . \ 32H_2O$), hydrocalumite ($Ca_4Al_2(OH)_{12}(OH)_2 \ . \ 4H_2O$), calcium silicate hydrate (3 $CaO \cdot 2 SiO_2 \cdot 4 H_2O$ - CSH) present in these waste (Barna *et al.*, 2000; Johnson *et al.*, 1995; Meima and Comans, 1997). High pH leads to an increase in the precipitation of metals in the form of carbonates and hydroxides; increased sorption of cations onto oxides of iron and manganese and increased sorption to humus material, hence decreasing trace element mobility and under low pH conditions the reverse becomes the case. The factor of pH also affects ion pair and complex formation, surface charge, organic matter solubility, metal hydroxide and carbonate solubility (Appel and Ma, 2001; Huang *et al.*, 2005; Lebourg *et al.*, 1998). The mineral dissolution – precipitation process, although occurring at a slow rate, is a key mechanism that governs the mobility of trace metals (Deverel *et al.*, 2012). Usually, if the element exceeds its solubility for a given compound in a solution, mineral precipitation occurs (Carrillo-González et al., 2006; Deverel *et al.*, 2012). On the other hand, if the concentration of a given component of the mineral phase is below its chemical equilibrium concentration, mineral dissolution occurs (Deverel *et al.*, 2012).

2.5.1.2 Complexation

At high pH, trace elements can bind with organic and inorganic ligands within a waste system thus enhancing their mobility via complex formation (Carrillo-González et al., 2006). Metal ions and ligands form soluble complexes in form of weakly bound ion pairs, metal-organic complexes and chelation (Gao *et al.*, 2003). Some of these ligands include naturally occurring compounds e.g. polysaccharides, amino acids, polyphenols, and aliphatic acids, humic substances e.g. humic and fulvic acids, and humin, hydroxyl, carbonates, sulfate, nitrate, chloride, and dissolved organic matter (DOM) (Carrillo-González et al., 2006). In most cases, a significant proportion of soluble trace elements occur in association with dissolved organic matter (Alberic *et al.*, 2000). DOM consist of a mixture of fulvic and humic acids hence the modelling of complexation is rather difficult due to the heterogeneity and variable chemical composition and structure of the organic substance. Also, the solubility of trace elements is expected to increase in the presence of a good source of DOM such as municipal compost by the formation of soluble organometallic complexes (Naidu and Harter, 1998). Chelating ligands form very stable associations with trace elements and are able to extract them even if they are bound to the organic matter (Carrillo-González et al., 2006). The chelation process is however affected by pH and the ionic concentration of the ligand species (Carrillo-González et al., 2006; Deverel *et al.*, 2012). For example, copper complexes dissociate at low pH while lead and chromium complexes are stable at low pH.

2.5.1.3 Coprecipitation

Coprecipitation is a common mechanism that control trace element leaching in waste. This process occurs via either one of three routes;

1) Substitution of the trace element into the lattice of the major mineral depending on the distribution coefficient between the trace and major element in a solid / solution system (Webb *et al.*, 1998). For example, if calcite was the major precipitating mineral, calcium becomes the major element.
2) Two minerals precipitating simultaneously with the dominant supersaturated mineral possessing a higher saturation index (Deverel *et al.*, 2012).
3) Adsorption of trace elements onto the surface of the precipitating mineral or metal oxides such as iron oxides, manganese oxides, aluminium oxides (Deverel *et al.*, 2012).

2.5.1.3.1 Secondary precipitates as metal sinks

Calcite has been shown to be an effective sink for various trace elements including rare earth elements, actinides, heavy metals, oxyanions like phosphate, selenate, arsenate, chromate (Alexandratos *et al.*, 2007 ; Tang *et al.*, 2007). It is able to achieve this either through adsorption or coprecipitation (Rouff *et al.*, 2004; Elzinga *et al.*, 2002; Zachara *et al.*, 1991). In some cases, the uptake mechanism can be a combination of both (Roman – Ross *et al.*, 2006). Calcite is able to allow for substitution of various substituents in its crystal structure due to the flexibility of its topology. Calcite structure is based on corner-sharing of triangular CO_3 groups with CaO_6 octahedra (Alexandratos *et al.*, 2007; Tang *et al.*, 2007).

Factors such as pH, reaction time, ionic strength, solution composition and adsorbing species, affect the distribution coefficient of a metal between the solid and liquid phase (Alexandratos *et al*., 2007). Generally, most studies involving metal uptake in calcite have been shown to occur in steps; a fast initial uptake followed by a slow removal process. The fast initial uptake is attributed to be due to chemisorptions to readily available surface sites (McBride, 1980) while the following slower uptake has been suggested to be due to co-precipitation (Franklin and Morse, 1983), diffusion to additional less accessible surface sites in fracture and pores, or adsorption to sites that have a lower reaction rate due to lower affinity (Davis *et al*., 1987; Stipp *et al*., 1992).

Ideally, trace elements are expected to incorporate homogenously into calcite in a thermodynamic manner. However, this is not the case in scenarios where active precipitation of calcite tends to occur e.g. in skeletal biogenic calcite. In such cases, other factors such as rate of reactions tend to have an impact on the mechanism of incorporation. A common way for determining the preferred phase for a trace element in a solid (calcite) – solution system is via the use of partition coefficient. If partition coefficient, D of a trace element exceeds 1, the trace element is preferentially concentrated in the calcite thus decreasing its mobility whereas a D value less than 1 implies that the trace element is preferentially excluded from the calcite precipitate and more mobile (Lea, 1999). Partition coefficients are calculated using the resulting trace element TE and calcium concentration according to the expression:

$$D_{TE} = \frac{\left(\frac{TE}{Ca}\right)_{solid}}{\left(\frac{TE}{Ca}\right)_{solution}} \qquad (2.8)$$

Partition coefficient, as defined in equation (2.8) is however an empirical measure of the trace element to calcium ratio in precipitated calcite to the same ratio in solution for a specific set of biological and physical conditions and is not representative of the thermodynamic property of the system (Lea, 1999).

Pingitore (1986), proposed two mechanisms for the incorporation of trace elements into foraminiferal calcite. They include through direct solid solutions, in which the trace element substitutes directly for Ca^{2+} in the calcite structure, and trapping, in which the trace elements occurs as a discrete phase or absorbed ion. The former, is more likely controlled by the thermodynamics of the system whereby trace elements with ionic radii similar to Ca^{2+} and chemical structures isomorphous with calcite tend to incorporate in this way. However, trace elements incorporated through trapping tend to have a more heterogenous mineral composition and is also regulated by kinetic factors such as precipitation rate (Reeder, 1983).

2.6 Leaching mechanisms of selected elements in high pH waste

The leaching rate of most elements in alkaline waste is dependent on the redox state of the element, pH and mineral solubility (Cornelis *et al.*, 2008). For instance, oxyanionic (negatively charged species containing O) elements such as Cr, Sb, Mo, V, As form various species in solution depending on the redox potential (negative redox potential tend to form more reducing species while solution with more positive redox potential produces oxidizing species). In most cases, the oxidized states are more mobile than the reduced species. Oxyanionic elements like vanadium and molybdenum are more soluble at high pH. Vanadium and molybdenum exists predominantly in the form of vanadate (VO_4^{3-}) and molybdate (MoO_4^{2-}) in alkaline waste (Cruywagen, 2000; Fillela *et al.*, 2002). The mechanism of leaching of these elements in high pH waste isn't clear-cut. Previous authors have shown that neither solubility control nor adsorption to iron and aluminium oxides can fully explain vanadium and molybdenum leaching at pH 10 - 14, the "natural" pH values of fresh alkaline inorganic waste (Cornelis *et al.*, 2005).

Vanadium is highly involatile even under high temperature processes (> 1100 °C) such as that which yield waste such as steel slag. Vanadium exist in the +4 or +5 oxidation state in the form of vanadate VO_4^{3-} in high pH waste and is highly mobile at alkaline pH (Moreno *et al.*, 2005). The geochemical behaviour of vanadium is slightly affected by redox transformation (Cornelis, 2008). The release of vanadium from alkaline waste is controlled by a number of mechanisms. One of such mechanisms is surface adsorption to minerals. Vanadate has been shown to adsorb to the surface of the mineral hydrotalcite ($Mg_6[Al(OH)_6]_2\text{-}CO_3 .4H_2O$) which has a positive charge that gets attracted to the negative surface of the alkaline waste (Ulibarri *et al.*, 1994). However in some alkaline waste such as cementitous waste, this mechanism is less effective (Lothenbach and Winnifeld, 2006).

Another control mechanism is the precipitation of calcium vanadates, this species plays a key role in controlling the solubility of vanadium under high pH conditions (Cornelis *et al.*, 2008). Vanadium is easily leachable from any high pH waste, even those with low Ca content (Cornelis *et al.*, 2008). The effect of adding more calcium to the high pH system will reduce the mobility of vanadium because Ca-vanadates precipitation will be encouraged, this is likely to continue until all the available soluble Ca has been used up and the leachate becomes undersaturated with respect to Ca-vanadate (Cornelis *et al.*, 2008). As a result, at pH > 12 the amount of

V lowers in the leachates. The mobility of vanadium can also be controlled through solid solution formation with ettringite. This mineral offers preferential uptake of vanadate regardless of its large ionic radius (Kumarathasan *et al*., 1990).

Molybdenum exists in the stable hexavalent state in the form of molybdate in most alkaline waste, although in some cases (e.g. steel slag) they can sometimes be found to exist in its elemental state (Belevi and Moench, 2000; Paoletti, 2002). The rate and extent of leaching of molybdenum increases at a fairly constant rate at pH range 7 – 12, however at pH 11.5, a slight decrease in pH is usually observed due to the incorporation of molybdate into the ettringite structure (Kumarathasan *et al*., 1990). Molybdenum (in the form of MoO_4^{2-}) has a larger size when compared to other oxyanions and this significantly reduces its uptake by ettringite. Alkaline waste with low sulphate content e.g. cement usually exhibit formation of monosulphate or hydrocalumite ($Ca_4[Al(OH)_6]_2(OH)_2 \cdot 6H_2O$ instead of ettringite (Gougar *et al*., 1996). These phases are stable at high pH and also reduce the mobility of molybdenum in low sulphur waste compared to alkaline waste with high sulphur content (Chrysochoou and Dermatas, 2006). The leaching behaviour of molybdenum in hyperalkaline leachates is also controlled via calcium metallate ($CaMoO_4$) precipitation and independent of the concentration of Ca in the hyperalkaline leachates due to the high solubility of Ca-molybdates (Querol *et al*., 2001).

Another possible mechanism that controls the leaching of molybdenum in cement is via solid solution formation with monosulphate (Kindness *et al*., 1994 a). This is possible due to the lower solubility product of molybdate compared to other oxyanions (selenite, sulphate). Calcite does not act as a good sink for molybdate because the latter is not trigonal, so it is only slightly retained by calcite (Goldberg *et al.*, 1996). Elevated sulphate concentrations also affect the incorporation of trace oxyanions regardless of its tetragonal coordination (Cowan *et al.*, 1990).

Iron and aluminium oxides are abundant in alkaline waste (Piantone *et al.*, 2004). These oxides have a high surface area which promotes adsorption of molybdate to its surface as a control mechanism to reduce leaching of molybdenum from alkaline waste (Piantone *et al.*, 2004). At low pH (<5), molybdenum sorbs to Fe and Al oxyhydroxides and this lowers its solubility in acidic waste (Ward *et al.*, 2009). The mobility of molybdenum can also be controlled via surface adsorption to portlandite or hydrotalcite (Cornelis *et al.*, 2006; Misra and Perrotta, 1992). Molybdate does not have an affinity for gypsum, as a result they undergo increased leaching when gypsum is formed instead of ettringite analogue phases during weathering (Cornelis *et al.*, 2008).

2.7 Chapter summary

This review has highlighted the increasing global production of alkaline waste particularly steel slag and lime waste, and their associated management challenges. These waste are not well characterised in terms of leaching behaviour in environmental settings. Also, highly alkaline leachates are damaging to aquatic environment, and are typically enriched with vanadium, molybdenum, and possibly nickel. The presence of elements of interest and opportunities for carbon offsetting are key management targets of the future and are hoped to be addressed in this work.

3

Methodology

This chapter describes the generic methods used in this research. A detailed description of the experimental methods designed specifically for the leaching tests carried out in this research have been provided in the related chapters (Chapters 5 and 6). Details of the procedure used for batch leaching of basic oxygen furnace (BOF) slag have been described in Chapter 5. Details of the methodology used for the column experiments investigating the weathering of steel slag using municipal compost have been highlighted in Chapter 6.

Here in this chapter, a detailed description of the reagents used in this work has been provided, including their associated suppliers and purity. Also, the theory and procedures of the analytical techniques employed in this study have been fully described. Details of field sampling and sample analysis (both field and laboratory) have been covered in this chapter.

3.1 Reagents

A list of all the reagents used during the course of this work has been presented in Table 3.1. High purity chemicals have been used, where possible.

Table 3.1: List of reagents used in this work including its supplier and associated purity

Reagent	Supplier	Purity
Sulphuric acid (H_2SO_4)	Fisher Scientific, UK	Analytical grade (96 %)
Nitric acid (HNO_3)	ROMIL, UK	67 – 69 %
Buffer solutions (pH 4, 7, 10)	Fluka analytical	N/A
Conductivity standard solution (Hanna 1413 µS/cm)	Fisher Scientific. UK	N/A
Phenolphthalein indicator	Fisher Scientific (Acros Organics), UK	98.5 %
Bromocresol green – methyl red indicator	Sigma Aldrich, UK	N/A
1000 ± 2 ppm element reference solutions (Al, Na, Fe, V, Ni, Mo, Ba, Li, As, Cr, Sb, Se, Sr, Ca, K, Mg, Si, S, Ti, Ga, In, Bi) made up in 0.5 M HNO_3 matrix.	ROMIL, UK	N/A
Hydrochloric acid	Fisher Scientific, UK	35 – 38 %
Ultrahigh quality (UHQ) water		18.2 MΩ
Sodium hydroxide pellets	Fisher Scientific, UK	98.3 %
Sodium chloride salt (NaCl)	Sigma Aldrich, UK	≥99.0 %
Sodium sulphate Na_2SO_4	Sigma Aldrich, UK	≥99.0 %
Certified reference material Estuarian sediment solution (matrix 4 % HNO_3)	High – purity standards	N/A
Blast furnace slag ECRM 802-1	Institut de Recherches de la Sidérurgie (IRSID) France	N/A
Calcein	Sigma Aldrich, UK	≥93 %

3.2 Instrumentation

This section has been split into two categories; the first group includes techniques that were used routinely for measurement purposes. They include inductively coupled plasma optical emission Spectrometry (ICP-OES), inductively coupled plasma mass spectrometry (ICP-MS) and ion chromatography (IC).

The other group consists of techniques that have been used primarily for sample characterization purposes. They include x-ray diffraction (XRD), scanning electron microscopy (SEM), thermogravimetric analysis (TGA) and surface area analysis.

3.2.1 THEORY - Measurement techniques

3.2.1.1 Inductively Coupled Plasma Optical Emission Spectrometry (ICP-OES)

ICP-OES is a key analytical technique for the determination of trace elements in various sample matrices e.g. agricultural, food, biological, geological, environmental, water samples (Boss and Freeden, 2004; Hou and Jones, 2000). In recent years, there has been a rapid development of ICP-OES in comparison to other techniques such as flame atomic absorption spectrometry (FAAS) and graphite furnace atomic absorption spectrometry (GFAAS), mainly due to some of its advantages such as simultaneous multielement capability, excellent detection limits, wide linear dynamic range, low background emission and low chemical interference (Hou and Jones, 2000).

3.2.1.1.1 Principle of operation: ICP-OES

This technique depends upon the spontaneous emission of photons from ions and atoms that have been excited in a radiofrequency (RF) discharge (Hou and Jones, 2000). ICP-OES can be used for the analysis of liquid, gaseous and solid samples.

The former two can be introduced directly into the instrument while the latter require some form of sample preparation usually in form of acid digestion in order to extract analytes into solution (Hou and Jones, 2000). The sample solution is converted to an aerosol and travels into the core of the plasma which is maintained at a temperature of about 10000 K, this high temperature causes the aerosol to vaporise rapidly. Elements are released as free atoms in the gaseous state. These atoms gets excited and promoted to higher energy state as a result of multiple collisions occurring within the plasma. Sufficient energy is often available to convert the atoms to ions and subsequently promote the ions to excited states. Both the atomic and ionic excited state species may then relax to the ground state through the emission of a photon. These photons have characteristic energies that are determined by the quantized energy level structure for the atoms or ions. Thus the wavelength of the photons can be used to identify the elements from which they originated. The total number of photons is directly proportional to the concentration of the originating element in the sample (Hou and Jones, 2000). The schematic of a typical ICP-OES system is shown in Figure 3.1.

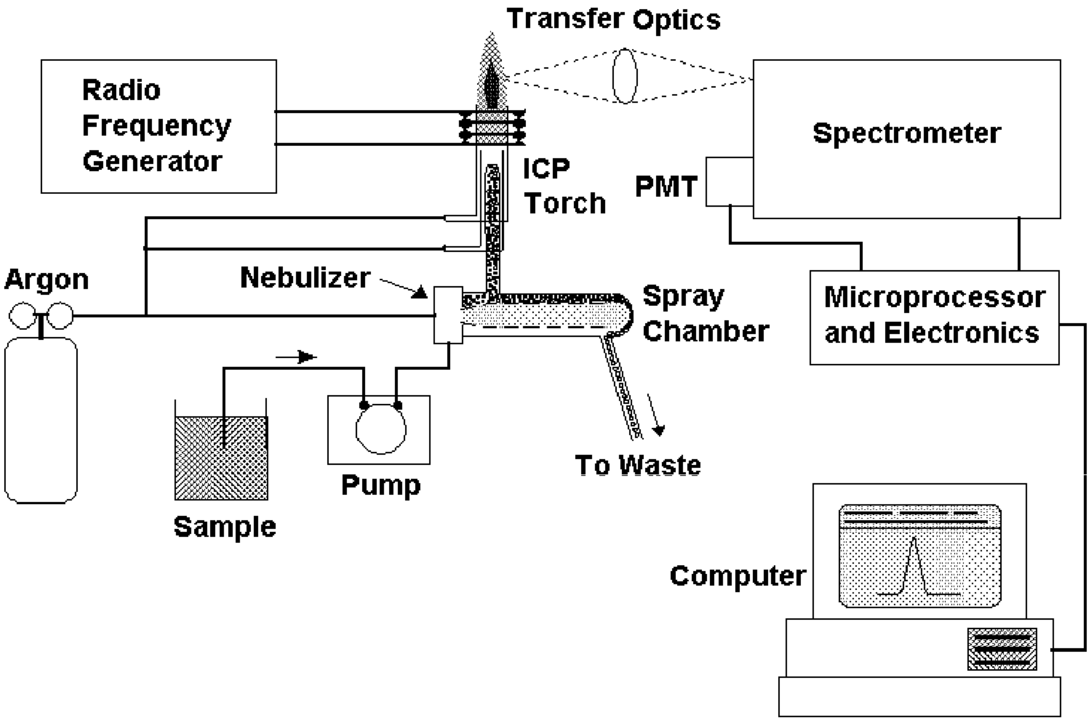

Figure 3.1: Schematic representation of an ICP-OES set-up (Boss and Fredeen, 2004)

3.2.1.1.2 Torch configuration – ICP-OES

Emissions from the ICP can be viewed in a radial (side-on), axial (end-on) and dual configuration (Boss and Freeden, 2004; Hou and Jones, 2000). A dual viewing combines axial and radial configuration. Only the former two viewing modes have been used in this work, as a result discussion will be limited to them. The choice of viewing mode depends mainly on the concentration of the analyte of interest in the sample, and each of them has its merits and demerits (Hou and Jones, 2000). The radial view is the traditional viewing mode for ICP-OES. With radial viewing, the plasma is operated in a vertical orientation, and the analytical zone is observed from the side of the plasma. Radial viewing is particularly useful when analytes concentrations are up to ppm levels, therefore giving it a lower sensitivity. This operation mode doesn't suffer the effect of potential spectral and background interferences. With the axial view, the plasma is rotated to a horizontal position and the analytical zone of the ICP is observed from the end of the plasma. The axial view provides better limits of detection (LODs) than radial view. This may be due to the longer viewing path available down the axis of the plasma. Thus, a better sensitivity and a 5- to 10- fold improvement in the LOD can be achieved. The disadvantages of the axial view include the increased potential for spectral interference and matrix-induced interferences (Boss and Freeden, 2004; Hou and Jones, 2000).

3.2.1.2 Inductively Coupled Plasma Mass Spectrometry (ICP-MS)

An Inductively coupled plasma mass spectrometry (ICP-MS) system comprises four main parts, namely; the sample introduction system, plasma region, interface and mass spectrometer region (see Figure 3.2).

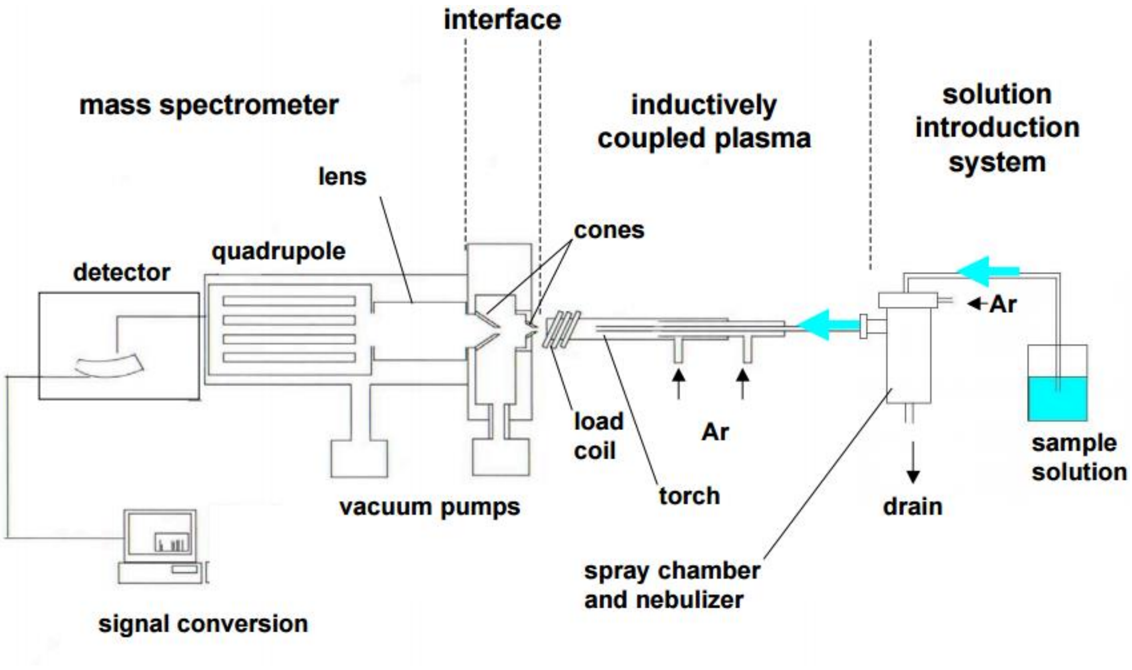

Figure 3.2: Schematic representation of a quadrupole ICP – MS set up (Source: Wolf, 2005)

The high temperature ICP source is responsible for conversion of the atoms of the elements in the sample to ions (Wolf, 2005). These ions are then transmitted to the mass spectrometer via the interface cones. At the interface region, the ions, travelling in the presence of argon sample stream at atmospheric pressure (1 – 2 torr), gets transferred to the mass spectrometer which is maintained at low pressure (10^{-5} torr). This is achieved through the combination of the sampler and skimmer cones which creates an intermediate vacuum region. The primary function of the cones is to sample the center portion of the ion beam coming from the ICP torch. Also, due to the small diameters of the orifices in the sampler and skimmer cones, ICP-MS has some limitations as to the amount of total dissolved solids in the samples (ideally less than 0.2 % total dissolved solids is recommended). A shadow stop blocks the photons coming from the ICP torch so as to prevent the intense light from reaching the mass spectrometer. The ions from the ICP source are then focused by the electrostatic lenses in the system. Once the ions enter the mass spectrometer, they are separated by their mass-to-charge ratio (Wolf, 2005). In this work, a quadrupole mass spectrometer instrument was used because they are reasonably priced and also provide good resolution (up to 1 atomic mass unit). Other types of mass spectrometer that could be interfaced to the ICP include the magnetic double sector, time of flight, ion cyclotron resonance analyzers, these are however expensive and mostly used for specialized applications such as isotope analysis which were not required in this work. Once the ions have been separated by their mass-to-charge ratio, they must then be detected or counted by a suitable detector such as a discrete dynode detector which operates either in a pulse – counting or analog mode (Wolf, 2005).

Internal standards are widely used in ICP-MS analyses to correct for variations in the instrument response as the analysis proceeds (drift) and to calculate the analyte concentrations of the samples. Accurate correction for non-spectral interferences is also possible using an internal standard with mass number close to that of the analyte element(s). The use of an internal standard with mass number close to that of the analyte improves the precision of data obtained from ICP-MS. When a number of elements over a considerable mass range are to be determined, several internal standards have to be used.

Some of the advantages ICPMS offer over other techniques such as graphite furnace atomic absorption spectroscopy (GFAAS) include its superior detection capability, higher sample throughput, and the ability to carry out isotopic analysis (Wolf, 2005).

3.2.1.2.1 Microwave assisted acid digestion of samples

Microwave digestion is used to prepare samples of all types (rocks, plant, soil, food, pharmaceuticals, plastics, metals) for elemental analysis by ICP-OES, ICP-MS, or AAS, which require the sample to be in the form of a solution in order to introduce it into the analyzer. The use of a microwave allows for a faster and more reliable quantitative measurement because it allows for analysis of a more representative sample unlike techniques like laser ablation which is less efficient for measuring representative composition. Furthermore, microwave digestion unlike the traditional open hotplate digestion, offers other advantages such as simultaneous heating of multiple samples thereby saving time, higher working temperatures, lower acid consumption, greater extraction efficiency and lower risk of contamination of samples.

Acid digestion is employed to break down the sample matrix leaving the analytes of interest in solution and ready for analysis. Microwave digestion systems rapidly break down a wide variety of sample matrices leaving behind a clear solution containing the elements of interest (CEM, 2011).

3.2.1.3 Ion chromatography

Ion chromatography (otherwise known as ion exchange chromatography) is an analytical technique used for the separation of ions and polar molecules based on their affinity to the ion exchanger. Ion-exchange chromatography retains analyte molecules on the column based on ionic interactions. The surface of the stationary phase displays ionic functional groups (R-X) that interact with analyte ions of opposite charge. This type of chromatography is further subdivided into cation exchange chromatography and anion-exchange chromatography. The ionic compound consisting of the cationic species M+ and the anionic species B- can be retained by the stationary phase.

Cation exchange chromatography retains positively charged cations because the stationary phase displays a negatively charged functional group:

$$R - X^-C^+ + M^+B^- \leftrightarrow R - X^-M^+ + C^+ + B^- \qquad (3.1)$$

Anion exchange chromatography retains anions using positively charged functional group:

$$R - X^+A^- + M^+B^- \leftrightarrow R - X^+B^- + M^+ + A^- \qquad (3.2)$$

The ion strength of either C+ or A- in the mobile phase can be adjusted to shift the equilibrium position, thus retention time (Haddad and Jackson, 1990).

3.2.2 THEORY - Characterization techniques

3.2.2.1 X-ray Diffraction (XRD)

X-ray diffraction is a versatile, non-destructive technique primarily used for phase identification of a crystalline material and can provide information on unit cell dimensions (Xiao-Ming *et al.*, 2013). X-ray diffraction is based on constructive interference of monochromatic X-rays and a crystalline sample. These X-rays are generated by a cathode ray tube, filtered to produce monochromatic radiation, collimated to concentrate, and directed towards the sample. The interaction of the incident rays with the sample produces constructive interference (and a diffracted ray) when conditions satisfy Bragg's law ($n\lambda=2d\sin\theta$). This law relates the wavelength of electromagnetic radiation to the diffraction angle and the lattice spacing in a crystalline sample. These diffracted X-rays are then detected, processed and counted. By scanning the sample through a range of 2θ angles, all possible diffraction directions of the lattice should be attained due to the random orientation of the powdered material. Conversion of the diffraction peaks to d-spacings allows identification of the mineral because each mineral has a set of unique d-spacings. Typically, this is achieved by comparison of d-spacings with standard reference patterns (Xiao-Ming *et al.*, 2013).

3.2.2.2 Scanning electron microscopy (SEM)

Scanning electron microscopy (SEM) is a technique for high-resolution imaging of surfaces (Amelinckx *et al.*, 2008). The SEM uses electrons for imaging much as a light microscope uses visible light. The advantages of SEM over light microscopy include much higher magnification (>100,000X) and greater depth of field up to 100 times that of light microscopy. Qualitative and quantitative chemical analysis information is also obtained using an energy dispersive x-ray spectrometer (EDX) with the SEM.

The SEM generates a beam of incident electrons in an electron column above the sample chamber. The electrons are produced by a thermal emission source, such as a heated tungsten filament, or by a field emission cathode. The energy of the incident electrons can be as low as 100 eV or as high as 30 keV depending on the evaluation objectives. The electrons are focused into a small beam by a series of electromagnetic lenses in the SEM column. Scanning coils near the end of the column direct and position the focused beam onto the sample surface. The electron beam is scanned in a raster pattern over the surface for imaging. The beam can also be focused at a single point or scanned along a line for x-ray analysis. The beam can be focused to a final probe diameter as small as about 10 Å (Amelinckx *et al.*, 2008).

The incident electrons cause electrons to be emitted from the sample due to elastic and inelastic scattering events within the sample's surface and near-surface material. High-energy electrons that are ejected by an elastic collision of an incident electron, typically with a sample atom's nucleus, are referred to as backscattered electrons. The energy of backscattered electrons will be comparable to that of the incident electrons. Emitted lower-energy electrons resulting from inelastic scattering are called secondary electrons. Secondary electrons can be formed by collisions with the nucleus where substantial energy loss occurs or by the ejection of loosely bound electrons from the sample atoms. The energy of secondary electrons is typically 50 eV or less. Detectors collect these backscattered and secondary electrons and convert them into a signal displayed in form of an SEM image.

3.2.2.3 Thermogravimetric analysis (TGA)

Thermogravimetric analysis (TGA) measures the mass changes of a sample over a range of temperatures. This change can be used to determine the composition of a material or its thermal stability, up to 1000 °C. Usually, a sample loses weight as it is heated up due to decomposition, reduction, or evaporation. A sample could also gain weight due to oxidation or absorption. While in operation, the TGA instrument tracks the change in weight of the sample via a microgram balance. Temperature is monitored via a thermocouple. The TGA can also track change in weight as a function of time. The output curve produced from a TGA analysis can therefore be a plot of weight percent or time vs temperature. If the material in question is stoichiometric, the molar weight of the component being burned off can be ascertained based on the weight percent lost and the total molar weight of the material (PerkinElmer Inc., 2010).

3.2.2.4 Surface area and porosity analysis

This analytical technique uses physical adsorption and capillary condensation principles to obtain information about the surface area and porosity of a solid material (Micromeritics, 2007). In this technique, the sample is placed in an empty sample tube, cooled to cryogenic temperature and then exposed to the analysis gas at a series of precisely controlled pressures. With each incremental pressure increase, the number of gas molecules adsorbed on the surface increases. The equilibrated pressure (P) is compared to the saturation pressure (P_0) and their relative pressure ratio (P/P_0) is recorded along with the quantity of gas adsorbed by the sample at each equilibrated pressure (Gregg and Sing, 1967).

As adsorption proceeds, the thickness of the adsorbed film increases. Any micropores in the surface are filled first, then the free surface becomes completely covered, and finally the larger pores are filled by capillary condensation. The process may continue to the point of bulk condensation of the analysis gas. Then, the desorption process may begin in which pressure systematically is reduced resulting in liberation of the adsorbed molecules. As with the adsorption process, the changing quantity of gas on the solid surface at each decreasing equilibrium pressure is quantified. These two sets of data describe the the adsorption and desorption isotherms. Analysis of the shape of the isotherm yields information about the surface and internal pore characteristics of the material (Micromeritics, 2007).

3.3 Procedures and instrument settings

3.3.1 ICPOES and ICPMS

3.3.1.1 Condition for ICPOES

The analyses (major elements) were carried out on a Perkin Elmer Optima 5300DV ICP – OES instrument under the preset operating conditions shown in Table 3.2.

Table 3.2: Typical operating conditions of ICP-OES instrument used in this work

Parameter	**Condition**
Plasma gas flow rate	15 L/min
Auxillary gas flow rate	0.2 L/min
Nebulizer gas flow rate	0.8 L/min
RF power	1300 W
Pump flow rate	1.5 mL/min
Purge gas flow	Normal (with the exception of sulphur – set as high flow)
Autosampler wash rate	1.5 mL/min
Autosampler wash time	30 seconds
Sample flow rate	1.5 mL/min
Replicates	3
Nebulizer type	Concentric

The viewing modes used for the various elements in this work have been listed in Table 3.3 below.

Table 3.3: Selected atomic emission lines for various elements and preferred torch configuration used in this work

Torch configuration	**Elements (Chosen analytical line in nm)**
Axial view	Aluminium (396.153), sodium (598.592), iron (238.204), vanadium (310.230), nickel (231.604), molybdenum (202.031) barium (493.408), lithium (670.784), arsenic (188.979), chromium (205.560), antimony (206.836), selenium (196.026)
Radial view	Strontium (407.771), calcium (317.933), potassium (766.490), magnesium (280.271), silicon (251.611),
Axial or radial view	Sulphur (180.669)

The choice of the atomic emission lines for the output data, as shown in Table 3.2 was based on the Perkin Elmer recommendations for the Optima 5300 DV spectrometer to prevent spectral interference. Although only one analytical line was chosen as being representative of the sample measurements, the reliability was tested by comparing its relative standard deviation (RSD %) with that of the other analytical lines for each element. The choice was deemed reliable as similar RSD % values were obtained for the analytical lines (Nolte, 2003).

Each analytical line was measured three times for both the samples and blank calibration solutions (2 % HNO_3) and the mean of these measurements presented in the output data. The standard deviation (s) and relative standard deviation (RSD) was calculated by the internal software (Winlab).

The RSD is calculated using the formulae:

$$R.S.D = \frac{s}{x} \qquad (3.3)$$

Where s is the sample standard deviation and x the mean of the measurements, multiplying by 100 % gives the RSD in percentage form. The precision of the instrument is determined by the relative RSD of the measurements and should optimally be about 1 % but not more than 3 % (Nolte, 2003).

3.3.1.2 Condition for ICPMS

All trace element analyses in this work were carried out using an Elan DRCII quadrupole ICP-MS with a CETAC ASX-510 autosampler instrument under the preset operating conditions shown in Table 3.4.

Table 3.4: Typical operating conditions of ICP-MS instrument used in this work

Parameter	**Condition**
Torch box temperature	38 °C
Vacuum pressure	10^{-6} Torr
Nebulizer gas flow	0.9 L/min
ICP RF power	1125 W
Lens voltage	6.2 V
Analog stage voltage	-1875 V
Pulse stage voltage	1050 V

3.3.1.3 Calibration methods and Certified reference materials

In order to establish the reliability of both ICP instruments, reference standards of selected elements were used to prepare solutions used for calibration for both the ICP-OES and ICP-MS prior to analysis of samples. In addition, a blank solution (2 % HNO_3 in UHQ water) was analysed after every 10 runs to check the precision of the instrument and the limit of detection (LOD), the LOD is calculated thus:

$$LOD = 3 * s \qquad (3.4)$$

Where s is the average standard deviation of the blank measurements.

Furthermore, certified reference materials (CRMs) were used to assess the quality and traceability of data, and also to validate analytical measurement methods. The accuracy of the output data obtained from the analysis of steel slag samples on the ICP was checked by the analysis of blast furnace slag ECRM 802-1 (IRSID France) while the data accuracy of the compost samples was assessed by the analysis of CRM estuarian sediment solution made in 4 % HNO_3 (see Chapter 5). Also, the reliability of the data obtained from the ICP-OES and ICP-MS was checked by analyzing a leachate sample (picked at random) and CRM on both instruments.

Table 3.5 provides a comparison between measured and real values obtained for selected analytes on leachate samples and CRM using ICP-OES and ICP-MS. All of the analytes passed the quality guidelines, as there was a good agreement (±3 %) between the measured and the real values of the analytes in the CRM.

Table 3.5: Measured values for selected analytes in chosen leachate sample and CRM using ICP-OES and ICP-MS

Element	**Leachate (ICP-OES) / ppb**	**Leachate (ICP-MS) / ppb**	**CRM estuarine sediment solution (measured by ICP-OES) / ppm**	**CRM estuarine sediment solution (certified value) / ppm**
Arsenic (As)	20.02 ± 0.08	14.73 ± 0.12	0.12 ± 0.01	0.09 ± 0.01
Nickel (Ni)	20.41 ± 0.04	22.61 ± 0.21	0.31 ± 0.05	0.34 ± 0.04
Chromium (Cr)	22.5 ± 1.2	21.1 ± 0.8	0.75 ± 0.11	0.83 ± 0.12
Lithium (Li)	60.0 ± 1.3	56.4 ± 0.4	-	-
Vanadium (V)	21.5 ± 1.3	22.4 ± 1.8	1.03 ± 0.02	1.02 ± 0.01

Finally, for ICPMS only, a solution comprising a mix of 10 ppb gallium, 10 ppb indium and 10 ppb bismuth was made up in 2 % HNO_3 in a 1 L flask. This was used as the internal standard for analyses so as to eliminate interferences.

3.3.1.4 Microwave digestion methods

Prior to microwave digestion, all samples were oven dried at 105 °C overnight. Details of the methods employed for the digestion of steel slag samples, municipal compost and sediments are provided in Table 3.6.

Table 3.6: Methods used for microwave assisted acid digestion of samples

Sample	Method used	Digestion procedure	Heating program
Steel slag	CEM method 5OS – 22	0.5 g of steel slag sample was added to a digestion vessel followed by the addition of 3 mL conc. nitric acid, 2 mL conc. hydrochloric acid, 5 mL conc. hydrofluoric acid and heated according to heating program (1), the vessel was allowed to cool followed by the addition of 30 mL of 4 % boric acid and heated according to heating program (2).	(1) Maximum power - 1200 W, Percent power – 100, Heating time – 25 minutes, Pressure – 180 psi, Temperature – 210 °C, Hold time – 15 minutes. (2) Max. Power – 1200 W, percent power – 100, heating time – 10 minutes, pressure – 100 psi, temperature – 170 °C, hold time – 5 minutes.
Municipal Compost	CEM method XprEN – 8	2 g of compost was added to a digestion vessel followed by the addition of 12 mL aqua regia (3:1 hydrochloric : nitric acid) and heated according to heating program (3)	(3) Maximum power – 1200 W, percent power – 100, Ramp time – 10 minutes, pressure – low, temperature – 160 °C, hold time – 15 minutes.
Sediment (secondary precipitate)	CEM method 5OS – 15	0.5 g of sediment sample was added to a digestion vessel followed by the addition of 10 mL deionised water, 5 mL conc. nitric acid, 1 mL conc. hydrochloric acid and heated in accordance with heating program (4), the vessel was allowed to cool followed by the addition of 30 mL of 4 % boric acid and heated according to heating program (5).	(4) Maximum power - 1200 W, Percent power – 100, Heating time – 30 minutes, Pressure – 175 psi, Temperature – 210 °C, Hold time – 20 minutes. (5) Max. Power – 1200 W, percent power – 100, heating time – 10 minutes, pressure – 100 psi, temperature – 210 °C, hold time – 5 minutes.

3.3.2 IC

Chloride and sulphate analysis of selected water samples were carried out using a Dionex ICS 2000 instrument with suppressed conductivity detection and gradient elution of 15 mM NaOH solution over 10 minutes run time.

Chloride and sulphate salts (see Table 3.1) were used to prepare standards for calibration of the ion chromatography system prior to analysis of samples. For this purpose, the appropriate mass of the salts were weighed out separately and made up in 100 ml flasks using deionised water to produce 1, 2, 3, 4, 5 ppm solutions. All real samples were diluted 500 times so that measured concentrations were within the range of the prepared calibration standards and analysed using the conditions listed in table 3.7 below.

Table 3.7: Settings for the ion chromatography instrument used in this work

Parameter	**Condition**
Pump flow rate	0.38 µl/min
Suppressor current	15 mA anion, 15 µA cation
Detector type	DS6 heated conductivity cell
Column	Dionex IonPac™ AS11-HC RFIC™ 2 X 250 mm
Guard column	Dionex IonPac™ AG11-HC RFIC™ 2 X 50 mm

3.3.3 XRD

In all cases, prior to XRD analysis, the samples were sieved to obtain the 50 µm size fraction. The samples were then oven dried at 105 °C for 3 hours in order to get rid of moisture. Mineral phases in the slag samples and secondary deposits were identified using a PANalytical Empyrean X-ray diffraction instrument with a Cuα radiation source and a PIXcel^{1D} detector. For data acquisition, the Cu anode was supplied with 40 kV and a current of 40 mA to generate Cu K-alpha1 (lambda = 1.54060 angstroms). The X-ray patterns were acquired in the 2θ (20 ° – 80 °) interval at a step size of 0.026 ° under fixed slit condition. The peaks were indexed and matched using Hiscore plus version 3.0e and PDF-2 database (ICDD, 2014).

3.3.4 SEM

Prior to SEM analyses, the steel slag and calcite precipitate samples were air dried in order to remove water. This was done because the presence of water in the vacuum would affect the formation of electrons, hence the quality of the SEM image. No further sample preparation was required for the samples. Morphological analyses of the samples were carried out with a Carl Zeiss EVO60 scanning electron microscopy (SEM) instrument (resolution 2 nm, maximum accelerating voltage 30 KV). Preliminary elemental analysis of the samples was achieved using an Oxford INCA 350 energy dispersive X-ray analysis (EDX) instrument (with an ultra-thin polymer window detector).

3.3.5 TGA

For this work, a Mettler Toledo TGA/DSC1 instrument coupled with a Mettler Star software version 12.0 was used. No gas controller was required since only nitrogen gas was required for thermal decomposition and not a mixture of gases. The instrument required 30 mg of powdered sample, which was weighed in a 70 µl alumina crucible and placed onto a frequently calibrated microbalance (10^{-3} mg sensitivity). The atmosphere inside the furnace was water – cooled in order to have proper control of the heating temperature. The sample was heated from 50 °C to 950 °C at a heating rate of 30 °C/minute and a nitrogen flow rate of 100 ml/min.

The method used was calibrated by running a blank (usually an empty crucible), thus correcting for drift.

3.3.6 BET

Surface area and porosity of the samples were determined by the Brunauer Emmett Teller (BET) and the Barrett Joyner Halenda (BJH) methods respectively using a Micrometrics ASAP 2000 (USA) adsorption instrument. Prior to surface area analysis of the steel slag samples, three empty test tubes (with lids) were placed in the flowing-gas degassing unit and dried with flowing nitrogen for 1 hour. One test tube was used for the analysis and the other two for calibrating the P_0 (saturation pressure). Approximately 0.1 g of the sample was introduced into the empty analysis test tube using a spatula and dried further for an additional 1 hour. Afterwards, the Dewar was filled with liquid nitrogen and placed on a platform within the instrument then the three test tubes were lowered into the liquid nitrogen followed by sample analysis.

3.4 Sample collection and storage

3.4.1 Water, Steel slag and sediments collection

During the course of this work, triplicate water samples were collected in 50 ml acid-cleaned polypropylene bottles at each sampling point (they were filled to the brim allowing no headspace), one of which was acidified (for total cations and trace element analysis), one of which was filtered (using a 0.45 µm Millex non pyrogenic filter) prior to acidification (dissolved cation and trace element analysis) and the other left untreated (for anion analysis). Acidification was achieved by adding 0.3 ml of ultrapure conc. nitric acid to the individual samples. Water samples were preserved at 4 °C so as to stabilize analyte concentrations for the required period of time hence preventing deterioration of the samples. These water samples were analyzed within 3 days of sampling.

Steel slag samples were collected from the Yarborough landfill, Scunthorpe and slag disposal sites at Consett County Durham (see Chapter 4 for details of sampling locations). Since the steel slag were co-deposited with other waste (mostly generated on site), extra care was taken through visual inspection to ensure that only steel slag were collected at the selected sampling locations. At these sampling locations, the steel slags were dug up using a spade. Approximately 3 kg of steel slag were collected from each sampling location and placed in sealed polyethylene bags. The average diameter of the sampled steel slag was 15 mm.

At most of the study sites, the interaction of atmospheric CO_2 with the alkaline material led to the formation of secondary precipitates (predominantly calcite) on the surface of the steel slag. These sediments (secondary deposits) forming at the sites were sampled and characterised in this work. Care was taken to avoid contamination of the sediments by vegetation growing alongside some of the deposits. Sediment samples were placed in sealed polyethylene bags and stored at 4 °C.

3.4.1.1 Physico-chemical parameters determination

3.4.1.1.1 pH, Eh and conductivity

Field measurements of major physical and chemical parameters of the water samples including pH, water temperature, electrical conductivity and Eh (redox potential) were recorded using a Myron L Ultrameter properly calibrated with pH

4, 7, and 10 buffer solutions and a 1413 µS/cm conductivity standard on each sample day.

Laboratory measurement of solution pH and redox potential was achieved using a frequently calibrated Fisherbrand hydrus 500 pH meter. The repeatability was < ± 0.02. The conductivity of solutions was determined in the laboratory using a Jenway 4510 conductivity meter.

3.4.1.1.2 Alkalinity determination

The alkalinity of the water samples was assessed in the field using a two-stage titration against 0.8 M H_2SO_4 with phenolphthalein (to pH 8.3) and bromocresol green-methyl red indicators (to pH 4.6) to facilitate calculation of the constituents of sample alkalinity (i.e. hydroxyl, carbonate and bicarbonate alkalinity) (USEPA, 2012).

Alkalinity is usually measured using sulfuric acid with a digital titrator. Sulfuric acid is added to the water sample in measured amounts until the three main forms of alkalinity (bicarbonate, carbonate, and hydroxide) are converted to carbonic acid. At pH 10, hydroxide (if present) reacts to form water (see Eqn. 3.5). At pH 8.3, carbonate is converted to bicarbonate (Eqn. 3.6). At pH 4.5, it is certain that all carbonate and bicarbonate are converted to carbonic acid (Eqn. 3.7). Below this pH, the water is unable to neutralize the sulfuric acid and there is a linear relationship between the amount of sulfuric acid added to the sample and the change in the pH of the sample. So, additional sulfuric acid is added to the sample to reduce the pH of 4.5 by exactly 0.3 pH units (which corresponds to an exact doubling of the pH) to a pH of 4.2 (USEPA, 2012).

$$H^+ + OH^- \rightarrow H_2O \qquad (3.5) \qquad at\ pH\ 10$$

$$H^+ + CO_3^{2-} \rightarrow HCO_3^- \qquad (3.6) \quad at\ pH\ 8.3$$

$$H^+ + HCO_3^- \rightarrow H_2CO_3 \rightarrow CO_2 + H_2O \qquad (3.7) \quad at\ pH\ 4.5$$

Laboratory alkalinity of solutions was measured using a Mettler Toledo T50 digital titrator in accordance with Hach method 8203 (EPA 310.2 equivalent). A 0.1 M HCl solution was used as the titrant. Usually a 50 ml sample volume was required for this analysis, however in cases where limited volumes of sample was available, the samples were made up to the mark using ultrapure deionised water at a dilution factor of 20.

3.4.1.2 Geochemical modelling of leachates

Geochemical modelling of the leachates helps in determining the saturation indices of minerals within the leachate. Saturation indices (SI) indicate thermodynamic tendency of minerals to dissolve or precipitate. An SI value < 0 would suggest that the solution is undersaturated with respect to that mineral and therefore will tend to dissolve. An SI value = 0 implies that the solution is saturated with respect to the mineral and at apparent equilibrium. An SI value > 0 indicates that the solution is supersaturated with respect to the mineral and will therefore tend to precipitate (Langmuir, 1997).

For this work, aqueous geochemical modeling of the water samples was carried out using the computer program WEB-PHREEQC v.1.5.10 with either the WATEQ4F (Ball and Nordstrom, 1991) or LLNL database to determine the saturation indices of relevant mineral phases on a log scale (Parkhurst and Apello, 1999). The choice of database applied in most cases would depend on the suite of input elements, for example, the LLNL database was used when vanadium was of key interest.

4

Environmental behaviour of alkaline leachates

Globally, due to the high volume of alkaline industrial residues being produced, an understanding of their broader environmental impact, either in disposal sites or during afteruse (e.g. as aggregates for road fill: Chaurand *et al.,* 2007), is much-needed to facilitate their effective management. There have been relatively few studies on the leaching behaviour of caustic waste in environmental settings (see Chapter 2). As such, the fate of potential contaminants of concern, as well as elements of potential value for recovery, is not well understood.

This chapter presents new data on the investigation of leaching behaviour and geochemical processes taking place at a series of disposal sites affected by highly alkaline drainage waters (see Appendix A2). Through integrating aqueous and solid phase analyses of alkaline residues, leachates and secondary mineral deposits at two steel slag and three lime spoil disposal sites, this chapter aims to improve our understanding of the geochemical nature and fate of notable contaminants in highly alkaline settings as well as their key management challenges.

4.1 Investigation of the Yarborough landfill site, Scunthorpe

4.1.1 Yarborough Landfill, Scunthorpe – Site description and methodology

The Yarborough landfill site, Scunthorpe (53°34′52.27″N, 000°35′23.34″W) was selected as the key study location for this work. This site is an active landfill site where slag (from an ironstone quarry in the area) dating as back as far as hundred years ago had been stored. Quarry operations were stopped at the site in 1981 and the site is currently being in-filled with steel making slag with the expectation of finally reclaiming the landfill once it reaches its original surface profile. Presently, a highly alkaline discharge is observed to be seeping out from the base of the heap of the waste. A wetland cell of area of about 1600 m^2 was constructed at this site by Tata steel, Scunthorpe in spring 2012 and is being trialled as a potential remedial tool.

At this site, basic oxygen furnace (BOF) slag were obtained from the landfill while desulphurised skimmed slag and ladle slag were provided by Paul Whitby (Environment manager, Tata steel Scunthorpe), these slags had been collected in January 2012 fresh from the production plant. Also, the desulphurised skimmed slag and ladle slag (see section 2.2.1.1.2 for definitions) were collected from this site and analysed in order to highlight key differences in the mineralogy and chemical composition of various slag types obtained from different manufacturing process. However, BOF slag was identified as precursors to leachates found at this site.

Leachate samples were collected from various locations within this site in accordance with the method described in section 3.4.1. These leachates were collected from several selected spots within the Yarborough site (Figure 4.1).

These locations include a leachate source zone (Sample point Yarborough YB1), a site boundary cut off ditch (a tributary of the Bottesford Beck) intercepting leachate from slag heaps comprising BOS (basic oxygen steelmaking) slag (Sample point Cut off ditch YB2) and a lagoon containing water that had been pumped from a borehole in the area sampled on 24/2/12 (YB3A) and on 25/6/12 (YB3B). The lagoon lies at a shallow depth of 2.5 m below ground and is filled with water pumped from a borehole. This water gets refilled occasionally when the lagoon gets dried up (usually in winter season). The floor of the lagoon is covered in superficial clay deposits and has a vigorous population of common reed (*Phragmites australis*) growing. These were transplanted from native populations receiving alkaline drainage in a site drain.

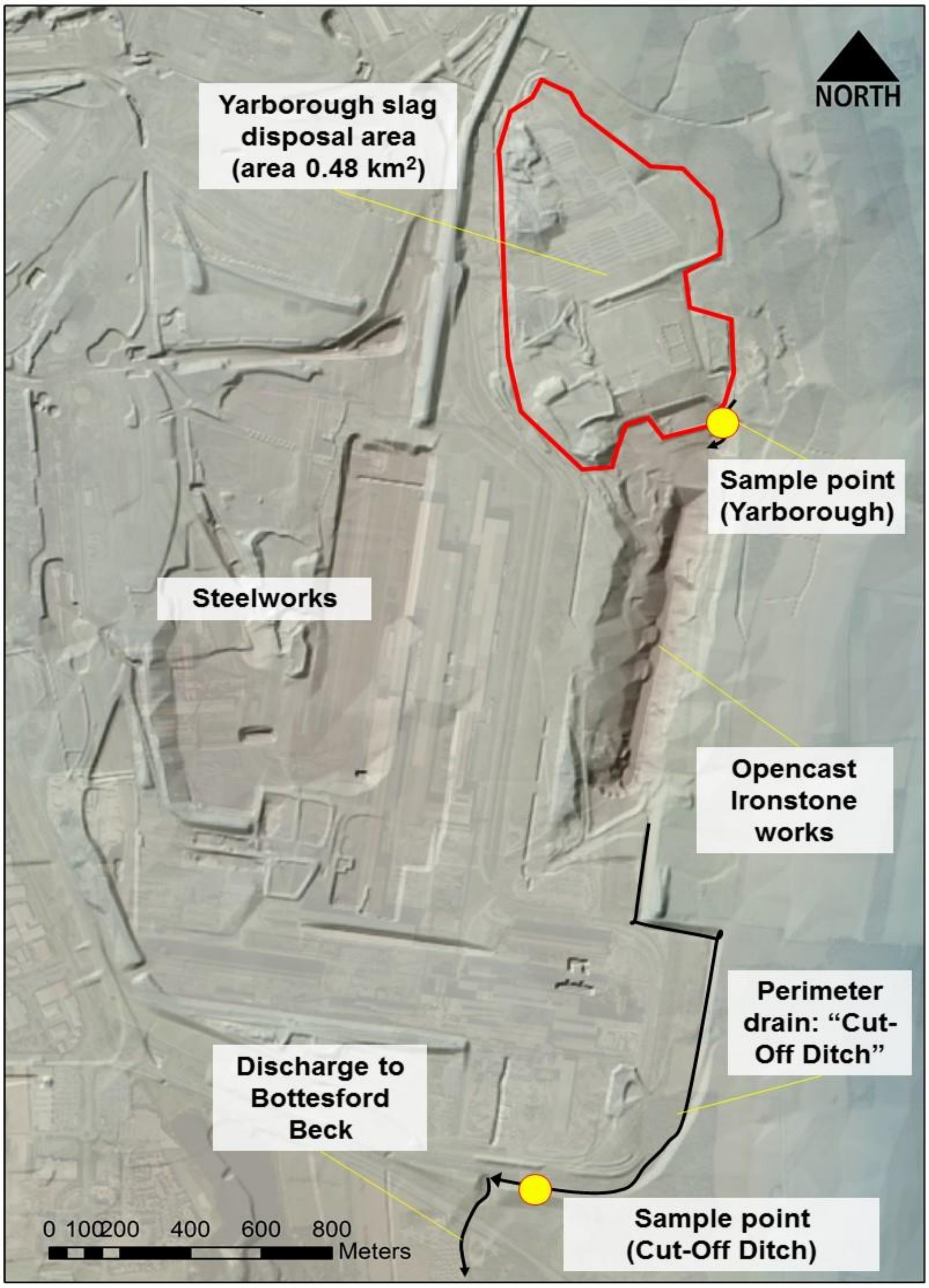

Figure 4.1: Map of Yarborough site highlighting key sampling locations

Steel slag samples (BOF, desulphurised skimmed and ladle slag) and secondary precipitates were collected at this site in accordance with section 3.4.1, air-dried and sieved to < 63 μm. Major element (Ca, Fe, Si, Al, Mg, Mn, S, Na, K, Ti, Sr, Zn) and trace element (As, Ba, Co, Cr, Li, Mo, Ni, Sb, V) composition were determined using ICPOES and ICPMS respectively according to the method described in section 3.3.1, after microwave assisted acid digestion in accordance with methods described in Table 3.6. Mineralogical analysis was determined using X-ray diffraction (section 3.3.3). Morphological analysis and preliminary elemental analysis of BOF slag and secondary precipitate from this site was determined using scanning electron microscopy (SEM) coupled with energy dispersive x-ray spectrometer (EDX) according to the method detailed in section 3.3.4. The characterisation of the decomposition pattern of the secondary precipitate was achieved using a thermogravimetric (TGA) instrument in accordance with the method described in section 3.3.5.

Furthermore, sampled leachates originating from the BOF slag at Yarborough were analysed for pH, conductivity and redox potential using a Myron Ultrameter (see section 3.4.1.1.1). Field alkalinity of the leachates was determined according to the method described in section 3.4.1.1.2. Metal concentrations in the leachates were determined using ICPOES (Ca, Na, K, Mg, Si, Sr) and ICPMS (Ba, Fe, Li, V, As, Sb, Ni, Mo, Pb) according to procedure described in section 3.3.1. Chloride and sulphate content of the leachates were determined using Ion chromatography according to method outlined in section 3.3.2.

4.1.2 Yarborough Landfill, Scunthorpe – Results

The images of the various slag types sampled at this site are presented in Plate 4.1. The key difference in the 3 slag types in terms of physical properties lie in their density and colour. Desulphurised skimmed slag was the least dense of all 3 sample types while BOF slag was darkest in colour. Based on visual inspection, the porosity of the ladle slag was higher than the other two samples.

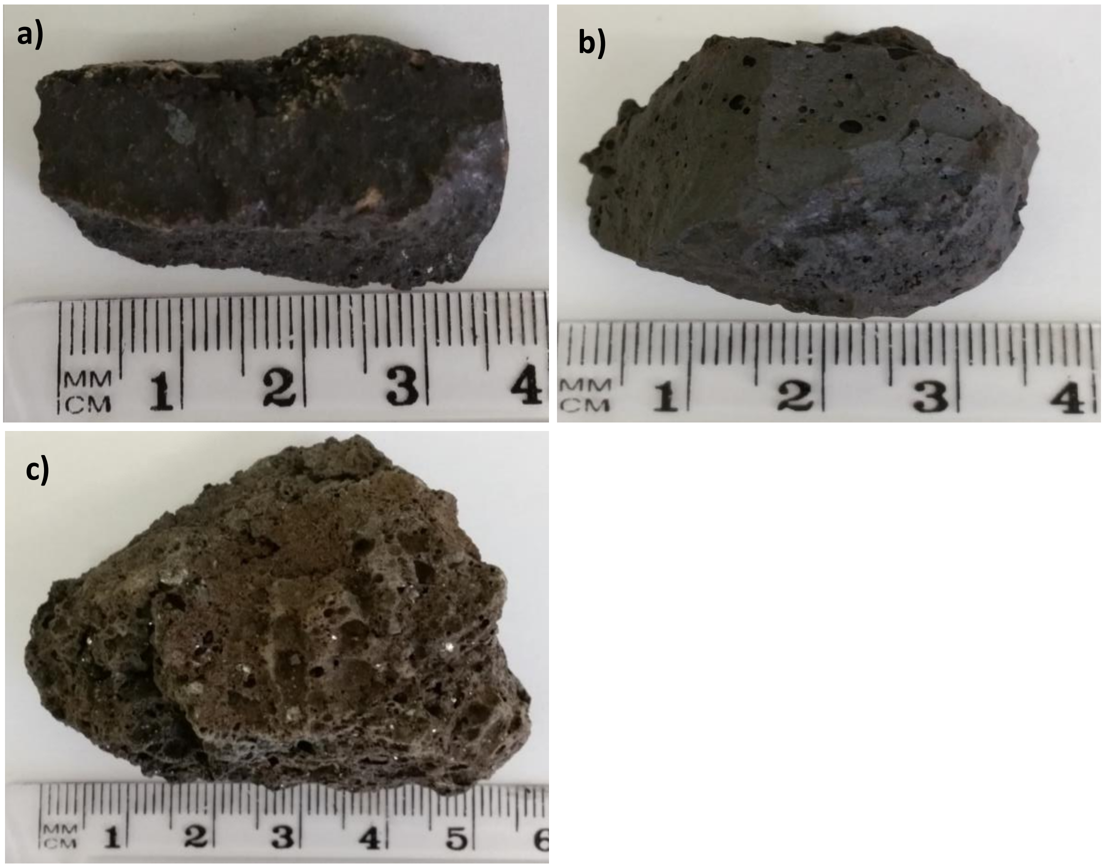

Plate 4.1: Images of a) Desulphurised skimmed slag b) Basic oxygen furnace slag c) Ladle slag

Table 4.1 presents data for total elemental composition of BOF (basic oxygen furnace), desulphurised skimmed and ladle slag obtained from the Yarborough site as determined using ICPOES and ICPMS.

The Yarborough BOF slag was dominated by calcium (20.0 ± 5.2 wt. %), iron (16.7 ± 3.2 wt. %), silicon (3.6 ± 0.4 wt. %), magnesium (2.0 ± 0.8 wt. %) and manganese (1.8 ± 0.9 wt. %). Other elements such as aluminium, sulphur, sodium, potassium, titanium, strontium and zinc accounted for < 1.2 wt. % of the total slag content. These concentrations have not been expressed in form of oxides hence the total value is not expected to be 100 %, which is mainly obtainable when the metal concentrations have been determined using XRF unlike in this work where ICP technique have been applied. Hence, in this analysis and for most of the ICP analysis carried out in this work, the unaccounted proportion could be due to oxygen.

Table 4.1: Major and minor elemental composition of digested steel slag samples from Yarborough, n = 3 where n is the number of replicate samples.

	Sample		
Major ions (% by weight)	**YARBOROUGH - BOF SLAG**	**YARBOROUGH – DESULPHURISED SKIMMED SLAG**	**YARBOROUGH – LADLE SLAG**
Ca	20.0 ± 5.2	20.6 ± 4.8	8.4 ± 2.3
Fe	16.7 ± 3.2	2.8 ± 0.8	3.5 ± 1.2
Si	3.6 ± 0.4	12.1 ± 1.3	2.9 ± 1.1
Al	0.6 ± 0.1	1.6 ± 0.4	5.3 ± 0.9
Mg	2.0 ± 0.8	4.3 ± 0.5	2.6 ± 0.2
Mn	1.8 ± 0.9	0.9 ± 0.4	1.2 ± 0.5
S	0.3 ± 0.1	2.6 ± 0.7	0.10 ± 0.03
Na	0.04 ± 0.01	3.1 ± 1.2	0.06 ± 0.02
K	0.010 ± 0.003	0.4 ± 0.1	0.020 ± 0.007
Ti	0.21 ± 0.08	0.4 ± 0.1	0.21 ± 0.07
Sr	0.020 ± 0.007	0.03 ± 0.01	0.010 ± 0.003
Zn	0.008 ± 0.002	0.0010 ± 0.0002	0.0010 ± 0.0003
Trace elements (mg/kg)			
As	23.6 ± 5.1	64 ± 10	1.0 ± 0.3
Ba	65.8 ± 3.4	172 ± 31	357 ± 38
Co	690 ± 21	55 ± 23	76 ± 28
Cr	1280 ± 20	39 ± 11	72 ± 14
Li	2.4 ± 1.0	22 ± 8	7.3 ± 1.2
Mo	20.3 ± 5.7	8 ± 2	4 ± 1
Ni	620 ± 34	8 ± 1	30 ± 11
Sb	0.5 ± 0.1	-	-
V	1910 ± 47	105 ± 11	125 ± 20

The dominant elements in the desulphurised skimmed slag were calcium (20.6 ± 4.8 wt. %), silicon (12.1 ± 1.3 wt. %), magnesium (4.3 ± 0.5 wt. %), sodium (3.1 ± 1.2 wt. %), iron (2.8 ± 0.8 wt. %), sulphur (2.6 ± 0.7 wt. %) and aluminium (1.6 ± 0.4 wt. %). Elements such as manganese, potassium, titanium, strontium and zinc collectively made up 1.73 wt. % of the total elemental composition of the material. The ladle slag was less enriched with respect to the studied elements compared to BOF and desulphurised slag. Concentration of major elements in the ladle slag were; calcium (8.4 ± 2.3 wt. %), aluminium (5.3 ± 0.9 wt. %), iron (3.5 ± 1.2 wt. %), silicon (2.9 ± 1.1 wt. %), magnesium (2.6 ± 0.2 wt. %) and manganese (1.2 ± 0.5 wt. %). Other major elements (sulphur, sodium, potassium, titanium, strontium and zinc) made up 0.40 wt. % of total elemental composition. The Yarborough BOF slag was more enriched, compared to the other slag types, with respect to elements such as cobalt (Co) – 690 ± 21 mg/kg, molybdenum (Mo) – 20.3 ± 5.7 mg/kg, nickel (Ni) – 620 ± 34 mg/kg and vanadium (V) – 1910 ± 47 mg/kg (see Table 4.1). Of the trace elements measured, barium was most abundant in the ladle slag than other slag types and antimony was the least abundant trace element in all the analysed steel slag.

Figure 4.2 displays the mineral phases present in the 3 steel slag samples. XRD analyses detected the presence of srebrodolskite ($Ca_2Fe_2O_5$), corundum (Al_2O_3), lime (CaO) and wustite (FeO) in the Yarborough BOF slag. In ladle slag, phases such as gehlenite ($Ca_2(Al_2SiO_7)$), larnite ($Ca_2(SiO_4)$, stishovite (SiO_2), spinel ($Mg (Al_2O_4)$) and periclase (MgO) were observed via XRD. Desulphurised skimmed slag was dominated by akermanite ($Ca_2Mg(Si_2O_7)$) and monticellite ($CaMgSiO_4$) phases.

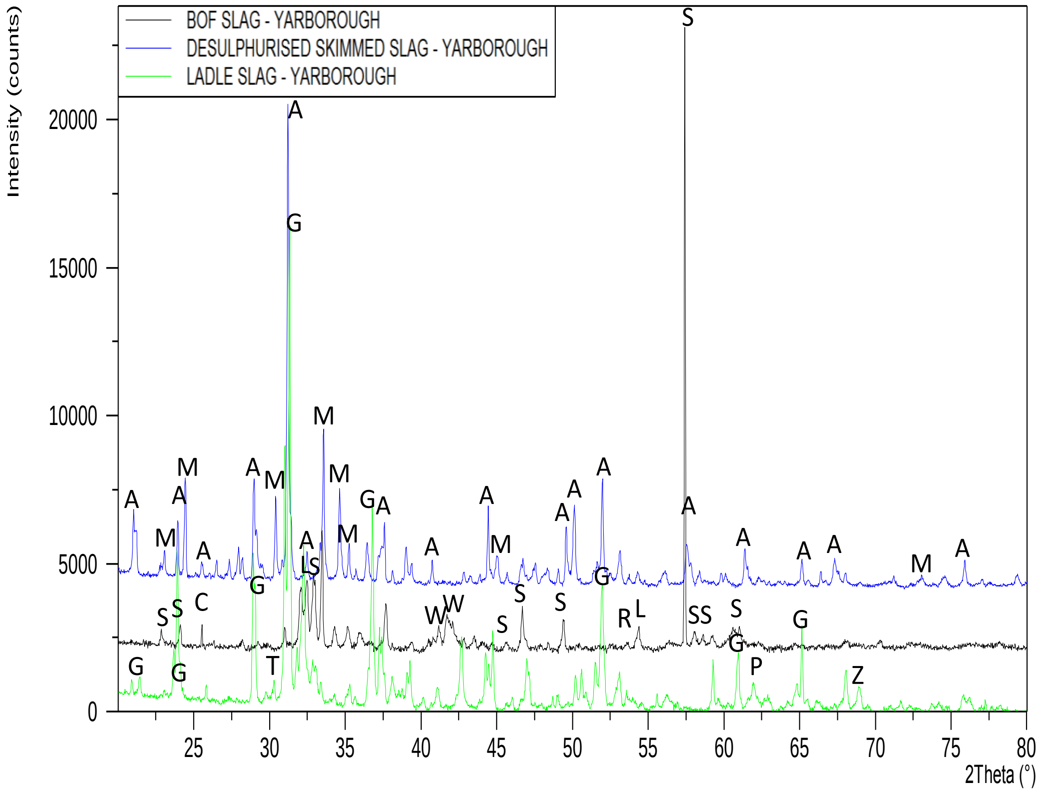

Figure 4.2: XRD diffractogram of steel slag at the Yarborough Site in Scunthorpe. C – Corundum (Al_2O_3), A – Akermanite ($Ca_2Mg(Si_2O_7)$), M – Monticellite ($CaMgSiO_4$), G – Gehlenite ($Ca_2(Al_2SiO_7)$, S – Srebrodolskite ($Ca_2(Fe_2O_5)$) ,P – Periclase (MgO) , Z – Spinel (Mg (Al_2O_4)) , W – Wustite (FeO), L – Larnite (Ca_2SiO_4), R - Lime (CaO), T - Stishovite (SiO_2).

Figure 4.3 shows a SEM/EDX analysis of BOF slag illustrating the heterogeneity of the material and the presence of a mix of mineral phases within the same material. SEM analysis revealed a surface with a glassy appearance and two distinct regions; a light coloured region A and a dark coloured region B. EDX analysis of BOF slag revealed the presence of calcium, iron, silicon, aluminium, oxygen with traces of carbon, magnesium, titanium, vanadium and manganese in both regions of the slag. Region B had an additional phosphorus peak. The iron peak was more intense in region A while calcium and silicon peaks were more intense in region B.

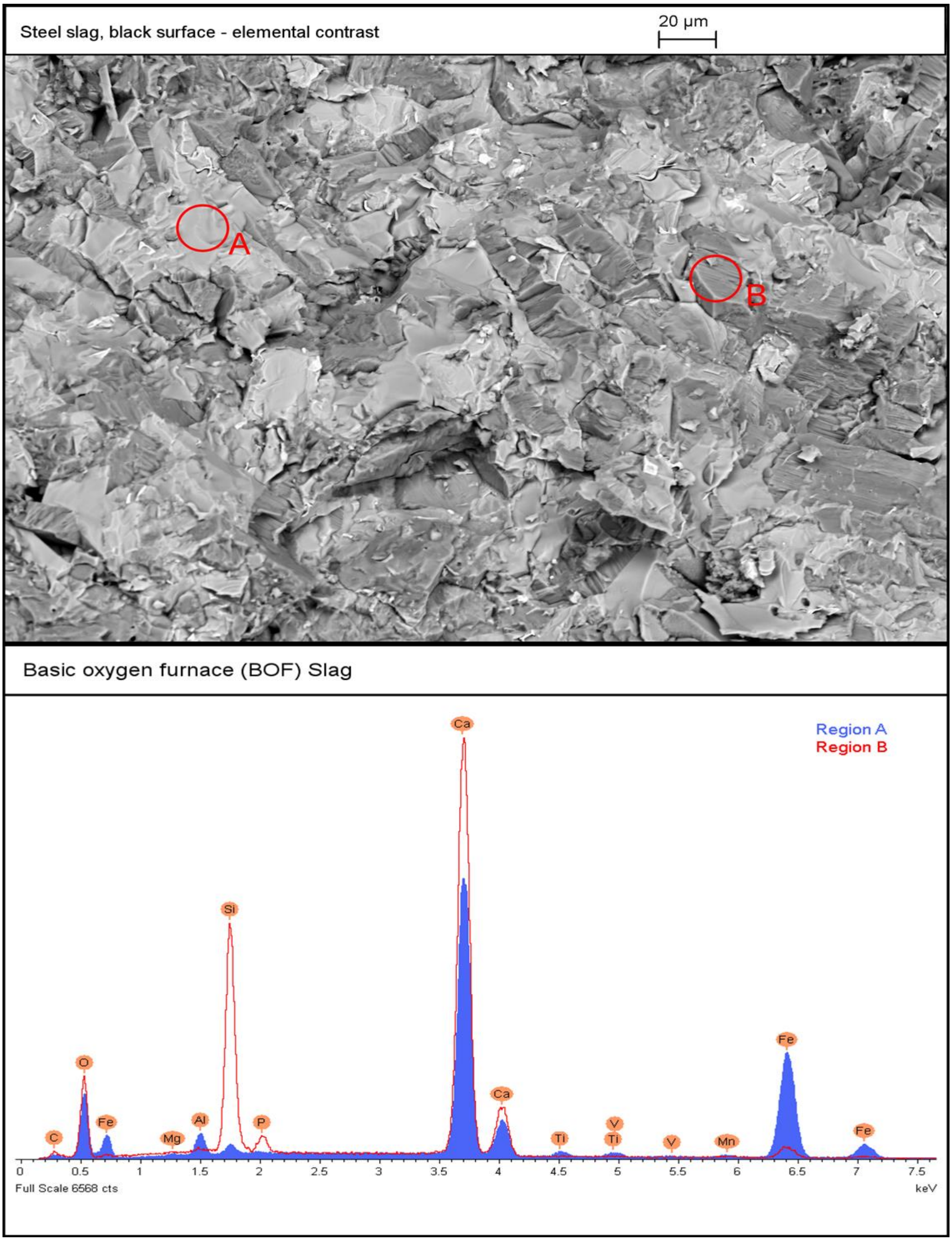

Figure 4.3: SEM micrograph and EDX analysis of Yarborough BOF slag. A –light region, B – dark region. The colour variation reflects elemental compositions in these regions.

The major elemental composition and selected physico-chemical properties of leachates sampled at the Yarborough site are shown in Table 4.2. The average pH of the waters associated with this site ranged from 9.3 ± 0.1 to 11.9 ± 0.2 (mean =

10.2, s = 1.2). The highest pH at this site was recorded at the source discharge area (YB1) while the lowest pH was recorded at the cut-off ditch (YB2). Redox potential values at this site were between -84 ± 4 and 92 ± 6 mV. Conductivity values ranged from 1354 ± 186 to 6523 ± 204 µS/cm. The pH and conductivity of the leachates sampled at the lagoon decreased over time from 10.2 ± 0.2 to 9.5 ± 0.2 and 6523 ± 204 to 3526 ± 193 µS/cm respectively. Total alkalinity of the leachates at source discharge in this site was 560 ± 23 mg/L as $CaCO_3$, mostly dominated by carbonate ions.

Table 4.2: Baseflow physico-chemical parameters and elemental constituent of filtered (0.45 µm) leachate samples from Yarborough. Data for Environmental Quality Standards (EQS) are presented alongside, where prescribed.

	Sample					
Determinand	Leachate source(YB1)	Cut off ditch (YB2)	Lagoon sampled on 24/2/12 (YB3A)	Lagoon sampled on 25/6/12 (YB3B)		EQS
pH	11.9 ± 0.2	9.3 ± 0.1	10.2 ± 0.2	9.5 ± 0.2		6-9
Temperature (°C)	15.5 ± 1.2	12.1 ± 0.9	10.4 ± 0.9	15.2 ± 1.4		
Conductivity (µS/cm)	5562 ± 231	1354 ± 186	6523 ± 204	3526 ± 193		
Eh (mV)	-84 ± 4	28 ± 3	-13 ± 3	92 ± 6		
Total alkalinity (mg/L as CaCO$_3$)	560 ± 23	98 ± 14	N/M	N/M		
OH modelled	196 ± 5	N/M	N/M	N/M		
CO$_3$ modelled	364 ± 10	18 ± 2	N/M	N/M		
HCO$_3$ modelled	0	80 ± 14	N/M	N/M		
Major ions(ppm)					LOD(ppm)	
Ca	23 ± 8	6 ± 2	1.0 ± 0.3	6 ± 1	0.010 ± 0.002	
Na	114 ± 23	13.3 ± 3.2	162.3 ± 22.1	818 ± 54	0.020 ± 0.006	
K	5 ± 1	1.8 ± 0.4	13.1 ± 3.2	40 ± 6	0.003 ± 0.001	
Mg	0.10 ± 0.01	8.2 ± 2.2	9.2 ± 2.3	16 ± 3	0.020 ± 0.006	
SO$_4^{2-}$	246 ± 40	29.6 ± 7.3	48.0 ± 4.3	815 ± 34	2.1 ± 0.2	
Cl$^-$	127 ± 21	N/M	N/M	N/M	0.79 ± 0.08	
Minor ions/trace elements(ppb)					LOD(ppb)	
Sr	3729 ± 176	499 ± 15	<LOD	<LOD	488 ± 10	1500
Ba	6 ± 1	<LOD	<LOD	<LOD	4.1 ± 0.3	110^
Fe	<LOD	<LOD	77.4 ± 6.7	<LOD	3.4 ± 0.2	1000+
Li	35 ± 5	49 ± 7	58.2 ± 5.1	20 ± 3	0.17 ± 0.02	260^

V	18 ± 3	32 ± 6	79.4 ± 8.7	12 ± 2	0.10 ± 0.03	60*+
As	41 ± 5	28 ± 3	54.5 ±	35 ± 6	0.51 ± 0.10	3.1
Sb	49 ± 7	4 ± 1	1.3 ± 0.4	0.4 ± 0.1	0.11 ± 0.02	30
Ni	61 ± 6	10 ± 1	48.6 ± 6.4	4 ± 1	0.22 ± 0.05	200*+
Mo	60 ± 8	55 ± 11	48.4 ± 5.7	35 ± 3	0.63 ± 0.11	1600^
Pb	75 ± 7	135 ± 13	<LOD	210 ± 45	71.9 ± 7.6	20*+
Si	114 ± 12	388 ± 16	338 ± 45	2490 ± 231	86 ± 13	

LOD = limit of detection, N/M = not measured, * = hardness related, value quoted for hardness values encountered here; $^{+}$ = as dissolved fraction which can pass through a 0.45μm filter. EQS taken from EU WFD with exception of '^' which are from Buchman (2008).

Leachates from the steel slag disposal sites at Yarborough were dominated by Na-CO_3-SO_4 ions. The sulphate and chloride content of the source leachates were 246 ± 40 ppm and 127 ± 21 ppm respectively. In order to estimate the easily leachable fraction of the selected elements, their leaching efficiencies (see Appendix A3) have been calculated using data from Tables 4.1 and Table 4.2 (assuming the majority of the slag in the landfill is due to BOF slag, which is true for this site). Here, the leaching efficiency of an element has been defined as the ratio of its concentration in the leachate to that in the original resource. The concentration of magnesium in the leachates obtained from source zone (YB1) was 0.10 ± 0.01 ppm, which represents only a very small fraction (0.0005 %) of the total magnesium concentration in the BOF slag. The calculated leaching efficiencies for calcium and silicon were 0.012 % and 0.00030 % respectively (see Appendix A3).

Trace elements concentrations of Yarborough BOF slag are presented in Table 4.2 above. Strontium levels at source discharge were 3729 ± 176 ppb, but were present in low concentration and below detection limit in the cut-off ditch and lagoon respectively (see Table 4.2). Certain elements such as barium and iron, although present in the source material (steel slag) in detectable amounts, were however below detection limits in the leachates sampled, with leaching efficiencies of 0.006 % and 0.000002 % respectively. The concentration of lithium, vanadium, nickel and molybdenum at the leachate source (YB1) were 35 ± 5 ppb, 18 ± 3 ppb, 61 ± 6 ppb and 60 ± 8 ppb respectively with representative leaching efficiencies of 1.46 %, 0.004 %, 0.01 % and 0.3 % respectively (Appendix A3). The concentrations of these elements were also observed to decrease with time (see Table 4.2).

Table 4.3 highlights the elemental composition of the secondary precipitate obtained from the Yarborough site. The bulk of the secondary precipitate was mainly due to major elements (approx. 99.8 %). Metal analysis showed calcium was the key element found in the precipitate, accounting for about 84 % of the total concentration of elements identified by ICPOES. In addition, about 9 % of the total major ions content was due to silicon. Trace elements accounted for about 0.2 % of the total elemental composition. Concentrations of elements like barium, chromium, vanadium, nickel and molybdenum in the precipitate were 195 ± 10 mg/kg, 130 ± 9 mg/kg, 110 ± 12 mg/kg, 30 ± 4 mg/kg and 8.4 ± 1.5 mg/kg respectively. The concentration of these elements exceeded threshold levels for sediments in surface waters (Table 4.3).

Table 4.3: Major ions and trace element composition of digested secondary deposits from Yarborough.

Major ions (% by weight)	**YB**	**EQS**
Ca	26.4 ± 1.2	
Mg	0.8 ± 0.1	
Si	2.7 ± 0.1	
S	0.40 ± 0.04	
Al	0.50 ± 0.01	0.26
K	0.10 ± 0.01	
Na	0.10 ± 0.02	
Sr	0.20 ± 0.07	0.01
Trace elements (mg/kg)		
As	21.6 ± 3.5	6
Ba	195 ± 10	0.7
Cr	130 ± 9	37.3
Li	11.1 ± 2.8	
Mo	8.4 ± 1.5	
Ni	30 ± 4	18
Sb	1.1 ± 0.2	0.2
V	110 ± 12	50

EQS – Environmental Quality Standard taken from Buchman (2008).

Figure 4.4 displays the mineral phases present in the secondary precipitate collected from Yarborough. XRD analyses revealed that the material was predominantly calcite with traces of quartz.

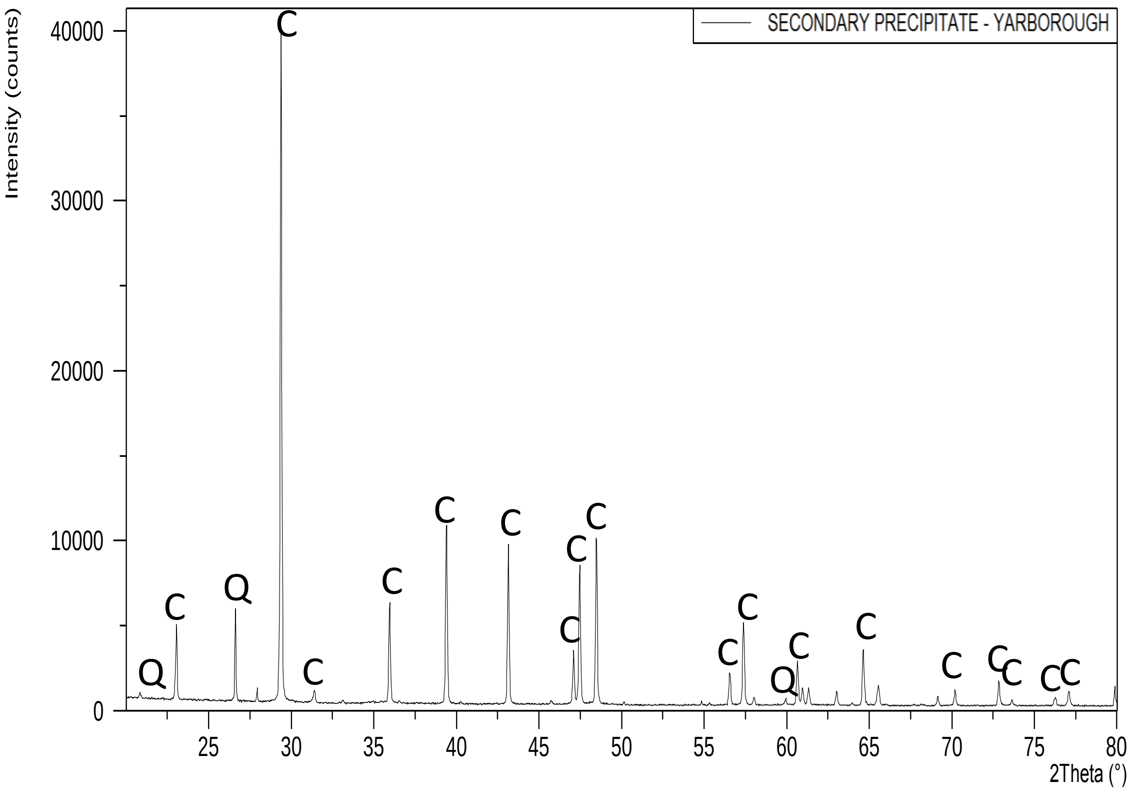

Figure 4.4: XRD diffractogram of secondary precipitate from Yarborough Site in Scunthorpe. C- Calcite ($CaCO_3$), Q – Quartz (SiO_2)

Figure 4.5 shows a SEM/EDX analysis of the secondary precipitate obtained from Yarborough. SEM (back scatter) analysis of the secondary precipitate reveals a structure with three distinct layers; labeled A, B, C (Figure 4.5). The outer layer (A) appears to be denser and more crystalline in appearance and is also apparently cleaner (judged by its white colour) and more likely to be experiencing recent crystal growth. The layers may have been formed as a result of several years of dumping activities at this site. The middle layer appears to be more compact compared to others but this may have been a deposition of some sort. EDX analysis of the outer region (A) revealed the presence of calcium, silicon, magnesium, carbon, oxygen with traces of iron, sodium, aluminium, sulphur, chloride, potassium, and manganese. EDX analysis of layer B confirmed the presence of carbon, oxygen, and calcium with traces of sodium, magnesium, aluminium, silicon, sulphur, and iron in this region. The lower region (C) was similar in composition to region B with the addition of manganese. The magnesium, silicon, oxygen and aluminium peaks were more pronounced in region A while the calcium peak was more pronounced in regions B and C.

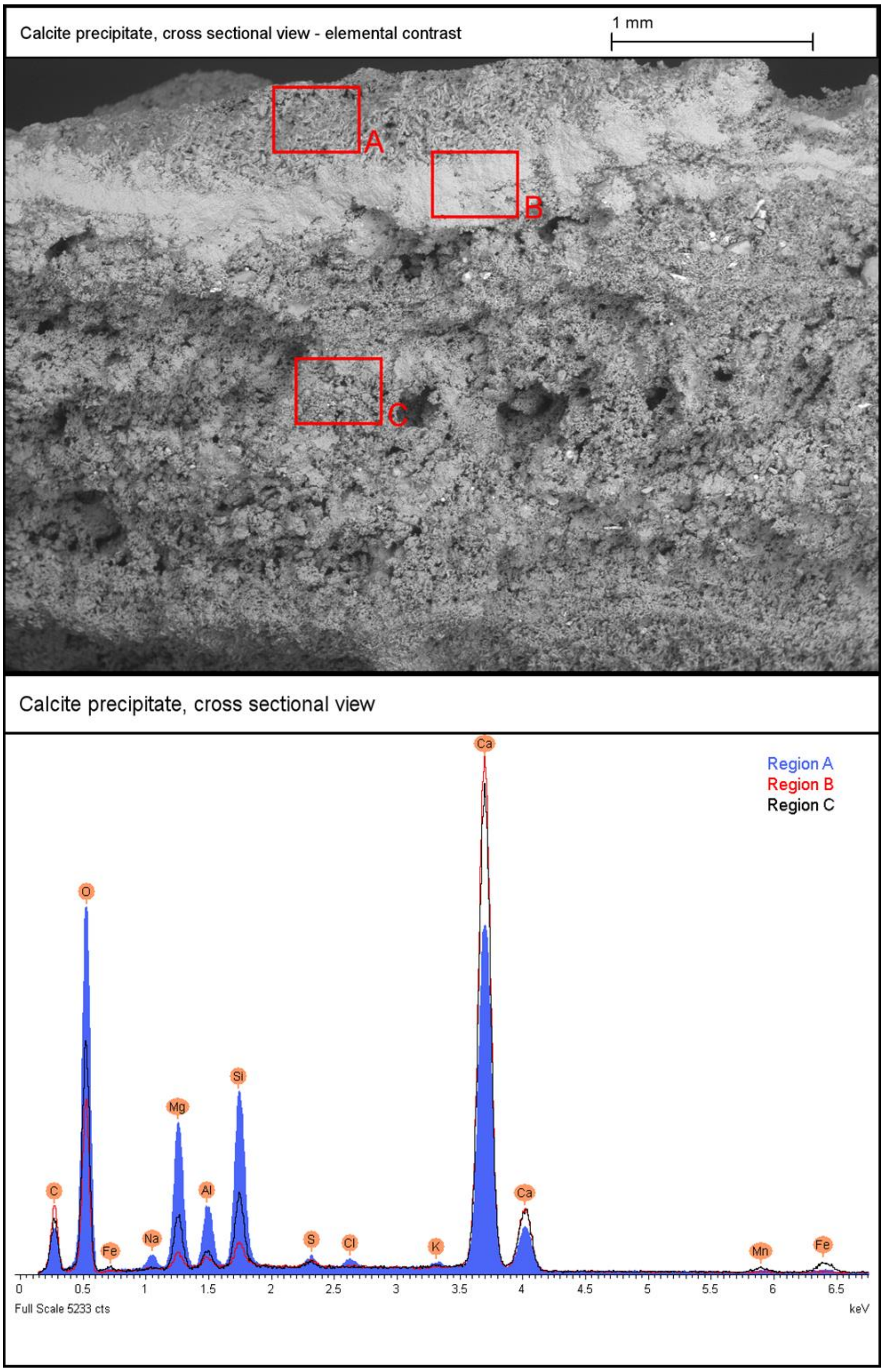

Figure 4.5: SEM micrograph and EDX analysis of secondary precipitate obtained from a steel slag disposal site.

Figure 4.6 displays the observed decomposition pattern for the secondary precipitate collected from Yarborough. Weight losses associated with moisture was not observed as there was no observable peak in the 100 ˚C region probably owing to the fact that the sample was oven dried for 5 hours prior to analysis. Decomposition of the secondary precipitate took place in the temperature range of 650 ˚C – 900 ˚C. Assuming the secondary precipitate was predominantly calcium carbonate (calcite) as confirmed via XRD. Then the expected typical decomposition pattern would be represented by equation (4.1)

$$CaCO_3 \rightarrow CaO + CO_2 \qquad (4.1)$$

Ideally, the expected mass loss should be equivalent to 44.00 % of the total mass (i.e the CO_2 fraction), however the analysis resulted in an actual mass loss of 36.63 % which would suggest that the decomposition of the precipitate was incomplete or the possibility of the presence of other mineral phases in the sample, most likely quartz, which was detected via XRD.

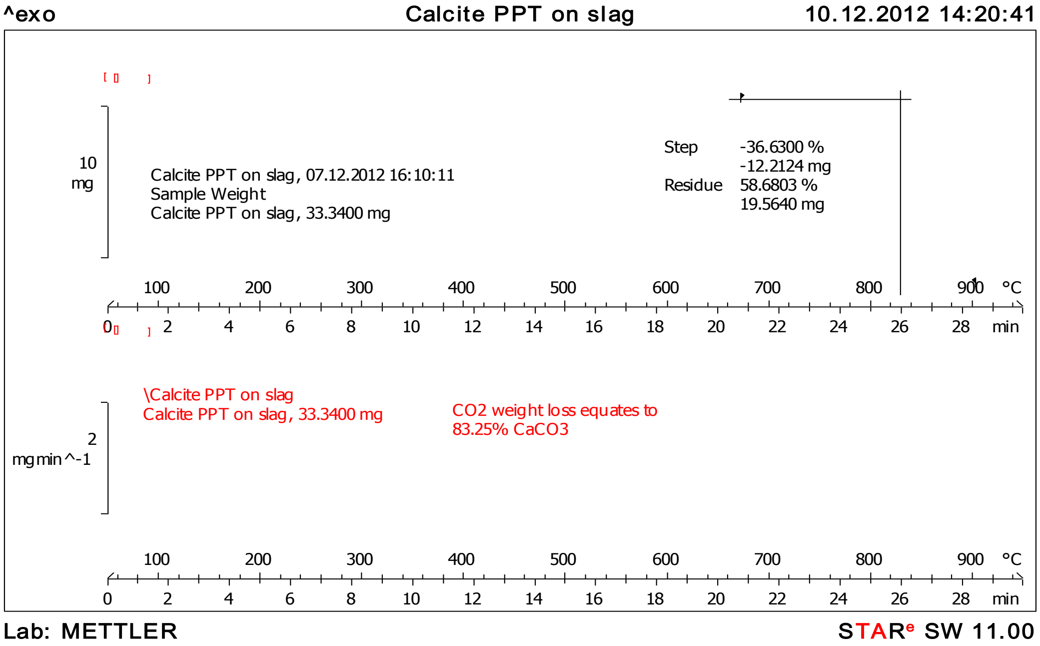

Figure 4.6: Thermogravimetric analysis of secondary precipitate from a steel slag disposal site.

4.2 Investigation of Consett steelworks, County Durham

4.2.1 Consett steelworks – Site description and methodology

Two watercourses draining extensive slag mounds associated with the former Consett Iron and Steel works in Northern England (54°50′32.9386″N, 001°51′32.5752″W and 54°51′11.7661″N, 001°51′38.0473″W) were sampled under baseflow conditions. These sites had been previously characterised by elevated pH (9.0 - 12.5) both during workings operation (when the waters were dosed with sulphuric acid) and throughout the three decades since the closure of the steel mill in 1980 (Mayes *et al.*, 2008). Under baseflow conditions, the Dene Burn (sample prefix DB) receives around half of its flow from a subterranean drainage network beneath the Grove Heaps area of the site. These heaps were used up until the closure of the workings in 1980 and consist of blast furnace bottom and steel slag (Mayes *et al*., 2008). The slag is deposited with other site waste (e.g. ashes and site demolition waste) over superficial alluvium and glacial till in the valley floors. Below this unconsolidated drift, the bedrock consists of Lower Coal Measures of Carboniferous (Westphalian) age. The Howden Burn (sample prefix HB) drains an area north of the Dene Burn previously occupied by the workings blast furnaces, power station and steel plant, again emerging from a large subterranean drainage system (Figure 4.7). The sampling locations at this site have been presented in Figure 4.7. Sampling locations for Dene Burn were labelled DB1 to DB10, where DB1 represents sampling locations closest to the source discharge and DB10 furthest from source. On the hand, sampling locations for Howden Burn were labelled HB1 to HB8 representing distance closest and furthest from source respectively (Figure 4.7).

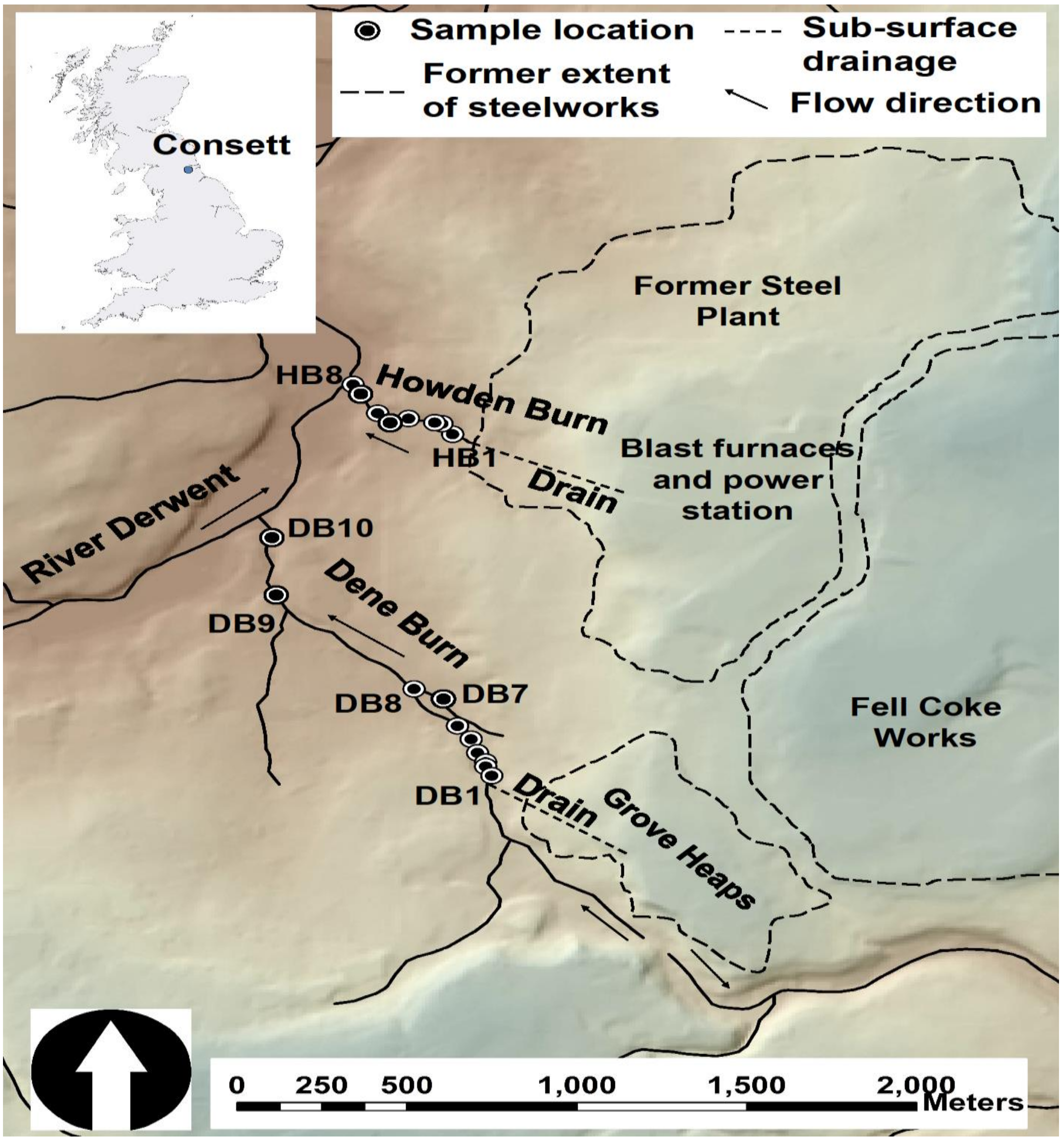

Figure 4.7: Sampling locations at the abandoned Consett steelworks, County Durham.

BOF slag, leachates and secondary precipitates were collected at this site in a similar way as the Yarborough site. Elemental composition of the slag and secondary precipitate were determined using ICPOES (Ca, Fe, Si, Al, Mg, Mn, S, Na, K, Ti, Sr, Zn) and ICPMS (As, Ba, Co, Cr, Li, Mo, Ni, Sb, V) while their mineralogy was determined using XRD (see section 3.3.3).

Physico-chemical parameters, field alkalinity, and dissolved metal concentrations of the leachates were analysed in the same way as that of the Yarborough site (see section 3.4.1.1). Dissolved oxygen was analysed using a YSI 85D meter. Saturation index for calcite was determined according to the procedure described in section 3.4.1.2.

At this site, flow measurements and multiple downstream sample locations (HB8 and DB8) were taken in order to assess the evolution of the waters with distance from discharge points. In addition to these geochemical analyses, stream flow rate was measured at each sample site at Consett to compute chemical mass loadings (which facilitate precipitation rate estimates through assessing Ca^{2+} loss between consecutive sample stations). The precipitation rate of secondary deposits (calcite) forming at this site was determined using the mass balance method. This parameter was derived using the mass balance between sequential sample stations and areal estimates of the stream bed from site surveys (Mayes *et al*., 2008). A Valeport 801 velocity meter with a flat electromagnetic sensor was deployed during base-flow sampling at this site. This device was particularly suited to measuring velocity in the streams studied at Consett given the typically shallow depth of water (generally < 0.05 m). Between 5 and 8 velocity measurements were taken in each cross-section. Unfortunately reliable flow measurements were not possible to obtain from the other study sites investigated in this work given the low flow rates (Yarborough) or highly dispersed nature of the drainage channels at these sites (Brook Bottom; see section 4.3.1 for site description).

Furthermore, in some cases where data did not conform to a normal distribution, even after log transformation (Kolmogorov Smirnov, $p < 0.05$), a non-parametric method (Spearman's Rank) have been used to assess relationships between key control variables. All graphs for this section were plotted using Microsoft Excel 2007 package.

4.3.2 Consett steelworks – Results

Table 4.4 presents the elemental composition of BOF slag from Howden Burn and Dene Burn Consett. The most abundant elements in the BOF slag collected from both sites were calcium, iron and silicon, with average concentrations of 27.0 ± 9.6 %, 17.8 ± 10.0 % and 10.9 ± 1.0 % across both sites respectively. Elements such as aluminium, manganese and magnesium were present in concentrations of 1.3 ± 0.6 %, 2.7 ± 0.1 %, and 0.8 ± 0.6 % respectively.

Table 4.4: Major and minor elemental composition of digested BOF slag samples from Consett steelworks (n=3).

	Sample		
Major ions (% by weight)	**CONSETT - BOF SLAG (HB)**	**CONSETT -BOF SLAG (DB)**	**Mean (HB, DB)**
Ca	20.2 ± 3.4 (16.3 – 22.8)	33.7 ± 43.6 (1 – 83.2)	27.0 ± 9.6
Fe	10.7 ± 6.9 (3.3 – 16.8)	24.8 ± 19.0 (3.3 – 39.4)	17.8 ± 10.0
Si	10.2 ± 4.9 (6.9 – 15.8)	11.6 ± 9.4 (6.2 – 22.4)	10.9 ± 1.0
Al	0.8 ± 0.6 (0.3 – 1.5)	1.7 ± 1.7 (1.8 -3.5)	1.3 ± 0.6
Mg	1.2 ± 0.2 (1.1 – 1.5)	0.4 ± 0.3 (0.1 – 0.6)	0.8 ± 0.6
Mn	2.8 ± 2.7 (0.01 – 5.5)	2.6 ± 1.5 (0.9 – 3.6)	2.7 ± 0.1
S	0.5 ± 0.2 (0.4 – 0.8)	0.3 ± 0.2 (0.04 – 0.5)	0.4 ± 0.1
Na	0.10 ± 0.02	0.11 ± 0.03	0.10 ± 0.02
K	0.1 ± 0.2 (0.02 – 0.3)	0.1 ± 0.1 (0.02 – 0.3)	0.10 ± 0.03
Ti	0.4 ± 0.2 (0.3 – 0.7)	0.4 ± 0.4	0.4 ± 0.1
Sr	0.04 ± 0.03 (0.01 – 0.06)	0.03 ±	0.04 ± 0.01
Zn	1.0 ± 0.8 (0.1 -1.7)	0.0010 ± 0.0002	0.5 ± 0.7
Trace elements (mg/kg)			
As	13.5 ± 13	15 ± 3	14.3 ± 1.1
Ba	421.7 ± 23.5	138.1 ± 33.5	279.9 ± 200.5
Co	3.9 ± 0.8	22.4 ± 3.6	13.2 ± 13.1
Cr	1411 ± 124	298.7 ± 10.4	854.9 ± 786.5
Li	21.8 ± 3.2	31.6 ± 5.4	26.7 ± 6.9
Mo	19.2 ± 2.1	18.6 ± 2.1	18.9 ± 0.4
Ni	242 ± 43	490 ± 43	366.0 ± 175.4
Sb	2.0 ± 0.5	4.0 ± 0.4	3.0 ± 1.4
V	1764 ± 122	1109 ± 87	1436.5 ± 463.2

Values in parentheses represent the range of triplicate sample measurement

Vanadium was the most abundant trace element present in the slag sample (1436.5 ± 463.2 %). Chromium, nickel and barium concentrations in the Consett BOF slag samples were 854.9 ± 786.5 %, 366.0 ± 175.4 % and 279.9 ± 200.5 %

respectively. Elements such as arsenic, cobalt, lithium, molybdenum were present in moderate concentrations of ≤ 26.7 ± 6.9 %. Antimony was the least abundant trace element in the BOF slag (Table 4.4).

The mineralogy of the BOF slag from the Consett sites are presented in Figure 4.8. XRD analysis detected the presence of brownmillerite ($Ca_2(Fe_2O_5)$), calcite ($CaCO_3$), hematite (Fe_2O_3), larnite (Ca_2SiO_4) and stishovite (SiO_2) in the BOF slag sample from Howden Burn while phases such as hematite (Fe_2O_3) and magnetite (Fe_3O_4) only were found in the BOF slag from Dene Burn.

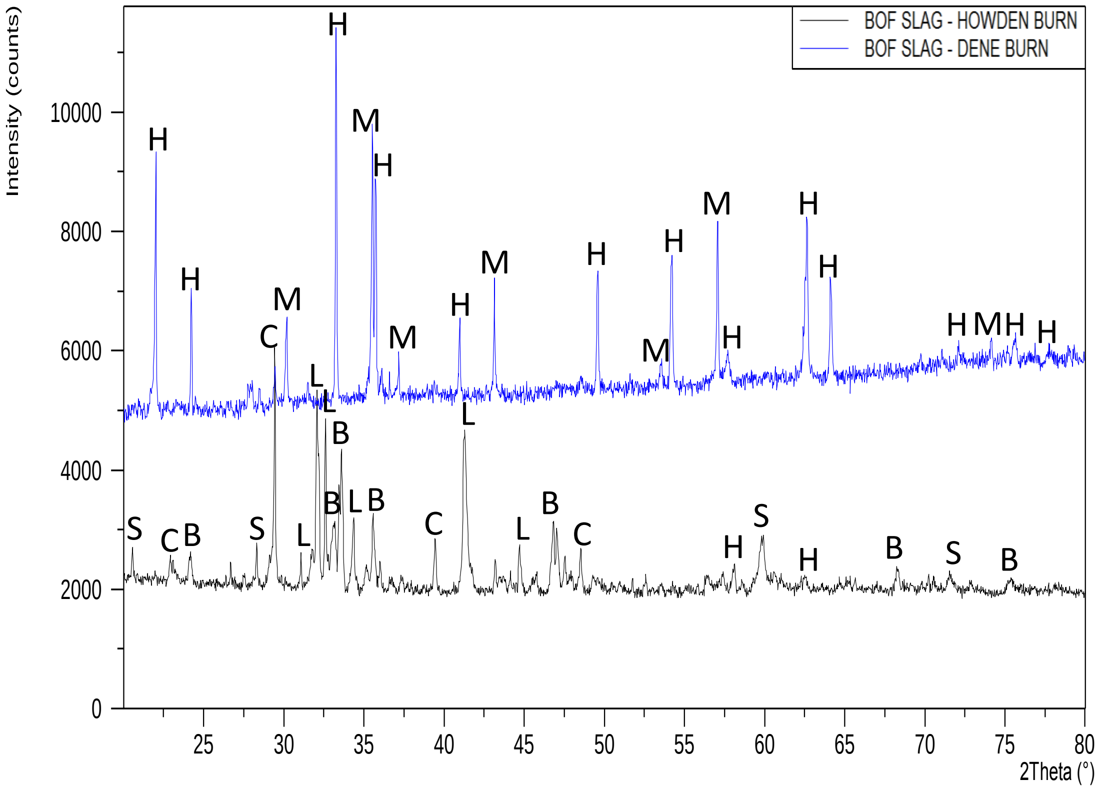

Figure 4.8: XRD diffractogram of BOF slag at the Consett Site in County Durham. H – Hematite (Fe_2O_3), M – Magnetite (Fe_3O_4), C – Calcite ($CaCO_3$), S – Stishovite (SiO_2), B – Brownmillerite ($Ca_2(Fe_2O_5)$), L – Larnite (Ca_2SiO_4).

The major elemental composition of leachates sampled at both source discharges and downstream locations at Consett are presented in Table 4.5. The average pH of the leachate obtained from the source discharges at Howden Burn (HB1) and Dene Burn (DB1) were 11.6 ± 0.3 and 10.7 ± 0.1, this value however decreased downstream by 0.3 pH units and 1.7 pH units at HB8 and DB8 respectively. Both the Howden and Dene Burn waters have pH values well above ambient aquatic life limits (pH 9). Leachates from the Consett site were mostly oxic (positive redox potential) in nature with the exception of the source discharge point at Dene Burn which was anoxic (Table 4.5). Dissolved oxygen concentrations were high at this site, ranging from 88 ± 2 to 99.4 ± 1.7 % sat., and increasing with distance downstream (Table 4.5), this was facilitated by the cascading, high gradient longitudinal profiles of both streams.

Table 4.5: Baseflow physicochemical parameters and major elemental constituent of slag leachates from Consett sites of filtered (0.45 μm) leachate samples from Consett sites. Source samples on each sampling site are presented alongside Environmental Quality Standards (EQS), where prescribed. HB - Howden Burn, DB - Dene Burn, EQS – Environmental quality standard

	Site				
Determinand	HB1	HB8	DB1	DB8	EQS
pH	11.6 ± 0.3	11.3 ± 0.2	10.7 ± 0.1	9.1 ± 0.1	6 – 9
Temperature (^oC)	13.0 ± 1.0	12.8 ± 0.3	12.5 ± 0.8	13.4 ± 1.3	
Electrical conductivity (μS/cm)	3193 ± 211	1563 ± 98	452 ± 32	438 ± 25	
E.h. (mV)	2.2 ± 0.4	2.5 ± 0.7	-1.1 ± 0.3	4.4 ± 1.0	
Dissolved oxygen (% sat.)	92.5 ± 1.2	96.5 ± 2.0	88 ± 2	99.4 ± 1.7	50
Distance downstream of source (m)	5	460	5	1660	
Major ions (mg/L)					
Ca	239 ± 12	110 ± 19	15 ± 2	11 ± 1	
Mg	1.0 ± 0.3	2.0 ± 0.4	2.0 ± 0.2	1.0 ± 0.2	
K	293 ± 23	172 ± 21	18 ± 4	19 ± 5	
Na	83 ± 4	56 ± 6	25 ± 4	24 ± 3	
Cl^-	42 ± 2	41 ± 4	18 ± 3	18 ± 2	
SO_4^{2-}	852 ± 43	546 ± 32	36 ± 5	36 ± 3	
NO_3	3.1 ± 0.5	4.0 ± 0.4	3.3 ± 0.7	3.2 ± 0.5	
Total P	0.05 ± 0.01	0.09 ± 0.01	0.03 ± 0.01	0.04 ± 0.02	
Total Alkalinity (as $CaCO_3$)	332 ± 21	84 ± 17	59 ± 10	66 ± 8	
OH^-	29 ± 3	13 ± 2	3.3 ± 0.5	1.0 ± 0.2	
CO_3^{2-}	139 ± 21	20 ± 3	18 ± 2	2.0 ± 0.4	
HCO_3^-	9 ± 1	3.0 ± 0.1	9 ± 1	37 ± 3	

Leachates from the Consett sites were dominated by the Ca-K-CO_3-SO_4 (Howden Burn), Na-K-SO_4 (Dene Burn) type waters. The Howden Burn had far greater ionic enrichment than the Dene Burn, with Ca^{2+}, OH^- and SO_4^{2-} as the major ions (Table 4.5). The concentration of dissolved magnesium at both sites was low (≤ 2 ppm), with a leaching efficiency of 0.008 %. Similarly, the leaching efficiencies of calcium and silicon at this site (Howden Burn, Consett) were 0.12 % and 0.001 % respectively (Appendix A3). The concentrations of the major ions decreased with increasing distance. The concentration of most of the trace elements in the leachate surveyed at this site was below threshold levels (EQS) except lithium, with a leaching efficiency of 3.8 % and strontium (Table 4.6; Appendix A3). The calculated leaching efficiencies for elements of interest such as vanadium, molybdenum, and nickel were 0.003, 0.12, and 0.004 % respectively (Appendix A3). In addition, at both sites, the concentrations of most trace elements fell with increasing distance although there were a few exceptions such as at Dene Burn where the concentrations of aluminium and strontium increased with distance (Table 4.6).

Table 4.6: Trace elemental constituent of filtered (0.45 µm) leachate samples from Consett sites. Source samples on each sampling site are presented alongside Environmental Quality Standards (EQS), where prescribed.

	Site				
Trace elements (µg/L)	HB1	HB8	DB1	DB8	EQS
Distance downstream of source (m)	5	460	5	1660	
Al	556 ± 23	13 ± 1	15 ± 1	40 ± 3	750
Ba	42.5 ± 3.2	32.8 ± 2.1	26 ± 4	4.6 ± 1.0	110^
Cd	2.0 ± 0.3	2.0 ± 0.2	2.0 ± 0.5	2 ± 0.3	5
Cr	8.4 ± 1.2	6.7 ± 1.3	2.5 ± 0.4	1.0 ± 0.1	50*+
Cu	1.0 ± 0.1	1.2 ± 0.2	1.0 ± 0.3	1.1 ± 0.2	28*+
Fe	980.7 ± 21.1	690.4 ± 34.2	137.6 ± 12.1	88.3 ± 10.3	1000+
Li	822 ± 21	703.6 ± 24.0	14.2 ± 2.1	4.4 ± 0.7	260^
Mn	32.2 ± 5.3	1.1 ± 0.2	17.4 ± 3.4	5.4 ± 1.3	
Mo	23.4 ± 2.1	13.3 ± 1.6	10.9 ± 1.2	2.8 ± 0.4	1600^
Ni	8.9 ± 2.3	4.8 ± 1.2	10.9 ± 2.2	0.3 ± 0.1	200*+
Pb	5.0 ± 1.0	5.0 ± 0.4	5.0 ± 0.3	5.0 ± 0.4	20*+
Sb	1.6 ± 0.4	1.1 ± 0.2	1.0 ± 0.4	0.10 ± 0.03	
Si	1290 ± 91	1160 ± 65	222 ± 54	203 ± 32	
Sr	2610 ± 187	1140 ± 121	213 ± 21	279 ± 19	15^
V	51.8 ± 1.5	34.2 ± 2.4	13.9 ± 2.3	1.6 ± 0.3	60*+
Zn	9 ± 1	2 ± 1	4 ± 1	3 ± 1	10.9*

* = hardness related, value quoted for hardness values encountered here; $^+$ = as dissolved fraction which can pass through a 0.45µm filter. EQS taken from EU WFD with exception of '^' which are from Buchman (2008). HB- Howden Burn, DB – Dene Burn

Figure 4.9 highlights how concentrations of selected elements (Ca, V) and key parameters (calcite precipitation rate, pH, and conductivity) behave as a function of distance downstream. There was a greater fall in pH of water samples at Dene Burn compared to Howden Burn as distance from source areas increased. Calcium carbonate precipitation rates, generally decreased with distance from the sources and is reflected in the downstream falls in conductivity (as ionic species are lost from solution) across the two streams at Consett (Figure 4.9). Similarly, the concentrations of Ca and V declined concomitantly with distance from the sources except in lower reaches of the Dene Burn where instream Ca^{2+} load gains were observed (Figure 4.9). Precipitation rates, as well as the saturation index, for calcite was higher in Howden Burn compared to Dene Burn.

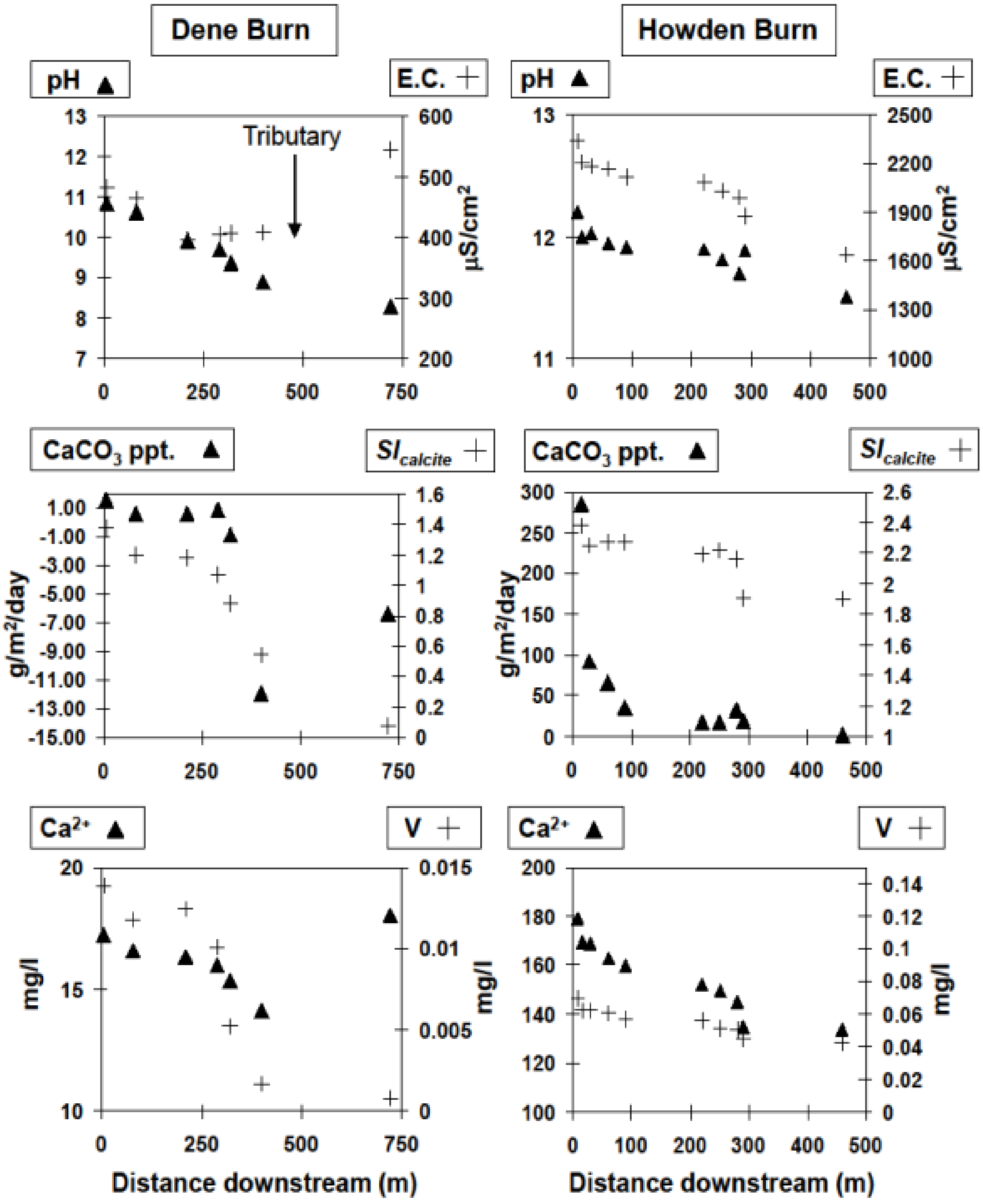

Figure 4.9: Baseflow patterns in selected major physico-chemical parameters and elemental concentrations along the Howden Burn and Dene Burn.

Results from previous work (Mayes *et al*., 2008), had shown that the secondary precipitates forming at the Consett site was mainly calcite, and in some cases, polymorphs of calcite such as vaterite were found in source areas. Table 4.7 presents data for the elemental content of the secondary precipitates obtained from Consett. Calcium and silicon were the most abundant elements in the secondary precipitates. They were however present in levels of about one order of magnitude lower than that in Yarborough. Most of the trace elements surveyed exceeded the threshold values for sediments in surface waters (Table 4.7). These elements include barium, arsenic, vanadium, nickel and antimony. The most abundant trace element in the secondary deposit was barium, ranging from 87.32 ± 8.67 to 354 ± 7 mg/kg while the least was antimony in levels ranging from 1.85 ± 0.23 to 1.98 ± 0.34 mg/kg.

Table 4.7: Major ions and trace element composition of digested secondary deposits from Consett slag disposal site (n = 3)

Major ions (% by weight)	**Howden Burn (HB)**	**Dene Burn (DB)**	**EQS**
Ca	1.96 ± 0.21	2.13 ± 0.15	
Mg	0.010 ± 0.001	0.15 ± 0.02	
Si	2.67 ± 0.13	2.92 ± 0.23	
S	0.76 ± 0.07	0.75 ± 0.12	
Al	0.23 ± 0.02	0.20 ± 0.03	0.26
K	0.03 ± 0.01	0.030 ± 0.006	
Na	0.010 ± 0.002	0.010 ± 0.004	
Sr	0.09 ± 0.02	0.003 ± 0.001	0.01
Trace elements (mg/kg)			
As	20.13 ± 2.12	22.38 ± 4.34	6
Ba	354.0 ± 7.0	87.32 ± 8.67	0.7
Cr	14.13 ± 1.62	7.55 ± 2.11	37.3
Li	11.87 ± 0.22	5.59 ± 1.24	
Mo	12.47 ± 0.45	6.03 ± 2.13	
Ni	22.47 ± 1.24	24.71 ± 3.42	18
Sb	1.98 ± 0.34	1.85 ± 0.23	0.2
V	219.07 ± 26.45	132.57 ±13.32	50

EQS – Environmental Quality Standard taken from Buchman (2008).

4.3 Investigation of Lime spoil sites, Derbyshire

4.3.1 Brook Bottom, Doveholes, and Newline Quarry Derbyshire – Site description and methodology

A number of lime spoil affected sites in the Buxton area, Derbyshire were investigated in this work. Sampling was carried out at Brook bottom, Buxton Derbyshire (Figure 4.10; 53°14′16.69″N, 001°54′33.60″W). Detailed descriptions of the features at this site have been provided elsewhere (Emery, 2013; Milodowski *et al*., 2013). The site is near Harpur Hill, in Derbyshire, UK. Large volumes of high pH waste that had been generated from the Hoffman lime kiln (well known for its lime roasting activities for the alkali carbonate industry) from 1872 until its closure in 1944 had been deposited into an adjacent valley to the northwest of the kiln (Anon, 2008). High pH leachates emanating from the base of the waste, flow downwards along the valley (Brook bottom) and on emergence to the atmosphere, forms a carbonate tufa which smothers the natural valley (Emery, 2013; Milodowski *et al*., 2013). Various locations were sampled at this site. They include two source areas from a seepage at the base of the spoil and a drainage sough from the adjacent Peak Dale valley. Downstream samples in the system were taken to assess the evolution of the waters downstream of emergence. These included the east side of the tufa, midpoint of the leachate source zone and an additional site around 400 m downstream of the site.

Leachate samples were also collected from other lime spoil affected waters at Doveholes discharge sample prefix DH (53°17′37.27″N, 001°53′12.16″W), a minor seepage and pond draining lime kiln spoil on the roadside of the A6, south of Dove Holes village, and from the Newline works Derbyshire sample prefix PD (53°17′46.93″N, 001°52′18.11″W), a roadside ditch (alongside Dale road in

Doveholes dale) receiving high pH discharges from the Newlime Quarry and limeworks (Figure 4.10).

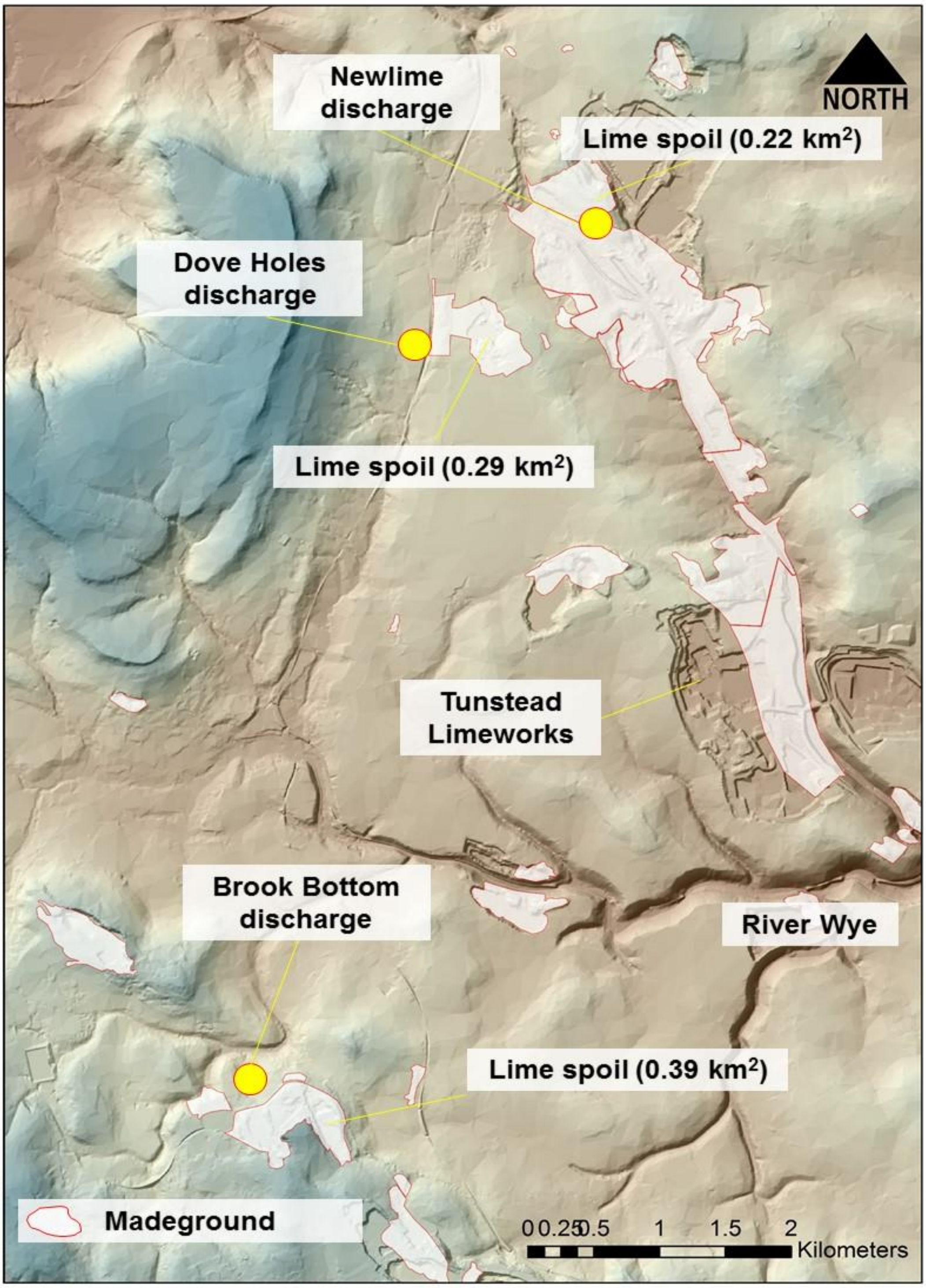

Figure 4.10: Map showing Lime-spoil sites sampled in the Buxton area

At these sites, only water samples and secondary precipitates were collected, and in accordance with method described in section 3.4.1. No source material was obtained at these sites. At the Brook bottom site, secondary deposits were obtained from 3 upstream sampling spots (BB1, BB2 and BB3) and a micrite-type sample was collected downstream of the site. The pH, conductivity and redox potential (Eh) of leachate samples at these sites were analysed in similar way as the Yarborough and Consett sites. Similarly, the field alkalinity of water samples from Brook bottom and Doveholes were determined using the same method as previous sites. Unfortunately, the alkalinity of the leachate sample from Peakdale was not reliably measured because the phenolphthalein indicator was insufficient at the time of sampling hence no geochemical modelling was done for this site. The major elements and trace elements in the leachates and secondary precipitates were analysed using ICPOES and ICPMS respectively, in same way as the previous sites. The mineralogy of the secondary precipitates was analysed using XRD.

4.3.2 Brook Bottom, Doveholes, and Newline Quarry Derbyshire – Results

The major and minor elemental composition of leachates sampled at the lime spoil sites are presented in Table 4.8.

Table 4.8: Baseflow major physical and chemical parameters and major and trace elemental constituent of filtered (0.45 μm) leachate samples from the lime spoil sites. Source samples on each sampling site are presented alongside Environmental Quality Standards (EQS), where prescribed.

	Site			
Determinand	BB	DH	PD	EQS
pH	13.0 ± 0.2	13.0 ± 0.1	11.3 ± 0.2	6 - 9
Temperature (^{o}C)	10.6 ± 0.2	14.5 ± 0.4	10.9 ± 3.2	
Electrical conductivity (μS/cm)	7652 ± 88	6775 ± 122	451 ± 34	
Eh(mV)	-0.07 ± 0.01	-0.07 ± 0.02	-0.03 ± 0.01	
Major ions (mg/L)				
Ca	615 ± 34	584 ± 54	11 ± 2	
Mg	19 ± 2	19 ± 4	1.3 ± 0.2	
K	88 ± 5	68 ± 5	13 ± 2	
Na	67 ± 7	10 ± 2	57 ± 4	
Cl^-		30 ± 3		
SO_4^{2-}		20 ± 4		
Total Alkalinity (as $CaCO_3$)	1562 ± 113	1606 ± 109	N.M	
OH^-	1486 ± 89			
CO_3^{2-}	76 ± 9	1459 ± 76		
HCO_3^-		147 ± 23		
Trace elements (μg/L)				
Ba	500 ± 45	2600 ± 102	1.6 ± 0.3	110^
Cr	7.3 ± 1.2	6.2 ± 1.3	7.4 ± 1.2	50*+
Li	363.5 ± 45.3	143 ± 12	23 ± 3	260^
Mo	12.5 ± 1.6	7 ± 2	11.5 ± 2.1	1600^
Ni	19.1 ± 1.5	19.2 ± 2.3	8.5 ± 1.3	200*+
Pb	26 ± 5	51 ± 3	12 ± 2	20*+
Sb	7.8 ± 1.7	1.8 ± 0.4	6.5 ± 1.1	
Si	37 ± 6	300 ± 13	960 ± 32	
Sr	1180 ± 32	1010 ± 93	160 ± 23	15^
V	2.2 ± 0.4	0.10 ± 0.02	0.10 ± 0.03	60*+

* = hardness related, value quoted for hardness values encountered here; $^{+}$ = as dissolved fraction which can pass through a 0.45μm filter. EQS taken from EU WFD with exception of '^' which are from Buchman (2008), N.M – not measured.

The average pH of the leachates across these sites range from 11.3 ± 0.2 to 13.0 ± 0.2. Leachates from all the lime spoil sites were strongly reducing in nature. Electrical conductivity was greatest at Brook bottom (7652 ± 88 µS/cm) and lowest in Peakdale (451 ± 34 µS/cm). Leachates from Brook bottom were of the Ca-OH type while leachates from Doveholes were dominated by Ca - CO_3 ions. Barium and strontium were the most abundant trace elements in the lime spoil leachates reaching maximum levels of 2600 ± 102 and 1180 ± 32 µg/L respectively, and exceeding regulatory limits. The concentrations of chromium, molybdenum, nickel and vanadium were below regulatory limits in the lime spoil leachates.

Figure 4.11 displays the mineral phases present in the secondary precipitate collected from Brook bottom, Doveholes and Peakdale. XRD analyses of secondary precipitates from Brook bottom revealed that the material was calcite. However, at Doveholes and Peakdale, the secondary precipitate was predominantly calcite with trace of quartz.

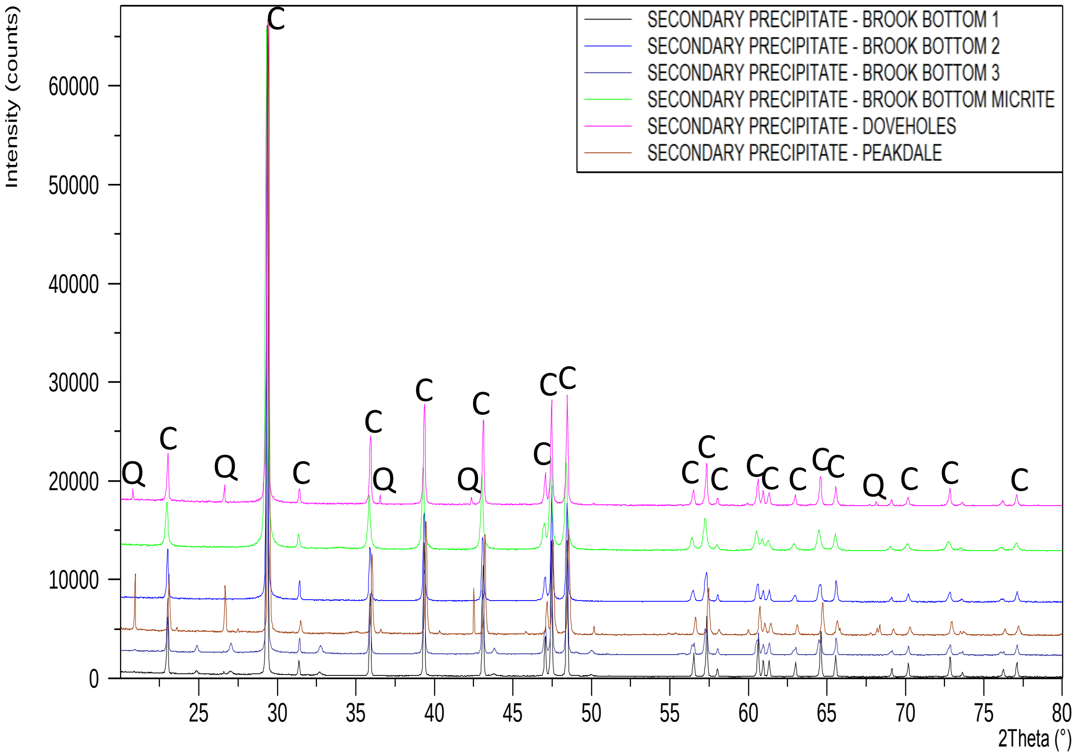

Figure 4.11: XRD diffractogram of secondary precipitates from the lime spoil sites at Brook bottom, Doveholes and Peakdale Derbyshire. C- Calcite ($CaCO_3$), Q – Quartz (SiO_2)

Table 4.9 presents data for elemental composition of secondary precipitates obtained from the lime spoil sites. Calcium was the most abundant element in the secondary precipitates. The concentration of barium, strontium and antimony in the secondary deposits, at the lime spoil sites, were higher than threshold values for sediments in surface waters (Table 4.9). The levels of arsenic, vanadium and nickel in the secondary deposits were below threshold values at the lime spoil sites (Table 4.9).

Table 4.9: Major ions and trace element composition of digested secondary deposits from lime spoil sites

	Site			
Major ions (% by weight)	**BB**	**DH**	**PD**	**EQS**
Ca	18.49 ± 0.41	8.82 ± 0.54	19.60 ± 3.23	
Mg	0.020 ± 0.003	0.010 ± 0.004	0.27 ± 0.06	
Si	1.52 ± 0.23	2.13 ± 0.32	5.14 ± 1.22	
S	0.18 ± 0.03	0.11 ± 0.02	0.26 ± 0.03	
Al	0.0010 ± 0.0001	0.0020 ± 0.0003	0.86 ± 0.11	0.26
K	0.03 ± 0.01	0.06 ± 0.01	0.26 ± 0.05	
Na	0.03 ± 0.01	0.03 ± 0.01	0.09 ± 0.01	
Sr	0.020 ± 0.003	0.021 ± 0.005	0.06 ± 0.01	0.01
Trace elements (mg/kg)				
As	3.9 ± 0.8	3.5 ± 1.2	9.6 ± 2.1	6
Ba	400 ± 21	900 ± 145	200 ± 23	0.7
Cr	1.3 ± 0.2	5.3 ± 1.2	34.4 ± 5.7	37.3
Li	4.3 ± 0.7	13.5 ± 3.2	22.4 ± 3.6	
Mo	2.8 ± 0.6	2.3 ± 0.6	-	
Ni	5.1 ± 1.2	5.4 ± 2.1	48.7 ± 7.8	18
Sb	3.4 ± 0.6	1.9 ± 0.7	6.0 ± 1.2	0.2
V	0.9 ± 0.3	5.4 ± 1.2	29.3 ± 3.5	50

EQS – Environmental Quality Standard taken from Buchman (2008). BB – Brook Bottom, DH – Doveholes, PD - Peakdales

4.4 Site investigation discussion

4.4.1 Chemistry of source material (Steel slag)

The chemical composition and mineralogy of the studied slag types were consistent with previous literature (Barra *et al.*, 2001; Manso *et al.*, 2005; Nicolae *et al.*, 2007; Radenovic *et al.*, 2013; Reddy *et al.*, 2006; Roadcap *et al.*, 2005; Shi, 2004; Yildirim and Prezzi, 2011). Calcium was the most abundant element in all the slag types. Typical weathering products of slag such as $CaCO_3$, $Ca_2Fe_2O_5$, SiO_2, and Fe_3O_4 were found in some of the steel slag, indicating that they are undergoing secondary mineralisation at the field disposal sites (Roadcap *et al*., 2005).

The BOF slag was rich in iron, hence phases such as hematite and srebrodolskite were detected in its mineralogy. Aluminium was more dominant in the ladle slag compared to other analysed slag types hence phases such as gehlenite and spinel minerals were observed by XRD (Manso *et al*., 2005; Tossavainen *et al*, 2007). The presence of minerals like akermanite and monticellite in the desulphurised skimmed slag was due to the abundance of magnesium and silicon in the sample (see Table 4.1). Magnesium was used as a desulphuriser in the steelmaking process in this case, to obtain low sulphur grade steel (International Magnesium Association, 2012), hence its higher abundance in desulphurised skimmed slag compared to the other slag types.

The steel slag samples were heterogeneous in nature. This could have been due to factors such as the manufacturing process used, age of slag, cooling technique and nature of co-deposited waste (Bayless and Schulz, 2003). This variability is reflected in the range of values, although narrow, obtained from analyses of replicate samples obtained from within the same disposal site (see Table 4.1), a similar observation to that reported by Harber and Forth, 2011. As such, there is a degree of uncertainty as to what values would be representative of the entire deposits of slag on average. The trace element composition of the various slag types varied depending on the nature of the sites and slag types (Table 4.1). Also, the concentrations of elements such as arsenic, barium, chromium, and lithium were consistent with values reported in literature (Roadcap *et al.*, 2005). The BOF slag was enriched with vanadium and chromium, hence making it a suitable feedstock for valuable metals recovery.

4.4.2 Leachate chemistry

4.4.2.1 Physico-chemical parameters and major elements

The highly alkaline nature of the steel slag leachates may be due to the weathering of calcium silicates present in the steel slag (see Figure 4.2; Eqn. 4.2) while the elevated pH of the lime spoil associated waters could be attributed to the hydrolysis of lime and subsequent dissociation of portlandite in solution (see Eqns. 2.1 – 2.2; Mayes *et al*., 2008; Roadcap *et al.*, 2005).

$$Ca_2SiO_4 \quad + \quad 4H_2O \quad \rightarrow \quad 2Ca^{2+} \; + \; H_4SiO_4 \; + \; 4OH^- \qquad (4.2)$$

The pH of the Dene Burn Consett leachates were however relatively low compared to other study sites, possibly due to the effect of the mixing of source samples with acidic surface runoff in subterranean drainage systems prior to emergence (Mayes *et al*., 2008), while the sulphate enrichment at the Howden Burn site was due to the dumping of sulphur-rich waste (such as fly ash, flue gas waste and coke works waste) at this site.

The calcium concentration in the leachates (both steel slag and lime spoil) appeared to correlate positively with pH (R^2 = 0.8252) and conductivity (R^2 = 0.641), hence implying that calcium may be a key controlling factor in this type of environment (Figure 4.12). This is consistent with other reported observations on work carried out at the Consett site (Hull *et al*., 2014), where correlations between major parameters and many trace elements showed strong positive relationships as summarized in Table 4.10.

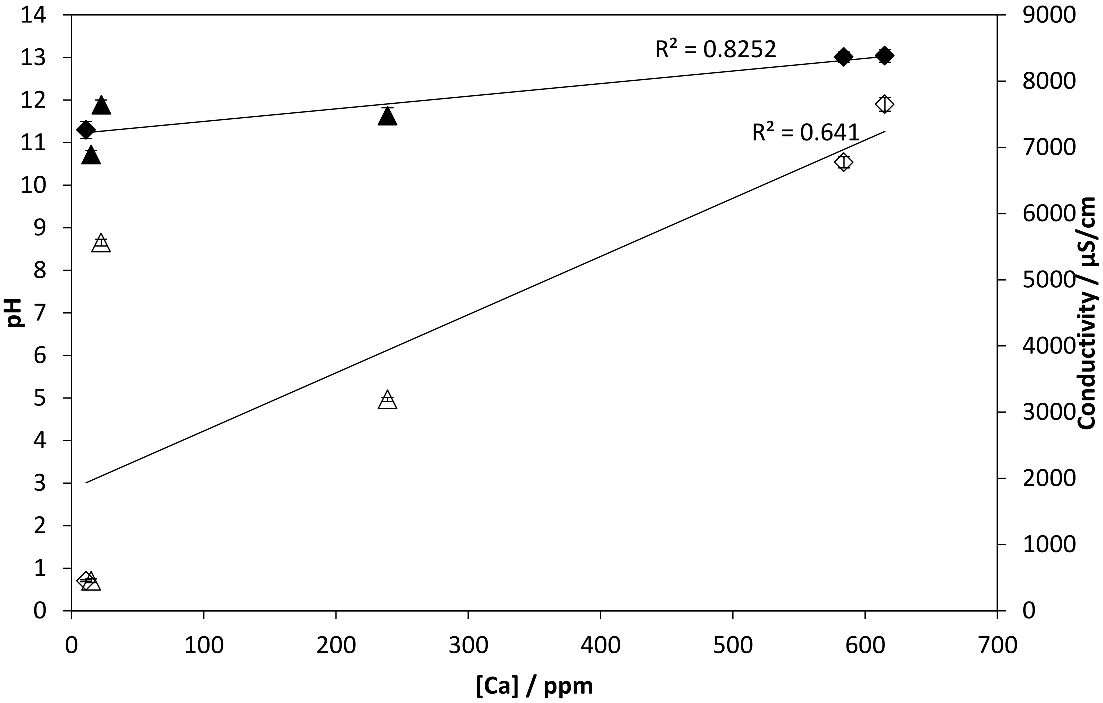

Figure 4.12: Combined plot of all study sites showing relationship between pH, conductivity versus [Ca]. (Shaded points – pH; unshaded points – conductivity; triangles – steel slag sites; diamonds – lime spoil sites). Error bars represent repeatability.

Table 4.10: Spearman's rank correlation matrix for selected major physical and chemical parameters and metals across the Dene and Howden Burns, *n* = 57 for all except those including $CaCO_3$ precipitation rate (*n* = 16). ** = *P* < 0.001.

	pH	Conductivity	$CaCO_3$ precipitation rate	Ca	Sr
Conductivity	0.778**				
$CaCO_3$ rate	0.965**	0.850**			
Ca	0.877**	0.896**	0.885**		
Sr	0.628**	0.781**	0.937**	0.743**	
V	0.761**	0.782**	0.920**	0.788**	0.761**

Carbonate alkalinity was the dominant source of fluid alkalinity at all the study sites with the exception of Brook bottom, a lime spoil site, in which about 95 % of total alkalinity was due to hydroxide (OH^-). The dominance of hydroxide ions at Brook bottom was responsible for the very high pH recorded here (Table 4.8). Leachates from most of the study sites were iron deficient and reducing in nature except at Howden Burn and Dene Burn Consett where water samples were slightly oxidizing possibly due to the oxidation of iron at this site (Table 4.5).

The high levels of dissolved oxygen at the Consett site was facilitated by the cascading, high gradient longitudinal profiles of both streams. Macronutrient concentrations in the waters were modest and reflect the groundwater-dominated sources for both streams, which themselves rise from predominantly made-ground (i.e. waste heaps associated with the former steelworks) with only a sparse cover of low-intensity grazing throughout the catchments (Table 4.5).

The hydrochemical facies of the leachate samples vary among sites with possible implications for secondary precipitation. For example, calcium levels in the leachates from Yarborough were about one order of magnitude lower than that obtained at Consett. This possibly suggests that secondary precipitates formed at Yarborough might be less Ca-rich compared to those at Consett. Futhermore, at Yarborough, the Na enrichment in leachates may likely be due to the use of sodium carbonate or sodium chloride as slag modifying agents in the steelmaking process in order to improve the fluidity of the slag and also reduce the amount of hot metal trapped within the slag (Li *et al.*, 2012). The precipitation of mineral phases such as calcite, aragonite, dolomite, and strontianite were thermodynamically favoured at all sites possibly due to the abundance of the carbonate ions (Appendix A4). The leachates were also supersaturated with brucite (Appendix A4). The leachates from both steel slag and lime spoil systems were undersaturated with respect to quartz, even though this mineral was observed via XRD, thus implying that the presence of quartz in the secondary precipitates may have been due to dirt contamination during sample collection. Some other phases such as chrysotile, diopside, forsterite were supersaturated in these waters (Appendix A4), however their origin remains uncertain because the kinetics of formation of these phases are far too slow to occur at surface temperature and pressure (Korytkova *et al*., 2007; Lüttge and Metz, 1993).

4.4.2.2 Minor elements

At all study sites, none of the trace elements surveyed exceeded prescribed aquatic life standards in the European Union at the hardness of the waters sampled with the exception of lead (up to 210 µg/L) (Table 4.2). However, lead (Pb) is insoluble at alkaline pH and as a result in most cases it isn't considered as a contaminant of regulatory concern in such waters (McLean and Bledsoe, 1992). Aluminium, which is a determinand of potential concern given mobility (as aluminate) at pH > 8 in surface waters, did not exceed prescribed Environmental Quality Standard (EQS) values and at most sample sites were below detection limits (5 µg/L). Iron (Fe), while present at some sites, was also not at concentrations that would warrant regulatory concern (Tables 4.2 and 4.6). Chromium, copper, nickel and zinc were either below prescribed EQS or detection limits in all samples. However, steel slag drainage can be characterised by enrichment in elements that are (a) not typically encountered in polluted wastewaters, and (b) not routinely monitored by regulatory agencies. These include steel additives and/or elements that are mobile under high pH conditions such as antimony, barium, lithium, molybdenum, strontium and vanadium, for which no formal European water quality standards are currently set. In as much as the aggregated aquatic life standards of Buchman (2008) have been used as an initial screening tool for the potential toxicity of some elements in this work, it must be stressed that standard toxicological tests rarely assess the broader chemical matrix of waters in the high pH spectrum.

The lime spoil sites were barium-rich and in most cases, exceeded screening values (Table 4.8) unlike the steel slag leachates where barium levels were low. It is apparent that strontium (Sr) exceeded provisional acute EQS values at all discharges. Lithium (Li) concentration of leachates sampled at the lime spoil site (Brook bottom) and slag disposal site (Howden Consett) surpassed recommended acute EQS values. Vanadium (V) was present at source in modest concentrations (< 52 μg/L) in all discharges (Table 4.6). While no formal ambient aquatic life standards are prescribed for V, concern has been raised for V in drinking waters with a suggested drinking water standard (DWS) of 15 μg/L (Gerke *et al*., 2010).

4.4.2.3 Downstream evolution of waters

At Dene Burn and Howden Burn, the concentrations of many elements declined with distance from the sources, thus implying that similar precipitation mechanisms was occurring at these sites which is most likely precipitation of calcite due to a rise in carbonate concentration (in-gassing of CO_2) into Ca-Si rich waters and precipitation of quartz due to falling pH. It must be stressed that the calcium content of the leachates, which is guided by the dissolution of calcium-rich phases in the source material, governs the pH and subsequent calcite precipitation rate in these alkaline stream systems (Frengstad and Banks, 2007). In most cases, the calcium content must exceed a threshold (not known in this case), in order for precipitation to occur. For example, in lower reaches of the Dene Burn, instream Ca^{2+} load gains were observed (< 20 mg/L; Figure 4.9) which is most likely ascribable to inputs of Ca^{2+}-rich waters from tributaries draining springs from Coal Measures strata (Mayes *et al.*, 2008). This amount is consistent with field observations in showing minimal, if any carbonate precipitation in these lower reaches (from 270 m from the source).

Precipitation rates at the source of the Howden Burn (up to 284 g $CaCO_3/m^2$/day) were an order of magnitude above the highest rates documented for natural tufa-precipitating streams, which are typically quoted in the range 0.2 - 10 g $CaCO_3/m^2$/day (Zaihua *et al.,* 1995; Miliša *et al*., 2006). The steep gradient stream morphology also lends itself to buffering of the waters with distance downstream (Figure 4.9), with thin films of leachate cascading over carbonate-crust barriers enhancing CO_2 in-gassing to the waters and subsequent calcite precipitation (Roadcap *et al.*, 2005). On the other hand, precipitation rates in the Dene Burn were towards the upper range of those found in natural karstic streams only in source areas (Figure 4.9). The precipitation rate data were also consistent with calculated calcite saturation indices (Figure 4.9), with values above +0.3 usually considered the threshold for heterogeneous calcium carbonate precipitation (Ford and Williams, 1991).

The Howden Burn retained a high $SI_{calcite}$ throughout its course at values above thresholds where homogeneous calcite precipitation would be anticipated from solution (quoted at +1.5: Ford and Williams, 1998). The high rates of carbonate deposition in source areas of both streams compare with those documented at other Ca-rich alkaline waters (Effler and Brooks, 1998) and are similar to mineral precipitation rates at analogous sites affected by other forms of inorganic post-industrial pollution, notably circum-neutral pH coal mine drainage (Edwards and Maidens, 1995; Jarvis and Younger, 1997).

4.4.3 Secondary products

Abundant secondary precipitates were apparent at all sites. These deposits were identified as primarily calcite, although in some cases there were traces of quartz and vaterite (at Consett). The observation of vaterite forming at the Consett sites was as a result of the rapid mineral precipitation occurring at this site, this phase appears to be short- lived and alters to the more stable calcite over time. Some potentially important trace elements (e.g. Sr, Ba and V) were attenuated in the calcite precipitates, this is in line with previous findings and a characteristic feature of alkaline settings (Mayes *et al.*, 2008). The formation of calcite at these sites seems to be governed by both biological activity and physico-chemical parameters.

4.5 Conclusions and management challenges

The chemistry of the source material (steel slag) obtained from the different sampling sites varied depending on the manufacturing process applied and the nature of the co-deposited waste. The composition of the waters draining from the slag mounds is consistent with previous studies at steel slag disposal sites in the UK (Mayes *et al*. 2006; 2008) and studies of slag leachate elsewhere in the world (e.g. Roadcap *et al.*, 2005). Alkaline leachates (both steel slag and lime-spoil) are characterised by elevated pH and alkalinity. In steel slag, this hyperalkalinity is primarily due to carbonate while hydroxide is the dominant ion responsible for alkalinity at the lime spoil sites. The waters showed several unusual features such as (a) enrichment of metals not routinely monitored by regulatory authorities and (b) very high mineral precipitation rates. The high pH, derived from dissolution of oxide and hydroxide phases in the slag (Roadcap *et al*., 2005), meant all sites exceed regulatory pH guidelines for large distances and is consistent with high ionic strength of source waters. Also, the native negative Eh (redox potential) of the leachates at some of the sites is most likely responsible for the near absence of iron at the sampling sites due to the reducing environment generated by the source material, which leads to the occurrence of iron in the form of less mobile sulphides. There was visible evidence of precipitation of secondary phases on the surface of the steel slag at these field disposal sites, highlighting the simultaneous dissolution and precipitation processes that highlight slag weathering. Secondary deposits formed at these alkaline sites were predominantly calcite, possibly acting as a sink for certain trace metals, and traces of quartz. The secondary precipitates exhibited a layered structure, suggesting a time related deposition. Also, calcite precipitation decreases downstream at steel slag sites and increases with pH.

Lithium, strontium and vanadium levels in the steel slag and lime spoil leachates were higher than those typically encountered in natural surface waters (e.g. Hem, 1985), and were at concentrations similar to those documented due to mineralisation or mining-related enrichment (Kszos and Stewart, 2003; Jones *et al*., 2013). Barium levels exceeded regulatory standards at the lime spoil sites but not in the steel slag sites, hence it is advisable that barium is monitored during toxicity studies at lime waste related sites. Vanadium should be a particular focus for toxicity studies in hyperalkaline waters, given it is usually observed in its pentavalent, and most toxic, form under high pH conditions (Chaurand *et al*. 2007; Burke *et al*., 2012 b) and retains mobility under circum-neutral pH (Takeno, 2006). The mineralogy of the source material appears to be the key factor governing the release of most of the metals of interest particularly calcium, magnesium, silicon iron, nickel, molybdenum and vanadium with very low leaching efficiencies. Main mineral phases present in the steel slag (akermanite, gehlenite, srebrodolskite and monticellite) have very slow dissolution kinetics at high pH and hence may be limiting the leaching of major ions like calcium, magnesium and silicon while the studied trace elements may also be locked within these phases. Another possible reason for the attenuation of these elements could be due to the instantaneous precipitation of insoluble mineral phases occurring within the subsurface system hence decreasing their mobility in field settings. These lines of thought will however be investigated in detail in subsequent chapters.

Furthermore, some of the elements present in the leachates are also of potential monetary value as critical raw materials (Naden, 2013), such as lithium, vanadium and chromium. This raises the possibility of approaches that combine remediation with potential value recovery from legacy disposal sites. Given the buffering of highly alkaline waters is dependent on carbonate precipitation, remedial approaches need to focus on ways of encouraging calcite precipitation in controlled settings which would minimise the potential downstream impacts of these discharges on aquatic biota. Such approaches are considered in subsequent chapters.

5

Accelerated metal release from steel slag

5.1 Introduction

Steel slag can serve as a secondary reserve for various metals given the production processes that enrich metals in by-products (Chapter 4). Some of these metals are however potentially harmful to the environment when leached (Chapter 2, Chapter 4). As a result, it is beneficial to recover metals from steel slag while encouraging slag utilisation. There is a rising interest in the utilisation of steel slag for metal recovery (Shen and Forssberg, 2003); not only due to the large scale at which it is generated annually, but also due to the abundance of legacy stockpiles at some sites, some of which have been in existence for a century (such as Yarborough landfill, Tata Steel Scunthorpe).

Leaching is a crucial step in the recovery of metals from steel slag. It can be achieved using an acid or a base (see Chapter 2). It is carried out so as to convert the metal of interest into more soluble forms which can then be recovered. In field scenarios, the concentration of metals within the leachate generated by the slag material at these disposal sites are not up to recoverable amounts (see Chapter 4), hence recovering metals from it would be expensive. In addition, directly digging up legacy sites is feasible, but is also expensive, energy intensive and would cause a lot of environmental disturbance. As a result, it would be desirable to develop a method that incorporates in-situ recovery as well as intensifies the concentration of metals of interest in the resultant leachate.

To this end, using batch leaching tests, this chapter aims to provide a comparative assessment of chemical leaching (with HCl) alongside organic amendments in intensifying the concentration of valuable metals (e.g. V, Ni, Li) in leachates prior to recovery, while promoting long term chemical stabilisation of weathered residues.

Rationale for the use of municipal compost as an organic amendment

Previous work carried out at the University of Hull UK investigating approaches for source minimisation of leachate generation from steel slag heaps, revealed that by capping steel slag with municipal compost, the concentration of metals (V, Mo, Cr, Li) were intensified by up to an order of magnitude compared to control experiments (slag only) (Dyson, 2013). This approach could act as a route for metal intensification prior to potential recovery using existing technologies.

Furthermore, municipal compost is cheap and readily available. It can also act as an additional source of carbon to the steel slag (Wright *et al.*, 2008), thus promoting carbonate precipitation within the alkaline system. The presence of dissolvable organic materials in the municipal compost could contribute towards enhancement of the weathering rate of the steel slag (Karlsson *et al.*, 2011; Renforth and Manning, 2011). Capping of steel slag at disposal sites with municipal compost can also help to minimise the production of surface dusts due to tipping activities.

The proposed approach, if successful, can be adopted as a potential route for offsetting carbon in the steel industry and the resultant leachate generated from the process can be treated with low – cost natural systems (wetlands), which could also serve as habitat for wildlife.

5.2 Methodology

5.2.1 Feedstock collection and preparation

BOF steel slag was collected from the Yarborough landfill site at Tata Steel, Scunthorpe because the landfill was composed of mainly BOF type slag. The steel slag were manually sorted (to eliminate stones and other unwanted materials) and crushed with a Tema mill (tungsten carbide) to reduce the size of the steel slag. The crushed steel slag was sieved to obtain a 63 μm – 420 μm size fraction for the leaching tests. This size fraction is consistent with the standardized batch leaching test procedures (BS EN 12457 – 2). Although care was taken to perform sufficient homogenization of the sample, a certain degree of variability and heterogeneity within the sample is bound to exist due to the complex nature of the waste matrix.

Municipal compost used in this experiment was collected from a waste recycling facility at Wastewise Hull. The compost was digested in accordance with CEM method XprEN – 8 (USEPA method 3051A equivalent; see Table 3.6) and analysed for selected elements using ICP-OES. Data obtained revealed that the compost was BSI PAS 100 compliant in terms of concentrations of potentially toxic elements as shown in Table 5.1. This implies that the municipal compost was fit for purpose and deemed reliably safe.

Table 5.1: Concentration of potential toxic elements in compost used in this work

Element	**PAS 100 Compost (upper limit value in mg/kg)***	**Municipal compost used in this work (mg/kg)**
Chromium	100	30 ± 2
Cadmium	1.5	1.20 ± 0.05
Copper	200	76 ± 6
Lead	200	97 ± 3
Mercury	1	0.010 ± 0.002
Nickel	50	43 ± 2
Zinc	400	209 ± 5

*Data obtained from BSI PAS 100: 2005

5.2.2 Batch leaching tests - Accelerated release of metals from BOF slag

Batch leaching tests are suitable for assessing the leaching behaviour of metals of interest on a laboratory scale. They are simple to construct, reproducible and also have short time requirements. Three treatments were investigated in this chapter. In the first investigation, BOF slag was leached with ultrapure deionised water only. Next, BOF slag was mixed with municipal compost and leached with ultrapure deionised water. These treatments have been described in this chapter as ‘control test’ and ‘compost test’ respectively. In the third treatment, BOF steel slag was leached with acid, described herein as ‘acid extraction test’. Four replicates of the individual treatments were set up. The BOF steel slag was subjected to a standardised leaching procedure in accordance with BS EN 12457 – 2. However there were some modifications made to this method as described below.

Ultra high quality water (18.2 MΩ) was used as the leaching fluid in the control test and compost test while 0.1 M HCl served as the leachant for the acid extraction test. The liquid /solid ratio for the control, compost and acid leaching tests were kept at 10:1. For the compost experiments, the DI water: steel slag: compost ratio used was 10:1:0.2. The leaching tests lasted for 72 hours and the flasks were agitated at a speed of 200 osc/min in a side to side rotation style at room temperature. Leachate aliquots (5 ml), representing about 2 % of the original volume, was sampled at different times (1, 3, 6, 24, 48, 72 hours) during the course of the experiments without replenishing the solution. The sampled volume was chosen in order to ensure minimal changes in the L/S ratio of the system and minimise equilibrium effects.

Leachates were filtered through 0.45 μm membranes filters, acidified with concentrated HNO_3 and subsequently analyzed for dissolved concentrations of major ions (Ca, K, S, Ba, Mg, Si, Na, Sr) and trace metals(Li, V, Ni, Mo) by ICP emission spectroscopy (ICP-OES; NF EN ISO 11885) and ICP-MS respectively. The pH and conductivity of the leachates were measured regularly according to method detailed in section 3.5.1.1.1. At the end of the leaching period, solid solution separation was achieved using a centrifuge at 6000 rpm for 10 minutes. The solids were rinsed with ultrapure UHQ water and oven dried at 90 °C for 6 hours in order to get rid of moisture and contaminants that might be present on the surface. Mineralogy, surface area and porosity of the leached and non-leached slag samples were determined using XRD, BET and BJH methods described in section 3.4.3 and section 3.4.6 respectively.

5.2.3 Statistical analyses

The Kruskal-Wallis test was conducted on the various treatments so as to ascertain the statistical differences in all treatments. This was achieved using Minitab software. Graphs were plotted using Microsoft Excel 2007, to display the leaching patterns of elements of interest over time in the various treatments.

5.3 Results

5.3.1 Physico-chemical parameters

Figures 5.1 (a) and (b) describes the effect of accelerated leaching of BOF slag on pH and conductivity. The pH in the acid experiments rose from 7.2 ± 0.6 to 10.1 ± 0.4 and remained relatively unchanged in the compost and control experiments with values of 11.7 ± 0.1 and 12.10 ± 0.04 respectively, during the 72 hrs. leaching period. The electrical conductivity of leachates from the acid extraction test rose from 2.4 ± 0.4 to 3.2 ± 0.3 mS/cm, 0.43 ± 0.13 to 0.46 ± 0.09 mS/cm for compost treatment, and declined from 0.72 ± 0.14 to 0.57 ± 0.14 mS/cm for control experiment during the leaching time.

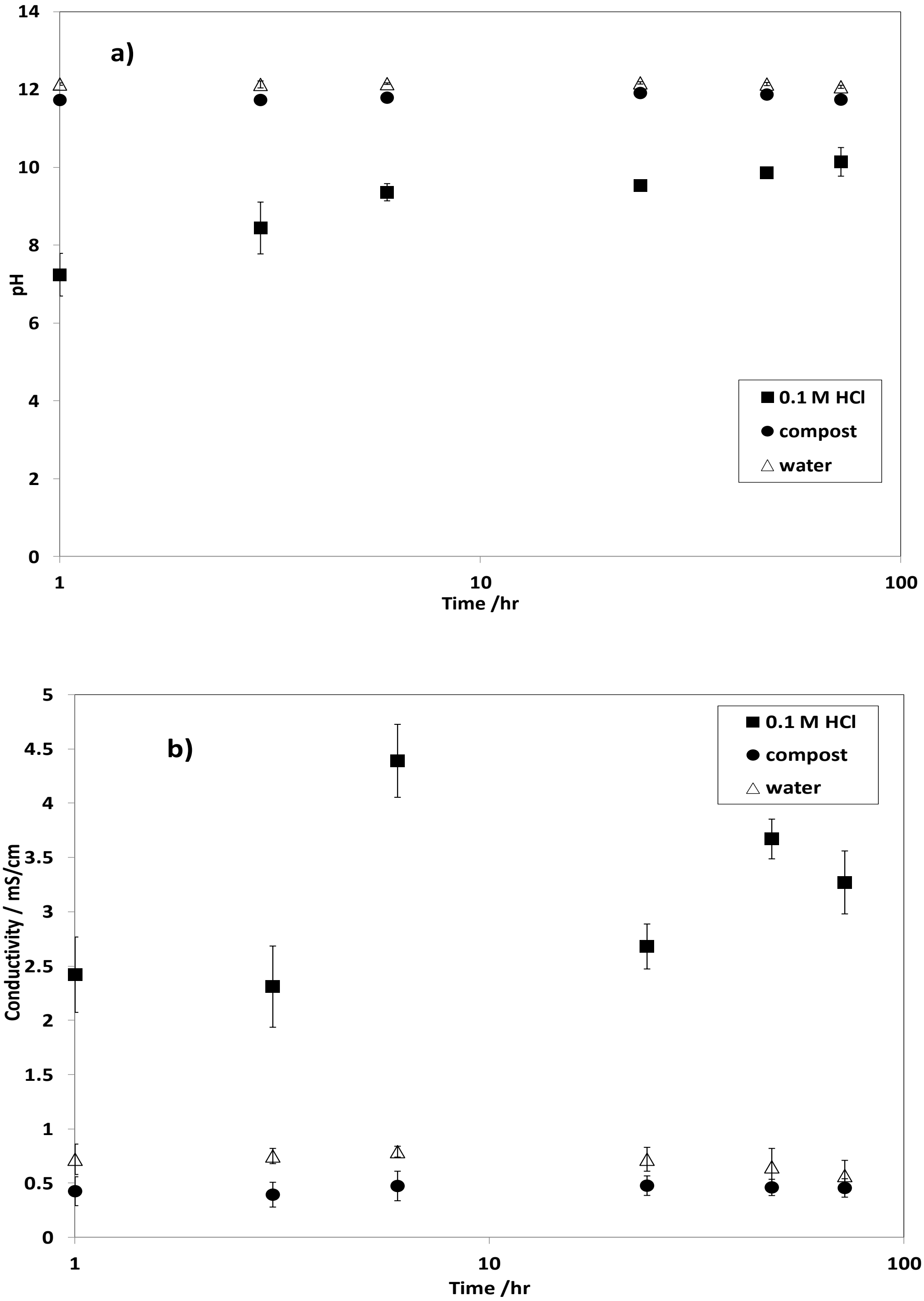

Figure 5.1: Effect of accelerated leaching of BOF slag on (a) pH (b) conductivity. Time axis is reported in log scale and errors bars represent repeatability (n=4).

5.3.2 Major elements

A series of batch tests were set up to investigate and compare the leaching behaviours of selected metals in BOF steel slag leached with either deionised water or dilute hydrochloric acid, and a mix of steel slag and municipal compost leached with deionised water. Figures 5.2 – 5.5 show the leaching patterns of selected metals over a 72 hour period in the treatments listed above. Note the log scale on the time axes. Error bars represent repeatability (n=4).

5.3.2.1 Calcium and Sulphur

As can be seen in Figures 5.2 (a) and (b), calcium and sulphur displayed a similar leaching pattern over time during acid extraction. There was an initial fall in amount leached within the first 3 hrs. followed subsequently by a steady rise in the amount of calcium and sulphur leached from t = 6 h onwards during acid leaching.

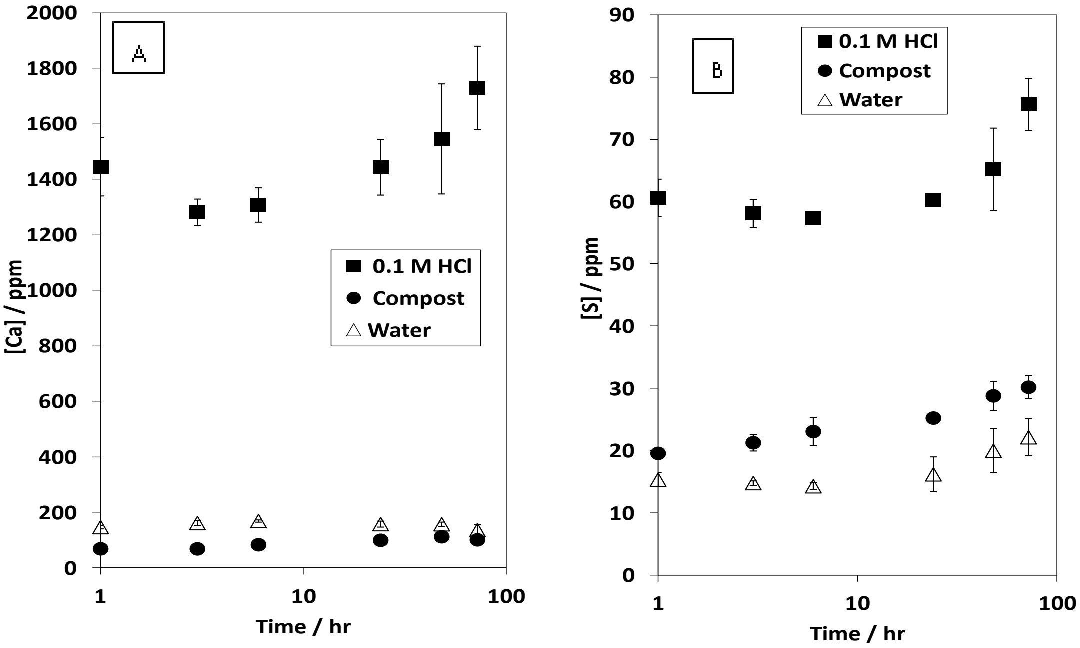

Figure 5.2: Effect of accelerated leaching of BOF slag on the leaching patterns of (a) calcium (b) sulphur. Time axis is reported in log scale and errors bars represent repeatability.

Calcium and sulphur leaching using acid was far higher, in some cases, by an order of magnitude, compared to water extraction (control) and compost amendment tests. In the water extraction and compost amendment tests, leaching of calcium was found to be relatively constant throughout the leaching period. However, the amount of calcium leached in the compost amendment test was marginally lower than that reported for the control test. The concentrations of calcium in the acid leached slag were 1445 ± 105 ppm and 1729 ± 150 ppm at the start and end of the experiment respectively. In the compost treatment, calcium levels were 68 ± 9 and 100 ± 6 ppm at the initial and final stages of the experiment. In the water extraction test (control), the amount of calcium leached dropped from 146 ± 6 to 136 ± 19 ppm by the end of the leaching period (72 hrs.).

As shown in Figure 5.2 (b), there was an initial decline in sulphur leaching within the first 3 hours followed by a gradual increase in amount of sulphur leached from the steel slag for the rest of the leaching period in the control test. In the compost amended steel slag, an initial rapid leaching of sulphur was observed within the first 6 hours of the experiment and the leaching reached equilibrium after 48 hours of leaching. The concentrations of sulphur in the acid leached slag were 61 ± 3 ppm and 76 ± 4 ppm at the start and end of the experiment. In the compost treatment, sulphur levels were 20 ± 1 and 30 ± 2 ppm at the initial and final stages of the experiment. In the water extraction test (control), the amount of sulphur leached rose from 15 ± 1 to 22 ± 3 ppm by the end of the leaching period (72 hrs.).

5.3.2.2 Magnesium and Silicon

It can be seen from Figure 5.3 (a) that the maximum concentration of magnesium leached from the steel slag was reached after 3 hours of leaching with acid, this was followed by a consistent fall onwards. The concentration of magnesium in the acid test dropped from 276 ± 26 ppm at 1 hr. of leaching to 65 ± 7 ppm after 72 hrs. of leaching. The concentration of magnesium leached in the control and compost experiments were negligible and below detection limits.

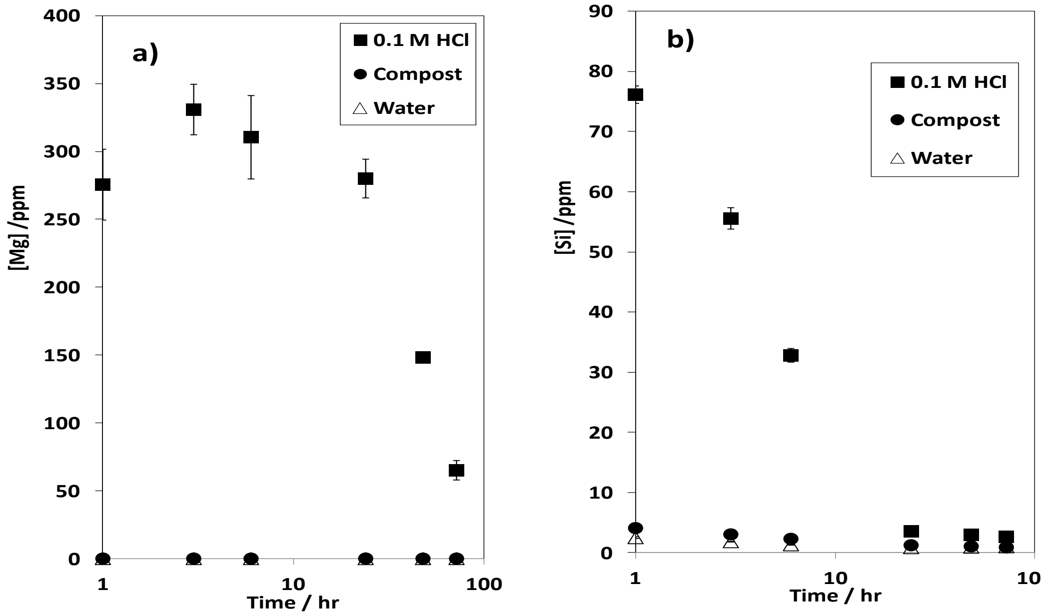

Figure 5.3: Effect of accelerated leaching of BOF slag on the leaching patterns of (a) magnesium (b) silicon. Time axis is reported in log scale and errors bars represent repeatability.

A steady fall in silicon leaching was observed in the acid leaching experiments, the most drastic fall was observed after 6 hours of leaching (see Figure 5.3 b). Silicon levels fell from 76 ± 1 to 2.6 ± 0.5 ppm by the end of the leaching experiment. Concentration of silicon leached in the compost experiment was slightly higher than that recorded for the control test, albeit significantly lower than the amount of silicon leached in the acid extraction test (see Figure 5.3 b). The initial and final concentrations of silicon were 4.6 ± 0.4 ppm and 0.9 ± 0.1 ppm in the compost test and, 2.5 ± 0.1 and 0.96 ± 0.04 ppm for the control. Magnesium and silicon show similar leaching trend in both the compost and control tests.

5.3.2.3 *Barium and strontium*

The leaching trend for barium and strontium during acid extraction were similar to that observed for calcium (see Figures 5.4 (a) and (b)). In the control (water) experiment, barium and strontium levels rose slightly in the first 6 hours before reaching equilibrium (as shown in Figures 5.4 a and b). In the compost amendment test, the levels of barium and strontium remained relatively unchanged throughout the leaching process. Barium and strontium release in the compost experiments were however lower relative to acid and control tests.

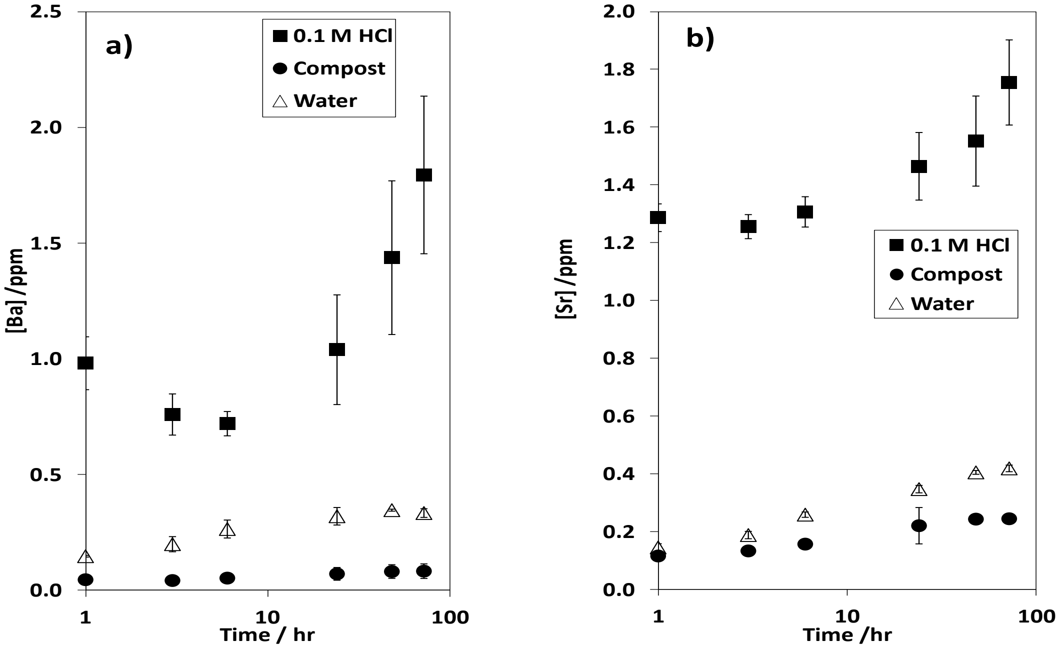

Figure 5.4: Effect of accelerated leaching of BOF slag on the leaching patterns of (a) barium (b) strontium. Time axis is reported in log scale and errors bars represent repeatability.

The concentrations of barium in the acid leached slag were 0.98 ± 0.11 ppm and 1.79 ± 0.34 ppm at the start and end of the experiment. In the compost treatment, barium levels were 0.04 ± 0.02 and 0.08 ± 0.03 ppm at the initial and final stages of the experiment. In the water extraction test (control), the amount of barium leached rose from 0.15 ppm to 0.33 ± 0.02 ppm by the end of the leaching period (72 hrs.).

On the other hand, the concentrations of strontium in the acid leached slag were 1.29 ± 0.05 ppm and 1.75 ± 0.15 ppm at the start and end of the experiment. In the compost treatment, strontium levels were 0.12 ± 0.01 and 0.24 ± 0.01 ppm at the initial and final stages of the experiment. In the water extraction test (control), the amount of strontium leached rose from 0.14 ± 0.01 ppm to 0.42 ± 0.01 ppm by the end of the leaching period (72 hrs.).

5.3.2.4 Potassium and sodium

Figures 5.5 (a) and (b) represent the release of potassium and sodium in the different extraction tests respectively. The highest levels of potassium and sodium were leached in the compost experiments while the control test leached the least levels.

Also, there was a steady increase in leaching of potassium and sodium throughout the leaching period. In the acid test, potassium levels increased from 12.1 ± 2.3 to 14.1 ± 2.1 ppm and sodium concentrations rose from 20.2 ± 1.6 to 23.5 ± 2.2 ppm. In the compost test, potassium levels increased from 46.9 ± 0.9 to 55.2 ± 1.6 ppm and sodium concentrations rose from 23.2 ± 0.5 to 31.5 ppm. In the water extraction (control) test, potassium levels increased from 6.7 ± 0.2 to 8.00 ± 0.04 ppm and sodium concentrations rose from 11.3 ± 1.3 to 18.3 ± 0.4 ppm.

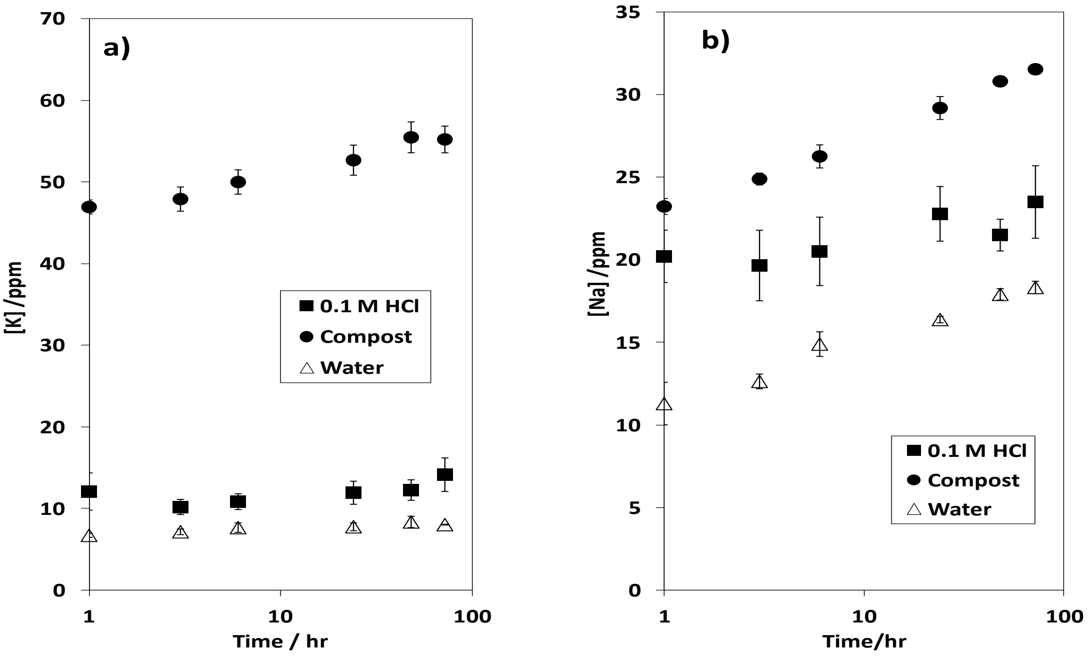

Figure 5.5: Effect of accelerated leaching of BOF slag on the leaching patterns of (a) potassium (b) sodium. Time axis is reported in log scale and errors bars represent repeatability.

5.3.3 Surface characterisation of leached product

The changes in surface properties of the BOF slag before and after leaching were examined using BET analysis (Table 5.2). Acid leaching of the BOF slag increased the BET surface area of the original material while the addition of compost led to a decrease of BET surface area by a factor of 2 (Table 5.2). The pore diameter of the material (non-leached BOF slag) falls within the mesoporous category (2 nm < *d* < 50 nm) and the obtained BET surface area results for all the treatments were far greater than that reported in Radenovic *et al*., 2013 (3.04 m^2 /g).

Table 5.2: Surface properties of leached BOF slag in batch experiments

	BET surface area (m^2/g)	Pore diameter (nm)
Non leached BOF slag	10.1 ± 0.4	16.3 ± 0.2
Water leached BOF slag (control)	12 ± 1	12.2 ± 0.5
Acid leached BOF slag	20 ± 2	10.0 ± 0.3
Compost amended BOF slag	5.5 ± 0.2	25.2 ± 3.4

5.3.4 Mineralogical characterisation

The changes in the mineralogy of BOF slag before and after leaching were examined using XRD analysis (Table 5.3). XRD analysis of the original material (non-leached BOF slag) used in this experiment, detected the presence of akermanite ($Ca_2MgSi_2O_7$), merwinite ($Ca_3Mg(SiO_4)_2$), portlandite ($Ca(OH)_2$), periclase (MgO), corundum (Al_2O_3), calcite ($CaCO_3$) and magnesite ($MgCO_3$). In the water extraction test, phases such as akermanite ($Ca_2MgSi_2O_7$), calcite ($CaCO_3$), corundum (Al_2O_3), quartz (SiO_2), periclase (MgO), magnetite (Fe_3O_4) and mullite ($Al_{4.44}Si_{1.56}O_{9.78}$) were detected.

Table 5.3: Mineral phases present in leached BOF slag (batch experiments); + phase detected

Phases	Original (Non leached BOF slag)	Water (control)	Acid (HCl)	Compost
Akermanite ($Ca_2MgSi_2O_7$)	+	+	+	
Quartz (SiO_2)		+		+
Calcite ($CaCO_3$)	+	+	+	+
Merwinite ($Ca_3Mg(SiO_4)_2$	+			+
Corundum (Al_2O_3)	+	+	+	+
Magnesite ($MgCO_3$)	+			
Periclase (MgO)	+	+	+	+
Portlandite ($Ca(OH)_2$)	+			
Magnetite (Fe_3O_4)		+		
Mullite ($Al_{4.44}Si_{1.56}O_{9.78}$)		+		
Calcium silicate hydrate ($Ca_2SiO_4.0.3H_2O$)			+	+
Brownmillerite $Ca_2(Fe_2O_5)$				+

In the acid extraction test, phases such as akermanite ($Ca_2MgSi_2O_7$), calcite ($CaCO_3$), corundum (Al_2O_3), periclase (MgO), and calcium silicate hydrate ($Ca_2SiO_4.0.3H_2O$) were present. In the compost test, mineral phases like quartz (SiO_2), calcite ($CaCO_3$), merwinite ($Ca_3Mg(SiO_4)_2$), corundum (Al_2O_3) periclase (MgO), calcium silicate hydrate ($Ca_2SiO_4.0.3H_2O$) and brownmillerite $Ca_2(Fe_2O_5)$ were observed.

5.3.5 Trace elements

The leaching patterns of selected trace elements over a 72 hour leaching period in the acid extraction, water extraction and compost amendment tests are presented in Figures 5.6 and 5.7.

5.3.5.1 Vanadium and molybdenum

The concentration of vanadium leached in acid, range from 245 ppb to 850 ppb. The highest level of vanadium was leached at 6 hours from the start of the experiment. Also, it can be seen that the leaching of vanadium occurred in two stages; an initial sharp leaching of vanadium in the first 6 hours followed by a decline in amount leached albeit at a slower rate for the rest of the period (Figure 5.6 a). The amount of vanadium released in the compost test was more than that recorded in the control (water) test. In the compost experiment, vanadium concentrations decreased from an initial concentration of 116 ± 19 ppb to a final concentration of 85 ± 1 ppb (Figure 5.6 a). Initial vanadium levels in the water extraction treatment were lower (40 ± 2 ppb) relative to the compost test, this amount decreased further by the end of the leaching period to a final value of 34 ± 2 ppb (see Figure 5.6 a).

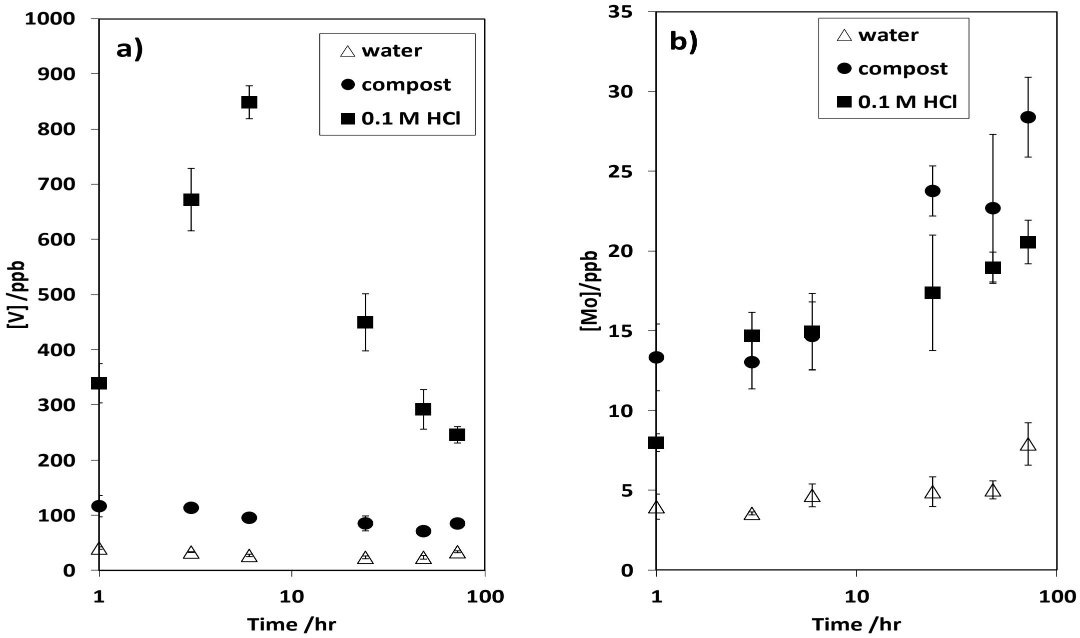

Figure 5.6: Effect of accelerated leaching of BOF slag on the leaching patterns of (a) vanadium (b) molybdenum. Time axis is reported in log scale and errors bars represent repeatability.

Acid leaching of the steel slag caused an increase in the leaching of molybdenum over time from 8.0 ± 0.6 ppb to 20.6 ± 1.4 ppb (see Figure 5.6 b). Molybdenum was more soluble in the compost experiment while the least Mo concentration was leached in water. The amount of molybdenum leached in the compost test rose from 13.3 ± 2.1 ppb to 28.4 ± 2.5 ppb, while in the case of the water extraction, the molybdenum level increased from 4.0 ± 0.8 ppb to 7.9 ± 1.3 ppb (Figure 5.6 b).

5.3.5.2 Lithium and nickel

During acid extraction, the amount of lithium and nickel leached from the BOF slag rose dramatically reaching concentrations of 125.3 ± 3.5 ppb and 142 ± 3 ppb respectively by the end of the leaching period of 72 hrs (see Figure 5.7). The levels of lithium and nickel leached using acid was in some cases 20 times greater than amounts recorded for the other treatments.

The release of lithium in water and compost tests were relatively constant during the leaching period, however concentration of lithium leached in water was somewhat higher compared to levels in the compost test (Figure 5.7 a). Lithium concentrations in the compost test decreased from 8.7 ± 1.0 to 6.6 ± 0.8 ppb, and dropped from 8.7 ± 1.0 ppb to 6.6 ± 0.8 ppb in the water extraction test (control).

As can be seen in Figure 5.7 b, there was no much difference in the amount of nickel leached for both the water and compost tests. Nickel concentrations in the compost test increased from 3.9 ± 0.9 to 8.7 ± 0.8 ppb, and dropped from 6.5 ± 0.1 ppb to 5.9 ± 0.3 ppb in the water extraction test (control).

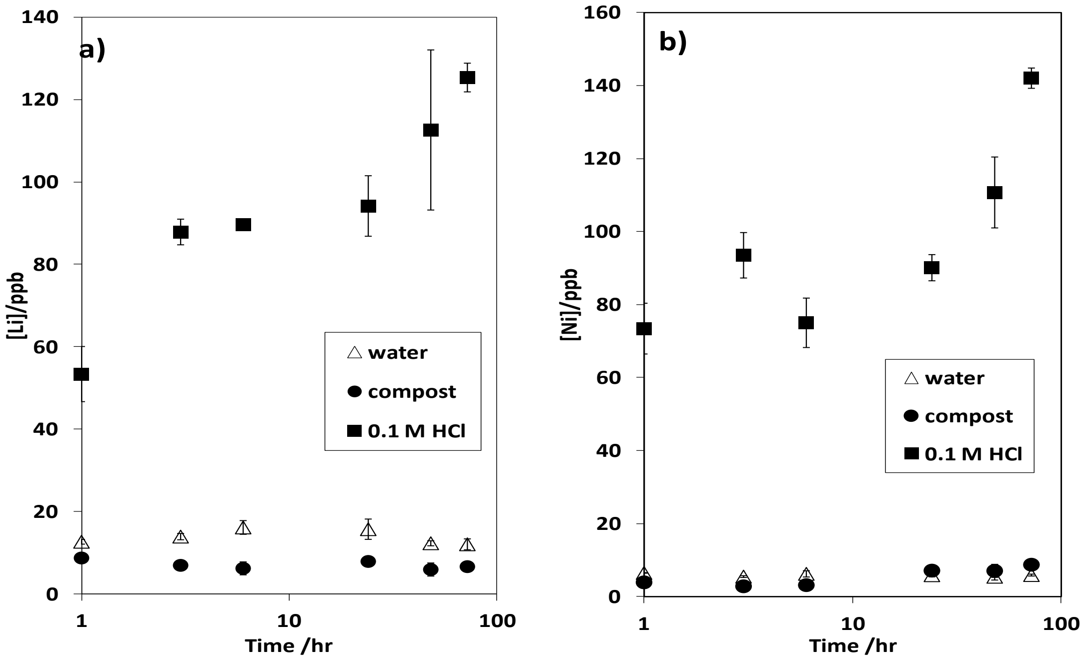

Figure 5.7: Effect of accelerated leaching of BOF slag on the leaching patterns of (a) lithium (b) nickel. Time axis is reported in log scale and errors bars represent repeatability.

5.4 Discussion

5.4.1 Leaching behaviour – Major elements

In the acid experiments, a greater amount of soluble species (e.g. Ca, Mg, Si, S) were leached from the slag matrix (Figures 5.2 & 5.3). Most of these elements are likely associated with calcium bearing phases and released through selective dissolution (Charun *et al.*, 2012; Mehrotra, 2011; Warren and Dudas, 1988). Acid leaching is a self-sustaining process which leads to formation of new available sites for dissolution of Ca-bearing phases. The increased surface area and lower pH of the acid-leached BOF slag compared to the control and compost tests also promotes the release of these elements. Acid leaching leads to an initial fall in the pH of the steel slag leachates via the production of protons which provides a buffering effect to the system. This effect is however short-lived, possibly due to the low strength of the acid used, in this case, 0.1 M HCl (Aarabi-Karasgani *et al.*, 2010), because most of the protons gets consumed within the first few hours of leaching.

5.4.1.1 Calcium

The observed leaching pattern for calcium in the acid experiments could possibly be due to an initial precipitation reaction and / or calcium sorption to negatively charged steel slag surface, followed by a later dissolution of calcium bearing phases possibly calcium silicate hydrate (Engström *et al.*, 2013). Also, in the batch experiments, there was a deviation from the usual pH dependent leaching behaviour for calcium. Usually, calcium release is favoured more at low pH, and becomes less soluble with increasing pH (Gitari *et al.*, 2009). This behaviour was however not observed in any of the batch experiments (Figure 5.2 a) where the effect of pH on calcium leaching was limited (Figures 5.1 a and 5.2 a). The amount of calcium leached from the steel slag in the compost experiment was relatively lower than the other treatments possibly because of the presence of brownmillerite (a less soluble calcium phase), in this treatment (see Table 5.3). The decrease in the surface area of compost amended steel slag observed due to the formation of calcite is also likely to be at least partly responsible for the lower levels of soluble species leached in this treatment.

5.4.1.2 Barium and strontium

The leaching trend for barium and strontium during acid extraction were similar to that observed for calcium, this would suggest that the controlling mechanism for these elements during acid extraction was the same. This is however not surprising because both barium and strontium are bivalent and can substitute calcium in the mineral phase controlling the dissolution. The slow release of barium and strontium in the water and compost tests could be due to incorporation of these elements in insoluble mineral phases such as $CaCO_3$, this is consistent with observations from a previous study (Gitari *et al*., 2009).

5.4.1.3 Magnesium and silicon

The leaching behaviour for magnesium and silicon in the all the batch experiments could be ascribed to be controlled by pH and the dissolution and precipitation of a magnesium silicate phase. The precipitation of magnesium silicate minerals are favourable at high pH and dissolution is promoted at lower pH (<9), hence there was an initial slight dissolution of this phase at pH < 8.4 in the acid treatment (Demadis, 2010). The use of ultrapure DI water as a leachant led to the release of lower levels of magnesium and silicon regardless of the abundance of these elements in the parent slag probably due to the poor selectivity of water towards these elements especially since they exist in less soluble phases (Gitari *et al*., 2009).

5.4.1.4 Potassium and sodium

In all the treatments, there was a steady increase in leaching of potassium and sodium throughout the leaching period, a unique pattern observed for Type 1 elements (Cappuyns *et al.*, 2008); this behaviour can be attributed to cation exchange reactions, in agreement with findings of Cappuyns *et al.*, (2008). However there was no visible relationship between the leaching of alkali metals and pH, thus implying that the effect of pH on the solubility and leaching of potassium and sodium into solution was limited, in line with the findings of Gitari *et al.*, (2009). The highest levels of potassium and sodium were leached in the compost experiments probably due to additional contribution from the leaching of soluble salts within the compost, while the control test leached the lowest concentrations.

5.4.2 Leaching behaviour – Trace elements

5.4.2.1 Vanadium and molybdenum

The release of vanadium and molybdenum in the compost tests is likely controlled by formation of soluble vanadium and molybdenum complexes. Municipal compost contains dissolved organic carbon and a number of organic species such as humic and fulvic acids which control heavy metal binding and aid the complexation process (Cappuyns *et al.* 2008). Complexation increases the mobility of vanadium and molybdenum via formation of soluble species. In addition, more soluble species are formed when the redox potential is positive, such as that recorded in the compost tests (+14 mV). This observation is in agreement with previous literature (Cornelis *et al.*, 2008; Karlsson *et al.*, 2011). The leaching behaviour of vanadium in the acid test could be attributed to a dissolution-precipitation type reaction involving the solubility controlling mineral phase, in this case probably a magnesium silicate phase which precipitates at high pH (Table 5.3; Aarabi-Karasgani *et al*., 2010; Demadis, 2010). An anomalous trend was observed between pH and oxyanion leaching. In the batch experiments, there was no visible positive correlation between pH and the leaching pattern for vanadium and molybdenum. This is in contrast with the findings of Centioli *et al*., 2008 and probably suggests that the effect of pH on the leaching of both elements is limited.

5.4.2.2 Lithium and nickel

Higher nickel leaching was observed in the acid leaching test (average pH 8.6) compared to the compost experiments (with mean pH 11.8). The increased solubility of nickel at lower pH may suggest that its release is governed by Ni $(OH)_2$, a mineral phase which precipitates at high pH and dissolves at lower pH. Hence, at high pH nickel tends to adsorb to this phase (Gitari *et al*., 2009). The precipitation of Ni $(OH)_2$ was further confirmed via geochemical modelling (data not shown here). Furthermore, the leaching behaviour of nickel in these experiments would suggest that the leaching of Ni is not governed by complexation reactions or dissolution of organic matter in the compost because these reactions are favoured at high pH, so more nickel would be expected to leach out of the slag instead of the rather low levels leached at high pH (Cappuyns *et al.* 2008). The solubility of lithium in acid was enhanced by up to a factor of 20 compared to the former two possibly due to a combination of increased surface area and the occurrence of cation exchange reactions promoted by its inherent conservative behaviour (Cappuyns *et al*., 2008).

5.4.3 Statistical analyses – interpretation

Statistical analyses of the various leaching methods showed significant differences ($P < 0.001$) between treatments for all variables ($H = 9.27 – 15.16$; $DF = 2$ for all) which are illustrated in Figures 5.1 – 5.7 and Appendix A9. However, the level of significance does vary with respect to some parameter e.g. silicon was not so significantly different between treatments (Figure 5.3 b, Appendix A9).

5.5 Conclusions

Acid leaching promotes the release of metals, especially those ones associated with calcium and magnesium bearing phases, from the matrix. On the other hand, addition of compost prior to leaching with water has little or no effect on the native pH of the system. Also, compost amendment, unlike acid leaching, suppresses calcite precipitation because this treatment reduces surface area available for carbonation reactions and also decreases the amount of calcium leached.

In laboratory conditions, addition of compost to steel slag prior to leaching with water intensifies the leaching of oxyanions such as molybdenum and vanadium relative to the control test. However, the concentrations of both elements were lower when compared with the acid leached sample (Table 5.4). Organic complexation could be a key controlling mechanism for leaching of such metals in the compost test.

Leaching of metals in the compost tests is not a function of surface area but controlled via organic complexation unlike the acid test where leaching is a function of surface area thus making it was the most weathered of all treatments as evidenced by XRD. The leaching of magnesium and silicon is pH-dependent and likely controlled by the dissolution and/or precipitation of magnesium silicates. Acid leaching of steel slag accelerates the release of lithium and nickel however addition of compost to BOF steel slag prior to leaching with water suppresses the release of these elements.

Concentrations of elements such as calcium, barium, strontium, lithium and nickel were lower in the compost experiments relative to the control tests most likely due to secondary precipitation reactions (Table 5.4). In most cases, the concentrations fell continuously over time with the exception of calcium and nickel. On the other hand, concentrations of elements such as sulphur, silicon, potassium, sodium, vanadium and molybdenum were higher in the compost amendment test compared to the control (Table 5.4). The concentrations dropped over time with the exception of sulphur and molybdenum.

In as much as acid leaching of steel slag accelerates the leaching of V and Mo compared to the compost test, the concentrations obtained via the acid leaching process are so low thus making the recovery process economically unviable e.g. concentrations of up to 94 ppm V, 40 ppm Mo, and 242 ppm Ni is sometimes required to achieve viability (Shen and Guo, 2015). The use of acids for leaching also tends to have a hazardous effect on the environment.

Consequently, it would be beneficial to adopt the use of a greener compost alternative for enhanced leaching of valuable metals like vanadium and molybdenum. However, from an environmental engineering perspective, V and Mo could be of potential environmental concern when steel slag are used for soil amendment purposes (in the presence of compost), hence a proper management system will be required if steel slag are to be used in an agricultural setting (and mixed with organics). As a result, further investigations on key factors that could affect leaching of these metals from compost amended steel slag have been carried out in subsequent chapters.

Table 5.4: Summary of leaching behaviour for selected elements in BOF slag leached with various media (concentrations in the acid and compost tests are expressed as a factor of amounts in control test)

Element	**Compost**		**Acid**	
	Start (1 hr.)	End (72 hr.)	Start (1 hr.)	End (72 hr.)
Calcium	0.5*	0.7^	10*	12.7^
Sulphur	1.3*	1.4^	4*	3.4^
Magnesium	*	2^	4500*	2170^
Silicon	1.6*	0.9^	30*	2.7^
Barium	0.3*	0.2^	6.5*	5.4^
Strontium	0.9*	0.6^	9.2*	4.2^
Potassium	7*	6.9^	1.8*	1.8^
Sodium	2*	1.7^	1.8*	1.3^
Vanadium	2.9*	2.5^	8.5*	7.3^
Lithium	0.7*	0.6^	4.2*	10.4^
Nickel	0.6*	1.5^	11.3*	24.1^
Molybdenum	3.3*	3.6^	2*	2.6^

* represents the elemental concentration in the control test at 1 hour from start of experiment

^ represents the elemental concentration in the control test at 72 hours from start of experiment

6

Leaching products of compost amended steel slag: Batch and column experiments

6.1 Introduction

Compost has been shown, in the previous chapter, to accelerate the leaching of some elements of potential commercial interest particularly vanadium and molybdenum (see Table 5.4). Covering slag waste piles with compost also has the benefit of suppressing fugitive dust production, supporting plant growth and contributing to a functioning ecosystem. Compost amendment therefore appears to be a viable strategy for widespread remediation of alkaline residue disposal areas.

However, if such a scheme was to be funded by extraction of trace elements, it is vital that factors which affect the release of elements from the matrix of the slag material are better understood. Landfill environments are seldom uniform, and thus will result in significant variation in leachant pH, redox, dissolved organic carbon (DOC), liquid to solid ratio, leachant type, biological activity and a range of other hydrochemical parameters (see Chapter 4; McLean and Bledsoe, 1992). This chapter aims to shed more light on the preliminary findings for two potentially economically viable components of the leachate, vanadium and molybdenum, so as to assess the key impacts of compost addition on leaching, and recarbonation of steel slags, and thus to underpin future research into metal recovery. To achieve this, batch leaching tests have been designed to investigate leaching under aerobic and anaerobic conditions, as well as some column leaching tests which provide the broader scale assessment of the leaching products and the effectiveness of these remedial interventions.

6.2 Methodology

6.2.1 Batch experiments investigating the effect of biological activity and redox on compost amended-BOF slag – Experiment 6A

6.2.1.1 Material preparation

Crushed BOF steel slag and compost were sieved so only particles with diameter between 420 µm and 63 µm were collected and used in this experiment. In order to obtain this desired size aggregate, two British standard sieves (mesh size of 420 µm and 63 µm) were combined by placing the 420 µm sieve above the 63 µm sieve prior to sieving.

A subset (half portion) of the sieved samples (slag and compost) was then removed and placed into two separate beakers and covered with aluminium foil. These were then sterilised in an autoclave at 120 °C for two hours so as to destroy all biological activity within the sample. The remaining half was however left unsterilized. Also, all the conical flasks used for this experiment were sterilised in the same way prior to the start of experiments so as to make sure that any observed biological activity was solely derived from the sample.

In these experiments (both aerobic and anaerobic), microcosms were set up in a controlled environment laboratory at 19 °C ± 1 °C in the presence of 8 hrs UV light daily (so as to simulate natural field conditions) over a 6 week period. Batch leaching tests were performed using deionised water (18.2 MΩ) so as to allow the waste material to control the redox environment thus reflecting the native Eh of the material.

6.2.1.2 Aerobic experiments – Experimental design and sample collection

Four different treatments were set up in separate 500 ml conical flasks as described in Table 6.1.

Table 6.1: Experimental set-up for the aerobic flask experiments (n = 4)

Treatment	Set-up
'slag only' – **control**	10 g of unsterilised slag + 100 ml UHQ deionised water
'sterile slag only' – **sterile control**	10 g of sterilised slag + 100 ml UHQ deionised water
'unsterilised (slag + compost)'	10 g of unsterilised slag + 2 g of unsterilised compost + 100 ml UHQ deionised water
'sterilised (slag + compost)'	10 g of sterilised slag + 2 g of sterilised compost + 100 ml UHQ deionised water

Next, all conical flasks were sealed with cotton wool and wrapped with aluminium foil material so as to regulate the amount of UV light entering the flasks. Subsequently, they were attached to a mechanical shaker and agitated from side to side at a speed of 100 osc/min (see Plate 6.1). Four replicates were set up for each treatment.

Plate 6.1: Experimental set – up for batch experiments under aerobic conditions

The flasks were carefully sampled over a 6 week period. Samples were collected at 4, 20, 24 hours from the start of the experiment and then sampling was done sequentially until the end of experiment. At each sampling time, 2 ml of the mix in the flask was collected using a syringe. The syringe was flushed with UHQ deionised water prior to sampling each time. The pH, Eh (redox potential), conductivity, alkalinity of the flask samples were analysed in the laboratory using a frequently calibrated pH meter, conductivity meter and digital titrator in accordance with the method described in sections 3.4.1.1.1 and 3.4.1.1.2. The alkalinity of the samples was measured only at the end of the experiment (assuming an initial zero alkalinity). Next, the collected leachate was filtered (0.45 μm), acidified with 2 % HNO_3 and subjected to ICPOES and ICPMS for major ions (Ca, Si, S, Mg, K, Na) and trace elements (Li, V, Ni, Mo) analysis respectively.

6.2.1.3 Anaerobic experiments – Experimental Set-up and sample collection

The set-up used in the anaerobic experiments was the same as that in the aerobic counterpart (Table 6.1), although with a slight modification (all samples were made up in 100 ml septum vials which were deoxygenated by bubbling with oxygen-free nitrogen immediately prior to use).

Similarly, four different treatments were investigated, namely ‘slag only - (control)’, ‘sterile slag only – (sterile control)’, ‘unsterilized (slag + compost)’, and ‘sterile (slag + compost)’. Four replicates were set up for each treatment. The samples were prepared in a glove bag flushed with nitrogen in order to create a near – anaerobic environment. The vials were immediately sealed as soon as all the materials had been added. Vials were rotated in a side to side motion during the experiments with a mechanical shaker at a speed of 200 osc/min.

The experiment lasted a period of 6 weeks and all treatment flasks were sampled during this time, however, the sampling of ‘sterile slag only’ and ‘sterilised (slag + compost)’ batches were not possible on Day 21 due to the lack of nitrogen. The pH, conductivity, Eh and alkalinity of the samples were measured using the same equipment as the aerobic experiment, except that these parameters were recorded only at the start and end of the experiment to avoid compromising the anaerobic conditions within the vials. For each sample, 2 ml of the leachate was collected with a nitrogen filled syringe. The sampled volume was filtered, acidified using 2 % HNO_3 and analysed for major ions (Ca, Si, S, Mg, K, Na) and trace elements (Li, V, Ni, Mo) using ICPOES and ICPMS respectively. Geochemical modelling of the leachates was done using PHREEQC v. 3.1.7-9213 with the LLNL database in line with the method outlined in section 3.4.1.2.

6.2.2 Effect of compost placement method in a compost-amended slag system; column experiments – Experiment 6B

6.2.2.1 Material preparation

The BOF slag was manually sorted to get rid of stones, leaves and other unwanted materials. They were then sieved to obtain steel slag with diameter greater than 8 mm but less than 19 mm using British standard sieves of mesh size 19 mm and 8 mm, this size fraction was chosen because it represented the average size of the uncrushed steel slag and would therefore cause minimal disturbance if the technology was applied in a field scenario since the need for crushing would be eliminated. The municipal compost was sorted to get rid of unwanted materials e.g. wood and plastics. No further processing was carried out on the compost.

6.2.2.2 Experimental design

Four mesocosms were constructed using PVC pipe of length 33 cm and width 11 cm with a tap at the bottom of the column for effluent collection (Figure 6.1).

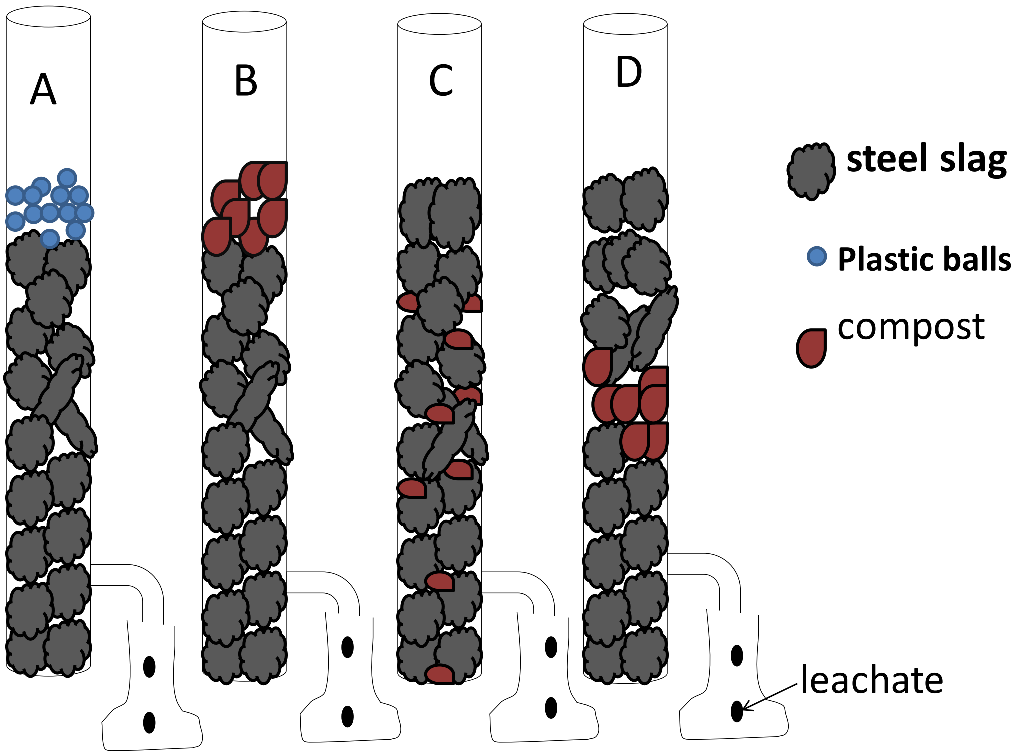

Figure 6.1: Different physical structures of slag-compost mixture. A – no compost, B – compost top, C – compost blend, D – compost intermediate.

For the column experiments, a slag to compost ratio of 5:1 was applied and set up in accordance with Table 6.2. This ratio translated to a depth of approximately 20 cm which is typical of soil amendment. Triplicates of each treatment were set up.

Table 6.2: Experimental set-up for column experiments (n = 3)

Treatment	Set-up
Column A (No compost)	2.25 kg of steel slag only + plastic balls (to bring this column to same level as others)
Column B (Compost Top)	450 g of compost layered over 2.25 kg of slag
Column C (Compost Blend)	2.25 kg of slag mixed vigorously with 450 g compost
Column D (Compost Intermediate)	450 g compost sandwiched between two layers of slag (total slag weight 2.25 kg)

Column A ('No compost') has been considered as a 'reference treatment' in this experiment since it lacks compost hence all other treatments have been compared against it. The slag samples were carefully introduced in the columns in such a way that does not create preferential flow of the leaching fluid by ensuring a near-even distribution of the slag material inside the column. UHQ deionised water was used as the leaching fluid in this experiment.

At the start of the experiment, 700 ml of the leaching fluid (pH = 5.7) dosed with 0.1 g calcein was added to the slag/compost mixture in all the columns. This volume of water was chosen so as to ensure that the water table in the column was within the slag region and below the interface between the steel slag and compost. Calcein, a fluorescent dye, was added to the water in order to stain fresh precipitates produced during the course of the experiment and also to allow for future examination of these precipitates under fluorescent UV/Visible light (see Chapter 7). The columns were set up in a controlled laboratory environment with average temperature of 20 °C ± 2 °C and exposed to 8 hours of daylight (UV light) daily, therefore simulating natural precipitation conditions. Furthermore, no filter was placed between the media and the tap. The tap was left open for free drainage only during sampling.

6.2.2.3 Solution chemistry: sampling and analyses

20 ml of the leachate from individual columns were sampled at different times over an initial sampling period of 100 days, however equilibration occurred within 50 days of sampling so data analysis was limited to this period. The sampled volume was replaced by the same volume of ultra-pure water (dosed with 10 mg calcein) in order to maintain a constant water table level in the columns and also

so as to limit the perturbation of the system. The physico-chemical parameters (pH, Eh, conductivity, alkalinity) of the sampled leachate were measured using calibrated instruments according to methods described in sections 3.4.1.1.1 and 3.4.1.1.2. Unfortunately, the alkalinity of samples from column D was only measured at 22 hours after the start of the experiment due to a fault developed by the instrument.

In addition, the water colour of the leachates was determined photoelectrically with a photometer at 410 nm, in accordance with standard method YSIP47 following filtration through a 0.45 µm filter to remove any suspended solids. This is because water colour is a useful surrogate measure for dissolved organic carbon in the samples.

The sampled leachate was filtered using a 0.45 µm filter, acidified (2 % HNO_3) and preserved at 4 °C. Major ions (Ca, S, K, Na) and trace elements (Li, V, Ni, Mo) of the stored samples were measured on ICP-OES and ICP-MS respectively within three days of sampling.

The saturation indices of possible mineral phases present in the leachates were determined at random times (Day 1, 19, 28 and 50) so as to create a better understanding of the thermodynamics of the system over time. This was achieved using the computer program WEB-PHREEQC version 3.1.7-9213 with the LLNL database (section 3.4.1.2).

Graphs were plotted using Microsoft Excel 2007, to display the leaching patterns of elements of interest over time in the various treatments. Also, the Kruskal-Wallis test was conducted on the various treatments so as to ascertain the statistical differences in all treatments. This was achieved using Minitab software.

6.3 Results

6.3.1 Batch experiments investigating the effect of biological activity and redox condition on compost amended-BOF slag – Experiment 6A

6.3.1.1 Physicochemical parameters - Aerobic

The changes in the pH, conductivity and Eh (redox potential) of the aerobic batch tests are presented in Figure 6.2. Under aerobic conditions, the pH for all the treatments fell approximately by an average of 1.4 pH units by Day 42. This decline in pH was more pronounced in the first 8 days followed by equilibration onwards (Figure 6.2 a). The pH of the non-sterile samples was also slightly lower than the sterilized ones. There was however no significant change in pH of the compost and non-compost amended slag treatments.

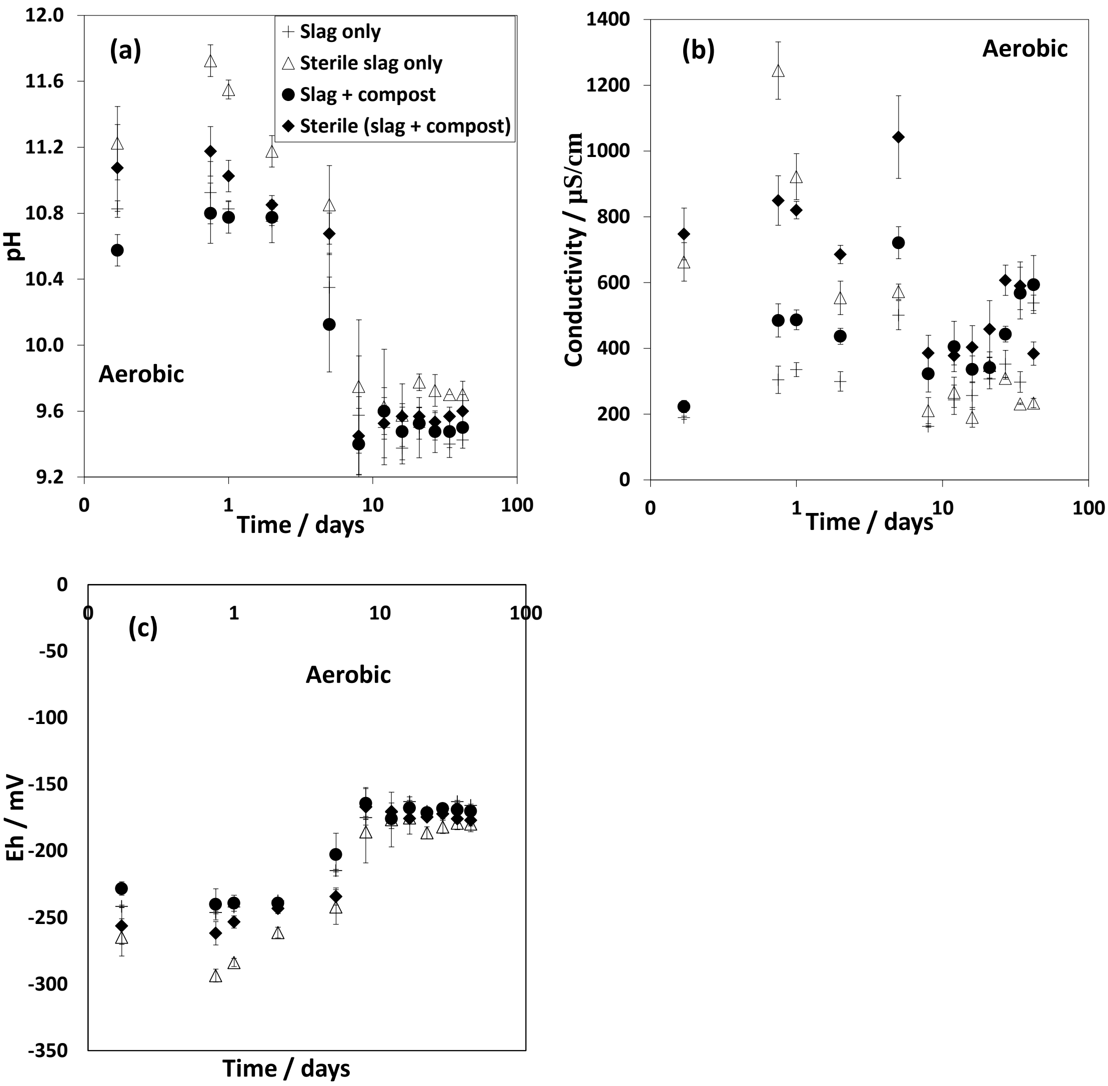

Figure 6.2: Changes in (a) pH (b) conductivity (c) Eh under aerobic conditions. Time axis is reported in log scale and errors bars represent repeatability.

Under aerobic conditions, no clear pattern was seen for the effect of the treatments on conductivity values (Figure 6.2 b). Conductivity values in the sterile samples were slightly higher than its unsterilized counterparts. The redox potential for all the treatments were negative (highly reducing). Similarly, as in the case of pH and conductivity, the sterile samples were more reducing compared to the non-sterile ones (Figure 6.2 c). For the aerobic experiments, alkalinity values at the end of experiment for the slag only, sterilized slag only, slag and compost, and sterilized slag and compost treatments were 515 ± 113, 577 ± 78, 984 ± 143, and 1259 ± 169 mg/L as $CaCO_3$ respectively (all assuming an initial zero alkalinity).

6.3.1.2 Physicochemical parameters - Anaerobic

Anaerobic (reducing) conditions led to a rise in pH in all the treatments (Table 6.3). The greatest rise of 1.5 pH units was observed for the unsterilized (slag and compost) treatment while the sterilized (slag plus compost) rose the least.

Table 6.3: Physicochemical parameters under anaerobic conditions (n=4)

	pH		Conduct. / µS/cm		Eh / mV	
	Initial	Final (6 weeks)	Initial	Final (6 weeks)	Initial	Final (6 weeks)
Unsterilized slag only	10.83 ± 0.05	12.15 ± 0.06	189 ± 5	2850 ± 518	-241.8 ± 4.38	-323.9 ± 3.63
Sterilised slag only	11.23 ± 0.22	12 ± 0	663 ± 58	1938 ± 91	-265 ± 14.01	-315.5 ± 1.72
Unsterilised (slag & compost)	10.58 ± 0.10	12.08 ± 0.05	223 ± 18	2625 ± 190	-228.3 ± 4.96	-320.5 ± 2.55
Sterilised (slag & compost)	11.08 ± 0.26	11.8 ± 0.0	748 ± 79	1434 ± 25	-256.4 ± 13.84	-301.6 ± 0.62

Batch leaching under anaerobic conditions led to a tremendous rise in conductivity (Table 6.3). This rise was more pronounced in the unsterilized samples, in some cases, by up to factor of 15 more than initial conductivity values. Also, the leachates were all strongly reducing, with the most reducing values in the sterile samples (Table 6.3).

The alkalinities in the anaerobic experiments were higher than the aerobic ones. For the anaerobic experiments, alkalinity values at the end of experiment for the slag only, sterilized slag only, slag and compost, and sterilized slag and compost treatments were 998 ± 88, 652 ± 21, 1168 ± 263 and 1249 ± 132 mg/L as $CaCO_3$ (all assuming an initial zero alkalinity).

6.3.1.3 Major elements – aerobic and anaerobic

6.3.1.3.1 Calcium, silicon and sulphur

The amount of calcium and silicon leached under anaerobic conditions was far higher compared to levels recorded under aerobic (oxidising) conditions (Figures 6.3 a - d). Under aerobic conditions, more calcium was leached from the sterilised treatments compared to the unsterilized ones (Figure 6.3 a). Conversely, silicon levels were higher in the unsterilized samples compared to the sterilized ones (Figure 6.3 c).

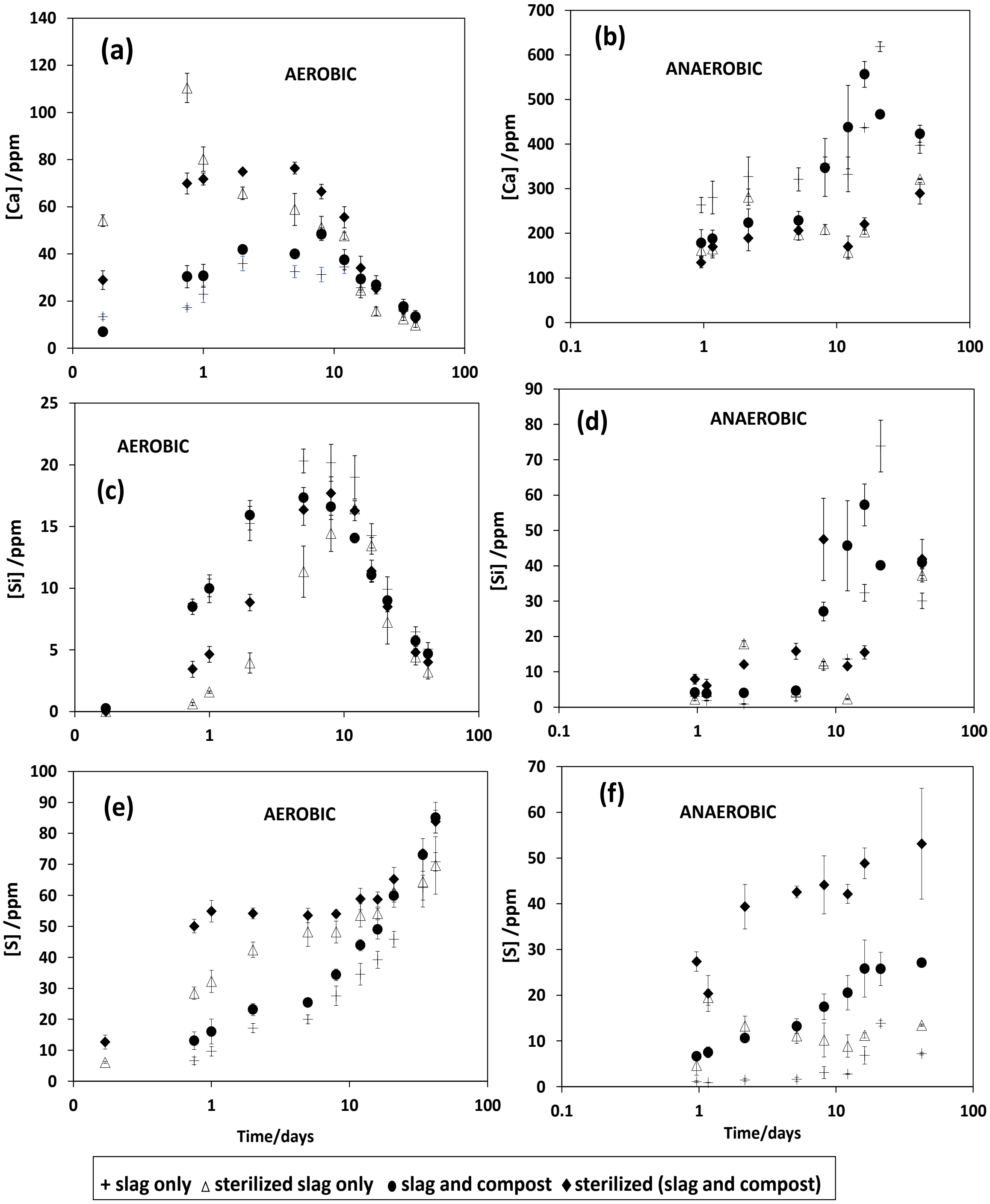

Figure 6.3: Leaching characteristics of selected major elements in compost amended BOF slag under varying redox conditions. (a) calcium – aerobic (b) calcium – anaerobic (c) silicon – aerobic (d) silicon – anaerobic (e) sulphur – aerobic (f) sulphur – anaerobic. Time axis is reported in log scale and errors bars represent repeatability.

Generally, for all treatments, the amount of calcium leached increased within first 5 days of leaching then drops onwards under aerobic conditions (Figure 6.3 a).

Similarly for silicon, an initial rise was observed within the first 8 days of leaching followed by a fall onwards in aerobic settings (Figure 6.3 c). On the other hand, under anaerobic conditions calcium and silicon levels rose continuously throughout the leaching period (Figure 6.3 b & d).

Sulphur leaching was slightly enhanced under aerobic conditions compared to anaerobic conditions (Figure 6.3 e & f). The sterilized treatments leached more sulphur compared to the unsterilized counterpart under anaerobic conditions. The leaching of sulphur was observed to increase continuously throughout the leaching period under both conditions (Figure 6.3 e & f).

6.3.1.3.2 Potassium and sodium

The level of potassium and sodium leached under aerobic environments was slightly lower than anaerobic treatments (Figures 6.4 a - d). The amount of sodium and potassium leached from the compost amended samples were higher than that recorded for the non-compost samples, and also independent of sterilization (Figures 6.4 a - d). The levels of alkali metals released from the slag matrix remained relatively constant throughout the leaching period (Figure 6.4).

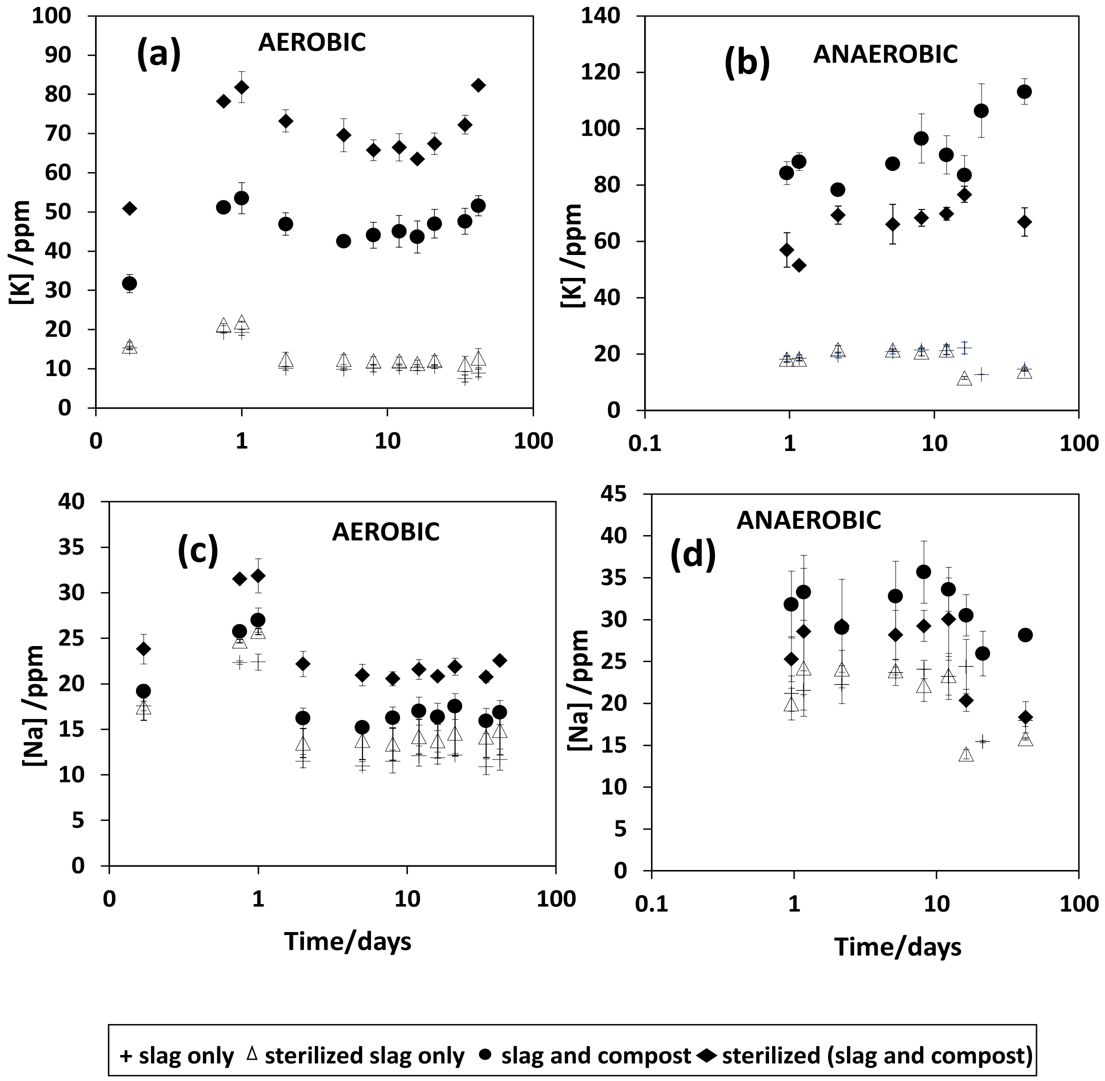

Figure 6.4: Leaching behaviour of potassium and sodium in compost amended BOF slag under aerobic and anaerobic conditions. (a) Potassium – aerobic (b) potassium – anaerobic (c) sodium – aerobic (d) sodium – anaerobic. Time axis is reported in log scale and errors bars represent repeatability.

6.3.1.4 Trace elements – aerobic and anaerobic

6.3.1.4.1 Lithium, vanadium, nickel, molybdenum

The leaching behaviour of lithium, vanadium, nickel and molybdenum in a compost-amended steel slag system investigated under aerobic and anaerobic settings have been presented in Figure 6.5.

Generally, anaerobic treatments depress the rate of leaching of lithium, vanadium and molybdenum but increases the amount of nickel leached.

The amount of lithium released increased steadily throughout the leaching period under both aerobic and anaerobic conditions. Also there was no noticeable difference in the amounts leached from the sterile and non-sterile samples.

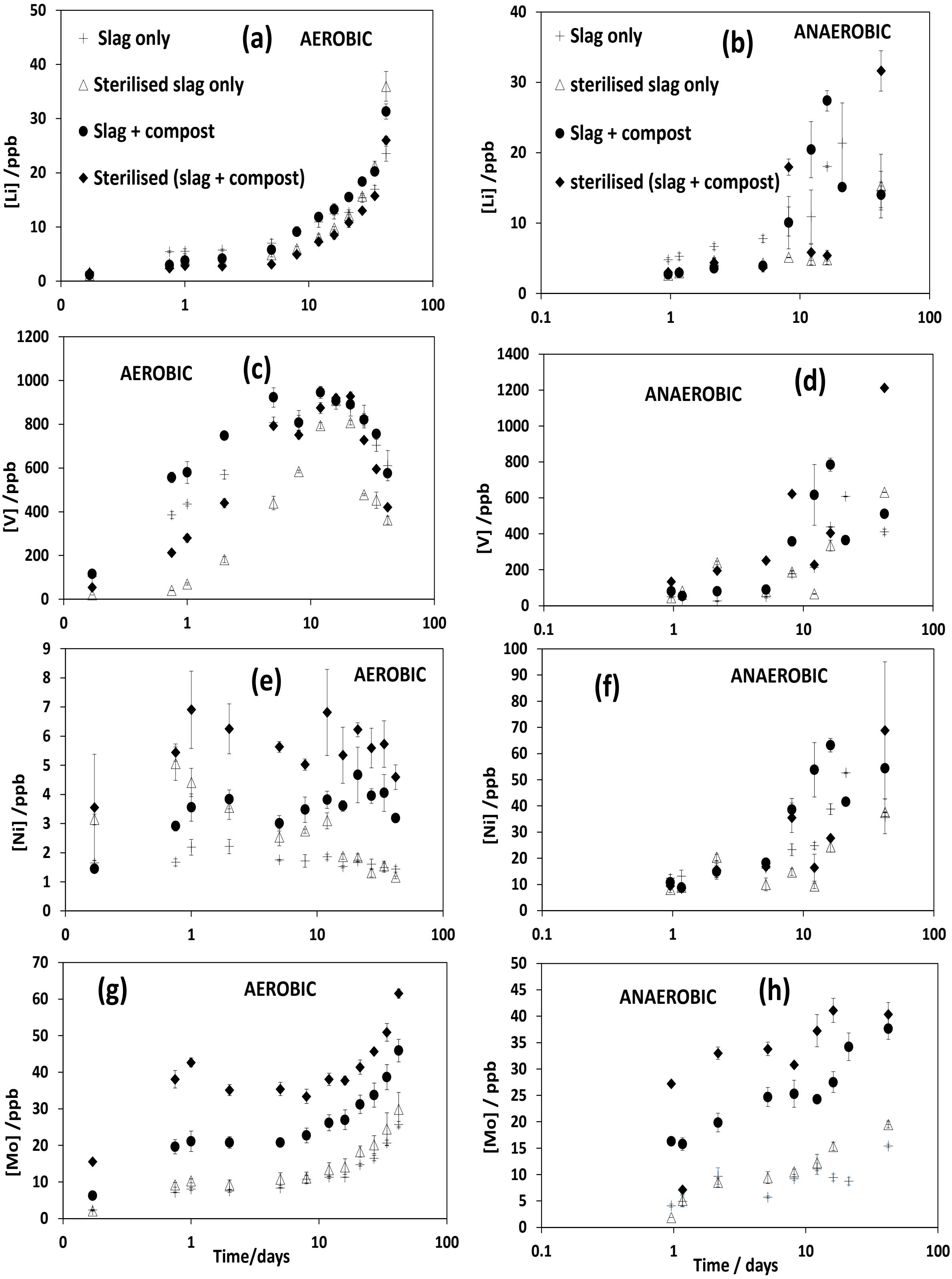

Figure 6.5: Leaching characteristics of selected trace elements in compost amended BOF slag under varying redox conditions. (a) Lithium – aerobic (b) lithium – anaerobic (c) vanadium – aerobic (d) vanadium – anaerobic (e) nickel – aerobic (f) nickel – anaerobic (g) molybdenum – aerobic (h) molybdenum – anaerobic. Time axis is reported in log scale and errors bars represent repeatability.

In the case of vanadium, aerobic leaching led to an initial rise in amount leached followed by a fall afterwards in leached levels. This pattern was similar to that observed for calcium and silicon. Aerobic leaching also favoured the release of vanadium. Anaerobic treatments led to a continuous, but slower, increase in the amount of vanadium leached. In the aerobic treatments, the amount of nickel leached fell progressively during the leaching period while during anaerobic leaching, there was a pronounced rise in leached nickel levels. The leaching pattern for molybdenum was similar in both the aerobic and anaerobic treatments; however the molybdenum levels in the aerobic treatments were slightly higher than its anaerobic counterparts.

6.3.2 Effect of compost placement method in a compost-amended slag system; column experiments – Experiment 6B

6.3.2.1 Physico-chemical parameters

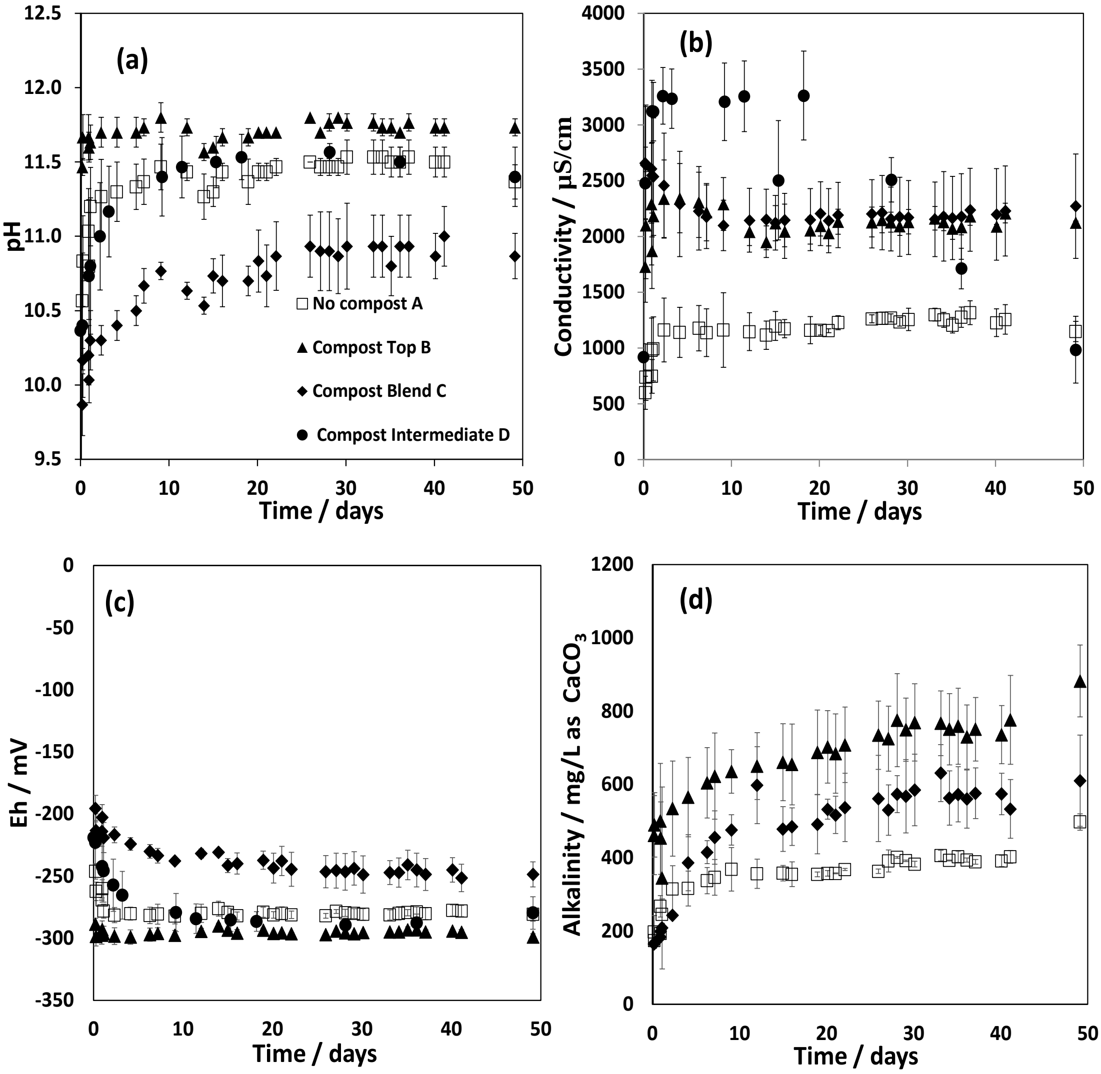

Figure 6.6: Effect of compost placement method of slag-compost mixtures on (a) pH (b) conductivity (c) redox potential (d) alkalinity

Figure 6.6 presents the physico-chemical parameters (pH, Eh, conductivity and alkalinity) of all the treatments investigated in the column experiments. There was a sharp rise in the pH of all the column treatments within the first 9 days of the column experiments followed by equilibration onwards (Figure 6.6). Column C (compost blend) had the lowest pH while column B (compost top) had the highest pH relative to column A (control). The pH of leachates in column C was 0.9 pH units lower than column A while the pH of leachates in column B was 0.4 pH units higher than column A by the end of the column leaching experiments. Also, there was little difference in the pH of the column D (compost intermediate) and column A.

The addition of compost increased the conductivity in all the treatments. The highest conductivity was recorded in column D (compost intermediate). The capped column (B) and blended column (C) showed similar conductivity pattern.

The leachates from all the columns were strongly reducing in nature, ranging from -196 ± 11 to -299 ± 2 mV. Column B (compost top) was the most reducing column while column C (compost blend) was the least reducing column of all the treatments. Alkalinities of the compost-amended samples were higher than the control treatment, and also increased over time. The greatest alkalinity was recorded in column B (compost top). The alkalinity in column B rose from 462 ± 108 to 883 ± 98 mg/L as $CaCO_3$ while that in column C rose from 165 ± 5 to 611 ± 125 mg/L as $CaCO_3$. The alkalinity for column D after 22 hours of leaching was 214 mg/L as $CaCO_3$.

Figure 6.7 shows a statistically significant difference (Kruskal Wallis: H: 30.7, d.f. 3, $P<0.001$) in water colour generation between the treatments (*n* = 6 for each treatment). Water colour generation was at or below detection limits in the control A (no organic amendment) and capped treatment B. Significantly higher water colour was apparent in the sandwich treatment D (median: 15 mg/L; range: 10-20 mg/L) and further more in the blended treatment (median: 100 mg/L; range: 70-150 mg/L).

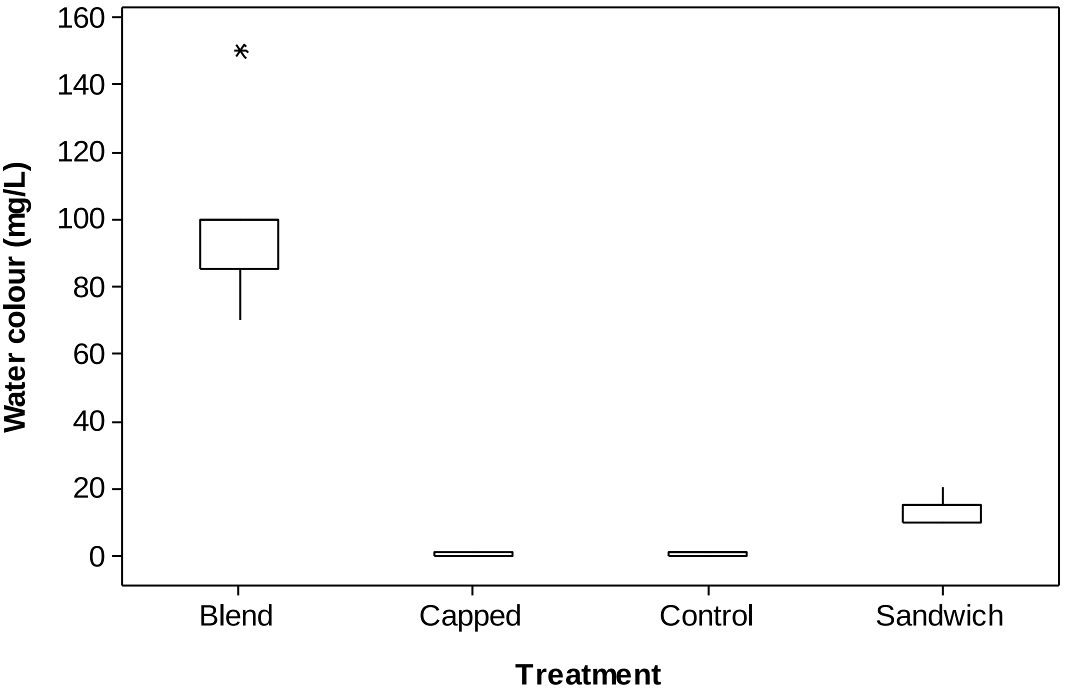

Figure 6.7: Water colour concentrations in various column treatments. Control – Column A, Capped – Column B, Blend – Column C, Sandwich – Column D.

6.3.2.2 Major elements

6.3.2.2.1 Calcium, sulphur, potassium and sodium

The leaching behaviour of calcium, sulphur, aluminium, potassium and sodium in the various column treatments are presented in Figure 6.8. The amount of calcium leached was highest in column D (compost intermediate) and lowest in column C (column blend). There was a rise in calcium leaching over time with the exception of calcium D, where calcium levels decreased over time (Figure 6.8 a). Sulphur release was greatest in column D and the leached levels remained relatively constant throughout the leaching period. Also, column C promoted the release of sulphur although in lower levels compared to column D (Figure 6.8 b).

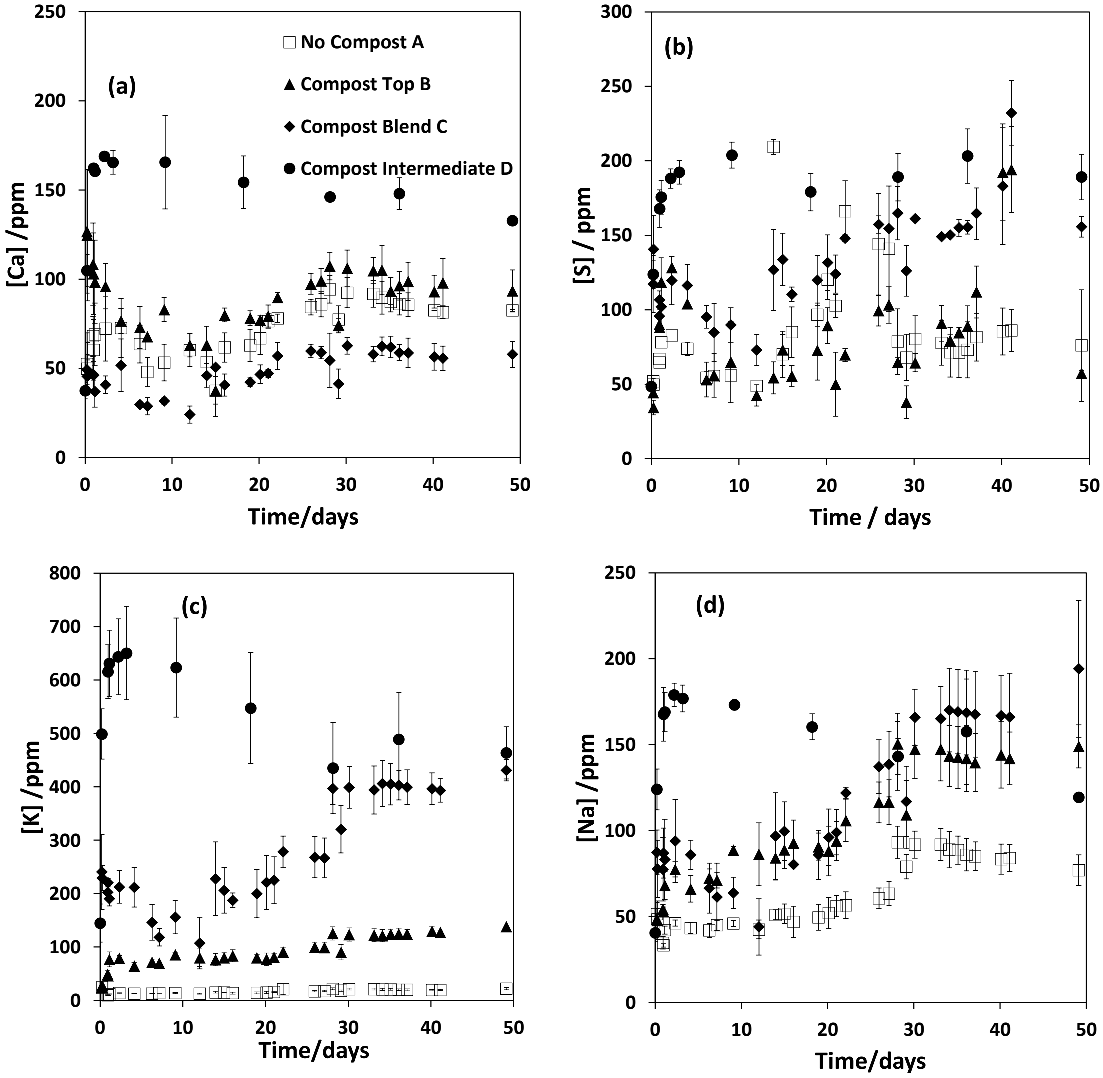

Figure 6.8: Effect of compost placement method of slag-compost mixtures on the leaching behaviour of (a) calcium (b) sulphur (c) potassium (d) sodium.

The addition of compost increased the leaching of potassium and sodium in all compost-amended samples (Figures 6.7 d & e). The greatest amount of these alkali metals was leached in column D. The concentration of potassium rose from 144.8 ± 35.6 to 463.7 ± 48.9 ppm while the sodium levels rose from 40.4 ± 4.8 to 119.2 ± 0.9 ppm in column D by the end of the leaching experiment. In column C, the concentration of potassium rose from 240.7 ± 70.4 to 430.9 ± 19.8 ppm while the sodium levels rose from 87.3 ± 13.1 to 194.1 ± 39.8 ppm by the end of the leaching experiment. The concentration of potassium and sodium rose from 24.9 ± 2.3 to

138.1 ± 0.6 ppm and 48.4 ± 9.8 to 148.9 ± 12.6 respectively in column B by day 50 of the leaching experiment (Figures 6.7 c & d).

6.3.2.2.2 Magnesium and silicon

Figures illustrating the leaching pattern for magnesium and silicon in the columns have not been presented here because most of the data obtained were anomalous and in most cases below detection limits of 0.030 ± 0.004 ppm and 0.040 ± 0.005 ppm for magnesium and silicon respectively.

The initial magnesium levels in columns A (no compost), B (compost top) and D (compost intermediate) were 0.30 ± 0.06, 0.10 ± 0.03 and 3.9 ± 1.1 ppm respectively (figures not shown here). After 4 days of leaching, this amount fell to 0.20 ± 0.02, 0.08 ± 0.01 and 1.1 ± 0.2 ppm respectively. Magnesium levels were below detection limit for the rest of the leaching period. However in column C (compost blend), the maximum amount of magnesium was leached on day 4 of the leaching experiments (8.0 ± 0.2 ppm), this amount dropped to 2 ppm by day 50 of the leaching experiments (Figure not shown here).

In the control treatment (no compost), silicon levels fell from 4.1 ± 0.2 to 1.6 ± 0.3 ppm by day 7 of the leaching period after which measured concentrations were below detection limit. Similarly, in column B (compost top), silicon concentrations decreased from 2.5 ± 0.6 to 1.6 ± 0.1 ppm by day 4 after which measured concentrations were below LOD. In column C, silicon levels rose steadily reaching concentration of up to 5 ppm by day 50 while in column D, there was an initial rise in silicon levels within the first 9 days of leaching, reaching levels up to 13 ppm, followed by a subsequent fall onwards.

6.3.2.3 Trace elements

6.3.2.3.1 Lithium, vanadium, nickel, molybdenum

The leaching characteristics of selected trace elements in the investigated column treatments are displayed in Figure 6.9. The leaching of lithium and vanadium were greatly enhanced in column D and suppressed in columns B and C. The concentration of lithium in column D increased over time rising from 10.9 ± 2.4 to 24.0 ± 5.1 ppb after 50 days of leaching. Contrary to this, lithium levels dropped in the other columns. In column A, lithium levels dropped from 17.9 ± 2.7 to 9.0 ± 1.1 ppb. In column B, lithium levels fell from 19.8 ± 5.3 ppb to 3.7 ± 0.4 ppb while in column C the lithium levels decreased from 18.9 ± 2.2 ppb to 6.3 ± 1.0 ppb.

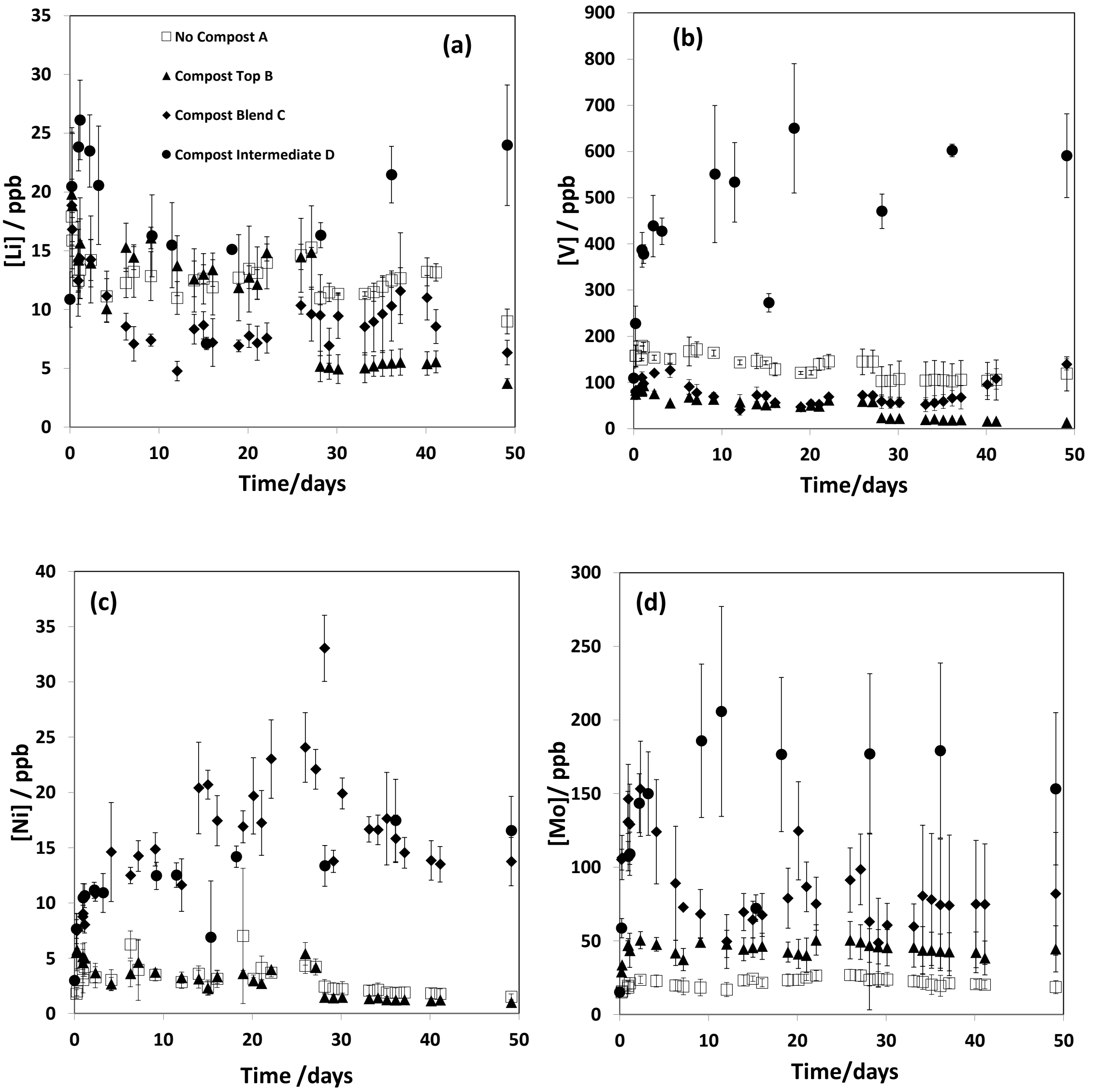

Figure 6.9: Effect of compost placement method of slag-compost mixtures on the leaching behaviour of (a) lithium (b) vanadium (c) nickel (d) molybdenum

In the case of vanadium, the initial and final concentrations in column A were 157.4 ± 22.7 and 118.7 ± 37.0 ppb respectively. In column B, vanadium levels fell from 74.5 ± 11.4 to 13.4 ± 3.0 ppb. Vanadium leaching in column C and D rose from 79.0 ± 3.3 to 139.1 ± 12.2 ppb and 109.3 ± 22.0 to 590.9 ± 90.6 ppb respectively. Nickel leaching was higher in columns C and D and lowest in column B relative to column A. In columns A and B, the amounts of nickel dropped from 1.8 ± 0.4 to 1.5 ± 0.3 ppb and 5.5 ± 1.6 1.0 ± 0.1 ppb respectively while in columns C and D, nickel levels rose from 7.7 ± 1.4 13.7 ± 2.2 ppb and 3.0 ± 0.1 16.5 ± 3.1 ppb respectively.

The leaching of molybdenum increased in all the compost amended steel slag. In column A (no compost), the initial and final levels were 15.1 ± 1.8 and 18.6 ± 4.4 ppb. Molybdenum levels rose from 29.1 ± 1.2 to 44.6 ± 15.7 ppb in column B while in column C, the amounts of molybdenum leached fell from 105.2 ± 7.1 to 82.0 ± 41.6 ppb. The greatest amount of molybdenum was leached in column D rising from 15.2 ± 1.7 to 153.3 ± 51.7 ppb.

6.3.2.4 Geochemical modelling

Here, the potential solubility controlling minerals were selected on the basis of the determined SI-values (i.e., closeness to zero) and the likeliness of their presence in steel slag. These minerals include calcite, aragonite, portlandite, quartz, corundum, ettringite, lime and larnite.

Leachates obtained from all the treatments (both control and compost-amended) were supersaturated with respect to calcite and aragonite, and undersaturated with respect to portlandite, lime, and larnite throughout the leaching period (Figure 6.10). In columns A, C and D, the leachates were initially saturated with respect to quartz in the first few days of leaching however by day 19, and for the rest of the leaching period, the leachates became undersaturated with quartz. Column B was undersaturated with respect to quartz throughout the leaching regime (Figure 6.10).

Corundum was supersaturated in all the columns throughout the leaching period with the exception of column D (column intermediate) in which this mineral phase remained undersaturated. Leachates in columns A and B were supersaturated with ettringite while columns C and D were undersaturated with respect to this phase (Figure 6.10).

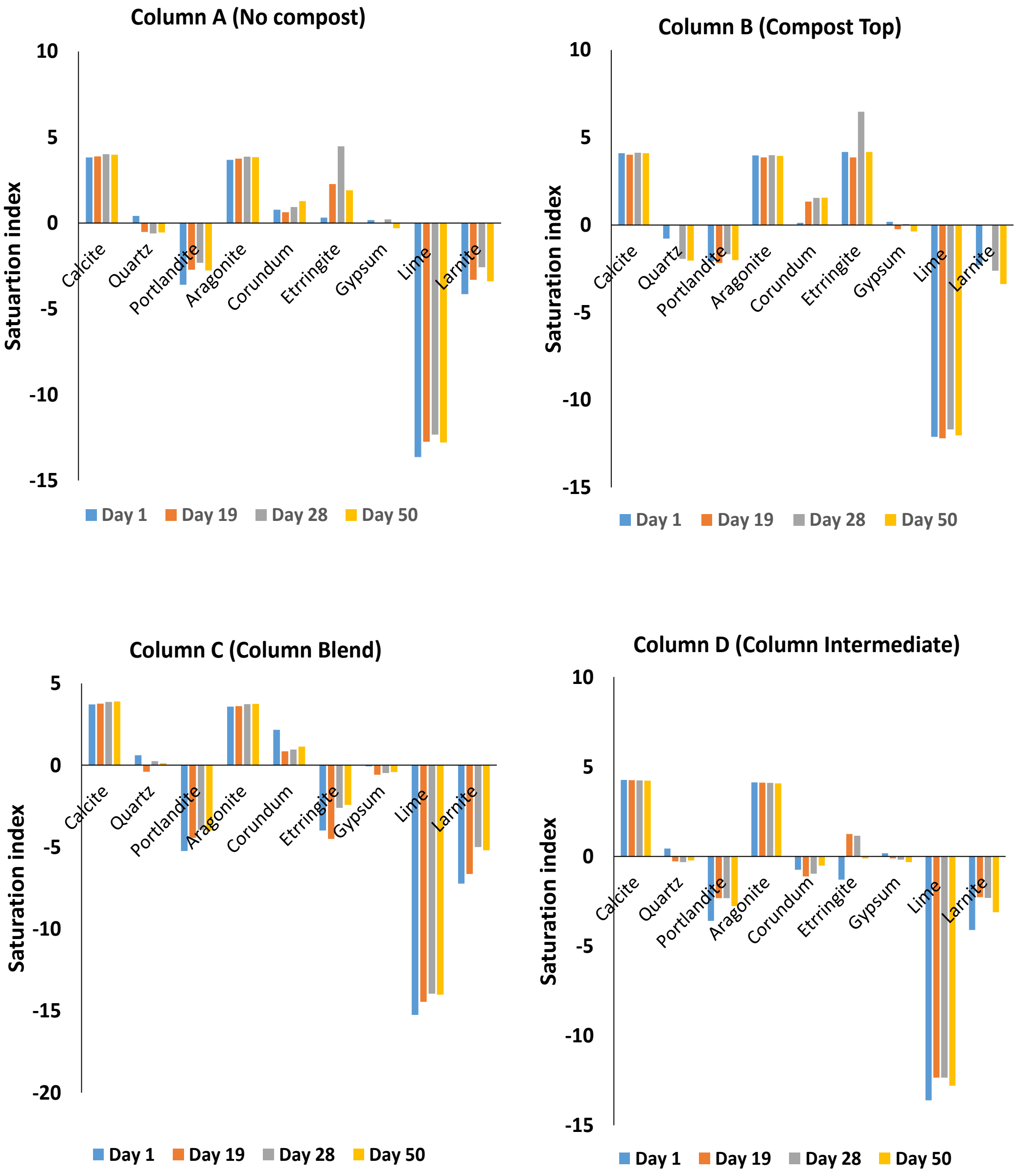

Figure 6.10: Evolution of key mineral phases in compost-amended steel slag over time. (Data obtained via aqueous modelling using WEB-PHREEQC version 3.1.7-9213 with the LLNL database).

6.4 Discussion (Batch and column experiments)

6.4.1 pH, Eh, and Alkalinity

Aerobic leaching lowers pH of the resultant leachates possibly due to the buffering effect provided by atmospheric $CO_{2(g)}$ rapidly reacting with the alkalinity of the samples hence leading to carbonation reactions and a fall in pH to values which may permit initiation of biological activity (pH < 10). Also, the decline in pH values under unsterilized aerobic conditions probably suggests that pH buffering may be partly biologically induced (Mayes *et al.*, 2006). The lack of carbonation reactions in the anaerobic flasks may be responsible for the lower redox potential and higher alkalinity values observed in this treatment, similar to previous findings in Dusing *et al.*, 1992.

Furthermore, a 'fully aerobic' environment wasn't established within the leaching period regardless of the CO_2 input from the atmosphere hence the negative redox potential values obtained, this is probably due to the inherent highly reducing nature of the slag material and also limited diffusion of CO_2 in the flask since most of it would travel in the upper zone of the flask. The higher alkalinities in the compost-amended samples probably suggests that the compost material contributes to the alkalinity in both aerobic and anaerobic conditions probably due to the slower diffusion rate of gases i.e. CO_2 in water and the release of alkaline species e.g. CO_3^{2-} from compost.

In column C (compost blend), the surface area available on the surface of the steel slag is reduced due to the closer interaction between the compost and slag. This decreases the leaching of calcium and also lowers the leachate pH by promoting the biological activity within this column.

6.4.2 Major elements

6.4.2.1 Calcium and silicon

The concentration of calcium in the aerobic leachates were lower compared to the anaerobic leachates possibly due to carbonation effect occurring as a result of the interaction of atmospheric CO_2 and calcium ions in the leachate (Comans *et al*., 2006), while the lower amount of silicon leached under aerobic conditions may be due to the precipitation of quartz, which is also promoted by the availability of atmospheric CO_2 (Bayless and Schulz, 2003). However, in anaerobic conditions, the leaching of calcium and silicon increased continuously and is probably governed by mineral dissolution only. Sterilization promotes the leaching of calcium and hinders the release of silicon in the aerobic tests, probably suggesting that biological activity could partly be responsible for the observed leaching behaviour of these elements (Figures 6.3 a and c).

In column C (compost blend), the surface area available on the surface of the steel slag is reduced possibly due to the closer interaction between the compost and slag. This decreases the leaching of calcium and also lowers the leachate pH by promoting the biological activity within this column.

6.4.2.2 Sulphur, potassium, and sodium

The leaching of sulphur was observed to increase continuously throughout the leaching period under both conditions, this may likely be associated with the dissolution of a highly soluble component such as sodium sulphate, which may have been formed as a result of the interaction between the sodium (4.3 ± 0.5 % Na ; see Table 4.1), derived from the use of sodium carbonate as an additive in the steel production process, and the abundant sulphur present in the slag (2.6 ± 0.3 %

S; see Table 4.1), The leaching of alkali metals was higher in the organic amended treatment in both aerobic and anaerobic environments regardless of sterilization probably due to the additional contribution of potassium and sodium naturally inherent in the compost.

6.4.3 Trace elements

The leaching of the selected trace elements (lithium, vanadium, nickel, molybdenum) were most likely solubility controlled and not governed by surface sorption. This is supported by the fact that typical sorptive surfaces such as amorphous aluminium oxides, hydrous ferric oxides and hydrotalcite, which have high affinity for these elements were not detected via geochemical modelling (see Appendix A4; Comans *et al*., 2006; Smith, 1999), possibly due to the fact that the concentrations of elements providing reactive hydro (oxide) surfaces for sorption such as aluminium, iron and magnesium were too low in the leachates.

6.4.3.1 Vanadium and molybdenum

The leaching behaviour of vanadium under aerobic environments was similar to that observed for calcium and silicon. This probably suggests that the leaching of vanadium is controlled by either a carbonate phase (possibly calcite) or a silicate bearing phases (Figure 6.3 a, c, and 6.5 c). On the other hand, the release of vanadium is greater under anaerobic conditions possibly due to the lack of carbonation reactions, hence the vanadium is released possibly due to the dissolution of a calcium vanadate or carbonate phase, this observation is in agreement with data from geochemical modelling results, with S.I = - 0.8 for $Ca_3(VO_4)_2$ (data not shown here), and previous literature (Comans *et al*., 2006).

Aerobic conditions enhances the release of vanadium, and molybdenum because these elements exist in a more oxidised form (+4 or +5 state) and this enhances the leaching of these elements unlike in an anaerobic environment where they exist in a form of lower oxidation state which decreases their mobility (see Chapter 2; Cornelis *et al.*, 2008). In addition, the concentrations of vanadium and molybdenum were higher in the compost amended samples. This could be ascribed to the formation of complexes with the humic substances in the compost (see Chapter 5). Complexed forms of heavy metals are generally highly soluble and therefore released more rapidly than uncomplexed forms. The release of vanadium and molybdenum was highest in the 'column intermediate, (D)' treatment, probably either due to the dissolution of calcium metallates or the alkaline hydrolysis of organics within the system (Figure 6.7). Leachates from all the columns were undersaturated with respect to highly soluble powellite ($CaMoO_4$) and calcium vanadate $Ca_3(VO_4)_2$ since calcium is precipitated as ettringite or calcite ($CaCO_3$) (see Appendix A5; Meima and Comans, 1997). On the other hand, alkaline hydrolysis of organics occur when high pH water from the upper layer of the column, which is a function of dissolution of lime phases, comes in contact with compost, hence more soluble vanadium and molybdenum complexes are formed and this enhances the mobility of these elements. The initial increase in the leaching of V and Mo in column D is likely controlled by the dissolution of ettringite while the decrease observed at day 15 (pH = 11.5) could be either due to the incorporation of these oxyanions into the ettringite structure or as a result of the incorporation of vanadate and molybdate into precipitated calcite (Figure 6.10; Van Gerven *et al.*, 2004; Cornelis *et al.*, 2005).

Ettringite $Ca_6Al_2(SO_4)_3(OH)_{12}{:}26H_2O$ is formed as a secondary phase during the leaching (weathering) of steel slag particularly in long term exposure scenarios. It has the potential to incorporate vanadate and molybdate into its lattice thereby decreasing their mobility. However, ettringite is unstable with respect to recarbonation reactions, and thus cannot be viewed as being an ultimate sink for oxyanions in exposed surface environments (Jones, 1995).

Portlandite also controls the leaching of V and Mo, however it is only stable at pH above 12.4. Hence in the column experiments, portlandite is eventually converted to more stable calcite (Meima and Comans, 1998). As a result, in fresh or mildly weathered steel slag, leaching of V and Mo is likely controlled by ettringite and portlandite while in long term scenarios calcite controls vanadium and molybdenum solubility.

6.4.3.2 Lithium and nickel

The leaching of nickel in the columns is most likely controlled by pH and Ni $(OH)_2$ solubility. The solubility of nickel increases with decreasing pH hence nickel was more mobile in column C because of the lower pH of the leachates in this column relative to other columns. On the other hand, nickel was highly immobile in column B due to the relatively high pH of leachates in this treatment (Quina *et al.*, 2009). The reason for the higher leaching of lithium in aerobic environments and nickel in anaerobic environments however remains unclear.

6.4.4 Statistical analyses – interpretation

Statistical analyses of the various column treatments showed significant differences ($P < 0.001$) between treatments for all variables ($H = 27.42 – 86.66$; $DF = 3$ for all) which are illustrated in Figures 6.6 – 6.9 and Appendix A10. It is however worth mentioning that in as much as the Kruskal Wallis test highlights the fact that some populations in the data are statistically different, it is unable to provide information on which specific variables may be involved.

6.5 Conclusions

Aerobic leaching of compost-amended steel slag buffers the pH and alkalinity of hyperalkaline leachates by promoting carbonation reactions and biological activity. This is however dependent on the position of the compost within the steel slag – compost system. Alkalinity and pH buffering is more effective by increasing the contact between slag and compost via thorough mixing. Contrary to this, the alkalinity and pH of steel slag leachates increases by capping the surface of the steel slag with compost. In addition, the mobility of calcium, silicon and nickel decreases when compost-amended steel slag are leached aerobically while the release of elements like vanadium, molybdenum and lithium are enhanced under same conditions. The leaching behaviour of certain elements like sulphur, potassium and sodium in a compost-amended steel slag environment is independent of the physico-chemical parameters of the leachates.

The leaching of most of the studied elements including sulphur, calcium, silicon, vanadium, molybdenum, lithium, and nickel were most likely controlled by the solubility of associated mineral phases. Similarly, the physical structural arrangement between the steel slag and the compost plays a key role in determining the leaching behaviour of the studied elements. By placing compost in between two layers of steel slag (Column D), the mobility of calcium, lithium, vanadium, and molybdenum were enhanced while thorough mixing of the slag and compost (Column C) increases the leaching of nickel, magnesium and silicon.

7

Solid phase assessment of compost amended steel slag

7.1 Introduction

The effect of redox and the placement method of compost within a "compost amended" slag system have been investigated in the previous chapter where it was shown that certain conditions favour the release of some E-tech elements (notably vanadium and molybdenum; see Chapter 6). However, the geochemical processes affecting these and other elements within the system are not well understood. A particular concern comes from the observation that several well-studied elements display complex behaviours in the batch and column experiments, e.g. magnesium and silicon (see Chapter 4 – 6). Consequently interpretation of the leaching behaviours of all elements is currently based on geochemical modelling rather than observed processes.

The research presented in this Chapter aims to provide a better understanding of the mechanisms controlling the leaching of these elements, and their fate. Since the flux of the metal leached into solution is a function of the dissolution flux minus reprecipitation flux, the very low levels of magnesium in solution (see Tables 4.2, 4.5, 4.8 and section 6.3.2.2.2) could be due to either very heterogeneous dissolution or very high reprecipitation. Any reprecipitation process will have its own set of co-precipitation and distribution properties, and so it is key to constrain this part of the system. The test is simple: is there a Mg-Si rich precipitate on the surface of the weathered solid?.

Here, we use lithium as a reference element following the observation drawn from previous chapters (Chapter 4) that it is behaving conservatively. We investigate other elements relative to this conservative behaviour, and estimate the distribution behaviour between the aqueous and solid phase for each element (see equation 2.7), relative to “conservative” lithium and “non conservative” magnesium. A better constraint on the controls on leaching behaviour of other elements (Si, Ca, V, Ni, Mo) is provided. By undertaking the solid phase assessment of the steel slag obtained at the end of the column experiments (Chapter 6), we also more fully elucidate the fate of elements of interest in steel slag deposits that are in lower concentration in the leachate than they would be were they perfectly conservative.

7.2 Experimental approach

7.2.1 Sample preparation

At the end of the column leaching experiment described in section 6.2.2, the columns were left to drain for a week until completely dry. Afterwards, the columns were split horizontally at 2 cm intervals using a cutting saw. The slag samples from the individual 2 cm sections were collected, recorded and sub-sampled.

7.2.2 Image analysis

The examination of the surface of all the calcein stained compost amended and non-amended slag from the columns, see section 6.2.2.3 for staining details, was done using fluorescent UV light (λ = 495 nm) and photographed using a 14 megapixels Fujifilm FinePixS camera attached to a Jessops TP.323 Tripod (see plate 7.1). The UV light stimulates fluorescence in the calcein, revealing where Ca or Mg-rich precipitates have formed on the surface of the weathered slag and within the compost. Images of the slag samples in the top, middle and bottom 2 cm interval of the various columns were taken so as to assess the evolution of the reprecipitation process in the columns as a function of depth.

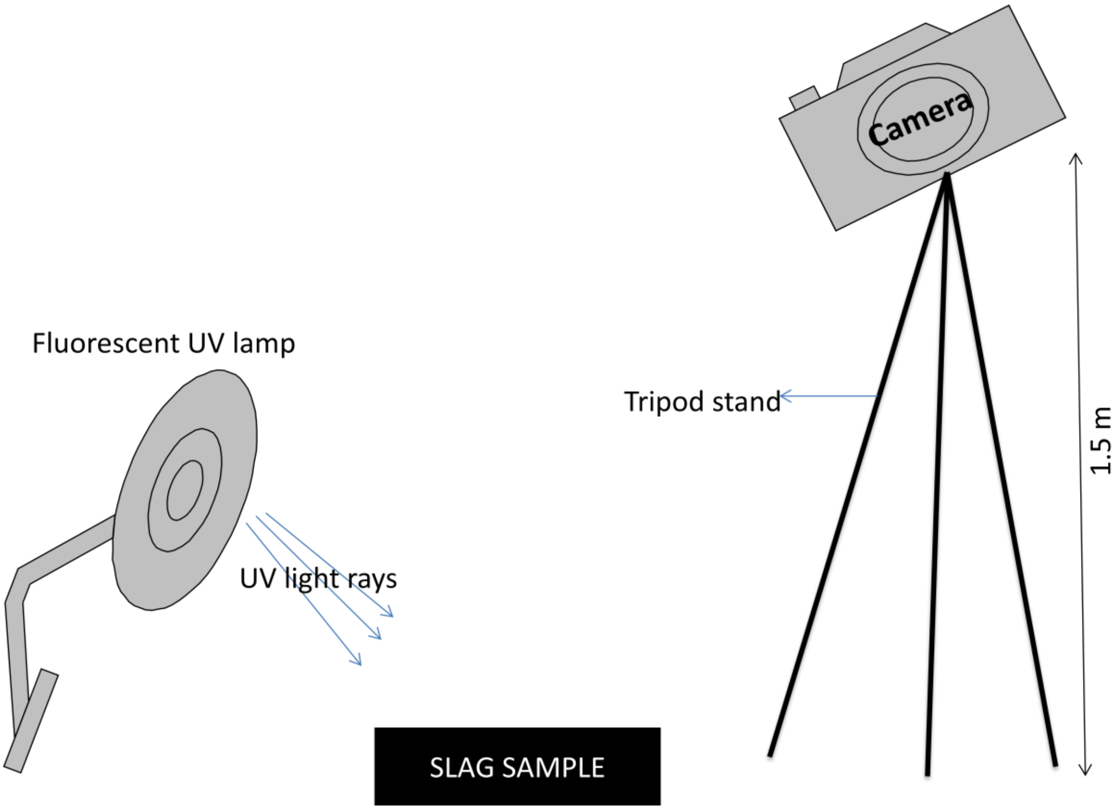

Figure 7.1: Schematic set –up used for image analysis of calcein stained steel slags

7.2.3 Thin section preparation

A slag sample was randomly selected from the top 2 cm zone of each of the columns. Each selected slag sample was horizontally cut into two-halves using a 6'' Buehler trim saw with a continuous rim diamond blade. One half was ground and prepared for XRD analysis (see section 3.3.3) while a thin section of the other half was prepared as described below.

The cut sample was polished using a Buehler metaserv grinding wheel fitted with a 40 micron diamond plate operating at a speed of 300 rpm and lubricated using water. The polished surface was gently smeared with an epoxy mixture (resin and hardener) and heated at 100 °C on a hot plate for a period of 15 minutes so as to allow adequate penetration of the resin into the sample. The sample was then further polished using a 10 micron diamond plate in order to obtain a finer surface. The finely polished slag sample was placed in a 30 ml mould and epoxy resin mix was introduced then left to cure overnight. Afterwards, the impregnated sample was further polished with a 10 micron diamond plate coated with a fine abrasive (aluminium oxide) and then placed in an ultrasonic bath to get rid of surface impurities. A final polishing stage was achieved by smearing the surface of the sample with 1 micron mono-crystalline diamond suspension followed by continuous polishing on a grinding wheel.

7.2.4 Microscopy and Mineralogy

Thin sections, which were left uncovered, were subjected to SEM analysis in accordance with the procedure detailed in section 3.3.4. In addition, the SEM instrument was operated in the variable pressure mode due to the non-conductive nature of the sample, so as to avoid charging of the sample and the production of low resolution images since no sample coating was required. EDX analysis was carried out on selected regions within the slag for composition analysis. Mineralogical analysis of the ground slag was determined via XRD following the method described in section 3.3.3.

7.3 Results

7.3.1 Weathered slag characterisation

Precipitated mineral phases were observed on the surface of the weathered slag samples (see Figure 7.1), these were mostly whitish in colour. Here, the extent of reprecipitation has been assessed qualitatively as a function of the intensity and number of fluorescent slag samples within the columns. In the control column (A), the reprecipitation process was enhanced particularly in the upper zone of the column. However, the precipitation process decreases with increasing depth since fewer fluorescent samples were observed in the deeper zones of column A. On the contrary, in the compost amended columns (B, C, D), there was little / no observable fluorescence (Figure 7.1).

Figure 7.2: Photographic image of control and compost amended steel slag showing secondary precipitation as a function of depth.

There were visible changes observed around the rim region on the surface of clasts, both within the control and compost capped slag treatment (column B) samples, however this was not observed for the compost blend (C) and intermediate (D) samples (Figure 7.3).

SEM analysis of the observed rim in the weathered slag samples (Figure 7.3), revealed the presence of three distinct zones. The inner zone was composed of large grey masses, with size > 1mm in most cases, and this made up the bulk of the core of the sampled slag (see point d, Figure 7.3 a). EDX analysis of the inner core (see Figure 7.3 a, point d) of the slag grain revealed that this zone was predominantly made of Mg and O, with traces of C, Ca and Si (Figure 7.3 b; see Appendix A6 for weight % composition). The majority of the grains were intact, but some had interstices which were filled with a bright coloured material (see point e, Figure 7.3 a). EDX analysis of the interstices (point e Figure 7.3 a) suggests that this zone was mainly composed of O and Mg with near-equal proportions of Ca, Si and C (Figure 7.3 b; Appendix A6).

The middle zone was composed of a mix of bright grey and dark grey irregular shaped masses. These small masses varied in size and were distributed in a random fashion within this region (see points b, c, and A3 Figures 7.2 a and c). EDX analysis of points b and c revealed a similarity in the elemental composition of both points consisting of O, Ca, C, Si and Mg (Figure 7.3 b; Appendix A6). EDX analysis of point A3 (Figure 7.3 c) confirms the presence of O, C, Mg, Ca, Si with traces of Al, Fe, Cr, Mn (Figure 7.3 d; Appendix A7).

The outer zone was composed of fine well-stacked crystals, with a shrubby-like appearance, and which extend vertically up to approximately 20 μm in length. Semi – quantitative EDX analysis of the outer layer (see points a, A1, and A2

Figures 7.2 a & c), confirmed the predominance of O, C and Mg in this region with traces of Ca and Si (see Appendix A6 and A7 for representative weight composition).

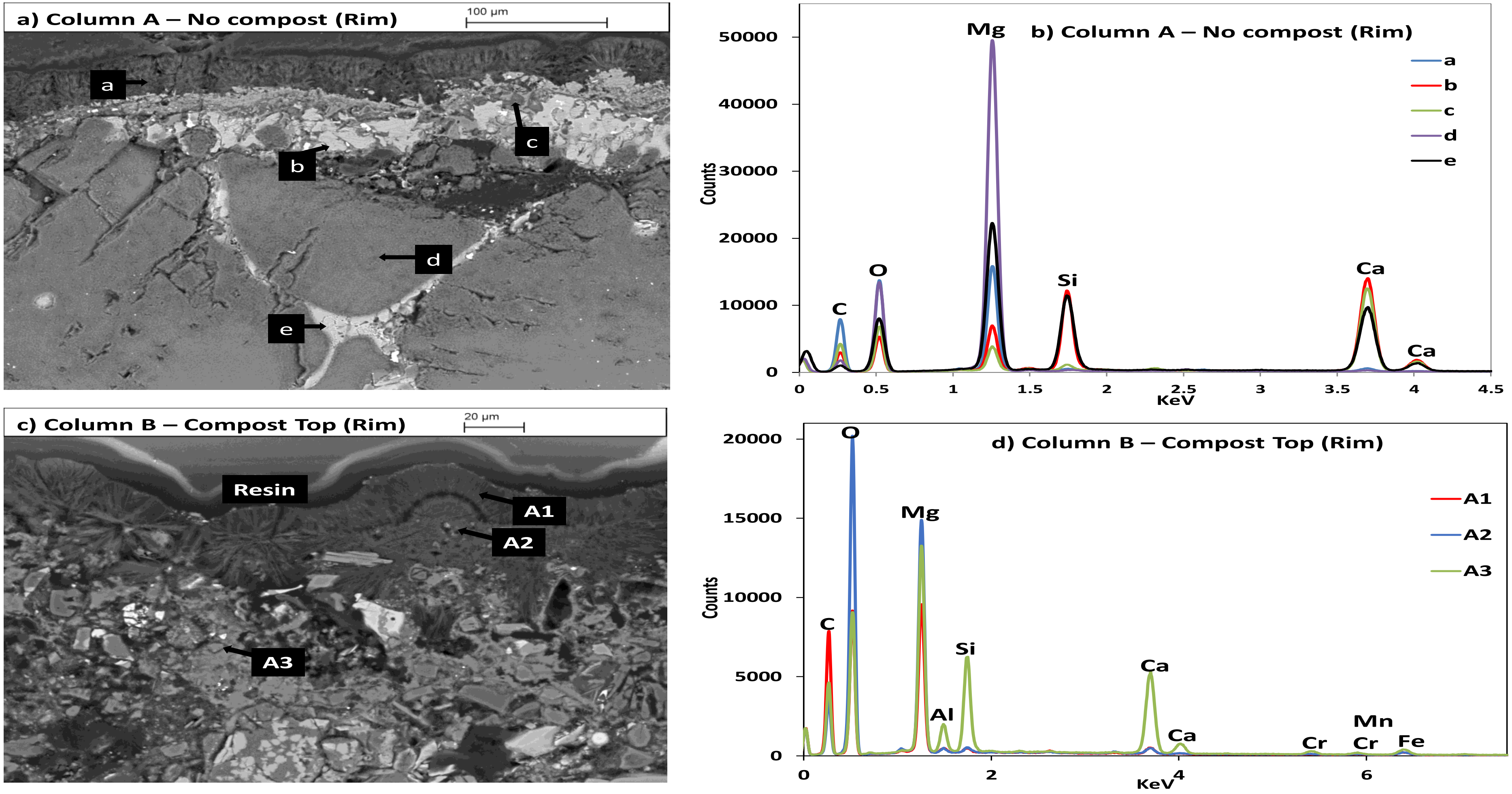

Figure 7.3: Reaction rim of (a) control column – SEM image (b) control column – EDX spectrum (c) compost amended column – SEM image (d) compost amended column – EDX spectrum.

Mineralogical analysis of the weathered material from the control column (Figure 7.4 a), confirmed the presence of periclase (MgO) as the main phase, with additional phases such as quartz (SiO_2), larnite (Ca_2SiO_4), calcite ($CaCO_3$), portlandite ($Ca(OH)_2$), and clinoenstatite ($MgSiO_3$). Also, XRD analysis of slag sample from compost amended column B (Figure 7.4 b) revealed the presence of calcite ($CaCO_3$), larnite (Ca_2SiO_4), dolomite ($Ca (Mg)(CO_3)_2$), lime (CaO), periclase (MgO) and merwinite ($Ca_3Mg(SiO_4)_2$.

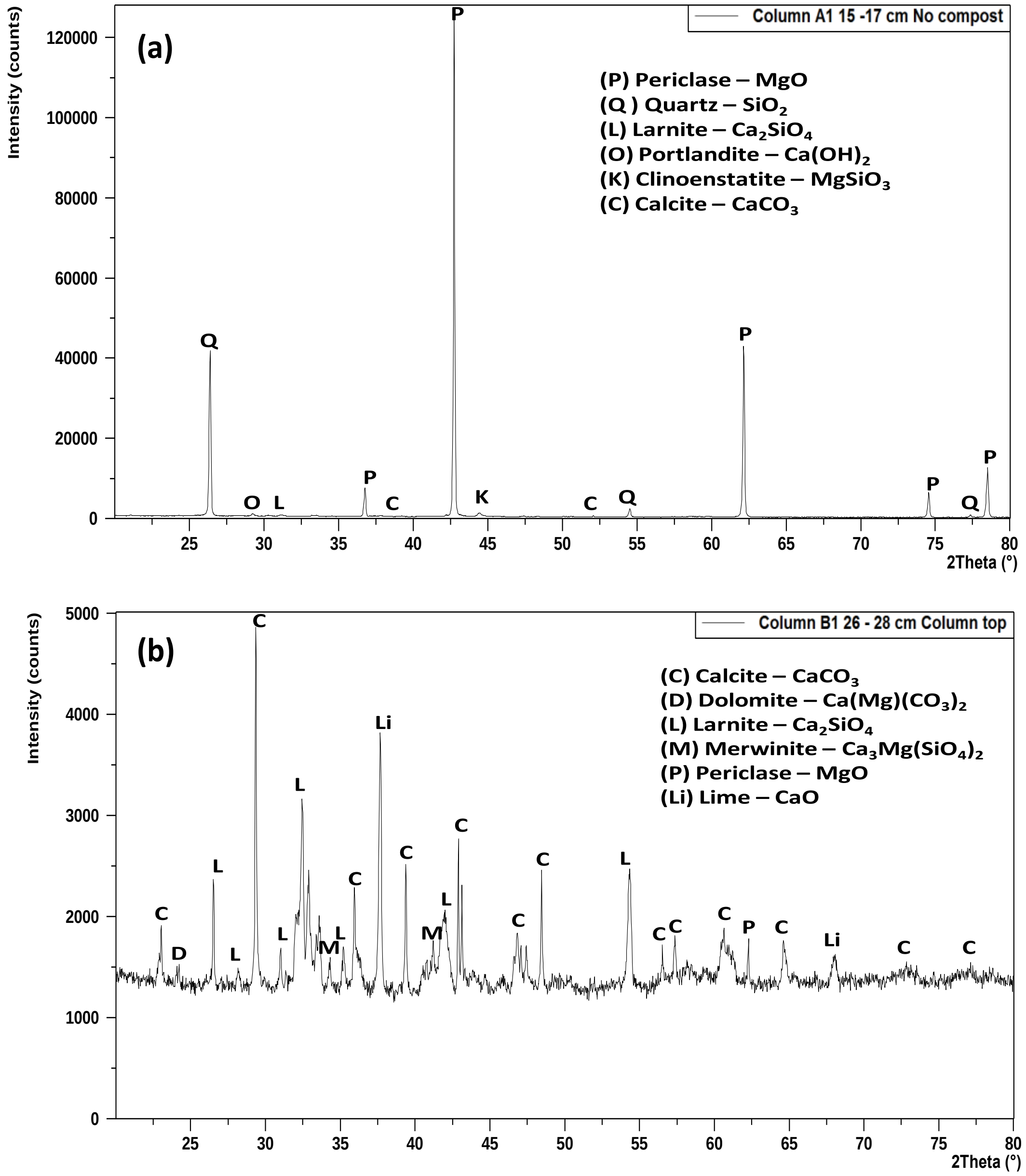

Figure 7.4: Mineralogical analysis of selected slag sample from (a) control column – no compost (b) compost amended column (column top).

7.3.2 Distribution and leaching behaviour of elements

In this section, the relative distribution coefficients of the elements of interest have been calculated (Equation 2.7), using lithium as the reference element due to its conservative behaviour (See Chapter 4). Similarly, elements such as sodium, potassium and sulphur also behaved in a conservative manner in the columns (see Appendix A8). The relative distribution coefficient help provide an understanding of the preferred phase for each element, relative to this conservative lithium species. The elements of interest that have been considered in this section include magnesium, calcium, silicon, nickel, vanadium and molybdenum.

7.3.2.1 Magnesium

Figure 7.5 presents a plot of the relative distribution coefficient (rK_D) of magnesium with respect to conservative lithium over time, in the various column treatments. Magnesium was initially semi-soluble in the control column (A), compost top column (B), and the column intermediate column (D) but became less soluble over time. On the other hand, magnesium was slightly soluble throughout the experiment in the compost blend column (C), although its solubility decreased over time.

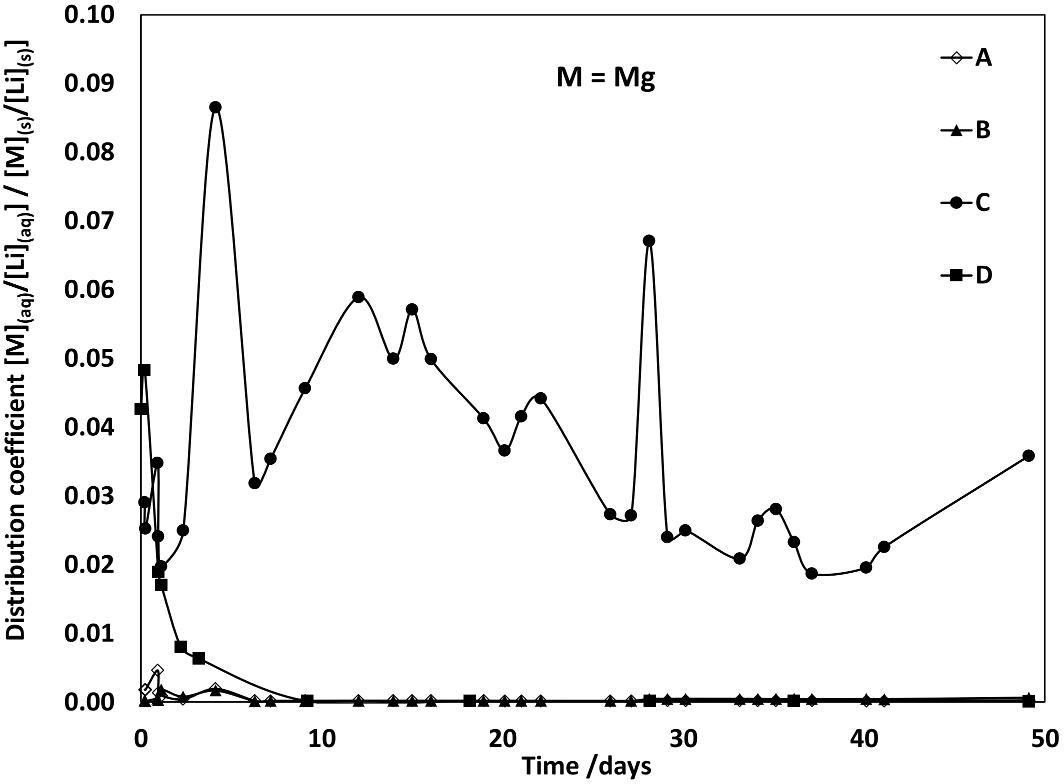

Figure 7.5: Relative distribution coefficient of magnesium in the investigated column treatments. A – Control, B - Compost top, C - Compost blend, D - Compost intermediate.

7.3.2.2 Calcium, silicon, nickel, and vanadium

Figure 7.6 presents plots of the relative distribution coefficient of calcium, silicon, nickel, and vanadium with respect to conservative lithium over time, in the various column treatments.

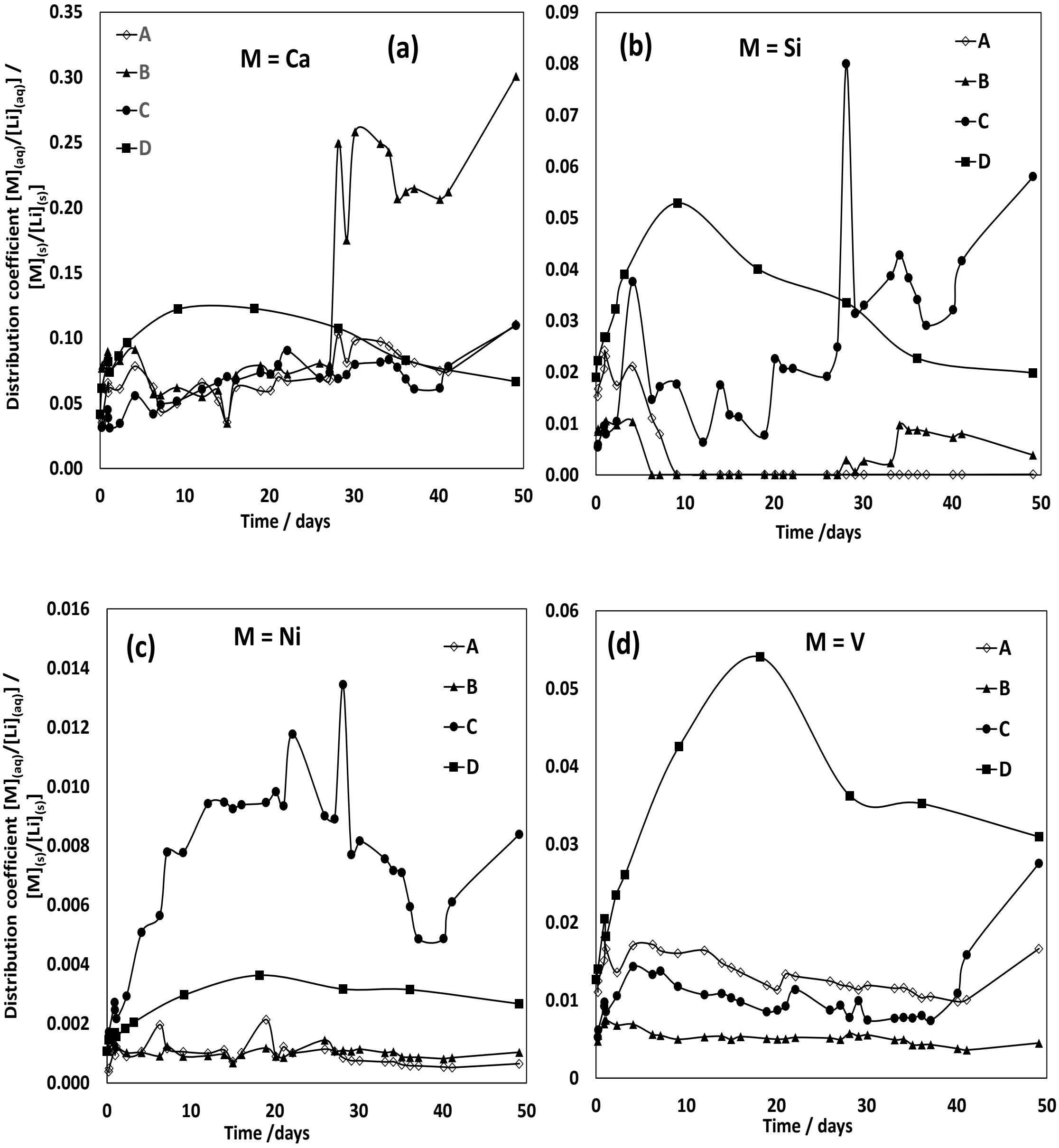

Figure 7.6: Relative distribution coefficient plots for (a) calcium (b) silicon (c) nickel (d) vanadium in column experiments. A – Control, B - Compost top, C - Compost blend, D - Compost intermediate.

Calcium solubility was low in all the columns and there were slight differences in leaching behaviour for the different columns (Figure 7.6 a). The solubility of calcium increased rapidly over time in column B, reaching a rK_D value of 0.30 by the end of the leaching experiment. The leaching behaviour of calcium in columns A and C were similar throughout the experiment, but were less soluble than column B and with a rK_D value of 0.10, reached by the end of the experiment. The distribution coefficient of calcium in column D plateaued after 10 days of leaching with a rK_D value of 0.12, after which the solubility of calcium decreased for the rest of the experiment (Figure 7.6 a).

Silicon was less soluble compared to calcium with a maximum rK_D value of < 0.08 (Figures 7.5 a and b). Similarly, just as calcium, silicon displayed different behaviours for the different treatments (Figure 7.6 b). In the control column A and column B, silicon became quite insoluble over time. In column D, silicon was initially semi-soluble however this decreased over time. The solubility of silicon was greatest in column C and also increased over time (Figure 7.6 b).

The solubility of nickel was very low in all the columns (Figure 7.6 c). In column A, B, and D, nickel solubility was relatively constant over time while in column C, there was increased nickel solubility, although this remained within low levels reaching a rK_D of 0.008 by day 50. Vanadium was slightly soluble in the columns, this solubility was however greater in column D compared to the other column treatments (Figure 7.6 d).

7.3.2.3 Molybdenum

Figure 7.7 presents a plot of the relative distribution coefficient of molybdenum with respect to conservative lithium over time, in the various column treatments. There was a variation in the behaviours of Mo in the various columns. Molybdenum exhibited a conservative behaviour and was more soluble in columns C and D while a non-conservative behaviour was observed in columns A and B.

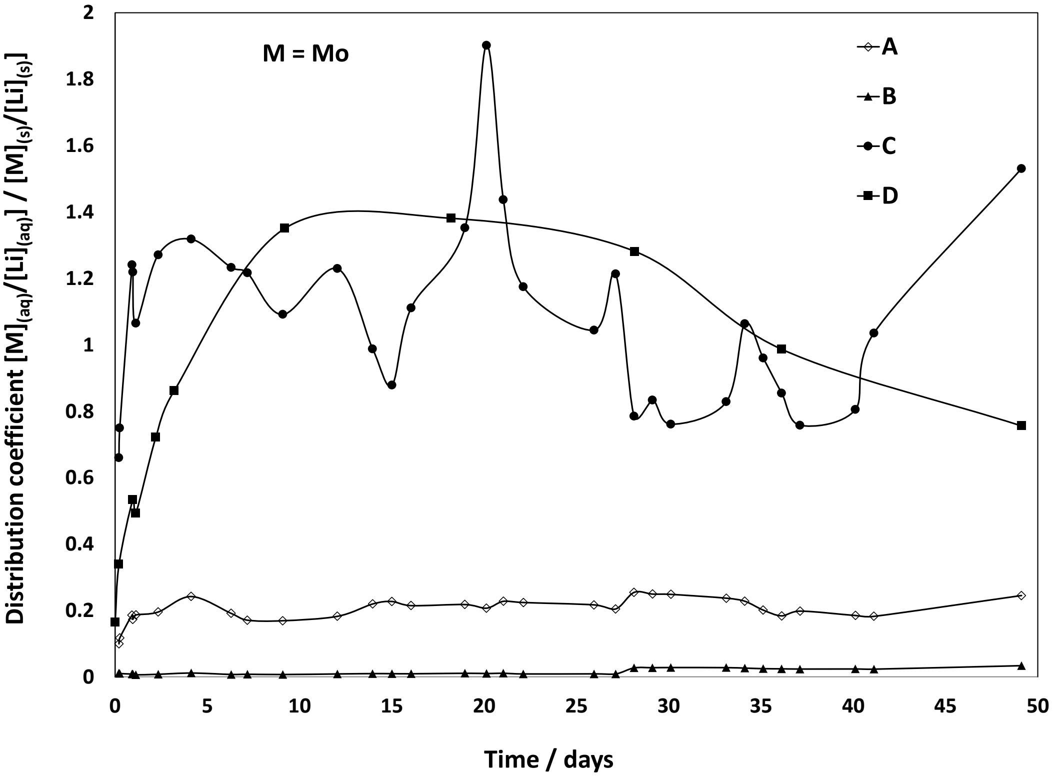

Figure 7.7: Relative distribution coefficient of molybdenum in the investigated column treatments. A – Control, B - Compost top, C - Compost blend, D - Compost intermediate.

7.4 Discussion

The surface reprecipitation process was greater in the control treatment compared to the compost-amended treatments (Figure 7.1), evidenced by the greater number of fluorescent samples and the low levels of calcium release in this column compared to others (Figure 6.8). This is likely due to the competition for available CO_2 between the compost and steel slag in the compost treatments and greater CO_2 diffusivity into the control column (Houst and Wittman, 1994). Mineral reprecipitation as a mechanism controlling the leaching of trace elements at high pH is widely reported (Baciocchi *et al.*, 2009; Huijgen *et al.*, 2005; Pan *et al.*, 2012). The examination of the weathered slag sample revealed that the inner zone was composed of predominantly unaltered MgO (periclase) grains (Figure 7.3 a and b; point d) and possibly traces of CaO (lime) (Figure 7.4 b). Periclase and lime are unstable over time hence tend to be converted to a more stable form (Zussman *et al.*, 2011). This is usually achieved via a 2 step process. In the case of lime, it alters to portlandite $Ca(OH)_2$ and subsequently calcite $CaCO_3$ (Bayless and Schulz, 2003).

Alternatively, periclase can weather to a carbonate phase via a 3 stage mechanism involving the initial alteration of periclase (MgO) to brucite $Mg(OH)_2$, subsequent transformation to hydromagnesite ($Mg_5(CO_3)_4(OH)_2{\cdot}4H_2O$) (Wogelius *et al.*, 1995), followed by surface dehydration. The weathered slag samples examined in this work show features typical of at least a two-step weathering process, for example the layered structure of the weathered material (Fig. 7.2) with the anticipated non-carbonate weathering products in the intermediate layer (Fig. 7.2) and the presence of intermediate products in the weathered slag (Figure 7.3 a, c). However, not all the weathering products are consistent with the pathways described above.

In the column experiments, simultaneous silification and carbonation initially occurs within the inner zone of the weathered slag. Here, the periclase and lime grains react with dissolved silica present in solution (0.11 ± 0.01 ppm; see Table 4.2) and atmospheric CO_2. The product is a mix of intermediary phases such as $MgSiO_3$ (clinoenstatite), Ca_2SiO_4 (larnite), $MgCO_3$ (magnesite), and $CaCO_3$ (calcite), found within the middle zone around the rim of the examined weathered slag samples (see points b, c, and A3; see equations 7.1 – 7.4). The presence of these products was further confirmed using a combination of the EDX data of this region and the XRD data of the slag sample (Figure 7.3).

$$MgO_{(s)} + SiO_{2_{(aq)}} \rightarrow MgSiO_{3_{(s)}} \quad (7.1)$$

$$2CaO_{(s)} + SiO_{2_{(aq)}} \rightarrow Ca_2SiO_{4_{(s)}} \quad (7.2)$$

$$MgO_{(s)} + CO_{2_{(aq)}} \rightarrow MgCO_{3_{(s)}} \quad (7.3)$$

$$CaO_{(s)} + CO_{2_{(aq)}} \rightarrow CaCO_{3_{(s)}} \quad (7.4)$$

Clinoenstatite ($MgSiO_3$) dominates within the middle (intermediate) zone (see Appendix A6 For quantification), reflecting the abundance of MgO in the bulk composition of the unweathered slag and the availability of dissolved silica compared to apparently low dissolved CO_2 concentration within the system. This magnesium silicate phase also extends between the interstices of the periclase grain (point e Figure 7.3 a). The presence of quartz (Fig. 7.3 a) is consistent with the clinoenstatite ($MgSiO_3$) from the middle zone reacting with $CO_{2(aq)}$ to form crystalline silicate and magnesite ($MgCO_3$). Magnesite constitutes the bulk of the outer precipitate zone of the slag sample (see points a, A1, A2 in Figure 7.3 a and c; equation 7.5). Consequently, we find the expected final weathering product and some of the reactions expected, but also evidence of an additional silica pathway for chemical weathering of these products.

$$MgSiO_{3_{(s)}} + CO_{2_{(g)}} \rightarrow MgCO_{3_{(s)}} + SiO_{2_{(s)}} \quad (7.5)$$

Magnesite and silica are more thermodynamically stable and unlikely to release further environmental pollutants. Furthermore, the precipitation of abundant insoluble magnesite on the surface of the slag adequately explains the unexpectedly low release of magnesium from these materials. Equally, the precipitation of quartz, detected via XRD (see Figure 7.4 a), could explain why little silica is released despite its expected high solubility at this pH (mean pH > 11.0 ± 0.3; Figure 6.6 a).

In the control column where the most magnesite precipitation was observed, calcium behaved in a non conservative manner. However, calcite is minor compared to magnesite, implying that the leaching of calcium is likely controlled via the formation of a solid solution between magnesite and calcite, rather than by the direct solubility of calcite itself. Magnesite and calcite are isomorphous, partially or fully replacing one another to form partial or full solid solution series (Cornelis *et al.*, 2008; Reeder, 1983). The electrical neutrality of the crystal is maintained regardless of substitution, as their ionic radii are relatively similar (0.99 Å in the case of calcium and 0.72 Å for magnesium; Barbalace, 2007), limiting the degree of distortion possible in the crystal lattice (Appelo and Postma, 2005). Consistent with this picture is the observation of dolomite in the weathered slag material (Figure 7.4 b). This is the stoichiometrically equal form ($Ca\ Mg\ (CO_3)_2$), and tends to assemble as alternating octahedral layers with slight rotation of the CO_3^{2-} groups to accommodate the slightly different radii (Boffa Ballaran *et al.*, 2007; Webb *et al.*, 1998).

In the column experiments, the solubility of nickel was controlled by the adsorption of nickel to magnesite forming on the slag surface. This is in line with the non-conservative behaviour observed for nickel in the control column (A) where magnesite precipitation was greatest, whereas in the blended column C, nickel exhibited a more conservative behaviour due to the relative unavailability of magnesite surfaces on which to bind (Figure 7.6 c). Indeed, the leaching behaviour of magnesium was similar to that observed for nickel in all the columns (Figure 7.5, Figure 7.6 c). The adsorption of nickel to mineral surfaces has been widely reported as a controlling mechanism for trace element mobility (Carrillo-González et al., 2006; Deverel *et al*., 2012; Smith, 1999). At pH values > 9.5, such as those reported in these experiments, sorption of nickel to the binding sites increases (Cappuyns and Swennen, 2008). This is because at such alkaline pH region, carbonate ions dominates, thus allowing the adsorbent surface (magnesite) to attract more positively charged Ni^{2+} to its surface (Deverel *et al*., 2012; Erol and Ozdemir, 2015).

The leaching behaviour for molybdenum and vanadium were quite similar in all experiments, in terms of the relative leaching performance of the various treatments (Figures 7.5 c and d). The solubility of both of these elements were most likely controlled by the availability of organic ligands for complexation reactions and not governed by mineral precipitation. This is in agreement with the fact that the mobility of these elements were enhanced in the compost blend column (C) and the compost intermediate column (D), which had significantly higher dissolved organic carbon (DOC) content of 100 mg/L and 15 mg/L respectively, compared to the other two columns (control (A) and compost top (B)) with negligible DOC content of < 1 mg/L (Figure 6.7). Where high pH waters are in contact with organics, alkaline hydrolysis gives rise to enhanced leaching of dissolved organic carbon in the blended and compost intermediate treatments (Figure 6.7). However, the architecture of these columns gives rise to different pH values, with the blended one (C) well-buffered by the mixed organic materials in solution. The humic and fulvic acids in the DOC are well known to chelate various metals including vanadium and molybdenum (Carrillo-González et al., 2006). Where the pH remains high and V mobile (such as in the compost intermediate treatment D) this leads to greater export of V from the column (See Figure 6.7). In the blended treatment the buffered pH is likely to limit the mobility of V and non conservative behaviour of V in the control and capped treatments were due to the absence of DOC in the columns. At pH <10, V solubility is typically limited by sorption to hydrous ferric oxides and other mineral surfaces (Cornelis *et al.* 2007).

7.5 Conclusions

The solubility of silicon and magnesium, in both the control and compost - amended steel slag, is likely governed by the precipitation of quartz and magnesite respectively on the surface of the slag. This precipitation process occurs via a two-step mechanism which leads to the formation of more stable reaction products. Magnesite is the main precipitating phase within the studied slag system and most likely controls the leaching of calcium and nickel. In the case of calcium, this leaching process is controlled by solid-solution formation with magnesite. On the other hand, the solubility of nickel within the studied slag system is controlled through surface adsorption to magnesite. In the case of vanadium and molybdenum, the leaching process is controlled by the availability of organic ligands for formation of organic complexes with either vanadium or molybdenum. . Compost amendment had an observable effect on the leaching behaviour for vanadium and molybdenum. The release of both elements is enhanced either by thoroughly mixing the compost and steel slag or leaching a high pH solution through the compost before contact with the steel slag. From a pollution control perspective where leaching is aimed to be prevented, leaching the steel slag in the absence of organics or capping the top of the steel slag with compost prior to leaching could be a viable approach. Also, since the reprecipitation process leads to the generation of silica, continuity in the formation of magnesite is ensured at the landfill site and also this process could also serve as a temporary storage for silica.

This knowledge could assist in the prediction of the long-term leaching behaviour of these wastes and possibly inform future remediation approaches.

8

Conclusions, future work and recommendations

8.1 Conclusions

Steel slag is an integral residue formed during the manufacture of iron and steel. It has established recycling potential due to its unique inherent physical and chemical properties. However, historically most steel slag residues were dumped in unregulated disposal sites and at present, a significant proportion of generated steel slag are disposed in active landfills. A review of alkaline waste production statistics suggests that around 2000 Mt are generated globally every year, and steel slag constitute about one-eighth of this amount (Gomes *et al.*, 2015).

Using field investigations (Chapter 4), this study has highlighted the consistencies and discrepancies in the chemistry of steel slag obtained from a range of disposal sites. Steel slag and analogous lime waste leachates are characterised by high pH and alkalinity due to the dissolution of free lime and calcium silicates. At such sites, elements such as lithium, sodium and potassium behave conservatively in steel slag and are easily leached out into solution. In addition, the source material and associated leachates were also smothered with secondary carbonate precipitates, formed through weathering processes and pronounced upstream, which act as a possible sink for certain metals. Elements such as calcium, magnesium, silicon, iron, nickel, molybdenum, and vanadium were not as easily leached possibly controlled by the slow dissolution or simultaneous precipitation of insoluble mineral phases, possibly magnesite, within the subsurface slag system. However, despite the precipitation of secondary phases containing trace elements, some exceed surface water regulatory guidelines e.g. vanadium and lithium, and thus pose environmental concern due to their toxic nature. As such, management of these leachates is likely to be an ongoing requirement of steel plants in the UK and beyond upon closure. Some of these elements that leach from the slag also hold some potential value if they were recovered, providing a potential win-win for minimising environmental toxicity and offsetting legacy treatment costs. To further investigate this, the scope for recovery of lithium, molybdenum, vanadium and nickel from steel slag leachates in microcosm experiments were undertaken.

Batch tests (Chapter 5) assessed some of the controls on leaching by comparative tests with water, strong acid and organic amendments. The HCl led to significantly higher leaching of elements of interest, notably vanadium, and achieved concentrations of V in leachates that approximate to those used in primary ore mining (Shen and Guo, 2015). However, such hydrometallurgical processes are unlikely to be viable due to cost at legacy sites. Organic amendments simulate the potential post-closure scenario for slag landfills and Chapter 5 demonstrated that compost amendment of steel slag enhances the leaching of molybdenum and vanadium by a factor of 3.6 and 2.5 respectively, above water leaching alone. This is most likely ascribable to organic complexation. The organic amendments also decreased the leaching of lithium and nickel, most likely through surface adsorption to negatively charged sites on the slag surface. As such, implications for leachate quality at amended slag sites needs to account for this potential preferential leaching of some oxyanion forming metals.

Furthermore, batch and column experiments (Chapter 6) were used to investigate the effect of redox and the physical positioning between steel slag and compost respectively, on the leaching characteristics of vanadium, molybdenum, nickel, and lithium in a compost amended steel slag system. The results demonstrate that the redox condition of the leaching environment and the configuration of the compost within the slag system, controls the leaching behaviour of the studied elements. For instance, the leaching of vanadium, molybdenum, and lithium from steel slag can be enhanced by placing compost between layers of steel slag prior to aerobic leaching. This is likely ascribable to alkaline hydrolysis of organics within the system. On the other hand, the release of nickel can be maximised by thoroughly mixing the steel slag with compost prior to leaching under anaerobic conditions.

Solid phase assessment of the weathered slag material obtained from the column experients (Chapter 7) were undertaken so as to provide a better understanding of the mechanisms controlling the leaching of elements of interest, and their fate. The results reinforced some of hypothesis made in previous chapters. The leaching of nickel was controlled by the adsorption to the precipitated phase (magnesite). Calcium release was governed by the formation of a solid-solution between calcite and magnesite. The results also showed that the precipitation of magnesite on the surface of the steel slag was not a single order process but at least two-step process. Furthermore, the results confirm that the leaching of vanadium and molybdenum was ascribed to organic complexation.

The aim of this project was to improve our understanding of the environmental risks and metal recovery opportunities associated with steel slag deposits and trial options for *in-situ* metal recovery. It can be seen from the results presented in this thesis, that steel slag deposits are enriched with various valuable metals, some of which holds potential environmental concern, however the recovery potential are enormous, and could serve as an established alternative reserve for metals given the large global demand for these metal resources. Furthermore, revenue generated from metal recovery can be used to compensate for the long term management of these residues.

8.2 Management Implications / Recommendations

This project demonstrated the potential issues with steel slag leachate under ambient leaching conditions at disposal sites. These centre on elevated pH above regulatory standards, excess rates of carbonate precipitation and enrichment of some trace elements above water quality standards (e.g. V, Li). Given the imminent need for long term legacy management at most steel plants in the UK (and to a lesser degree western Europe), there is a clear need for management plans to be formulated that can manage enduring issues of leachate production (Critchlow, 2015; Farrell and Smith, 2015; Farrell *et al.*, 2015). Furthermore, steel production continues to grow globally, particularly in China, and as such opportunities for valorisation of steel by-products is also a priority within the industry (Li and Guo, 2014; Morone *et al.*, 2014).

The approach trialled in this project could potentially offset treatment costs associated with disposal and management. Some of these disposal sites have been generating alkaline leachates for over four decades and would potentially benefit from recovering material of modest value from these heaps. However, there are broader implications associated with the proposed compost amendment approach. Compost amendment could help in terms of recovering vanadium and molybdenum from steel slag and possibly stabilise the slag material. However, compost cover could limit potential bulk reuse of the steel slag for other applications e.g. construction.

8.3 Additional work

There are various lines of future enquiry highlighted throughout the thesis, these are summarised in Table 8.1. The proposed future investigations primarily focus on material quantification, scaling up laboratory trials to field conditions, development of efficient metal recovery technologies, and assessment of the influence of microbes on the leaching of e-tech metals from alkaline residues, some of which are currently been addressed by various workers elsewhere (Gomes *et al*., 2015; Hocheng *et al*., 2014). This will reduce uncertainty in estimating the exact metal recovery potential of steel slag, and also help the future sustainable management of these leachates which are particularly timely given the dwindling state of the global steel industry and the closure of some, particularly in the UK.

Table 8.1: Proposed future investigations for this thesis

Research needs	Outcome
Material quantification: - In Chapter 2, the global production of alkaline residues due to industries was estimated to be in the region of 2000 Mt/yr. While some of these waste streams are globally quantified (steel slag, coal fly ash, red mud), there has never been a precedent for measuring others particularly lime waste and paper and pulp waste. Furthermore, the fate and quantity of alkaline residues at abandoned legacy sites worldwide is unknown and it is likely that some of these historical sites hold a significant proportion of secondary metal reserves. Hence, a global mapping exercise is needed to fully locate these legacy deposits and exploit their maximum metal recovery potential.	- Additional work is required in collaboration with material producers to create monitoring and reporting systems to understand the full extent of residue generation, disposal routes, possible reuse options and the potential for metal recovery.
Laboratory trials - Optimisation of laboratory leaching process (e.g. parameters such as slag to compost ratio, particle size, contact time) - Sequential analysis of compost amended steel slag - Development of efficient metal recovery techniques from alkaline leachates (e.g. solvent extraction, ion exchange) - Investigation on microbial influence on leaching of metals	- Maximise leachable volumes and modes of recovery - Improve understanding of the partitioning of metals of interest between organic and aqueous phases - Create an understanding of the importance and identity of microbes, if any, within a compost-amended steel slag system.
Field trials : compost amendment under environmental conditions -Scaling up laboratory trials to field scale -Investigation of possible methods of remediation of leachates from aftermath of metal recovery (e.g constructed wetlands)	- Greater certainty of leachable volumes with restoration strategies - Further improve the understanding of the influence of microbial and physical heterogeneity on treatment efficiency. - Greater certainty in flow rates, metal recovery rates and leachate buffering rates which will facilitate more robust engineering design guidance for remedial systems.

REFERENCES

Aarabi-Karasgani, M., Rashchi, F., Mostoufi, N., Vahidi, E., 2010. Leaching of vanadium from LD converter slag using sulfuric acid. *Hydrometallurgy,* **102**, 14–21.

Adriano, D.C., Page, A.L., Elseewi, A.A., Chang, A.C., Straughan, L., 1980. Utilisation and disposal of fly ash and other coal residues in terrestrial ecosystem: a review. *Journal of Environ. Quality*, **9**, 333 – 334.

Akcil, A., 2004. Potential bioleaching developments towards commercial reality: Turkish metal mining's future. *Minerals Eng.,* **17**, 477–480.

Akcil, A. and Deveci, H., 2010. Mineral biotechnology of sulphides, In *Geomicrobiology*, ed by Jain S, Khan A and Rai MK. Science Publishers, Enfield, NH, USA, 101–137.

Akcil, A., Erust, C., Gahan, C.S., Tuncuka, A., Deveci, H., 2013. Biohydrometallurgy of secondary metal resources: a potential alternative approach for metal recovery. *J Chem Technol Biotechnol.,* **88**, 2115–2132.

Alberic, P., Viollier, E., Jezequel, D., Grosbois, C., Michard, G., 2000. Interactions between trace elements and dissolved organic matter in the stagnant anoxic deep layer of a meromictic lake. *Limnology & Oceanography,* **45**, 1088-1096.

Alexandratos, V.G., Elzinga, E.J., Reeder, R.J., 2007. Arsenate uptake by calcite: Macroscopic and spectroscopic characterization of adsorption and incorporation mechanisms. *Geochimica et Cosmochimica Acta,* **71**, 4172 – 4187.

Amelinckx, S., Van Dyck, D., Van Landuyt, J., Van Tendeloo, G., (Editors) 2008. Electron Microscopy: Principles and Fundamentals. John Wiley and sons Inc., 527 pages.

Andrews, J.E., Gare, S.G., Dennis, P.F., 1997. Unusual isotopic phenomena in Welsh quarry water and carbonate crusts. *Terra Nova*, **9**, 67-70.

Anjum F., Shahid, M., Akcil, A., 2012. Biohydrometallurgy techniques of low grade ores: a review on black shale. *Hydrometallurgy,* **117–118**:1–12.

Anon, 2008. Flame which Burned in Harpur for decades. Buxton Advertiser Buxton, Johnston Press Digital Publishing.

Appel, C. and Ma, L., 2001. Concentration, pH and surface charge effect on cadmium and lead sorption in three tropical soils. *J. Environ. Qual.,* **31**, 581–589.

Appelo, C.A.J., and Postma, D., 2005. Geochemistry, Groundwater and Pollution, Second edition. Taylor & Francis, London. 668 pages.

Asokan, P., Saxena, M., Asolekar, S.R., 2005. Coal combustion residues: environmental implications and recycling potentials. *Resources, Conservation and Recycling,* **43**, 239 – 262.

Auer, M. T., Johnson, N. A., Penn, M. R., and Effler, S. W., 1996. Pollutant sources, depositional environment and the surficial sediments of Onondaga Lake, New York. *Journal of Environmental Quality*, **25**, 46-55.

Baciocchi, R., Costa, G., Bartolomeo, E, Polettini, A., Pomi, R., 2009. The effects of accelerated carbonation on CO_2 uptake and metal release from incineration APC residues. *Waste Management,* **29(12)**, 2994–3003.

Ball, J.W. and Nordstrom, D.K., 1991. User's manual for WATEQ4F, with revised thermodynamic data base and text cases for calculating speciation of major, trace, and redox elements in natural waters. U.S. Geological Survey Open-File Report 91-183.

Barbalace, K., 2007. Periodic Table of Elements - Sorted by Ionic Radius. EnvironmentalChemistry.com. 1995 - 2015. Accessed on-line: 12/11/2015 http://EnvironmentalChemistry.com/yogi/periodic/ionicradius.html

Barna, R., Bae, H., Me´hu, J., Van der Sloot, H.A., Moszkowicz, P., Desnoyers, C., 2000. Assessment of chemical sensitivity of Waelz slag. *Waste Management,* **20**, 115 – 124.

Barnes, I., O'Neil, J.R., Trescasses, J.J., 1978. Present day serpentinization in New Caledonia, Oman, Yugoslavia. *Geochim. Cosmochim. Acta*., **42**, 144 - 145.

Barra, M., Ramonich, E.V, Munoz, M.A., 2001. Stabilization of soils with steel slag and cement for application in rural and low traffic roads, In Proceedings of the Beneficial Use of Recycled Materials in Transportation Application, 423 – 432, RMCR University of Durham, Arlington, VA.

Bayless, E.R. and Schulz, M.S., 2003. Mineral precipitation and dissolution at two slag-disposal sites in northwestern Indiana, USA. *Environmental Geology,* **45**, 252–261.

Belevi, H. and Moench, H., 2000. Factors determining the element behavior in municipal solid waste incinerators: Field studies. *Environ. Sci. Technol*., **34**, 2501 – 2506.

Boffa Ballaran, T., Bromiley, F.A., Langenhorst, F., Seifert, F., 2007. Order and miscibility in the otavite–magnesite solid solution. *American Mineralogist,* **92**, 829 – 836.

Bonenfant, D., Kharoune, L., Sauve, S., Hausler, R., Niquette, P., Mimeault, M., Kharoune, M., 2008. CO_2 sequestration potential of steel slag at ambient pressure and temperature. *Ind. Eng. Chem. Res.,* **47**, 7610 – 7616.

Boss, C. B. and Fredeen, K. J., 2004. Concepts, Instrumentation and Techniques in Inductively Coupled Plasma Optical Emission Spectrometry. Perkin Elmer, USA.

Brierley, CL., 2010. Biohydrometallurgical prospects. *Hydrometallurgy,* **104**: 324–328.

British Lime Association, 2015. Lime Uses. http://www.britishlime.org/lime_uses/ accessed on 15/04/2015.

BS EN 12457-2:2002. Characterisation of waste. Leaching. Compliance test for leaching of granular waste materials and sludges. One stage batch test at a liquid to solid ratio of 10 l/kg for materials with particle size below 4 mm (without or with size reduction).

BSI PAS 100: 2005. http://www2.wrap.org.uk/downloads/Introduction_to_BSI_PAS_100-20052.3f664cd1.2181.pdf accessed on 12/8/14.

Buchman, M.F., 2008. *NOAA Screening Quick Reference Tables*, NOAA HAZMAT Report 99-1, Seattle WA. Coastal Protection and Restoration Division, National Oceanic and Atmospheric Administration, 12pp.

Burgstaller, W., Schinner, E., 1993. Metal Leaching with Fungi in *Biohydrometallurgical Techniques*, ed by Torma AE, Wey JE and Askshmanan VL. The Mineral, Metal and Materials Society, Warrendale, PA, 325–333.

Burke, I.T., Whittleston, R., Palani, S., Mortimer, R., Lockwood, C., Ashley, D., Stewart, D., 2012a. Biogeochemical reduction processes in a hyper-alkaline leachate affected soil profile. *Geomicrobiology,* **29**, 769 – 779.

Burke, I.T., Mayes, W.M., Peacock, C., Brown, A.P., Jarvis, A.P., Gruiz, K., 2012b. Speciation of arsenic, chromium, and vanadium in red mud samples from the Ajka spill site, Hungary. *Environ. Sci. Technol*., **46**, 3085 – 3092.

Cairns, J., Dickson, K. L., Crossman, J. S., 1972. The biological recovery of the Clinch River following a fly ash pond spill. In *Proceedings* of *25th Industrial Waste Conference* Purdue University, West Lafayette, Indiana, USA. 182-192.

Cappuyns, V. and Swennen, R., 2008. The application of pHstat leaching tests to assess the pH-dependent release of trace metals from soils, sediments and waste materials. *Journal of Hazardous Materials,* **158**, 185–195.

Carini, S.A. and Joye, S.B., 2008. Nitrification in Mono Lake, California: Activity and community composition during contrasting hydrological regimes. *Limnology and Oceanography,* **53 (6)**, 2546–2557.

Carrillo-Gonza´lez, R., Sˇimu˚ne, J., Sauve´, S., Adriano, D., 2006. Mechanisms and pathways of trace element mobility in soils. *Advances in Agronomy*, **91** 111 – 178.

CEM, 2011. http://www.cem.com/acid-digestion.html visited 20/06/14. Acid digestion microwave digestion.

Centioli, D., Comans, R.N.J, Gaudino, S., Galas, C., Belli, M., 2008. Leaching tests: useful tools for the risk assessment of contaminated sediments. *Ann Ist Super Sanità,* **44 (3)**, 252-257.

Chang, E.E., Chen, C.H., Chen, Y.H., Pan, S.Y., Chiang, P.C., 2011a. Performance evaluation for carbonation of steel-making slag in a slurry reactor. *J. Hazard. Mater*. **186**, 558 – 564.

Chang, E.E., Pan, S.Y., Chen, Y.H., Chu, H.W., Wang, C.F., Chiang, P.C., 2011b. CO_2 sequestration by carbonation of steelmaking slag in an autoclave reactor. *J. Hazard. Mater.* **195**, 107 – 114.

Charles, J., and Nemmer, P.E., 2006. User guideline manual on the use of waste and byproduct materials in pavement construction. Office of Engineering, Research and Development, Federal Highway Administration. Http://www.tfhrc.gov/hnr20/recycle/waste/ssa1.htm

Charun, B., Sudarat, T., Juntima, C., 2012. Leaching of steelmaking slag using acetic acid solution and deionized water for CO_2 sequestration. Paper presented at the 10th International PSU Engineering Conference, Thailand.

Chaurand, P., Rose, J., Briois, V., Olivi, L., Hazemann, J.-L., Proux, O., Bottero. J-Y., 2007. Environmental impacts of steel slag reused in road construction: A crystallographic and molecular (XANES) approach. *Journal of Hazardous Materials,* **139**, 537–542.

Chritchlow, A., 2015. 'China's dumped steel leaves UK industry facing fight for survival', The Telegraph, 20 September. Available online at : http://www.telegraph.co.uk/finance/commodities/11878679/Chinas-dumped-steel-leaves-UK-industry-facing-fight-for-survival.html (Accessed: 15/11/15).

Chrysochoou, M. and Dermatas, D., 2006. Evaluation of ettringite and hydrocalumite formation for heavy metal immobilization: Literature review and experimental study. *Journal of Hazard. Materials,* **136**, 20 – 33.

Clark, I. D., Fontes, J.C., Fritz, P., 1992. Stable isotope disequilibria in travertine from high pH waters: Laboratory investigations and field observations from Oman. *Geochimica et Cosmochimica Acta,* **56**, 2041 - 2050.

Cornelis, G., Van Gerven, T., Vandecasteele, C., 2005. The effect of calcium-bearing minerals on the solubility of molybdate and antimonate in alkaline wastes. Paper presented at WasteEng05, International Conference on Engineering for Waste Treatment edition:1 location:Albi, France date : May 17-19.

Cornelis, G., Saikia, N., Van Gerven, T., Vandecasteele, C., 2006. Leaching of Antimony and Molybdenum from Municipal Solid Waste Incinerator Residues.

In: Ilic, M., Goumans, J.J.J.M., Miletic, S., Heynen, J.J.M., Senden, G.J. (Eds), Proc. WASCON, May 30–June 2, Belgrade, pp. 205 – 216.

Cornelis, G., Johnson, C.A., Van Gerven, T., Vandecasteele, C., 2008. Leaching mechanisms of oxyanionic metalloid and metal species in alkaline soild waste (Review*). Applied Geochem*., **23**, 955 - 976.

Costa, G., Baciocchi, R., Polettini, A., Pomi, R., Hills, C.D., Carey, P.J., 2007. Current status and perspectives of accelerated carbonation processes on municipal waste combustion residues. *Environ. Monit. Assess.* **135**, 55 – 75.

Costa, G., 2009. Accelerated carbonation of minerals and industrial residues for carbon dioxide storage. Università Degli Studi Di Roma.

Council decision 2003/33/EC. Establishing criteria and procedures for the acceptance of waste at landfills pursuant to Article 16 of and Annex II to Directive 1999/31/EC. http://eur-lex.europa.eu/LexUriServ/LexUriServ.do?uri=OJ:L:2003:011:0027:0049:EN:PDF.

Council Directive 1999/31/EC of 26 April 1999 on the landfill of waste *Official Journal L 182, 16/07/1999 P. 0001 – 0019. http://eur-lex.europa.eu/legal-content/en/ALL/?uri=CELEX:31999L0031.*

Cowan, C.E., Zachara, J.M., Resch, C.T., 1990. Solution ion effects on the surface exchange of selenite on calcite. *Geochim. Cosmochim. Acta,* **54**, 2223 – 2234.

Cruywagen, J.J., 2000. Protonation, oligomerization, and condensation reactions of vanadate (V), molybdate (VI), and tungstate (VI). *Adv. Inorg. Chem.* 49: 127 – 182.

Czop, M., Motyka, J., Sracek, O., Szuwarzyński, M., 2011. Geochemistry of the Hyperalkaline Gorka Pit Lake (pH>13) in the Chrzanow Region, Southern Poland. *Water Air Soil Pollution,* **214**, 423 – 434.

Dai, S., Zhao, L., Peng, S., Chou, CL., Wang, X., Zhang, Y., Li, D., Sun, Y. 2011. Abundances and distribution of minerals and elements in high-alumina coal fly ash from the Jungar power plant, China. *Int. J. Coal Geol.* **81:** 320 - 332.

Davis, J. A., Fuller, C. C., Cook, A. D., 1987. A model for trace metal sorption processes at the calcite surface: Adsorption of Cd^{2+} and subsequent solid solution formation. *Geochim. Cosmochim. Acta,* **51**, 1477 – 1490.

De Windt, L., Chaurand, P., Rose, J. 2011. Kinetics of steel slag leaching: batch tests and modeling. *Waste Manag*. **31**, 225 – 235.

Defra, 2015. UK Statistics on Waste – 2010 to 2012. https://www.gov.uk/government/uploads/system/uploads/attachment_data/file/416471/UK_Statistical_release_UPDATEv6_19_03_2015.pdf accessed on 10/1/2014.

Dellantonio, A., Fitz, W.J., Repmann, F., Wenzel, W.W., 2010. Disposal of coal combustion residues in terrestrial systems. *Journal of Environmental Quality,* **39,** 761-775.

Demadis, K.D., 2010. The Science and Technology of Industrial Water Treatment: Recent Developments in Controlling Silica and Magnesium Silicate Foulants in Industrial Water Systems. Taylor and Francis Group Boca Raton, FL 33487-2742.

Dethlefsen, V. and Rosenthal, H., 1973. Problems with dumping of red mud in shallow water. A critical review of selected literature. *Aquaculture,* **2**, 267 – 280.

Deverel, S., Goldberg, S., Fujii, R., 2012. Chemistry of trace elements in soils and groundwater. In W.W. Wallender and K.K Tanji (eds) ASCE Manual and Reports on Engineering practice No. 71. Agricultural salinity assessment and management (2nd edition) ASCE Reston VA CHAPTER 4 Pg 89-137.

Doucet, F.J., 2010. Effective CO_2-specific sequestration capacity of steel slag and variability in their leaching behaviour in view of industrial mineral carbonation. *Miner. Eng.* **23**, 262–269.

Dragun, J., and Chiasson, A., 1991. Elements in North American Soils. Hazardous Materials Control Resources Institutes, Greenbelt MD.

Duff, R., Webley, M., Scott, O., 1963. Solubilization of minerals by 2-ketogluconic acid producing bacteria. *Soil Sci.,* **95**:105 – 114.

Dusing, D.C., Bishop, P.L., Keener, T.C., 1992. Effect of redox potential on leaching from stabilized/solidified waste materials. *Journal of Air waste management association,* **42**, 56 – 62.

Dwivedi, A., and Jain, M.K., 2014. Fly ash – waste management and overview: A Review. *Recent Research in Science and Technology,* **6(1)**, 30-35.

Dyson, 2013. Compost treatment of steel slags. Unpublished Masters dissertation. Geography, Earth and Envionmental Science University of Hull, UK.

Edwards, P.J., and Maidens, J.B., 1995. *Investigations Into the Impacts of Ferruginous Minewater Discharges in the Pelenna Catchment on Salmonid Spawning Gravels*. (Environment Agency) Welsh Region Internal Report No. PL/EAW/95/6. National Rivers Authority, Cardiff, UK.

Effler, S. W., 1987. The impact of a chloro-alkali plant on Onondaga Lake and adjoining systems. *Water, Air and Soil Pollution*, **33**, 85-115.

Effler, S. W., Matthews Brooks, C. M., Driscoll, C. T., 2001. Changes in deposition of phytoplankton constituents in a Ca^{2+} polluted lake. *Environmental Science and Technology*, **35**, 3082 - 3088.

Effler, S.W., and Brooks, C.M., 1998. Dry Weight Deposition in Polluted Onondaga Lake, New York, U.S.A. *Water, Air, and Soil Pollution,* **103(1)**, 389 - 404.

Eloneva, S., Teir, S., Salminen, J., Fogelholm, C.J., Zevenhoven, R., 2008a. Fixation of CO_2 by carbonating calcium derived from blast furnace slag. *Energy,* **33**, 1461 – 1467.

Eloneva, S., Teir, S., Salminen, J., Fogelholm, C.J., Zevenhoven, R., 2008b. Steel Converter Slag as a Raw Material for Precipitation of Pure Calcium Carbonate. *Ind. Eng. Chem. Res.* **47**: 7104 – 7111.

Eloneva, S., Teir, S., Revitzer, H., Salminen, J., Said, A., Fogelholm, C.J., Zevenhoven, R. 2009. Reduction of CO_2 emissions from steel plants by using steelmaking slag for production of marketable calcium carbonate. *Steel Res. Int.* **80**, 415 – 421.

Elzinga, E. J., Reeder, R. J., Withers, S. H., Peale, R. E., Mason, R.A., Beck, K. M., Hess, W. P., 2002. EXAFS study of rare earth element coordination in calcite. *Geochim. Cosmochim. Acta,* **66**, 2875 – 2885.

Emery, J. J., 1982. Slag Utilization in Pavement Construction; *Extending Aggregate Resources*. ASTM Special Technical Publication **774**, American Society for Testing and Materials, Washington, DC.

Emery, L., 2013. Extreme environments: tufa formation at high pH from lime kiln waste, South Wales School of Earth and Ocean Sciences, Cardiff University, Cardiff, UK. CF10 3YE. PhD Thesis

Erol, S., and Özdemir, M., 2015. Removal of nickel from aqueous solution using magnesite tailing. *Desalination and Water Treatment*, DOI: 10.1080/19443994.2014.1003971.

Engström, F., Adolfsson, D., Samuelsson, C., Sandström, Å., Björkman, B., 2013. A study of the solubility of pure slag minerals. *Minerals Engineering,* **41**, 46–52.

Environment Agency, 2010. Waste acceptance at landfills. https://www.gov.uk/government/uploads/system/uploads/attachment_data/file/296422/geho1110btew-e-e.pdf accessed on 24/09/2015.

Euroslag, 2010. Typical compositional ranges of iron and steel slag. http://www.euroslag.com/products/properties/ accessed on 23/05/14.

Euroslag, 2013. http://www.euroslag.com/products/statistics/2012/ accessed on 16/09/2014

Farrell, S., and Smith, D., 2015. 'Redcar Steel plant to close with 1700 job losses', *The Guardian*, 28 September. Available online at : http://www.theguardian.com/business/2015/sep/28/redcar-steel-plant-to-close-with-1700-job-losses (Accessed: 16/11/15).

Farrell, S., Brooks, L., West, K., 2015. 'Tata Steel confirms 1200 job losses as industry crisis deepens', The Guardian, 20 October. Available online at : http://www.theguardian.com/business/2015/oct/20/tata-steel-expected-to-announce-1200-job-losses-in-uk (Accessed : 16/11/15).

Felföldi, T. S.; Somogyi, B. R.; Márialigeti, K. R.; Vörös, L., 2009. Characterization of photoautotrophic picoplankton assemblages in turbid, alkaline lakes of the Carpathian Basin (Central Europe). *Journal of Limnology,* **68** (2).

Fernández Bertos, M., Li, X., Simons, S.J.R., Hills, C.D., Carey, P.J., 2004. Investigation of accelerated carbonation for the stabilisation of MSW incinerator ashes and the sequestration of CO_2. *Green Chem*. **6**, 428 – 436.

FHWA, 2012. User Guidelines for Waste and Byproduct Materials in Pavement Construction. http://www.fhwa.dot.gov/publications/research/infrastructure/structures/97148/bfs1.cfm accessed 13/04/2014

Filella, M., Belzile, N. and Chen, Y.-W., 2002. Antimony in the environment: a review focused on natural waters. I. Occurrence. *Earth Science Rev.*, 57, 125-176.

Ford, D. C., and Williams, P. W., 1991. Karst Geomorphology and Hydrology; Chapman and Hall: Cambridge, U.K.

Franklin, M. L. and Morse, J. W., 1983. The interaction of manganese(II) with the surface of calcite in dilute solutions and seawater. *Mar. Chem*. **12**, 241 – 254.

Frengstad, B. and Banks, D., 2007. Universal controls on the evolution of groundwater chemistry in shallow crystalline rock aquifers: the evidence from empirical and theoretical studies. In Krásný J., and John M. Sharp (eds), Chapter 18: Groundwater in Fractured Rocks: IAH Selected Paper Series, Volume 9 CRC Press.

Gao, Y., Kan, A. T., and Tomson, M. B., 2003. Critical evaluation of desorption phenomena of heavy metals from natural sediments. *Environ. Sci. Technol*. **37**, 5566–5577.

Geelhoed, J.S., Johannes, C.L.M., Hillier, S., Lumsdon, D.G., Thomas, R.P., Farmer, J.G., Paterson, E., 2002. Identification and geochemical modeling of processes controlling leaching of Cr (VI) and other major elements from chromite ore processing residue. *Geochimica et Cosmochimica Acta*. **66**, 3927 – 3942.

Geiseler, J., 1996. Use of steelworks slag in Europe. *Waste Management,* **16**, 59-63.

Gerdemann, S.J., O'Connor, W.K., Dahlin, D.C., Penner, L.R., Rush, H., 2007. Ex Situ Aqueous Mineral Carbonation. *Environ. Sci. Technol.* **41**: 2587 – 2593.

Gerke, T.L., Scheckel, K.G., Maynard, J.B., 2010. Speciation and distribution of vanadium in drinking water iron pipe corrosion by-products. *Science of the Total Environment*, **408**, 5845-5853.

Gitari, W.M., Fatoba, O.O., Petrik, L.F., Vadapalli, V., 2009. Leaching characteristics of selected South African fly ashes: Effect of pH on the release of major and trace species. *Journal of Environmental Science and Health, Part A: Toxic/Hazardous Substances and Environmental Engineering,* 44 (3) 206-220.

Goldberg, S., Forster, H.S., Godfrey, C.L., 1996. Molybdenum adsorption on oxides, clay minerals, and soils. *Soil Sci. Soc. Am. J.* **60**, 425 – 432.

Gomes, H.I., Mayes, W.M., Rogerson, M., Stewart, D.I., Burke, I.T., 2015. Alkaline residues and the environment: A review of impacts, management practices and opportunities. *Journal of Cleaner Production* doi: 10.1016/j.jclepro.2015.09.111.

Gougar, M.L.D., Scheetz, B.E., Roy, D.M., 1996. Ettringite and C–S–H portland cement phases for waste ion immobilization: a review. *Waste Management,* **16**, 295 – 303.

Gregg, S.J. and Sing K.S.W., 1967. Adsorption, surface, area and porosity. Academic Press, London and New York.

Haddad, P.R. and Jackson, P.E., 1990. Ion Chromatography: Principles and Applications. *Journal of Chromatograpy Library,* 46, 776 pages.

Harber, A. J. and Forth, R. A., 2001. The contamination of former iron and steel works sites. *Environmental Geology*, **40**, (3), 324-330.

Haslam, S. M., 1990. *River Pollution - an Ecological Perspective.* John Wiley and Sons, London.

Heidrich, C., Feuerborn, HJ. Weir, A. 2013. Coal combustion products: A global perspective. *World of Coal Ash Conference*. Lexington, KY, USA

Hendrick G. van Oss, 2015. Iron and steel slag. U.S. Geological Survey, Mineral Commodity Summaries.

HM Revenue & Customs, 2015. Landfill tax rates. https://www.gov.uk/government/publications/rates-and-allowances-landfill-tax/landfill-tax-rates-from-1-april-2013#contents accessed 25/08/2015.

Hocheng, H., Su, C., Jadhav, U.U., 2014. Bioleaching of metals from steel slag by Acidithiobacillus thiooxidans culture supernatant. *Chemosphere,* **117**, 652-657.

Hou, X. and Jones, B.T., 2000. Inductively Coupled Plasma/Optical Emission Spectrometry. *Encyclopedia of Analytical Chemistry*, pp. 9468 – 9485. John Wiley & Sons Ltd, Chichester.

Houst, Y.F. and Wittman, F.H., 1994. Influence of porosity and water content on the diffusivity of CO_2 and O_2 through hydrate cement paste. *Cement and Concrete Research,* **24**, 1165–1176.

Hsieh, T. H., Chen, J. J., Chen, L. H., Chiang, P. T., Lee, H. Y., 2011. "Time-course gait analysis of hemiparkinsonian rats following 6-hydroxydopamine lesion". *Behavioural Brain Research,* **222** (1): 1–9. doi:10.1016/j.bbr.2011.03.031.PMID 21435355

Huang, P. M., Violante, A., Bollag, J. M., and Vityakon, P., 2005. "Soil abiotic and biotic interactions and impact on the terrestrial ecosystem and human welfare." Science Publishers, Plymouth, UK.

Huijgen, W.J.J., Witkamp, G.J., Comans, R.N.J., 2005. Mineral CO_2 sequestration by steel slag carbonation. *Environ. Sci. Technol.*, **39**, 9676 – 9682.

Huijgen, W.J.J. and Comans, R.N.J., 2006. Carbonation of Steel Slag for CO_2 Sequestration: Leaching of Products and Reaction Mechanisms. *Environ. Sci. Technol*. **40**, 2790-2796.

Hull, S.L., Oty, U.V., Mayes, W.M, 2014. Rapid recovery of benthic invertebrates downstream of hyperalkaline steel slag discharges. *Hydrobiologia,* **736**, 83 – 97.

ICDD, 2014. The International Centre for Diffraction Data. http://www.icdd.com/products/pdf2.htm.

Iizuka, A., Fujii, M., Yamasaki, A., Yanagisawa, Y., 2004. Development of a new CO_2 sequestration process utilizing the carbonation of waste cement. *Ind. Eng. Chem. Res*. **43**, 7880 – 7887.

International Magnesium Association, 2012. Desulfurizing Steel: Magnesium is the Reagent of Choice. Mg Showcase Issue 19, Spring edition pg 1 – 4.

Ishida, T. and Maekawa, K., 2000. Modeling of pH profile in pore water based on mass transport and chemical equilibrium theory. *Proc. JSCE,* **648**, 203 – 215.

Jarvis, A.P. and Younger, P.L., 1997. Dominating chemical factors in mine water induced impoverishment of the invertebrate fauna of two streams in the Durham Coalfield, UK. *Chemistry and Ecology,* **13**, 249-270.

Jia, L., Anthony, E.J., Charland, J.P., 2002. Investigation of vanadium compounds in ashes from a CFBC firing 100% petroleum coke. *Energ. Fuel*. **16**, 397–403.

Johnston, D., Potter, H., Jones, C., Rolley, S., Watson, I., Pritchard, J., 2008. Abandoned mines and the water environment. *Environment Agency Science project,* **SC030136-41**.

Johnson, C.A., Brandenberger, S., Baccini, P., 1995. Acid neutralising capacity of municipal waste incinerator bottom ash. *Environ. Sci. Technol*. **29**, 142 – 147.

Jones, D.R., 1995. The leaching of major and trace elements from coal ash. In: Swaine, D.J., Goodarzi, F. (Eds.), Environmental Aspects of Trace Elements in Coal. Springer publishers Netherlands.

Jones, A., Rogerson, M., Greenway, G., Potter, H.A.B., Mayes, W.M., 2013. Mine water geochemistry and metal flux in a major historic Pb-Zn-F orefield, the Yorkshire Pennines, UK. *Environmental Science and Pollution Research,* **20**, 7570 – 7581.

Juckes, L.M., 2003. The volume stability of modern steelmaking slag. *Mineral Processing and Extractive Metallurgy*, **112**, 177 – 197.

Juckes, L., 2011. Basics of slag production. www.globalslag.com accessed on 23/05/14.

Karlsson, S., Sjöberg, V., Todd, K., Sartz, L., 2011. Impact of organic carbon in the release of vanadium from LD-slag. *Proceedings of IMWA 2011* "Mine Water – Managing the Challenges" Aachen, Germany.

Kindness, A., Macias, A., Glasser, F.P., 1994a. Immobilisation of chromium in cement matrices. *Waste Management* **14**, 3 – 11.

Kindness, A., Lachowski, E.E., Minocha, A.K., Glasser, F.P., 1994 b. Immobilisation and fixation of molybdenum (VI) by Portland cement. *Waste Manage*. **14**, 97–102.

Klauber C., Power G., Grafe M., 2009. Review of bauxite residue alkalinity and associated chemistry. CSIRO Document DMR-3610.

Kodama, S., Nishimoto, T., Yamamoto, N., Yogo, K., Yamada, K., 2008. Development of a new pH-swing CO_2 mineralization process with a recyclable reaction solution. *Energy,* **33**, 776 – 784.

Koryak, M., Stafford, L. J., Reilly, R. J., and Magnuson, M. P., 2002. Impacts of steel mill slag leachate on the water quality of a small Pennsylvania stream. *Journal of Freshwater Ecology*, **17**, 461 – 465.

Korytkova, E.N., Pivovarova, L.N., Gusarov, V.V., 2007. Influence of iron on the kinetics of formation of chrysotile nanotubes of composition $(Mg, Fe)_3Si_2O_5(OH)_4$ under hydrothermal conditions. *Geochemistry International,* **45 (8)**, 825-831.

Kotuby-Amacher, J. and Gambrell, R.P., 1988. Factors affecting trace metal mobility in subsurface soils. Project summary USEPA/600/S2-88/036.

Kszos, L.A. and Stewart, A.J., 2003. Review of lithium in the aquatic environment: distribution in the United States, toxicity and case example of groundwater contamination, *Ecotoxicology,* **12**, 439-447.

Kumar, S., Kumar, R., Bandopadhyay, A., 2006. Innovative methodologies for the utilization of waste from metallurgical and allied industries. *Resources, Conservation and Recycling,* **48**, 301–314.

Kumarathasan, P., McCarthy, G.J., Hasset, D.J., Pflughoeft- Hasset, D.F., 1990. Oxyanion substituted ettringites: synthesis and characterization, and their potential role in immobilization of As, B, Cr, Se, and V. *Mat. Res. Soc. Symp. Proc*. **178**, 83 – 104.

Lackner, K.S., 2002. Carbonate Chemistry for Sequestering Fossil Carbon. *Annu. Rev. Energy Environ*. **27**: 193 – 232.

Langmuir, D., 1997. Aqueous Environmental Geochemistry, Chapter 1: Thermochemical Principles. Prentice hall Upper Saddle River, New Jersey 07458.

Lanzén, A., Simachew, A., Gessesse, A., Chmolowska, D., Jonassen, I., Øvreås, L., 2013. Surprising Prokaryotic and Eukaryotic Diversity, Community Structure and

Biogeography of Ethiopian Soda Lakes. PLoS ONE 8(8): e72577. doi:10.1371/journal.pone.0072577

Lea, D.W., 1999. Trace elements in foraminiferal calcite. In *Modern Foraminifera (*ed Barun K. Sen Gupta), Kluwer Academic Publishers, Great Britain 259 – 277.

Lebourg, A., Sterckeman, T., Ciesielski, H., Proix, N., 1998. Trace metal speciation in three unbuffered salt solutions used to assess their bioavailability in soil. *J. Environ. Qual*. **27**, 584–590.

Lekakh, S.N., Rawlins, C.H., Robertson, D.G.C., Richards, V.L., Peaslee, K.D., 2008. Kinetics of aqueous leaching and carbonization of steelmaking slag. *Metall. Mater. Trans. B* **39**, 125 – 134.

Li, Z., Bugdol, M., Crama, W., 2012. Optimisation of hot metal desulphurisation slag in the CaO/Mg co-injection process to improve slag skimming performance. *Proceedings of the 9th International Conference on Molten Slag, Fluxes and Salts (MOLTEN 12)*, Beijing, China.

Li, G. and Guo, M., 2014. Current Development of Slag Valorisation in China. *Waste Biomass Valor.* **5**,317–325.

Lim, M., Han, G.C., Ahn, J.W., You, K.S., 2010. Environmental Remediation and Conversion of Carbon Dioxide (CO_2) into Useful Green Products by Accelerated Carbonation Technology. *Int. J. Environ. Res. Public Health*. **7**: 203 – 228.

Lopez Gomez, F.A., Aldecoa, R, Fernandez Prieto, Julia M., 1999. Preparation of NPK fertilizers from ferrous-metallurgy. *Simoes C Eur Commun*. [Rep];**18616**:1–57.

Lothenbach, B. and Winnifeld, F., 2006. Thermodynamic modeling of the hydration of Portland cement. *Cement Concrete Res*. **36**, 209 – 226.

Lüttge, A. and Metz P., 1993. Mechanism and kinetics of the reaction: 1 dolomite + 2 quartz = 1 diopside + 2 CO_2: a comparison of rock-sample and of powder experiments. Contributions to Mineralogy and Petrology, 115 (2) 155-164.

Mack, B. and Gutta B., 2009. An analysis of steel slag and its use in acid mine drainage (AMD) treatment. Paper presented at the 2009 National Meeting of the American Society of Mining and Reclamation, Billings, MT. Revitalizing the

Environment: Proven Solutions and Innovative Approaches. R.I. Barnhisel (Ed.) Published by ASMR, 3134 Montavesta Rd., Lexington, KY 40502.

Madsen, J. D., Bloomfield, J. A., Sutherland, J. W., Eichler, L. W., Boylen, C. W., 1996. The aquatic macrophyte community of Onondaga Lake: Field survey and plant growth bioassays of lake sediments. *Lake and Reservoir Management¸* **12**, 73-79.

Manerikar, R.S., Apte, A.A., Ghole,V.S., 2008. In vitro genotoxicity of fly ash leachate in earthworm coelomocytes. *Toxicol.Environ.Chem*. **90**,293 – 300.

Manso, J.M., Losañez, M., Polanco, J.A., and Gonzalez, J.J., 2005. Ladle furnace slag in construction. *Journal of Materials in Civil Engineering,* **17 (5)**, 513–518.

Maslehuddin, M., Alfarabi, A.M., Sharif, M., Shameen, M., Ibrahim, M., Barry, M.S., 2003. Comparison of properties of steel slag and crushed limestone aggregate concretes. *Construct Build Mater*. **17(2)**:105–12.

Mayes, W.M., Large, A.R.G., Younger, P.L., 2005. The impact of pumped water from a de-watered Magnesian limestone quarry on an adjacent wetland: Thrislington, County Durham, UK. *Environmental Pollution,* **138**, 443 - 454.

Mayes, W.M., Younger, P.L., Aumônier, J., 2006. Buffering of alkaline steel slag leachate across a natural wetland. *Environ Sci Technol*. **40(4)**, 1237-43.

Mayes, W.M., Younger, P.L., Aumônier, J., 2008. Hydrogeochemistry of alkaline steel slag leachates in the UK. *Water, Air & Soil Pollution*, **195**: 35-50.

Mayes, W.M., Aumônier, J., Jarvis, A.P., 2009. Preliminary evaluation of a constructed wetland for treating extremely alkaline (pH 12) steel slag drainage. *Water Sci Technol*. **59(11)**, 2253 - 2263.

Mayes, W.M., Jarvis, A.P., Burke, I.T., Walton, M., Feigl, V., Klebercz, O., Gruiz, K., 2011a. Dispersal and attenuation of trace contaminants downstream of the Ajka bauxite residue (red mud) depository failure, Hungary. *Environ. Sci. Technol*. 45:5147-5155.

Mayes, W.M., Jarvis, A.P., Burke, I.T., Walton, M., Gruiz, K. 2011b. Trace and rare earth element dispersal downstream of the Ajka red mud spill, Hungary. *Proceedings of IMWA Congress*, Aachen Germany.

McBride, M. B., 1980. Chemisorption of Cd^{2+} on calcite surfaces. *Soil Sci. Soc. Am. J.* **44**, 26 – 28.

McLean, J.E. and Bledsoe B.E., 1992. Ground Water Issue. Behaviour of Metals in Soils. United States Environmental Protection Agency Office of Solid Waste and Emergency Response Office of Research and Development EPA/540/S-92/018.

Mehrotra, V., 2011. Leaching of calcium ion (Ca^{2+}) from calcium silicate. In: Sundaram S.K., Ohji T., Fox K.M., Hoffman E. Advances in Materials Science for Environmental and Nuclear Technology II, Ceramic transactions Volume **227** John Wiley and sons, New jersey pg. 301-311.

Meima, J.A. and Comans, R.N.J., 1997. Geochemical modelling of weathering reactions in municipal solid waste incinerator bottom ash. *Environ. Sci. Technol.* **31**, 1269 – 1276.

Meima, J.A. and Comans, R.N.J., 1998. Reducing Sb leaching from municipal solid waste incinerator bottom ash by addition of sorbent materials. *J. Geochem. Expl.*, **62**, 299-304.

Michigan Department of Environmental Quality (MDEQ), 2014. A Guide for Compliance with the Air Regulatory Requirements for Particulate Matter Generation Managing Fugitive Dust.

Micromeritics Instrument Corporation, 2007. TriStar 3000 Operator's Manual V6.08. http://www.micromeritics.com/repository/files/tristar_3000_operators_manual_v6.08.pdf accessed 12/08/15.

Miliša, M., Kepčija, R.M., Radanović, I., Ostojić, A., Habdija, I., 2006. The impact of aquatic macrophyte (*Salix* sp. and *Cladium mariscus* (L.) Pohl.) removal on habitat conditions and macroinvertebrates of tufa barriers (Plitvice Lakes, Croatia) *Hydrobiologia*, **573 (1)**, pp. 183-197

Milodowski, A.E., Shaw, R.P., Stewart, D.I., 2013. The Harpur Hill Site: its geology, evolutionary history and a catalogue of materials present. *British Geological Survey Commissioned Report*, **CR/13/104** 43pp.

Mishra, D., Kim, D.J., Ahn, J.G., Lee, J.C., 2004. Bacterial leaching of metals from sulphide minerals and industrial waste. *KIGAM Bull.* **1**:48–57.

Mishra, D. and Rhee, Y., 2010. Current research trends of microbiological leaching for metal recovery from industrial wastes. http://www.formatex.info/microbiology2/1289-1296.pdf accessed on 13/05/2014.

Misra, C., Perrotta, A.J., 1992. Composition and properties of synthetic hydrotalcites. *Clays Clay Min*. **40**, 145 – 150.

Morel, F.M.M. and Hering, J.G., 1993. Principles and Applications of Aquatic Chemistry. John Wiley & Sons, New York.

Moreno, N., Querol, X., Andrés, J.M., Stanton, K., Towler, M., Nugteren, H., Janssen-Jurkovicová, M., Jones, R., 2005. Physico-chemical characteristics of European pulverized coal combustion fly ashes. *Fuel,* **84**, 1351 – 1363.

Morone, M., Costa, G., Polettini, A., Pomi, R., Baciocchi, R., 2014. Valorization of steel slag by a combined carbonation and granulation treatment. *Minerals Engineering,* **59**, 82–90.

Mukherjee, A.B. and Zevenhoven, R., 2006. Mercury in coal ash and its fate in the Indian subcontinent: A synoptic review. *Sci Total Environ.* **368(1)**, 384 - 392.

Mukherjee, A. and Chakraborty R., 2009. Mutagenicity and genotoxicity of coal fly ash water leachate. *Ecotoxicol Environ Saf.* **72(3)**, 838-842.

Naden, J., 2013. Science and Implementation Plan. Security of Supply of Mineral Resources (Nadin Minerals) Research Programme 2012–2017; Natural Environment Research Council p 15.

Naidu, R. and Harter, R. D., 1998. Effect of different organic ligands on cadmium sorption by and extractability from soils. *Soil Sci. Soc. Am. J*. **62**, 644–650.

Nandy, N.C. and Deo V.B., 1961. Origin of Lonar lake and its alkalinity. Tata Iron and Steel Company (TISCO), *Jamshedpur,* **8**, 1 - 12.

National Slag Association, 2007. Guide for the Use of Steel Slag in Agriculture and for Reclamation of Acidic Lands http://www.nationalslag.org/sites/nationalslag/files/ag_guide909.pdf accessed 12/07/2013.

National Slag Association, 2013. Common Uses for Slag. http://www.nationalslag.org/common-uses-slag accessed 15/09/2014.

Nicolae, M., Vîlciu, I., Zăman, F., 2007. X-ray diffraction analysis of steel slag and blast furnace slag viewing their use for road construction. *UPB Scientific Bulletin Series B*,**69(2)**, 99–108.

Nolte, J. 2003. ICP Emission Spectrometry: A practical guide. Wiley – VCH, Germany.

Ozeki, S., 1997. Properties and usage of steel plant slag. *ENCOSTEEL*- Steel for Sustainable Development -**135**. Stockholm, June.

Pagano, G., Meric, S., De Biase, A., Laccarino, M., Petruzelli, D., Tünay, O., Warnaus, M., 2002. Toxicity of bauxite manufacturing by-products in sea urchin embryos. Ecotoxicoloy and Environmental Safety **51**, 28 – 34.

Pan, S., Chang, E.E., Chiang, P., 2012. CO_2 capture by accelerated carbonation of alkaline waste: A review on its principles and applications. *Aerosol and Air Quality Research,* **12**, 770 – 791.

Paoletti, F., 2002. Behaviour of oxyanions forming heavy metals in municipal solid waste incineration. PhD. Thesis , Univ. Stuttgart.

Parkhurst, D.L. and Appelo C.A.J., 1999. User's guide to PHREEQC--*A computer program for speciation, batch-reaction, one-dimensional transport, and inverse geochemical calculations*. U.S. Geological Survey Water-Resources Investigations Report 99 - 4259.

Patrick, W. H. Jr. and Khalid, R. A., 1974. Phosphate release and sorption by soils and sediments: effect of aerobic and anaerobic conditions, *Science,* **186**, 53-54.

PerkinElmer Inc., 2010. Thermogravimetric Analysis (TGA). A Beginner's Guide. http://www.perkinelmer.co.uk/CMSResources/Images/44-74556GDE_TGABeginnersGuide.pdf accessed on 23/08/2014.

Piantone, P., Bodenan, F., Chatelet-Snidaro, L., 2004. Mineralogical study of secondary mineral phases from weathered MSWI bottom ash: implications for the modelling and trapping of heavy metals. *Appl. Geochem.* **19**, 1891 – 1904.

Pingitore, N.E., 1986. Modes of coprecipitation of Ba^{2+} and Sr^{2+} with calcite. In *Geochemical Processes at Mineral Surfaces*, American Chemical Society, Washington D.C., 574 – 586.

Poeppelmeier, K.R., Pless, J.D, Bardin, B., Kim, H., Ko, D., Smith, M.T., Hammond, R.R., Stair, P.C., 2004. Catalytic oxidative dehydrogenation of propane over Mg–V/Mo oxides. *Journal of Catalysis,* **223**, 419–431.

Pokhrel, D. and Viraraghavan, T., 2004. Treatment of pulp and paper mill wastewater: a review. *Science of the Total Environment,* **333**, 37 – 58.

Pósfai, M., Gelencsér, A., Kováts, N., Turóczi, B., Rostási, Á., Hoffer, A., Imre, K., Nyirő-Kósa, I., Csákberényi-Malasics, D., Tóth, Á., Czitrovszky, A., Nagy, A., Nagy, S., Ács, A., Kovács, A., Ferincz, Á., Hartyáni, Z., 2011. The red mud accident in Ajka (Hungary): characterization and potential health effects of fugitive dust. *Environ. Sci. Technol. 45*, 1608 – 1615.

Power, G., Gräfe, M., Klauber, C., 2009. Review of current bauxite residue management, disposal and storage: practices, engineering and science. CSIRO Document DMR-3608

Pradhan, J., Das, S.N., Thakur, R.S., 1999. Adsorption of hexavalent chromium from aqueous solution by using active red mud. *Journal of Colloid and Interface Science,* **217**, 137–141.

Pradhan, N., Das, B., Gahan, C.S., Kar, R.N., Sukla, L.B., 2006. Beneficiation of iron ore slime using *Aspergillus niger* and *Bacillus circulans*. *Bioresource Technol.* **97**:1876–1879.

Proctor, D.M., Fehling, K.A., Shay, E.C., Lee, B. *et al.*, 2000. Physical and chemical characteristics of blast furnace, basic oxygen furnace, and electric arc furnace steel industry slag. *Environmental Science and Technology*, **34**, 1576 – 1582.

Querol, X., Umaña, J.C., Alastuey, A., Ayora, C., Lopez-Soler, A., Plana, F., 2001. Extraction of soluble major and trace elements from fly ash in open and closed leaching systems. *Fuel,* **80**, 801 – 813.

Quina, M.J., Bordado, J.C.M., Quinta-Ferreira, R.M., 2009. The influence of pH on the leaching behaviour of inorganic components from municipal solid waste APC residues. Waste Management, **29**, 2483–2493.

Radenovic, A., Malina, J., Sofilic, T., 2013. Characterization of ladle furnace slag from carbon steel production as a potential adsorbent. *Advances in Materials Science and Engineering.* Vol. **2013**, Article ID 198240.

Reddy S., Pradhan, R.K., Chandra, S., 2006. Utilization of Basic Oxygen Furnace (BOF) slag in the production of a hydraulic cement binder. *International Journal of Mineral Processing,* **79(2)**, 98–105.

Reeder, R.J., 1983. Crystal chemistry of the rhombohedral carbonates. In *Carbonates: Mineralogy and Chemistry* (ed. R.J Reeder), pp 1 - 47, Mineralogical Society of America, Washington D.C.

Renforth, P. and Manning, D.A.C., 2011. Laboratory carbonation of artificial silicate gels enhanced by citrate: Implications for engineered pedogenic carbonate formation. *International Journal of Greenhouse Gas Control,* **5**, 1578–1586.

Roadcap, G. S., Kelly, W. R., Bethke, C. M., 2005. Geochemistry of extremely alkaline (pH > 12) ground water in slag-fill aquifer. *Ground Water*, **43**, 806 – 816.

Roman-Ross, G., Cuello, G. J., Turrillas, X., Fernandez-Martinez, A., Charlet, L., 2006. Arsenite sorption and co-precipitation with calcite. *Chem. Geol*. **233**, 328 – 336.

Rouff, A. A., Elzinga, E. J., Reeder, R. J., Fisher, N. S., 2004. X-ray absorption spectroscopic evidence for the formation of Pb(II) inner-sphere adsorption complexes and precipitates at the calcite-water interface. *Environ. Sci. Technol*. **38**, 1700 – 1707.

Ruhl, L., Vengosh, A., Dwyer, G.S., Hsu-kim, H., Deonarine, A., Bergin, M., and Kravchenko, J., 2009. Survey of the potential environmental and health impacts in the immediate aftermath of the coal ash spill in Kingston, Tennessee. *Environ. Sci. Technol.* ***43,*** 6326 – 6333.

Shacklette, H.T. and Boerngen, J.G., 1984. Element concentrations in soils and other surficial materials of the conterminous United States. *USGS professional paper*, **1270**.

Shafyei, A., Madhavian, A., Keshavarz Alamdari, E., Haghshenas, D.F., 2006. Recovery of vanadium from Esfahan steel company steel slag: optimizing of roasting and leaching parameters. *International journal of ISSI*, **3**, 17 - 21.

Shen, H. and Forssberg, E., 2003. An overview of recovery of metals from slags. *Waste Management,* **23** 933–949.

Shen, Y. and Guo, W., 2015. Recovery of molybdenum and vanadium from acidic sulfate leach solution of blue sludge by ion exchange. *Environmental Progress & Sustainable Energy*. DOI: 10.1002/ep.12220.

Shi, C., 2004. Steel slag—its production, processing, characteristics, and cementitious properties. *Journal of Materials in Civil Engineering,* **16(3)**, 230–236.

Siddiqi, S.Z., 2008. Limnological profile of high impact meteor crater lake Lonar, Buldana, Maharashtra, India: an extreme hyperalkaline, saline habitat. *Proceedings of Taal2007: The 12th world lake conference*, 1597 - 1613.

Singleton Birch, 2015. A-Z of Lime Uses. http://www.singletonbirch.co.uk/lime/uses accessed on 12/03/2015.

Smith, K.S., 1999. Metal sorption on mineral surfaces: An overview with examples relating to mineral deposits. *Reviews in economic geology volumes 6A and 6B*. U.S. Geological Survey, Denver, CO 80225-0046.

Steelconstruction.info. http://www.steelconstruction.info/Steel_manufacture accessed on 23/05/14.

Stipp, S. L., Hochella, M. F., Parks, G. A., Leckie, J. O. 1992. Cd^{2+} uptake by calcite, solid-state diffusion, and the formation of solid-solution—interface processes observed with near-surface sensitive techniques (XPS, LEED and AES). *Geochim. Cosmochim. Acta,* **56**, 1941–1954.

Stubbles, J., 2015. The Basic Oxygen Steelmaking (BOS) Process. American Iron and Steel Institute https://www.steel.org/making-steel/how-its-made/processes/processes-info/the-basic-oxygen-steelmaking-process.aspx accessed 14/06/2015.

Sutar, H., Mishra, S.C., Sahoo, S.K., Chakraverty, A.P., Maharana, H.S., 2014. Progress of Red Mud Utilization: An Overview. *American Chemical Science Journal,* **4(3)**, 255-279.

Tai, C.Y., Chen, W.R., Shih, S.M., 2006. Factors affecting wollastonite carbonation under CO_2 supercritical conditions. *AlChE J*. **52**, 292 – 299.

Takeno, 2006. Atlas of Eh-pH diagrams Intercomparison of thermodynamic databases Geological Survey of Japan Open File Report No.419.

Tang, Y., Elzinga, E. J., Lee, Y. J., Reeder, R. J., 2007. Coprecipitation of chromate with calcite: batch experiments and X-ray absorption spectroscopy. *Geochim. Cosmochim. Acta,* **71**, 1480 – 1493.

Teir, S., 2008. Fixation of carbon dioxide by producing carbonates from minerals and steelmaking slag. Doctoral Dissertation, Department of Energy Technology, Helsinki University of Technology.

Teir, S., Kronqvist, P., Kaartinen, T., Parviainen, T., 2015. Leaching of Residual Steel Slag from a Mineral Carbonation Process. Paper presented at the 5th International Conference on Accelerated Carbonation for Environmental and Material Engineering (ACEME) New York, USA.

Tossavainen, M., Engstrom, F., Yang, Q., Menad, N., Larsson, M.L., and Bjorkman, B., 2007. Characteristics of steel slag under different cooling conditions. *Waste Management,* **27 (10)**, 1335–1344.

Trieff, N.M., Romana, L.A., Esposito, A., Quiniou, F., Iaccarino, M., Alcock, N., Ramanujam, V.M.S., Pagano, G., 1995. Effluent from bauxite factory induces developmental and reproductive damage in sea urchins. *Archives of Environmental Contamination and Toxicology* **28**, 173 – 177.

Ulibarri, M.A., Labajos, F.M., Trujillano, R., Kagunya, W., Jones, W., 1994. Comparative study of the synthesis and properties of vanadate-exchanged layered double hydroxides. *Inorg. Chem.* **33**, 2592 – 2599.

US EPA, 1995. EPA office of compliance sector notebook project: profile of pulp and paper industry. Washington, DC 20460, USA: EPA/ 310-R-95-015.

USEPA, 2012. Total alkalinity. Retrieved from http://water.epa.gov/type/rsl/monitoring/vms510.cfm on 13/06/2015.

USGS, 2013. *Mineral Commodities Summary.* USGS, Virginia, USA.

Vahidi, E., Shahnazi, A., Rashchi, F., 2012. A kinetics study on the hydrometallurgical recovery of vanadium from LD converter slag in alkaline media. Conference paper presented at EPD Congress Annual Meeting & Exhibition Orlando, Florida, USA.

Van Gerven, T., Imbrechts, K., Van Keer, E., Vandecasteele, C., Jaspers, M., Wauters, G., 2004. In: Gaballah I., B. Mishra, R. Solozabal and M. Tanaka (eds.), Proceedings on Rewas '04, Global symposium on Recycling, Waste Treatment and Clean Technology, Madrid, 26-29 September.

Wang, Q. and Yan, P., 2010. Hydration properties of basic oxygen furnace steel slag. *Constr. Build. Mater.* **24**, 1134–1140.

Ward, C.R., French, D., Jankowski, J., Dubikova, M., Li, Z., Riley, K.W., 2009. Element mobility from fresh and long-stored acidic fly ashes associated with an Australian power station. *International Journal of Coal Geology,* **80**, 224 – 236.

Warren, C.J. and Dudas M.J., 1988. Leaching behaviour of selected trace elements in chemically weathered alkaline fly ash. *The Science of The Total Environment,* **76**, 229-246.

Watkinson, A.P. and Brimacombe J.K., 1982. Limestone calcination in a rotary kiln. *Metallurgical Transactions B,* **13(3)**, 369 - 378.

Webb, J., Rimstidt, D., Balog, A., 1998. Distribution of trace elements between carbonate minerals and aqueous solutions. *Geochimica et Cosmochimica Acta,* **62 (11)**,1851–1863.

Whittleston, R.A., Stewart, D.I., Mortimer, R.J., Tilt, Z.C., Brown, A.P., Geraki, K., Burke, I.T., 2011. Chromate reduction in Fe(II)-containing soil affected by hyperalkaline leachate from chromite ore processing residue. *Journal of Hazardous Materials,* **194**, 15 - 23.

Wogelius, R.A., Refson, K., Fraser, D.G., Grime, G.W., Goff, J.P., 1995. Periclase surface hydroxylation during dissolution. *Geochimica et Cosmochimica Acta,* **59(9)** 1875- 1881.

Wolf, R.E., 2005. What is ICP-MS? ... and more importantly, what can it do? USGS/Central Region/Crustal Imaging and Characterization Team.

Wright, A.L., Provin, T.L., Hons, F.M., Zuberer, D.A., White, R.H., 2008. Compost impacts on dissolved organic carbon and available nitrogen and phosphorus in turfgrass soil. *Waste Management,* **28**, 1057–1063.

Xiao-Ming, L., Xu-Jia, H., Yue-Peng, C., 2013. Chapter 1: Development and application of X-Ray diffraction technique for single crystal. In: Kaimin Shih (ed.) X-Ray Diffraction: Structure, Principles and Applications Nova Science publishers New York, USA.

Yang, X., Hou, Q., Yang, Z., Zhang, X., Hou, Y., 2012. Solid-solution partitioning of arsenic (As) in the paddy soil profiles in Chengdu Plain, Southwest China. *Geoscience Frontiers,* **3(6)**, 901–909.

Yildirim, I.Z. and Prezzi, M., 2011. Chemical, Mineralogical, and Morphological Properties of Steel Slag. *Advances in Civil Engineering*; Hindawi Publishing Corporation, 1 -13.

Yildirim, I. and Prezzi M., 2015. Steel Slag: Chemistry, Mineralogy, and Morphology. *IFCEE*, 2816 - 2825.

Zachara, J. M., Cowan, C. E., Resch, C. T., 1991. Sorption of divalent metals on calcite. *Geochim. Cosmochim. Acta,* **55**, 1549 – 1562.

Zaihua, L., Svensson, U., Dreybrodt, W., Daoxian, Y., Buhmann, D., 1995. Hydrodynamic control of inorganic calcite precipitation in Huanglong Ravine, China: Field measurements and theoretical prediction of deposition rates. *Geochimica et Cosmochimicha Acta.* **59,** 3087-3097.

Zussman, J., Bowles, J.F.W., Howie, R.A., Vaughan, D.J., 2011. In Rock-forming Minerals: Non-silicates: oxides, hydroxides and sulphides. 2nd edition, Vol **5A** published by the Geological Society London.

Appendix

A1: Published paper and conference presentation abstracts

(i)

Hull S.L., Oty U.V., Mayes W.M., 2014. Rapid recovery of benthic invertebrates downstream of hyperalkaline steel slag discharges. *Hydrobiologia* **736**, 83–97.

Abstract

This study assesses the physical and chemical characteristics of hyperalkaline steel slag leachate from a former steelworks on two streams in England and their impacts on benthic invertebrate communities. Using multivariate methods (CCA), we related invertebrate richness and diversity with chemical parameters along the environmental gradient from point sources to less impacted sites downstream. Point discharges are characterised by high pH (10.6–11.5), high ionic strength (dominated by Ca–CO3–OH waters), elevated trace elements (notably Li, Sr and V) and high rates of calcium carbonate precipitation. This combination of stressors gives rise to an impoverished benthic invertebrate community in source areas. The total abundance, taxonomic richness and densities of most observed organisms were strongly negatively correlated with water pH. Analysis using biological pollution monitoring indices (e.g. BMWP and Functional Feeding Groups) shows the system to be highly impacted at source, but when pH approaches values close to aquatic life standards, some 500 m downstream, complex biological communities become established. In addition to showing the rapid recovery of invertebrate communities downstream of the discharges, this study also provides a baseline characterisation of invertebrate communities at the extreme alkaline range of the pH spectrum.

(ii)

Conference paper delivered at the 21st meeting of the International Mineralogical Association 1-5 September 2014 Johannesburg, South Africa.

Oty, U., Rogerson, M., Greenway, G., Mayes, W., 2014. Accelerated weathering of steel slag using organic amendments, in: Chetty, D., Andrews, L., Villiers, J.d., Dixon, R., Nex, P., Reimold, W.U., Richards, J., Smith, B., Smith, C., Verryn, S., Viljoen, F. (Eds.), 21st meeting of the International Mineralogical Association (IMA), Johannesburg, South Africa.

Abstract

The leaching of oxyanionic metals such as V, Mo and Cr from steel slag at high pH can pose environmental problems at disposal sites and in slag used as aggregate. This study presents a novel biologically-mediated approach that both (1) accelerates the rates of slag weathering so the timescales over which environmental impacts are apparent is reduced, and (2) provides an opportunity for the recovery of valuable e-tech metals such as V and Li from leachates. A series of column and batch experiments were set up to investigate the effect of organic amendment of steel slags using municipal solid waste (MSW) compost. The impact of the physical structure of the treatments and the effect of microbial or redox controls versus the leaching rate of V and Li were also studied. Results showed that capping of steel slag with municipal compost accelerated the release of V and Li from initial concentrations of 250 ppb and 12 ppb to a four-fold and three-fold increase respectively within the equilibration period of 50 days. The leaching rate of various elements were found to be dependent on the structural arrangement of the compost within the slag, with high pH (10-11.5) water in contact with organic layers crucial for the solubilisation of V and Li. This is likely explicable by organic complexation of metals. Batch experiments highlighted that with and without organic amendment, under aerobic conditions, V concentrations in leachate from slag reached 1000 ppb a full order of magnitude faster than under anaerobic conditions. The effect of microbial processes on the leaching process however remains uncertain, even though the V concentration in sterilised aerobic flasks was lower compared to the unsterilised ones. In addition to the potential value recovery of materials from these by-products, the compost amendment holds the

promise to reduce the lifetimes over which polluting waters are released from the slag and minimise the hazard of fugitive dusts.

(iii)

Poster presented at the 24th Goldschmidt conference 8 – 13 June, Sacramento California USA.

Poster title: Hyperalkaline waters: occurrence, impacts and management

Oty U[1]*, Rogerson M[2], Greenway G[3], Mayes W[1]. [1] - Centre for environmental and marine sciences, University of Hull, UK. *u.v.oty@2010.hull.ac.uk [2] - Geography, earth and environmental sciences University of Hull. [3] - Department of chemistry, University of Hull.

Abstract

High pH leachates arising from steel slag and lime spoil disposal sites can pose serious threats to aquatic life and also cause groundwater pollution. Data are presented detailing the hydrogeochemistry of leachates (of average pH > 12) from two steel slag disposal sites and three lime spoil affected sites in the UK.

Waters at the steel slag disposal sites are of the Na-CO_3 type (Yarborough, Tata steel Scunthorpe), and Ca – OH type (Consett steelworks). Leachates from selected lime spoil affected areas in Derbyshire are dominated by Ca-OH type (Brook Bottom), Ca – CO_3 type (Doveholes), Na and Cl^- type (Peakdale Cement) waters. Caustic leachates at these sites are often supersaturated with secondary calcite deposits which can act as a sink for certain metals. Concentrations of trace elements such as V, Mo and Ni in these waters reach levels of up to 97, 60 and 61 μg/L respectively.

The potential for applying constructed wetlands to buffer the pH to acceptable levels by attenuating carbonate sediments is being trialled at the Scunthorpe site. The background to the system design and broader management options are discussed, including the potential for recovery of these valuable metals from these waters.

Appendix A2: Sampling locations used in this research

Appendix A3: Leaching efficiencies of selected elements in steel slag (field samples)

	Yarborough			**Consett**		
Element	slag concentration / mg/kg	leachate concentration / ppm	**Leaching efficiency / %**	slag concentration / mg/kg	leachate concentration / ppm	**Leaching efficiency / %**
Mg	20000	0.1	**0.001**	12000	1	**0.008**
Ca	200000	23	**0.012**	202000	239	**0.118**
Si	36000	0.114	**0.0003**	102000	1.29	**0.001**
Li	2.4	0.035	**1.46**	21.8	0.822	**3.77**
V	1910	0.079	**0.004**	1764	0.0518	**0.003**
Mo	20.3	0.06	**0.296**	19.2	0.0234	**0.122**
Ni	620	0.061	**0.010**	242	0.0089	**0.004**
Ba	65.8	0.0041	**0.006**	422	0.0425	**0.010**
Fe	167000	0.0034	**0.000002**	107000	0.98	**0.001**

Appendix A4: Geochemical modelling data for the study sites showing predicted mineral phases.

	Sites			
Phases	**YB**	**HB**	**BB**	**DH**
Aragonite ($CaCO_3$)	1.76	2.29	2.17	3.21
Barite ($BaSO_4$)	-0.37	0.96	N.D	0.91
Brucite ($Mg(OH)_2$)	0.29	0.82	4.33	4.26
Calcite ($CaCO_3$)	1.91*	2.43*	2.32*	3.35*
Chrysotile ($Mg_3Si_2O_5(OH)_4$)	3.71	8.41	11.89	12.67
Clinoenstatite ($MgSiO_3$)	-2.09	-0.05	-0.11	0.39
Diopside ($CaMgSi_2O_6$)	0.87	5.09	4.56	5.19
Dolomite ($CaMg(CO_3)_2$)	1.68	2.63	2.82	5.22
Forsterite (Mg_2SiO_4)	-2.03	0.52	3.96	4.4
Magnesite ($MgCO_3$)	-0.72	-0.29	0.02	1.37
Merwinite ($Ca_3MgSi_2O_8$)	-10	-4.76	0.67	0.86
Monticellite ($CaMgSiO_4$)	-1.94	0.67	3.64	3.83
$Ni(OH)_2$	1.81	1.49	0.72	0.42
Strontianite ($SrCO_3$)	2.1	1.17	0.2	1.66
Quartz (SiO_2)	-3.83*	-2.3	-5.87	-5.31*
Wollastonite ($CaSiO_3$)	-1.65	0.46	-0.05	0.17

*Denotes presence of solid phase confirmed by XRD, N.D – not detected

YB – Yarborough, HB – Howden Burn, BB – Brook bottom, DH – Doveholes

Appendix A5: Saturation indices of potential solubility controlling phases in leachates for column experiments. N.D – not detected

Mineral	**Formula**	**A1**	**A19**	**A28**	**A50**	**B1**	**B19**	**B28**	**B50**	**C1**	**C19**	**C28**	**C50**	**D1**	**D19**	**D28**	**D50**
Calcite	$CaCO_3$	**3.83**	**3.89**	**4.01**	**3.99**	**4.11**	**4.02**	**4.13**	**4.1**	**3.71**	**3.75**	**3.86**	**3.89**	**4.27**	**4.25**	**4.24**	**4.22**
Quartz	SiO_2	**0.42**	**-0.51**	**-0.61**	**-0.54**	**-0.78**	**ND**	**-1.94**	**-2.03**	**0.6**	**-0.41**	**0.24**	**0.13**	**0.44**	**-0.28**	**-0.32**	**-0.23**
Portlandite	$Ca(OH)_2$	**-3.6**	**-2.72**	**-2.31**	**-2.76**	**-2.09**	**-2.17**	**-1.67**	**-2.01**	**-5.24**	**-4.44**	**-3.95**	**-3.99**	**-3.6**	**-2.33**	**-2.33**	**-2.77**
Brucite	$Mg(OH)_2$	**0.21**	**ND**	**ND**	**ND**	**1.01**	**ND**	**ND**	**ND**	**0.02**	**0.86**	**1.6**	**1.07**	**1.33**	**ND**	**ND**	**ND**
Corundum	Al_2O_3	**0.78**	**0.64**	**0.94**	**1.28**	**0.12**	**1.34**	**1.55**	**1.56**	**2.16**	**0.84**	**0.96**	**1.13**	**-0.75**	**-1.12**	**-0.97**	**-0.52**
Aragonite	$CaCO_3$	**3.68**	**3.75**	**3.87**	**3.84**	**3.97**	**3.87**	**3.99**	**3.95**	**3.57**	**3.61**	**3.72**	**3.74**	**4.13**	**4.11**	**4.1**	**4.07**
Strontianite	$SrCO_3$	**3.38**	**3.73**	**3.38**	**4.36**	**3.82**	**4.02**	**3.96**	**4.52**	**3.38**	**3.58**	**ND**	**ND**	**4.49**	**4.23**	**4.18**	**3.4**
Dolomite	$CaMg(CO_3)_2$	**6.39**	**ND**	**ND**	**ND**	**6.24**	**ND**	**ND**	**ND**	**7.59**	**7.73**	**8.18**	**7.76**	**8.38**	**ND**	**ND**	**ND**
Ettringite	$Ca_6Al_2(SO_4)_3(OH)_{12}{:}26H_2O$	**0.32**	**2.27**	**4.47**	**1.91**	**4.18**	**3.86**	**6.47**	**4.18**	**-3.99**	**-4.5**	**-2.61**	**-2.42**	**-1.3**	**1.25**	**1.15**	**-0.11**
Gypsum	$CaSO_4{:}2H_2O$	**0.18**	**-0.01**	**0.22**	**-0.3**	**0.18**	**-0.24**	**0.05**	**-0.37**	**-0.07**	**-0.59**	**-0.48**	**-0.42**	**0.18**	**-0.11**	**-0.19**	**-0.32**
Periclase	MgO	**-4.83**	**ND**	**ND**	**ND**	**-4.03**	**ND**	**ND**	**ND**	**-5.02**	**-4.18**	**-3.44**	**-3.96**	**-3.71**	**ND**	**ND**	**ND**
Lime	CaO	**-13.63**	**-12.74**	**-12.33**	**-12.78**	**-12.11**	**-12.19**	**-11.69**	**-12.02**	**-15.26**	**-14.46**	**-13.96**	**-14.01**	**-13.61**	**-12.34**	**-12.34**	**-12.79**
Wollastonite	$CaSiO_3$	**1.62**	**1.57**	**1.88**	**1.5**	**1.93**	**ND**	**1.19**	**0.77**	**0.16**	**-0.05**	**1.09**	**0.93**	**1.64**	**2.2**	**2.16**	**1.8**
Larnite	Ca_2SiO_4	**-4.14**	**-3.3**	**-2.58**	**-3.4**	**-2.3**	**ND**	**-2.62**	**-3.38**	**-7.23**	**-6.64**	**-5**	**-5.2**	**-4.1**	**-2.27**	**-2.32**	**-3.11**
Rankinite	$Ca_3Si_2O_7$	**-2.2**	**-1.4**	**-0.38**	**-1.58**	**-0.04**	**ND**	**-1.11**	**-2.29**	**-6.75**	**-6.37**	**-3.59**	**-3.94**	**-2.13**	**0.25**	**0.16**	**-0.99**
Forsterite	Mg_2SiO_4	**1.58**	**ND**	**ND**	**ND**	**1.98**	**ND**	**ND**	**ND**	**1.38**	**2.05**	**4.17**	**3.02**	**3.83**	**ND**	**ND**	**ND**
Akermanite	$Ca_2MgSi_2O_7$	**1.94**	**ND**	**ND**	**ND**	**3.39**	**ND**	**ND**	**ND**	**-1.16**	**-0.74**	**2.29**	**1.45**	**3.12**	**ND**	**ND**	**ND**
Merwinite	$MgCa_3(SiO_4)_2$	**-2.29**	**ND**	**ND**	**ND**	**0.67**	**ND**	**ND**	**ND**	**-7.03**	**-5.81**	**-2.29**	**-3.17**	**-1.1**	**ND**	**ND**	**ND**
Calcium aluminium silicate	$Ca_3Al_2(SiO_4)_3$	**13.31**	**13.03**	**14.26**	**13.47**	**13.61**	**ND**	**12.81**	**11.55**	**10.32**	**8.37**	**11.92**	**11.62**	**11.87**	**13.15**	**13.19**	**12.58**
Spinel	Al_2MgO_4	**-2.04**	**ND**	**ND**	**ND**	**-1.9**	**ND**	**ND**	**ND**	**-0.85**	**-1.32**	**-0.46**	**-0.82**	**-2.44**	**ND**	**ND**	**ND**

Appendix A6: Semi –quantitative EDX analysis of weathered slag from control column (Rim region)

All results in weight %					
Region	C	O	Mg	Si	Ca
zone a	34.79	49.37	13.93	0.21	0.61
zone b	20.41	38.29	7.09	11.49	22.40
zone c	20.06	50.75	4.75	0.91	22.34
zone d	12.38	41.87	45.25	0.07	0.23
zone e	9.50	41.60	21.90	12.10	14.50

Appendix A7: Semi –quantitative EDX analysis of weathered slag from compost amended column (Rim region)

All results in weight %										
Region	C	O	Mg	Si	Ca	Fe	Al	Cr	Ti	Mn
zone A1	40.14	45.94	10.94	0.30	0.72	0.85	0.29	0.14	0.00	0.18
zone A2	20.18	60.43	16.58	0.31	0.60	0.73	0.29	0.15	0.00	0.19
zone A3	27.74	42.29	12.40	5.73	7.56	1.36	1.61	0.59	0.05	0.34

Appendix A8: Distribution coefficient values for selected conservative elements for different column treatments

		Column A			Column B			Column C	
Time (days)	Na	K	S	Na	K	S	Na	K	S
0.2	17.2	33.4	2.3	14.6	30.1	1.8	27.8	369.7	5.0
0.3	18.3	36.6	2.5	15.2	36.1	1.5	27.7	384.4	6.7
0.9	16.7	19.7	4.3	22.5	81.4	5.0	37.3	468.5	6.1
1.0	16.0	18.6	4.1	22.3	78.1	5.0	36.7	432.7	6.0
1.1	18.8	21.4	4.7	26.1	117.7	6.1	34.8	397.2	5.7
2.3	19.5	22.9	4.7	33.3	135.7	7.4	39.5	431.6	6.7
4.1	23.3	27.3	5.3	39.3	153.8	8.3	46.3	479.7	8.4
6.3	20.5	25.0	3.6	28.4	112.2	2.8	46.6	480.8	8.9
7.2	20.4	24.7	3.4	29.5	115.5	3.1	52.0	522.3	9.6
9.1	21.4	25.9	3.5	33.0	128.0	3.2	51.7	506.4	9.7
12.0	23.2	27.4	3.6	37.7	140.0	2.5	55.2	540.2	12.2
14.0	24.5	28.5	13.4	40.1	145.6	3.4	69.7	656.0	12.2
15.0	24.5	28.1	4.4	41.0	147.5	4.5	69.0	572.0	12.4
16.0	23.6	27.3	5.7	41.6	149.6	3.3	67.0	626.2	12.3
19.0	23.4	26.7	6.1	45.8	161.4	4.9	74.5	694.2	13.9
20.1	23.2	26.7	7.2	41.5	145.2	5.6	74.3	683.9	13.6
21.0	25.7	29.0	6.3	46.4	159.7	3.3	83.1	756.3	13.9
22.1	24.2	35.7	9.5	42.8	146.9	3.8	96.6	882.4	15.6
26.0	24.8	27.9	7.9	48.2	164.9	5.5	79.5	622.3	12.2
27.1	24.8	27.6	7.4	47.0	160.0	5.6	86.6	666.6	12.9
28.1	50.9	47.4	5.7	174.8	583.2	10.0	90.5	885.0	13.9
29.1	41.3	38.1	4.7	128.8	425.5	6.0	101.4	987.0	14.6
30.1	48.6	45.0	5.7	179.1	599.9	10.4	105.5	1015.3	13.7
33.1	48.6	45.0	5.5	175.4	581.7	14.4	116.1	1108.8	14.0
34.1	46.5	42.6	5.0	165.5	560.1	12.2	113.7	1086.8	13.4
35.1	44.5	40.9	4.8	158.0	548.4	12.5	105.6	1011.6	12.9
36.1	41.3	38.3	4.7	156.2	548.4	13.1	98.3	939.2	12.1
37.1	40.2	37.4	5.2	151.7	540.8	16.2	87.0	829.3	11.4
40.1	37.9	34.9	5.2	159.9	575.5	28.4	91.0	865.2	13.3
41.1	38.3	35.2	5.2	153.5	550.8	28.0	116.5	1103.6	21.7
49.1	51.4	59.1	6.8	239.7	889.1	12.3	183.8	1631.9	19.7

		Column D	
Time (days)	Na	K	S
0	22.3	303.4	3.6
0.2	36.3	526.2	4.8
1.0	42.2	561.7	5.6
1.1	38.8	526.9	5.4
2.2	45.7	601.6	6.4
3.2	51.6	691.2	7.5
9.2	63.8	852.3	10.0
18.2	63.6	789.4	9.5
28.2	52.6	639.8	9.3
36.1	44.0	473.1	7.6
49.1	29.8	400.5	6.3

Appendix A9: Statistical analyses showing differences in the various leaching (flask) treatments

Kruskal-Wallis Test: pH versus Treatment

```
Kruskal-Wallis Test on pH

Treatment   N  Median  Ave Rank      Z
Acid        6   9.445       3.5  -3.37
Compost     6  11.765       9.5   0.00
Water       6  12.140      15.5   3.37
Overall    18               9.5

H = 15.16  DF = 2  P = 0.001
H = 15.19  DF = 2  P = 0.001  (adjusted for ties)
```

Kruskal-Wallis Test: Cond versus Treatment

```
Kruskal-Wallis Test on Cond

Treatment   N  Median  Ave Rank      Z
Acid        6  2.9750      15.5   3.37
Compost     6  0.4585       3.5  -3.37
Water       6  0.7200       9.5   0.00
Overall    18               9.5

H = 15.16  DF = 2  P = 0.001
H = 15.17  DF = 2  P = 0.001  (adjusted for ties)
```

Kruskal-Wallis Test: Ca versus Treatment

```
Kruskal-Wallis Test on Ca

Treatment   N   Median  Ave Rank      Z
Acid        6  1443.85      15.5   3.37
Compost     6    90.72       3.5  -3.37
Water       6   156.85       9.5   0.00
Overall    18                9.5

H = 15.16  DF = 2  P = 0.001
```

Kruskal-Wallis Test: S versus Treatment

```
Kruskal-Wallis Test on S

Treatment   N  Median  Ave Rank      Z
Acid        6   60.39      15.5   3.37
Compost     6   24.12       9.0  -0.28
Water       6   15.73       4.0  -3.09
Overall    18               9.5

H = 14.00  DF = 2  P = 0.001
```

Kruskal-Wallis Test: Mg versus Treatment

```
Kruskal-Wallis Test on Mg

Treatment   N     Median  Ave Rank      Z
Acid        6  277.74657      15.5   3.37
Compost     6    0.06404       9.2  -0.19
Water       6    0.02462       3.8  -3.18
Overall    18                  9.5
```

```
H = 14.36  DF = 2  P = 0.001
```

Kruskal-Wallis Test: Si versus Treatment

```
Kruskal-Wallis Test on Si

Treatment   N  Median  Ave Rank      Z
Acid        6  18.182      14.7   2.90
Compost     6   1.756       8.3  -0.66
Water       6   1.130       5.5  -2.25
Overall    18               9.5

H = 9.27  DF = 2  P = 0.010
```

Kruskal-Wallis Test: Ba versus Treatment

```
Kruskal-Wallis Test on Ba

Treatment   N   Median  Ave Rank      Z
Acid        6  1.00957      15.5   3.37
Compost     6  0.06097       3.5  -3.37
Water       6  0.29146       9.5   0.00
Overall    18                9.5

H = 15.16  DF = 2  P = 0.001
```

Kruskal-Wallis Test: Sr versus Treatment

```
Kruskal-Wallis Test on Sr

Treatment   N  Median  Ave Rank      Z
Acid        6  1.3854      15.5   3.37
Compost     6  0.1880       4.7  -2.72
Water       6  0.3023       8.3  -0.66
Overall    18               9.5

H = 12.78  DF = 2  P = 0.002
```

Kruskal-Wallis Test: K versus Treatment

```
Kruskal-Wallis Test on K

Treatment   N  Median  Ave Rank      Z
Acid        6  12.001       9.5   0.00
Compost     6  51.337      15.5   3.37
Water       6   7.705       3.5  -3.37
Overall    18               9.5

H = 15.16  DF = 2  P = 0.001
```

Kruskal-Wallis Test: Na versus Treatment

```
Kruskal-Wallis Test on Na

Treatment   N  Median  Ave Rank      Z
Acid        6   21.00       9.7   0.09
Compost     6   27.72      15.3   3.28
Water       6   15.63       3.5  -3.37
Overall    18               9.5

H = 14.75  DF = 2  P = 0.001
```

Kruskal-Wallis Test: V versus Treatment

```
Kruskal-Wallis Test on V

Treatment   N  Median  Ave Rank      Z
Acid        6  394.33      15.5   3.37
Compost     6   90.02       9.5   0.00
Water       6   29.86       3.5  -3.37
Overall    18               9.5

H = 15.16  DF = 2  P = 0.001
```

Kruskal-Wallis Test: Mo versus Treatment

```
Kruskal-Wallis Test on Mo

Treatment   N  Median  Ave Rank      Z
Acid        6  16.168      12.0   1.40
Compost     6  18.683      13.0   1.97
Water       6   4.803       3.5  -3.37
Overall    18               9.5

H = 11.47  DF = 2  P = 0.003
```

Kruskal-Wallis Test: Li versus Treatment

```
Kruskal-Wallis Test on Li

Treatment   N  Median  Ave Rank      Z
Acid        6  91.870      15.5   3.37
Compost     6   6.770       3.5  -3.37
Water       6  13.277       9.5   0.00
Overall    18               9.5

H = 15.16  DF = 2  P = 0.001
```

Kruskal-Wallis Test: Ni versus Treatment

```
Kruskal-Wallis Test on Ni

Treatment   N  Median  Ave Rank      Z
Acid        6  91.786      15.5   3.37
Compost     6   5.470       6.5  -1.69
Water       6   5.866       6.5  -1.69
Overall    18               9.5

H = 11.37  DF = 2  P = 0.003
```

Appendix A10: Statistical analyses showing differences in the column treatments

Kruskal-Wallis Test: pH versus C1

```
Kruskal-Wallis Test on pH

C1         N  Median  Ave Rank      Z
ColumnA   31   11.43      53.5  -0.01
ColumnB   31   11.70      90.5   7.96
ColumnC   31   10.77      20.2  -7.16
ColumnD   13   11.40      44.7  -1.10
Overall  106              53.5

H = 82.16  DF = 3  P = 0.000
```

```
H = 82.31  DF = 3  P = 0.000  (adjusted for ties)
```

Kruskal-Wallis Test: Cond versus C1

```
Kruskal-Wallis Test on Cond

C1         N  Median  Ave Rank      Z
ColumnA   31    1173      17.8  -7.69
ColumnB   31    2129      57.1   0.78
ColumnC   31    2192      74.3   4.49
ColumnD   13    3120      80.3   3.36
Overall  106              53.5

H = 66.42  DF = 3  P = 0.000
H = 66.43  DF = 3  P = 0.000  (adjusted for ties)
```

Kruskal-Wallis Test: Eh versus C1

```
Kruskal-Wallis Test on Eh

C1         N  Median  Ave Rank      Z
ColumnA   31  -280.0      53.2  -0.06
ColumnB   31  -295.6      16.0  -8.07
ColumnC   31  -241.0      88.4   7.52
ColumnD   13  -279.3      60.2   0.84
Overall  106              53.5

H = 86.66  DF = 3  P = 0.000
H = 86.66  DF = 3  P = 0.000  (adjusted for ties)
```

Kruskal-Wallis Test: Ca versus C1

```
104 cases were used
2 cases contained missing values


Kruskal-Wallis Test on Ca

C1         N  Median  Ave Rank      Z
ColumnA   31   72.63      51.0  -0.32
ColumnB   31   93.47      71.9   4.27
ColumnC   31   49.22      21.1  -6.93
ColumnD   11  154.45      90.5   4.42
Overall  104              52.5

H = 64.06  DF = 3  P = 0.000
```

Kruskal-Wallis Test: S versus C1

```
104 cases were used
2 cases contained missing values


Kruskal-Wallis Test on S

C1         N  Median  Ave Rank      Z
ColumnA   31   77.76      38.1  -3.17
ColumnB   31   73.06      36.0  -3.63
ColumnC   31  131.62      71.7   4.22
ColumnD   11  188.09      85.5   3.83
Overall  104              52.5

H = 41.97  DF = 3  P = 0.000
```

Kruskal-Wallis Test: K versus C1

```
104 cases were used
2 cases contained missing values


Kruskal-Wallis Test on K

C1          N  Median  Ave Rank      Z
ColumnA    31   17.02      16.0  -8.03
ColumnB    31   83.45      47.6  -1.08
ColumnC    31  229.28      78.3   5.68
ColumnD    11  547.60      96.4   5.10
Overall   104              52.5

H = 92.03  DF = 3  P = 0.000
```

Kruskal-Wallis Test: Na versus C1

```
104 cases were used
2 cases contained missing values


Kruskal-Wallis Test on Na

C1          N  Median  Ave Rank      Z
ColumnA    31   52.00      25.7  -5.89
ColumnB    31   92.76      56.7   0.92
ColumnC    31   98.91      64.4   2.63
ColumnD    11  160.34      82.5   3.49
Overall   104              52.5

H = 40.74  DF = 3  P = 0.000
```

Kruskal-Wallis Test: Li versus C1

```
Kruskal-Wallis Test on Li

C1          N  Median  Ave Rank      Z
ColumnA    31  12.622      59.7   1.34
ColumnB    31  12.743      50.5  -0.66
ColumnC    31   8.971      36.1  -3.75
ColumnD    13  20.471      87.5   4.25
Overall   106              53.5

H = 27.42  DF = 3  P = 0.000
H = 27.42  DF = 3  P = 0.000  (adjusted for ties)
```

Kruskal-Wallis Test: V versus C1

```
Kruskal-Wallis Test on V

C1          N  Median  Ave Rank      Z
ColumnA    31  142.52      76.8   5.02
ColumnB    31   53.67      23.4  -6.48
ColumnC    31   70.84      41.6  -2.56
ColumnD    13  438.61      98.1   5.58
Overall   106              53.5

H = 79.52  DF = 3  P = 0.000
```

Kruskal-Wallis Test: Ni versus C1

```
Kruskal-Wallis Test on Ni

C1          N  Median  Ave Rank      Z
ColumnA    31   3.014      32.8  -4.46
ColumnB    31   3.110      31.3  -4.79
ColumnC    31  14.852      87.9   7.40
ColumnD    13  11.156      73.9   2.56
Overall   106              53.5

H = 74.75  DF = 3  P = 0.000
```

Kruskal-Wallis Test: Mo versus C1

```
Kruskal-Wallis Test on Mo

C1          N  Median  Ave Rank      Z
ColumnA    31   21.61      17.0  -7.87
ColumnB    31   44.56      48.3  -1.13
ColumnC    31   78.04      80.9   5.89
ColumnD    13  150.04      87.8   4.30
Overall   106              53.5

H = 85.47  DF = 3  P = 0.000
```